東北大学反応化学研究所

炭素資源反応研究センター報告書

１９９４年５月

Research Center for Carbonaceous Resources

Institute for Chemical Reaction Science

Tohoku University

東北大学反応化学研究所

炭素資源反応研究センター報告書

１９９４年５月

Research Center for Carbonaceous Resources

Institute for Chemical Reaction Science

Tohoku University

目　次

巻頭言

炭素資源反応研究センター長　　富田　彰

最近、前世紀末のエネルギー状況を調べる機会があった。当時のわが国の主要エネルギー源は薪炭であり、石炭が急速に伸びて薪炭に迫ろうとしている状況であった。ごく僅かの石油が使用されているが、原子力、天然ガスはおろか水力さえも存在しない時代であった。彼らが百年後の今日を予測することは不可能に近いことであったろう。われわれが百年後のことは予測することはさらに難しい。そうかといって将来を成り行きに任せるというのでは無責任すぎよう。百年とは言わないが、３０年後位のことならある程度分かる。核融合の利用は遠く、増殖炉は実現していたにしてもごく僅かで、太陽光発電も全エネルギーの１０％には達していまい。石油、天然ガスが底をつくことはないが、先行きの心細さ感は急速に顕在化していよう。一方、人口とエネルギー消費の伸びは一向に衰えない。３０年前に炭素税云々と言っていたのが信じられないくらい石炭に依存する時代になっている可能性は少なくない。石炭を有効にしかもクリーンに利用する手段を準備しておくことがわれわれの大きな使命である。

１９９１年４月に、非水溶液化学研究所が反応化学研究所に改組するにあたり、「石炭処理部門」と「石炭化学実験施設」を継承して“石炭・重質油・バイオマスなどの炭素質をクリーンな燃料や高度な機能をもつ素材に変換するための総合的なプロセスの開発”を目的とする本センターが設置された。これは、石炭をはじめとする重質炭素資源の研究が一見緊急を要しないようでいながら、長期的には人類の存亡にかかわる重要課題であると文部省、大学当局が認識されたもので、その判断に深い敬意と謝意を表するものである。

改組前の石炭グループの成果は「東北大学における石炭研究の概要（１～５）」として報告してきた。センター発足以来、「変換プロセス研究部」では石炭の溶媒抽出や石炭の高次構造の研究で、「変換触媒研究部」では石炭のガス化やクリーン化の研究でいずれも優れた成果を挙げてきたので、協力分野も含めて成果を紹介するための報告書を作ることにした。ここには、研究業績のほか、諸活動の記録をも含めた。国際協力の項などを見ていただけると本センターの幅広い活動状況を御理解いただけることと思う。事実、昨年バンフで開催された国際石炭科学会議において、本センターを含む本学からの参加者数が世界の研究機関の中で最も多かったことは、本学が世界の石炭研究の中心の一つになっていることを示している。このような意味でも、本センターの任務は重大なものがある。諸賢の厳しい御鞭撻と暖かい御支援を衷心よりお願い申し上げる次第である。

炭素資源反応研究センター設立の経緯

西山 誼行

東北大学非水溶液化学研究所において新しいエネルギー源を作るという観点で石炭変換研究が始められたのは1973年である。この研究は従来の石炭科学の流れとは切り離された形で、全く新しい発想にもとづいて、石炭の液体アンモニア（液安）への溶解性を調べることからスタートした。その成果が内外の注目を惹くところとなり、当時のエネルギー問題にも助勢されて、急速な研究体制の整備、拡充が求められるところとなり、1981年に石炭化学実験施設が設置された。その間の経緯を、1981年度概算要求の説明文から抜萃させて頂く。

「非水溶液化学研究所無機化学研究部門では昭和46年以来炭素質の触媒を用いたガス化の研究を行い、47年には成果の一部をJournal of Catalysisに発表した。翌昭和48年にいわゆる第１次石油危機が発生し、エネルギー源としての石炭の重要性が協調されるに至り、当部門でも大学としての石炭に関する基礎研究の必要を認め石炭ガス化の研究を開始、最初の成果が49年に「石炭の液体アンモニア前処理を伴う触媒ガス化」として発表されたが、これは世界的反響を呼び西独の著名な石炭研究所Bergbau Forschung から共同研究の申込を受け、国有特許として日米英独仏蘭加豪印の９ヶ国の認可を得ている。次いで非水溶液化学研究所として関連５部門に工学部応用化学科の１講座も加え、石炭ガス化のプロジェクト研究を開始した。直ちに文部省に研究助成を要請し、昭和50年度2240万円、51年度6000万円、その他54年度現在総額1億4千万円の交付を受けた。東北大学における石炭関連研究もきわめて活発で、例えば卒業論文として工学部応用化学科、化学工学科、非水溶液化学研究所全体で53年度８研究室11編、54年度６研究室8編が発表されている。

この様な経過と成果をふまえ、益々国家的重要性を増しつつある石炭化学の基礎研究を強力に推進する方途について検討を重ねたが、研究者の数の不足が最大の障害であると認めざるを得ない。石炭化学者は我が国においては極めて少なく、その教育要請のためにも関連研究部門および施設の増設が急務と思われる。」

この1981年度の予算要求は、文部省の認めるところとなり、まず石炭化学実験施設（専任教官：助教授１、助手１）が時限10年で設置され、ついで1983年には石炭処理化学研究部門（専任教官：教授１、助教授１）が同じく時限10年で認められた。

石炭化学実験施設の時限が目前に感じられるようになった1988年頃から、松田施設長（当時）を中心に石炭研究の将来について討議され、石炭グループ教授間で次期の研究組織構想が固められて来た。その骨子は　①石炭利用技術の開発はまだまだ進めるべき事項が多く、研究を継続する必要がある、②附属施設の陣容を強化して石炭研究の中核としての役割を明確にし、かつ学生の配属も確保する形が望まし

い、という２点であり、1980年構想の2部門・1施設を一つの研究組織とする形であった。

平行して非水溶液化学研究所の組織運営の見直しが1984年頃から開始され、1991年には大部門制で反応化学の総合化と体系化を目指す反応化学研究所へと改組・転換されたが、その見直し作業の全期間を通して、石炭変換研究は研究所の三つの中心課題の一つとして捉えられ、その推進は多数の共通理解であった。1989年に提出された1990年度概算要求では新センターは次の形で要求された。

名称　有機資源高度利用研究センター

変換プロセス研究部	教授	1	助教授	1	助手　1
変換触媒部	教授	1	助教授	1	
高度利用システム研究部	教授（客員）	1	助教授（客員）	1	

研究所自体の改組検討作業の変遷につれて、この研究センター構想も紆余曲折があり、名称、人員配置について何度か修正を余儀なくされたが、骨格は変えないで炭素資源反応研究センターとして設置されることになり、研究所の改組・転換と同時に1991年4月12日省令が公布され、新組織が発足した。

産業エネルギーを取り巻く社会情勢は年々急速に変化しているが、石炭利用方法の高度化、環境への適合化は社会の強い要請であり、石炭を中心とする炭素資源の変換研究が新しい研究所の中心的な研究課題であることは変わりない。

センターは反応制御研究部門の固体反応制御研究分野、界面反応制御研究分野などの所内研究陣はもちろん、工学部、素材研などの学内組織、他大学、国公立機関と連携して、炭素資源の新規かつ高度な利用研究を推進することとしている。

炭素資源反応研究センターの構成員

センター長（併）・教授	富田　彰	（固体反応制御研究分野・内線2758）
教授(兼)	松田　實	（分子配列制御研究分野・内線2873）
教授(兼)	西山　詔行	（界面反応制御研究分野・内線2879）

（変換プロセス研究部）

教授	飯野　雅	（内線2278）
助手	鷹觜　利公	（内線2533）
技術補佐員	石垣　美紀	（内線2533）

（変換触媒研究部）

助教授	大塚　康夫	（内線2524）
技術補佐員	庄子　あゆみ	（内線2833）

連絡先

〒980-77　反応化学研究所・炭素資源反応研究センター

電　　話：022-227-6200（代表）

ファックス：022-223-8956（研究所共通）

研究概要と活動状況

炭素資源反応研究センター・変換プロセス研究部

飯野　雅

1.　石炭の総合変換プロセスの構築

石炭を高効率、クリーンに変換する事を目的として、溶媒抽出、触媒分解、触媒ガス化を組み合わせた石炭の総合変換プロセスの構築に関する研究を、本センターの変換触媒研究部、本研究所の反応制御部門界面反応制御研究分野と共同で行っている。この総合変換プロセスのフローシートを図１に示す。石炭は不均質であり、化学的に異質な成分より構成されているが、このプロセスは石炭の各成分に適した変換反応を行い、トータルとしての利用効率を向上させることを目的としている。本研究部は溶媒抽出の部分を受け持ち、高性能選択的抽出溶媒の開発および抽出物の利用について研究をしている。褐炭に対して有効な溶媒の探索を行い、室温で高い抽出率を与える溶媒系を見出している。

2.　石炭の混合溶媒抽出

二硫化炭素を１成分とする混合溶媒、特に二硫化炭素－*N*－メチル－2－ピロリジノン（CS_2-NMP）混合溶媒が歴青炭の室温抽出で非常に高い抽出率（30-65％）を与える事を約10年前に見出して以来、この混合溶媒による抽出機構、得られた抽出物、残渣の化学構造と性状について研究してきた。最近の結果としてはこの混合溶媒にごく少量（10％程度）の電子受容体（テトラシアノエチレン（TCNE）など）を加えて抽出を行うと抽出率が更に増加することを見出した。この原因は電子受容体が

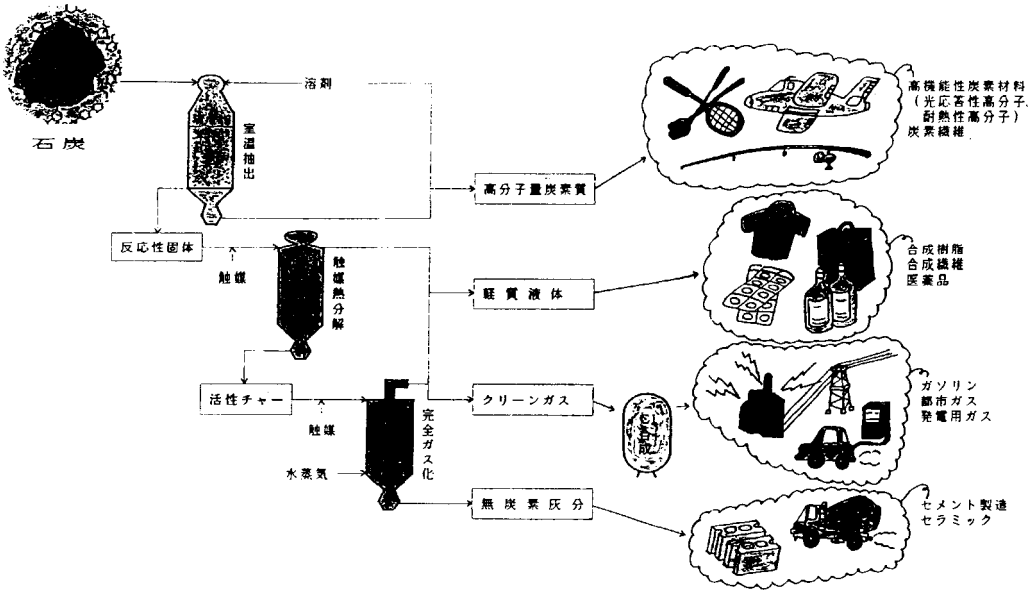

図１　石炭の総合変換プロセスのフローシート

石炭分子間会合を開裂させるためであることを明らかにした。又、混合溶媒抽出に対する石炭微細組織成分の挙動の相違についても明らかにした。

3. 石炭の化学構造

3.1 石炭分子間相互作用

石炭中には水素結合、π電子－π電子相互作用、電荷移動相互作用などの分子間相互作用が強く働き、分子会合体を形成していると考えられている。我々は石炭の溶媒抽出の溶解度に及ぼす添加剤の影響を調べた。その結果、石炭分子と上記の相互作用をそれぞれもつフェノール、アニリン、アントラセン、TCNE、TCNQなどの添加により抽出物の溶解度が増加し、その増加の程度から石炭分子間相互作用についての情報が得られることが分かった。

3.2 石炭の高次構造

石炭は共有結合で結び付けられている溶媒不溶の三次元架橋構造とその中にトラップされている比較的少量の溶媒可溶成分（抽出物）から成ると従来考えられてきた。しかし、混合溶媒抽出による60%以上の高い抽出率、石炭分子間相互作用による会合体の生成は上記の共有結合による架橋構造の存在に疑問を投げかけており、石炭の真の構造は比較的低分子量の溶媒可溶成分が上記の水素結合などの種々の分子間相互作用による巨大な会合体である可能性を強く示唆している。このような観点から、現在、石炭をカラム充填剤とするインバース液体クロマトグラフ、石炭、抽出物、残渣の溶媒膨潤と溶媒の拡散、抽出物から膜形成能、石炭－溶媒系の粘弾性、表面張力などの面から石炭高次構造の研究に着手している。

3.3 コンピュータシミュレーションによる石炭構造モデル

高次構造を含めた石炭の三次元構造モデルの計算機支援分子設計法（Computer-Aided Molecular Design, CAMD）による構築を目指して研究している。現在、第１段階として構造パラメータ、元素分析値、官能基分析からのデータから得られた石炭抽出物の構造モデルに対して分子力学法と分子動力学法を用いるCAMDによるコンピュータシミュレーションを行い、非共有結合による分子集合体（会合体）が安定に存在することを認めている。会合体の１例を図２に示す。

4. 石炭可溶化反応機構

温和な条件下で高効率で進行する石炭液化プロセスの設計を最終目標として石炭液化の初期過程である種々の溶媒中での熱可溶化反応機構を研究している。室温で

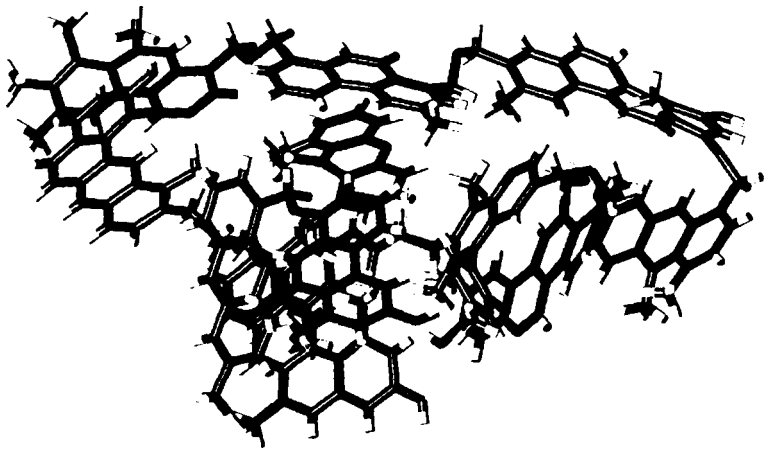

図２　分子構造シミュレーションによる石炭の分子集合体構造

高い抽出率を与えるCS2-NMP混合溶媒を可溶化反応後の抽出溶媒に用いる事により、より重質な溶媒可溶成分の挙動を知ることができた。通常の液化温度（400-550℃）よりはるかに低い温度（175-300℃）で石炭の可溶化反応が水素供与性溶媒中で起こり、一方、水素供与性の低い溶媒では逆に重質化反応が進行する事が見出された。この知見は石炭前処理を巧みに行うことにより、上記の最終目標を達成できる可能性を示している。

又、高炭化度の無煙炭のNMP溶媒中アルカリにより室温可溶化反応機構についても研究している。

5.　石炭の軟化溶融機構

高炉用コークスを広範囲の炭種を用いることのできる、環境適合、省エネルギー、高効率次世代コークス製造法の確立が製鉄における重要な課題となっている。本研究部ではコークス製造の最も重要な過程である石炭の軟化溶融機構を熱による化学構造の変化の観点からの研究に着手している。

以上が本研究部での研究機構であるが、これらの研究の遂行にあたり、文部省科研費による日米、日豪、日中国際共同研究を行っており、詳細は後述する。又、国際学会にも平成３年から現在まで、石炭国際会議２回（ニューキャスル（イギリス）、平成３年およびバンフ（カナダ）、平成５年）、日中シンポジウム（大阪、平成５年）、アメリカ化学会シンポジウム（シカゴ、平成５年）など数多く出席し、講演を行っている。

炭素資源反応研究センター・変換触媒研究部

大塚　康夫

1．石炭の事前窒素法の開発

石炭中の窒素は、燃焼時にはFuel NOxとなり酸性雨や光化学スモッグの原因となり、熱分解タール中の多環窒素化合物は、発ガン性や突然変異性を示すことが知られている。 通常の微粉炭燃焼では、NOx発生量の大部分がFuel窒素に由来するので、窒素を事前に除去することができれば、排煙処理工程の負担軽減やシステムの簡素化に結びつくと期待される。しかし、石炭中の窒素は化学的に安定であるため、その事前除去は至難というのがこれまでの常識であった。

ところが、鉄触媒を担持した褐炭を単に加熱すると、石炭窒素の50～60%が無害なN_2として除去できることを発見した。 図1はその例であり、触媒量は1%程度と少く、高価な水素が不要であるのも大きな特徴である。このように、鉄存在下では、N_2生成量が劇的に増加する一方、NH_3やHCNの発生量は減少し、チャーやタール中に残留する窒素量も著しく小さくなった。

ここでは、塩化鉄水溶液より褐炭上に沈殿担持した微細な水酸化鉄を用いており、水酸化鉄は、石炭熱分解時に還元されて20～50 nmの超微粒子となる。 脱窒素のメカニズムとしては、鉄微粒子上でのVolatile Nitrogenの二次分解と、 固相におけるChar Nitrogen（もしくはCoal Nitrogen）からの脱N_2反応が考えられる。

固相での脱窒素反応を検証するために、ポリアクリロニトリルより調製した炭素質に市販の金属鉄超微粒子を添加して熱処理したところ、 約600℃の低温からN_2が脱離することが明らかとなった。鉄微粒子は極めてMobileで反応性に富むため、炭素質に溶解して窒化鉄を生成するが、窒化鉄は熱的に不安定なため分解してN_2を放出する、というメカニズムが想定される。

このように、微細な鉄触媒は、石炭もしくはチャー中を移動しながら脱N_2反応を促進していると結論できる。

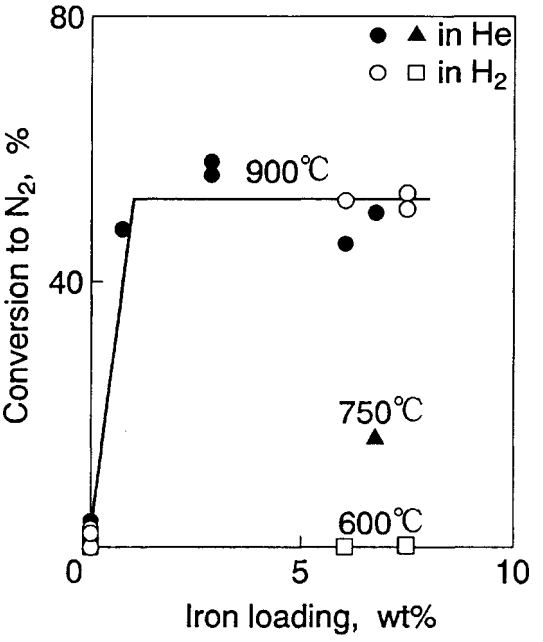

図1　鉄触媒による脱窒素

現在、炭化度の異なる多くの石炭に対して、本法の有効性を検討しており、さらに、X線光電子分光法（XPS）を用いて、石炭のN 1s XPSスペクトルの測定も行なっている。今後、Nitrogen Functionalityと脱窒素率の関係を確立することにより、新しい事前脱窒素プロセスの設計が可能になると思われる。

2　安価な触媒を用いる石炭の低温ガス化法の開発

石炭のガス化は現在、約1500℃の高温で操業する灰溶融型噴流床方式が主流であるが、環境調和性、総合熱効率、灰処理トラブル、ガス精製効率などを考慮すると、触媒を用いる低温ガス化は、次世代のガス化方式の一つとして期待される。

しかし、その実現には、安価で、かつ、高い活性を持つ触媒の開発が不可欠である。これまでの研究より明らかなことは、触媒の担持状態が活性を左右し、イオン交換のような原子状分散に近い場合ほど顕著な効果が得られるのである。従って、実用可能な触媒の開発には、安価な原料を用いて、活性成分のみをいかに高い分散状態で石炭上に担持するかが、キーポイントとなる。

（1）塩化鉄の利用

鉄はガス化触媒の有望な候補であり、原料としては、鋼板の酸洗過程で大量に排出される鉄酸廃液が有力である。 その主成分の$FeCl_3$を加水分解すると、単分散酸化鉄微粒子が得られるので、多量のイオン交換サイトを持つ褐炭への触媒担持法としてこの手法を応用した。 図２左に示すように、$Ca(OH)_2$を用いて調製した鉄触媒

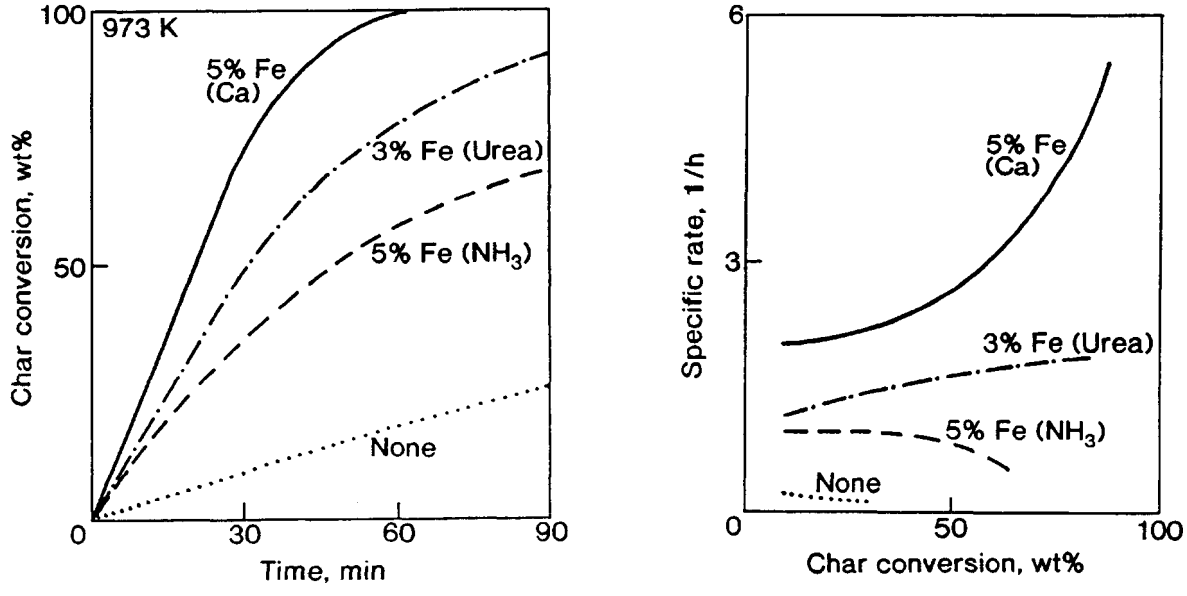

図２　塩化鉄より沈殿担持された鉄触媒による水蒸気ガス化

（5%Fe(Ca)）が、最も著しいH_2Oガス化促進効果を発揮し、 700℃、60分で完全ガス化を達成した。完全ガス化に要する時間は750℃では30分に短縮された。 鉄を用いてこのように高い低温活性を実現した例は、今回が初めてである。

この鉄触媒ガス化の特徴は、反応の進行とともにガス化速度が増大する（図２右）ことであり、従来観測されていた急激な速度低下とは全く対照的である。FTIRやメスバウアーなどの測定結果より、担持段階では、Feイオンは石炭中のCOOH基と強い相互作用を持ち、 5 nm以下のFeOOH超微粒子（またはクラスター）が生成し、この高い分散性がガス化速度の増大に寄与していることが明らかとなった。しかし、詳細なメカニズムの解明は今度の課題である。

（２）炭酸カルシウムの利用

カルシウムも鉄と同様に有力なガス化触媒候補である。これまでは主に、石灰水（$Ca(OH)_2$）を用いてH_2Oガス化や炉内ガス精製を行なってきたが、 $Ca(OH)_2$は石灰石（$Ca(CO)_3$）を焼成して得られるCaOより製造されるので、石灰石そのものを触媒原料とするほうが実際的である。

図３は、褐炭を$CaCO_3$と常温水中で混合した後のFTIRスペクトルを示す。 原炭にはCOOH基に由来する鋭い吸収が観測されたが、 混合試料（Impregnated）では吸収ピークは消失した。これは、予想外なことだが、次式で表わされるイオン交換反応が起こるためであり、イオン交換量に相当するCO_2の発生が確認された。

$$CaCO_3 + 2(\text{-COOH}) = (\text{-COO})_2Ca + H_2O + CO_2$$

$CaCO_3$は水に難溶であるが、褐炭を水に分散させると弱酸性となるので、$CaCO_3$の溶解度は高くなり、 かつ、CO_2が発生するので、上記の反応は室温でも速やかに進行する。

イオン交換Caの生成から予測されるように、$CaCO_3$担持炭のH_2Oガス化反応性は非常に大きく、 700℃での速度は原炭の70倍に上り、ガス化は30分という短時間で終了した。石灰石の主成分のCalcite型$CaCO_3$に比べて、貝殻中に存在するAragonite型$CaCO_3$を用いると、ガス化速度は原炭の100倍にも達した。

以上のように、安価な原料を高活性なガス化触媒に転換することに成功した。今後は、これらの脱窒素・脱硫機能を生かして、炉内での同時ガス精製を組み合わせた触媒ガス化方式に展開することが重要と思われる。

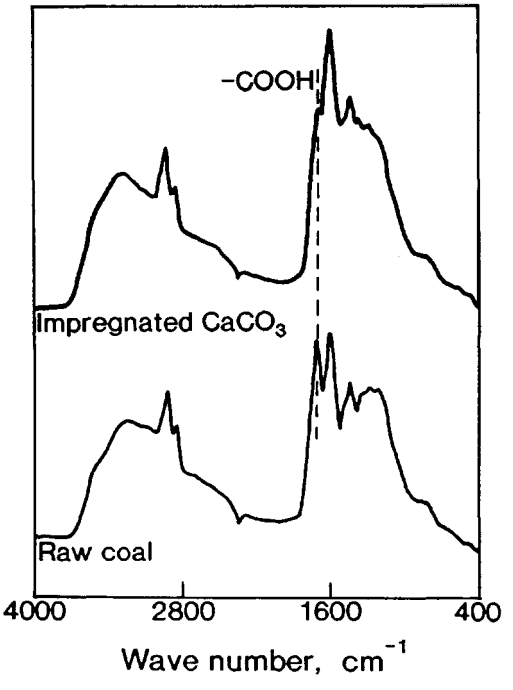

図３　$CaCO_3$担持炭のIRスペクトル

3．メタンと二酸化炭素の反応によるC_2炭化水素の合成

天然ガスの新しい直接変換法として、 CH_4の酸化カップリングによるC_2H_6やC_2H_4の合成法が注目されており、触媒の開発が活発に行なわれている。しかし、現段階では触媒性能が充分でないため、カップリング反応が実用化可能な速度で進行する条件下では、均一気相反応が併発して起こり、C_2収率の低下が避けられない。

そこで、O_2の代わりにCO_2を酸化剤として用い、 副反応を伴わずにC_2炭化水素を製造することに着目した。反応は次式で表わされ、注目する温度域（800～900℃）でのCH_4の平衡転化率は15～35%になる。

$$2CH_4 + CO_2 = C_2H_6 + CO + H_2O$$

$$2CH_4 + 2CO_2 = C_2H_4 + 2CO + 2H_2O$$

しかし、このような研究は世界的にも始まったばかりであり、触媒の有効性に関する基礎的理解は極めて乏しい。1991年度から石油産業活性化センター・石油学会の委託を受けて、無担持の金属酸化物固有の活性や選択性を系統的に調べている。図4に示すように、多くの酸化物が上記の反応を促進するが、なかでも、ランタノイド酸化物が比較的高いC_2選択性を示した。現在、反応機構の解明と触媒性能の向上を進めている。

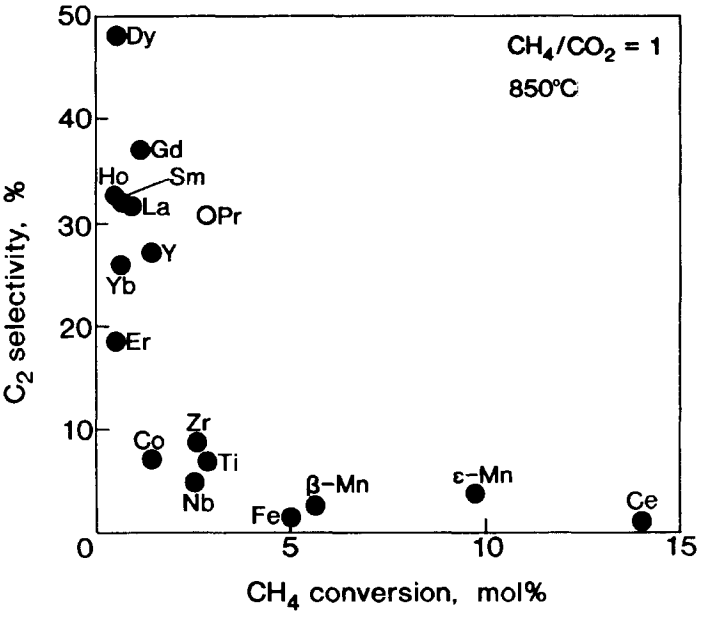

図4　酸化物触媒上のでCH₄転化率とC₂選択率

上記の研究以外に、高分子金属錯体を炭素化して高分散金属超微粒子を合成し、その触媒機能を調べており、また、鉄鋼協会特基研究会「コークス製造のための乾留制御部会」（1991.4～1993.3）の一環として、急速加熱した石炭の軟化溶融性を研究してきた。おもな対外的な活動として、朝見賢二助手と筆者が、文部省科研費「日本－カナダ共同学術研究」（代表者：京都大学工学部橋本健治教授）の分担者として、それぞれ1992、1993年度にCANMETで共同研究を実施した。なお、当研究部の前身（石炭化学実験施設）からの共同研究者であった朝見助手は、 1994年4月大阪市立大学工学部講師に昇任した。氏の一層の活躍を期待したい。

外国人研究者訪問リスト

王　栄，王　建華，韓　怡卓，郭　樹珍，張　碧江，周　敬来，崔　永又
中国科学院煤制合成汽油技考査団（中国）（1991.4.5）

K. J. Mccullough
Heriot-Watt University（イギリス）（1991.4.13～4.14）

江　英彦
中国科学院化学研究所（中国）（1991.6.28）

Earl Whiteney
The University of Utah（アメリカ）（1991.7.8）

Ben de hange, Wolter Tager
Groningen State University（オランダ）（1991.10.19）

F.P. Miknis
Western Research Institute（アメリカ）（1991.11.13）

Peter Silveston
University of Waterloo（カナダ）（1992.1.10）

Edward Karakhanov
Moscow State University（ロシア）（1992.6.24）

David L. Morgan
CSIR（南アフリカ）（1992.9.3～9.6）

Jonathan Clark
Elsevier Science Publishers B.V.（オランダ）（1992.10.24）

John W. Larsen
Lehigh University（アメリカ）（1991.11.17）

L.R. Radovic
Pennsylvania State University（アメリカ）（1992.11.17）

程　懋圩，李　保庆
中国科学院山西煤炭化学研究所（中国）（1993.3.1～3.4）

Yongseung Yun
Institute for Advanced Engineering（韓国）（1993.3.10）

Allan Chambers, John Chen
（株）日立製作所 日立研究所（1993.4.12）

朱 起明, 潘 衛
清華大学（中国）（1993.5.18～5.21）

Ed Furimsky
CANMET（カナダ）（1993.6.3）

A.P. Watkinson
The University of British Columbia（カナダ）（1993.6.3）

E.M. Suuberg
Brown University（アメリカ）（1993.6.1～6.3）

胡 浩权, 郭 樹才, 杜 宝昇, 沙 興中
胡 浩权 ; 大連理工大学（中国）
郭 樹才 ; 大連理工大学（中国）
杜 宝昇 ; 東北内蒙古石炭公社・多種経営公社（中国）
沙 興中 ; 華東化工学院（中国）（1993.6.4～6.6）

D.E. Mainwaring
Swinburne University of Technology（オーストラリア）（1993.6.4～6.5）

Woong Moo Lee
Ajou University（韓国）（1993.6.23）

Stephanie Rothenberg
Lehigh University（アメリカ）（1993.7.1～7.6）

Peter Guy
Coal Corporation of Victoria（オーストラリア）（1993.8.29～11.18）

H.H. Schobert
Pennsylvania State University（アメリカ）（1993.10.8）

Ronald R. Martin
The University of Western Ontario（カナダ）（1993.11.1）

張 秋民
大連理工大学（中国）（1993.10.21～11.9）

張 済宇, 趙 連仲
中国科学院山西煤炭化学研究所（中国）（1993.11.1）

2. 炭素質のガス化反応の基礎的研究

昇温脱離法、過渡応答法、X線吸収微細構造、二次イオン質量分析、拡散反射FTIR、X線光電子分光などの表面分析手法を駆使し、石炭などの炭素質のガス化反応ガス化反応における触媒の働き、あるいは炭素表面含酸素化合物の役割を分子レベルで理解する試みを行っている。ガス化した炭素上の含酸素表面化合物の形態を実際にFTIRで捕まえ、それらがガス化反応中にどのようなダイナミック挙動をするかを明らかにすることが目的である。反応ガスに同位体ガスを用いることにより、表面化合物の役割を詳細に観察することができる。また、酸性雨あるいはオゾン層破壊などの原因となる窒素酸化物の除去のため、炭素とNOの反応の基礎研究を行っている。反応中に酸素原子だけでなく、窒素原子も炭素中に取り込まれ、その後反応の進行とともに窒素分子として脱離するるといった興味ある新事実を見いだした。含窒素化合物はXPSで調べるとピリジンおよびピロール型で、不活性雰囲気下ではかなり安定なものであるが、反応条件下では容易に脱離できる。これは表面の化合物のガス化時のダイナミックスを考える上で大きな示唆を与える。これらの一連の研究は、東北大学と姉妹校であるペンシルベニア州立大学のRadovic博士らと共同で進めたが（1991.4～1994.3）、学生への刺激なども含め、色々な意味で非常に有意義な成果を挙げることができた。

3. 新しい炭素材料の創製

新しい炭素材料創製のため、分子オーダーでその構造を制御しうる材料作成法の開発研究を科学技術振興調整費（1990.4～1995.3）により行っている。すなわち、構造のはっきりとした無機物質を鋳型とし、その孔隙内に導入した有機物を熱処理することにより炭素材料を合成すると、鋳型として用いたテンプレートの特性を反映した特色ある新炭素材料を設計することができる。たとえば、粘土化合物の層間という2次元空間を炭素化の場として利用することで、高結晶性の薄片状炭素が合成できる。予め成膜した層状粘土化合物を用いてその層間で有機物を炭素化すると、結晶性・配向性に優れていながら、しかも可撓性を合わせ持つという特異な新炭素材料の合成が可能となる。電磁シールド材、電極材、電池セパレータなどへの応用が期待される。また、多孔性のゼオライトを鋳型としてその細孔内で有機物を熱処理すると、大きな表面積をもつだけでなく、細孔の大きさが従来の活性炭より大きく、加熱しても表面積が減少しないという、新しいタイプの炭素を合成することに成功した。特殊吸着剤としての応用が期待される。

界面反応制御研究分野

西山 誼行

1． 石炭の接触ガス化に関する研究

当研究室では1978年以来、石炭のガス化に対して触媒を利用する研究を進めて来た。触媒の使用はガス化反応の温度を大幅に低下させ操業の容易なプロセスを構成する可能性がある一方、触媒自体のコストや添加、使用後の処理といった問題を生じるから、少量で高度に活性な物質・使用法でなければ実用的な意味がない。

炭素資源反応研究センターや固体反応制御研究分野でも触媒ガス化研究が展開されていることを考慮して、当研究室での研究では触媒の活性を支配する因子を解明し、効率的な触媒使用方式を探索することを主目的として来た。その結果、鉄系触媒に対してはアルカリ土類塩の添加が有効であること、炭素系基質の表面状態を制御することにより触媒の活性が大きく変わり、少量の触媒、短時間で高い転化率が得られることを明らかにしている。

1991-1993年度では、これらの触媒活性発現因子を整理すると共に、触媒ガス化の一つの展開として石炭類を溶媒抽出した残りを熱分解してその残渣を水蒸気ガス化することにより、有用成分を高度に活用するプロセスの構築を試みた。これは炭素資源反応研究センターとの共同研究であり、溶媒抽出、熱分解、水蒸気ガス化を組み合わせることにより、石炭中の炭素質が有効に利用できる可能性が示された。

2．褐炭のイオン交換能と表面状態

褐炭はその表面に多くの含酸素官能基を有しており、それらは種々の金属カチオンとイオン交換することが知られている。当研究室では褐炭の高度利用技術開発の基礎として、褐炭の表面状態がイオン交換能に及ぼす影響、そして交換イオンが熱分解、ガス化、液化などの褐炭転化反応に及ぼす影響を検討している。

表面修飾とイオン交換能　褐炭試料としては、オーストラリア褐炭のLoy Yangを用い、不活性雰囲気下での低温熱処理(LTH)、水熱処理(LTW)、硝酸酸化およびスルホン化を施し、ナトリウム、カルシウム、ニッケル、および亜鉛で交換した。

LTH炭では処理温度(HTT)とともに表面官能基の減少が見られ、イオン交換量(ECE)が減少した。しかし赤外分光法やナトリウム滴定法から求めた表面官能基の減少量に比べてECEの減少率は大きく、LTHはイオン交換性官能基量を減らすというより「イオン交換に関与しない官能基」に変えると考えられる。イオン交換時のpHを1～12の間で変化させるとpHの上昇に伴いECEは上昇する。顕微鏡下での直接観察によると高pHにおいて石炭粒子の凝集構造が緩和することが観測された。また、LTW炭は水に対する濡れ性の向上が見られ、同じ温度でのLTH炭と比較するとECEは５倍以上の高い値を示した。以上の事実より、「イオン交換に関与しない官能基」は褐炭粒子

に内包された状態であると考えられる。

イオン交換時のエタノール添加効果　褐炭は極性溶媒に対して体積膨潤を示す。そこでイオン交換時にエタノールを添加しイオン交換能を調べた。約30%迄の添加でECEは３倍程度までに増加し、それ以上のエタノール分率では飽和する傾向が見られた。また、水溶液系ではECEが殆どゼロであるLTH(HTT>250℃)炭も、エタノールを加えることによりECEの増加が見られた。この方法はイオン種を石炭粒子の内部にまで導入するのに有効な方法で、熱分解や液化などの転化反応の前処理として有望と考えられる。

３．　カチオン交換褐炭の炭素化

鉄イオン交換褐炭　褐炭の表面官能基の修飾により新しい機能性炭素材料、例えばガスセンサー、触媒電極、触媒など、を得ることを目的として、イオン交換をベースとした褐炭の利用を試みた。我々はこれまで、鉄共存下での炭素化により炭素化物の電気物性を制御できることを見出している。本研究ではイオン交換法により導入した鉄が高分散であることに注目し、炭素化褐炭の物性を主に炭素化度と電気伝導度について検討した。

400℃炭素化物で鉄交換炭(4-LY)の電気伝導度は10^{-11} S/cmで、無添加炭(A-LY)のそれ(10^{-13} S/cm)に比べて100倍大きいが、炭素化温度とともにその比は小さくなる傾向を示した。鉄導入による電気伝導度の増大は、炭素化が鉄により促進されているためであることがわかった。FTIRより鉄は200～400℃においてカルボキシル基の分解を促進すること、SEMより未炭素化試料に特徴的な網目状構造から粒子状構造への変化がA-LYでは425℃、4-LYでは300℃付近から見られること、がわかった。網目状構造は褐炭の官能基間の水素結合による高次構造に特徴的なものである。

以上より、鉄は褐炭中の水素結合を破壊してイオン交換し、官能基の分解を起こりやすい状況にする、そして鉄の触媒作用で芳香環同士の合体などが容易に起こるようになり炭素化が促進されるもの、と考えられる。

アルカリ・アルカリ土類交換炭　カチオンの存在が上記の電気物性のほかに生成炭素の物性に影響するかを、表面積の観点から検討した。900℃で生成した炭素質の窒素BET表面積はニッケル交換炭では交換量によらず一定で未交換炭と同じであるが、カルシウムとナトリウムでは交換量とともに減少する。特にナトリウムでは約2～3%で1 m^2/g以下になることが特徴的である。またSEM観察によるとニッケル交換炭では表面形状が粗であるのに対し、ナトリウム交換炭では滑らかであることが示された。これは熱分解の過程が共存イオンによって異なることを示唆するものと考えている。

研究設備リスト

ハンマークラッシャー
ロータップ篩振とう器
卓上縮分器
元素（C, H, N）分析装置
全硫黄分析装置
微量窒素分析装置
高温炉（2800, 1800, 1500℃）
熱天秤ガス化装置（赤外線イメージ炉）
流動層熱分解装置（ゴールド炉）
加圧キュリーポイントパイロライザ
ガスクロマトグラフ（TCD, FID, FTD検出器）
高速ガスクロマトグラフ（TCD検出器）
赤外ガス分析計（CO, CO_2, CH_4）
微量酸素センサー
ＮＯxメータ
冷却式高速遠心分離機
石炭反射率測定顕微鏡
自動表面積測定装置
原子吸光分析装置
赤外分光光度計（拡散反射・顕微FTIR付属）
昇温Ｘ線回折装置
四重極質量分析計
走査型電子顕微鏡（EDAX付属）
透過型電子顕微鏡
走査トンネル顕微鏡
Ｘ線光電子分光装置
二次イオン質量分析装置

関連活動報告

日本－オーストラリア共同研究
ビクトリア褐炭の構造，反応性と新しい利用技術

西山　誼行

1．　研究目的

オーストラリア国ビクトリア州のラトローブ地方を中心とする褐炭は総埋蔵量2000億トンの膨大な化石資源であるが、現在ではその一部が発電やブリケットに使用されているにすぎない。これは主としてこの褐炭が50～67%の水分を含むので遠隔地での活用が困難なためである。しかしこの褐炭は炭化度が低いことから化学燃料として有用な成分を多量に含有しており、かつ、灰分や硫黄分が極めて少ないため、クリーンな燃料源としても高い潜在価値を持っており、この化学資源の人類社会での活用のため早急に方策を講じる必要がある。そのためにはまずこの褐炭の化学的特性、特に水分との相互作用や鉱物質の状態、有機質の化学反応性を明確にし、その知見にもとづく合理的な利用法式を樹立する必要がある。本研究ではビクトリア褐炭の化学特性を明確にし、新しい活用法を提出することを目的とする。

2．　研究組織

[研究代表者]

西山 誼行	東北大学・反応化学研究所・教授	総括,褐炭の表面特性、熱分解特性

[研究分担者]

真田 雄三	北海道大学・工学部・教授	褐炭構造解析
持田　勲	九州大学・機能物質科学研究所・教授	褐炭液化触媒の開発、褐炭の反応性解析
飯野　雅	東北大学・反応化学研究所・教授	褐炭と溶媒との相互作用、ゲル構造解析
D. J. Allardice	Victoria州石炭公社・開発研究部長（現理事長）	オーストラリア側代表 褐炭と水との相互作用
W. R. Jackson	Monash大学・化学科・教授	褐炭の構造と反応性、液化触媒開発
F. E. Larkins	Melbourne大学・教授・副学長代理	褐炭変換触媒の構造解析
D. E. Mainwaring	Swinburne工業大学・教授	褐炭表面解析、溶媒との相互作用

[研究協力者]

坂西 欣也	九州大学・機能物質科学研究所・助手	褐炭液化触媒の開発

尾崎 純一	東北大学・反応化学研究所・助手	褐炭の熱分解と生成物の特性
鷹觜 利公	東北大学・反応化学研究所・助手	褐炭と溶媒との相互作用、構造解析
P. J. Guy	Victoria州石炭公社・研究員	褐炭と水との相互作用

3. 学術交流

国際学術研究では国内と国外との研究者交流が重要な柱となっている。本共同研究においてもビクトリア褐炭を直接の対象としての研究経費は主として各研究機関の負担によることとし研究者の交流による討議および外国研究機関での実地の実験研究に主眼をおいた。本共同研究経費により派遣、招へいされた研究者は次の通り。

	氏 名	職	期 間
[派遣]	持 田 勲	九州大機能研 教授	1992.11.28より8日間
	真田 雄三	北海道大工学部 教授	1993.10.30より8日間
	飯野 雅	東北大反応研 教授	1993.10.30より10日間
	坂 西 欣 也	九州大機能研 助手	1992.11.3より57日間
	鷹 觜 利 公	東北大反応研 助手	1992.11.25より66日間
	尾 崎 純 一	東北大反応研 助手	1993.1.10より65日間
[招へい]	D.E.Mainwaring	Swinburne工業大学 教授	1993.5.23より14日間
	P.J.Guy	ビクトリア州石炭公社研究員	1993.9.26より54日間

4. 研究成果の概要

本共同研究ではビクトリア褐炭の化学的特性を明らかにして，新しい利用技術を開発することを眼目とし，構造，反応性などの基礎的諸性質，水分や溶媒との相互作用など多角的に研究を進めた。

持田，坂西，Jacksonらは褐炭の硫酸処理と引く続くイオン交換法で鉄やスズを担持して高分散液化触媒を調製する方法を開発した。また，褐炭の脱鉱物処理及び乾燥前後の性状・構造変化を調べ，褐炭のCO/H_2O条件下において高活性を発揮する触媒($NaAlO_2$)は安価であり，350℃前後においてCO/H_2O条件下で効果的にWater-Shift反応を進行させ，褐炭の解重合に対して高活性を示すことを確認した。

一方真田，Jacksonらは電荷移動錯体をモデルとする石炭の構造と反応性の研究を展開した。その結果，^{1}H-NMR固体法で得られるスピン－格子緩和時間のヨウ素添加効果が提供された試料の間で著しく異なったが，これはアスファルテンの反応性の相違と対応づけられる。この点を明確にするために試料のヘキサン抽出試験とヘキサン可溶分中の芳香族環構造の分布を高速液体クロマトグラフィにて検討した結果，

両者にはヘキサン抽出量に相違のないことを明かにした。さらにAllardice博士とも共同して褐炭の脱水過程のシミュレーションを試み，脱水，水の再吸着プロセスは室温においても可逆的に行い得ないこと，通常の熱的乾燥法による脱水は褐炭の構造を大きく変え，反応性に影響を及ぼすことが判明した。これらの基礎研究は工業プロセス化が検討されている水熱乾燥法(Hydrothermal Dewatering Process)の設計に対して基礎的知見となることが期待される。

飯野，鷹觜，Mainwaring教授らは亜瀝青炭のCollie炭（西オーストラリア），褐炭のLeigh Creek炭（南オーストラリア）と， Loy Yang 炭（ビクトリア）の種々の溶媒における溶媒抽出率，溶媒膨潤値を測定した。 また Loy Yang 炭とN-メチル-2-ピロリジノン(NMP)のサスペンジョンを作製し，レオメータを用いて粘弾性の測定を行った。その結果水の場合にLoy Yang炭の膨潤値が他の石炭に比べて小さく，Loy Yang炭が構造内に多くの水分を有しているためであると考えられること，膨潤値の比較ではピリジン，NMPを用いた時にCollie炭，Loy Yang 炭で２以上の高い膨潤値を与えることが分かった。以上の結果から，Loy Yang褐炭は他のオーストラリア亜瀝青炭に比べて多くの溶媒可溶成分を有し，また極性溶媒と相互作用する極性置換基を多く含む構造からなるものと考えた。

西山，尾崎，Perry，Allardice博士らは褐炭上のカルボキシル基にイオン交換法により導入した鉄が高分散であることに着目し，このような鉄により褐炭の低温炭素化はどの様に修飾されるか，そして微分散鉄の担体として鉄交換褐炭をPVDCの炭素化に用いた場合，炭素化物の物性はどう変化するかを，主に炭素化度と電気伝導度の観点から検討した。その結果，鉄は表面官能基の分解を促進することにより，電気伝導度にして最大約２桁に相当する炭素化の進行を促すことを見出した。今後，褐炭上の表面官能基を用いた炭素化の制御による新規な材料の開発が期待される。

招へい者Mainwaring教授は褐炭のコロイド性，ゲルの電解質特性，粘弾性など我国研究者の中では不十分であった視点からの有益な知見を提供し，褐炭の特性の理解に大きな貢献をなした。またもう一人の招へい者Guy氏は東北大学グループと共同で褐炭ブリケットの性状に対する溶媒効果を解明し，メチル化による疎水化がブリケットの安定化につながることを明らかにし，水との相互作用の定量的な解析に示差熱分析法が有用であることなどの知見を得，今後の展開の大きな足がかりが得られた。

以上のように本共同研究の結果として，褐炭の構造，巨視的物性に結びつく水や溶媒との相互作用が解明され，今後の高度利用に結びつく十分な成果が得られたものと考えている。

日米国際共同研究（平成４年度～５年度）報告

飯野　雅・鷹觜利公

1. 研究の経緯

この共同研究の経緯は、真田雄三教授（北大工）の米国のゴードン研究会議での招待講演が契機となり、石炭構造についての日米の研究者の交流が始まり、幸いに平成元年度～２年度の文部省の科学研究費国際学術研究に採択され（代表・真田雄三教授）、共同研究が行われ、多大な成果が挙げられた。

日本側の研究者はこの共同研究を引き続き行い、石炭構造をさらに明らかにすることが必要であると考えていたが、米国側も平成５年１月、飯野雅教授（本センター変換プロセス研究部）との協議および前代表者である真田雄三教授宛の書簡で引き続き共同研究を行うことを強く希望した。

そこで、日米双方の研究代表者、分担者が前回の共同研究の成果をもとにして協議した結果、石炭構造の中で新しい石炭変換プロセスの開発に直結している石炭の架橋構造に的を絞って共同研究を行うことが緊急の課題であるとの合意に達し、改めて申請を行ったところ、平成４年度～５年度の国際学術研究に採択され（代表・飯野雅教授）、「石炭の架橋構造の解明と新しい石炭変換プロセスの設計」という研究課題名で本共同研究が行われた。

2. 研究の組織

平成４年度～５年度の本研究の研究組織は次の通りである。

飯野　雅	東北大学・反応化学研究所・教授	総括：石炭の溶媒抽出
真田雄三	北海道大学・工学部・教授	石炭と試薬との相互作用
野村正勝	大阪大学工学部・教授	石炭構造のモデリング
相田哲夫	近畿大学・九州工学部・教授	石炭の膨潤速度
中村和夫	大阪ガス（株）・基盤研究所・課長	石炭変換プロセス
J. W. Larsen	リハイ大学・化学科・教授	石炭の高分子物性
E. M. Suuberg	ブラウン大学・工学科・教授	石炭中への物質の拡散速度

3. 米国側研究者のプロフィール

米国側の共同研究者であるLarsen教授は石炭化学の世界的リーダーであり、現在アメリカ化学会の「Energy & Fuels」誌の編集長である。Larsen教授の研究業績は枚挙にいとまがないが、本研究でテーマに挙げた石炭の架橋構造に関する研究では、第一に1985年にアメリカ化学会誌に発表した論文が挙げられる。これは架橋構造形

成に非共有結合性の相互作用が重要な寄与をしていることを見いだしたもので、従来の石炭の架橋構造の概念をくつがえす大きなインパクトを全世界の石炭研究者に与え、その後のこの分野のめざましい展開の端緒となった研究である。Larsen教授のこの仕事はアメリカ化学会で大きく認められ、アメリカ化学会賞を受賞している。その後Larsen教授は石炭の高分子物性から架橋構造解明へのアプローチ、石炭構造の異方性の発見、石炭生成過程と架橋構造との関連、石炭孔隙構造、石炭液化機構などの多くの面で顕著な成果を挙げている。これらの研究の一部は前回の国際共同研究で行われたものである。

Suuberg教授は現在40才の若さであるが、既に多くの研究業績を挙げている新進気鋭の研究者で、1987年、1989年、1990年に米国で開催された燃料および燃焼に関する学会、シンポジウムの企画委員長、組織委員長を務め、また現在アメリカ化学会燃料部会の会長の要職についている。Suuberg教授は、石炭構造、燃焼機構、燃料からの公害物質の除去などの幅広い研究を行っているが、架橋構造については主として石炭中への試薬の拡散と種々の溶媒による石炭の膨潤の点から研究を行っている。前者については拡散の速度を正確に測定する装置を考案し、得られたデータを理論的に考察し、拡散機構を明らかにして理論的解釈を試み、従来から用いられているフローリー・レーナー式では架橋密度を正しく評価できないことを明らかにし、それに代わる手法を提案した。Suuberg教授はこの研究で1990年、英国で行われた「石炭の構造と反応性に関するシンポジウム」に招待され特別講演を行っている。

4. 研究の目的

埋蔵量が多く、世界に広く分布している石炭の新しい高効率変換プロセスを確立し、石油に代わる燃料、化学原料を安定に供給することは、来世紀に向けての最も重要な課題の一つであることは言うまでもない。また、石炭利用プロセスの高効率化は現在、大きな環境問題となっている炭酸ガス濃度増加に対する当面の現実的に可能な解決策の一つである。本研究は、新たな展開を見せている石炭の架橋構造（石炭の三次元構造）の分子レベルでの解明と新しい高効率石炭変換プロセスの設計を目的とした。すなわち、架橋構造を形成している化学結合の種類およびその寄与の程度を明らかにし、さらに得られた知見をもとに架橋構造と密接に関連している石炭液化と熱分解の新しい高効率変換プロセスの設計を行うことを目的とした。

5. 研究の意義

最近の石炭の溶媒抽出、溶媒膨潤および石炭と試薬の相互作用の研究は、石炭の架橋構造についての従来の定説をくつがえすものであった。すなわち、石炭は従来、強固な共有結合で結び付けられた架橋構造を形成していると考えられていたが、本

共同研究の研究成果から、もっと弱い結合である水素結合、電荷移動相互作用などの非共有結合が重要な寄与をしていることを示した。しかしながら炭種による非共有結合の寄与の程度は異なり、詳細については不明のままであり、本研究を進めていく中で、この点が重要なテーマの一つになった。

石炭架橋構造の解明は上記のような石炭化学の根本に関わる問題であると同時に、石炭利用技術の面においても新しい画期的な高効率変換プロセスの開発につながる可能性が大きい緊急を要する重要課題である。この点は本共同研究の全メンバーの一致する認識であり、本研究とは別にこうした石炭構造に関する研究者が日本・アメリカを代表として徐々に増加する傾向がある。

6. 研究内容の概要

平成４年度は日本側から飯野雅教授（研究代表者）、熊谷治夫助手（研究協力者、北大）、村田聡助手（研究協力者、阪大）、米国側からLarsen教授（米国側研究代表者）、Yun博士（研究協力者、ブラウン大学）が、それぞれ派遣または招聘された。飯野教授、Larsen教授は共同研究の打ち合わせ、研究分担者との意見交換、石炭関連研究施設の見学および石炭構造に関する講演を行った。熊谷氏はSuuberg教授の研究室にて褐炭分子と水との相互作用に関する研究を行った。村田氏はLarsen教授の研究室にて石炭構造モデルのコンピュータによる構築、Yun氏は飯野教授の研究室にて石炭抽出物、抽出残渣の加熱による架橋構造変化に関する研究を行った。

平成５年度は日本側から相田哲夫教授、真田雄三教授、鷹觜利公助手（研究協力者、東北大）、米国側からSuuberg教授、Rothenberg氏（研究協力者、リハイ大学）がそれぞれ派遣、招聘された。相田教授は石炭膨潤、石炭分子間相互作用に関する意見交換を行い、真田教授は褐炭における石炭分子と水との相互作用、瀝青炭における石炭分子とテトラシアノキノジメタン（TCNQ）などの電子受容体との電荷移動相互作用に関する意見交換（共著の論文を発表予定）を行った。Suuberg教授は阪大、近畿大、東北大、北大などを訪問し、石炭架橋構造、石炭分子間相互作用についての討論と講演を行った。鷹觜氏はSuuberg教授の研究室にて前年度のYun氏の東北大における研究の継続としての溶媒抽出物、抽出残渣、原炭の加熱過程における構造緩和、リハイ大学のLarsen教授の研究室にて石炭分子と電子受容体との電荷移動相互作用、BCR国立研究所（ピッツバーグ）にて溶媒抽出物、抽出残渣の溶媒膨潤に関する研究を行った。Rothenberg氏は東北大にて溶媒抽出物を用いた石炭分子－電子受容体との電荷移動相互作用、北大にて石炭と電子受容体との錯体の電荷伝導度に関する研究を行った。

以上２年間に渡り日米合わせて１０名の研究者の交流があり、国のレベルを越えた研究者相互の緊密な議論と共同研究が実現された。

7. 研究成果の要約

石炭架橋構造に関する研究は日本および米国で最近活発に行われている分野の一つであり、これまでは本共同研究の研究グループごとに行われてきた。一方でこの研究の最終目的である新しい石炭変換プロセスの設計の実現のためには、早急に前記の基礎研究を進める必要があり、日米双方のこの分野の専門家が共同研究することは重要な意味を有するものであった。特に前述のように近年石炭の化学構造について、石炭が実際は共有結合よりはるかに弱い結合である水素結合、電荷移動相互作用などの非共有結合によりなる巨大な会合体である可能性が示唆されている。これは石炭化学の根本に関わる問題であると同時に、石炭利用技術の面においてもこの新しい構造概念をプロセス設計の指針とすることにより、画期的な無公害、高効率石炭利用プロセスの開発に結び付く重要な知見である。

本研究では複雑な石炭の架橋構造を分子レベルで評価するために、石炭と電子受容体あるいは水との相互作用に関する研究、石炭の高分子物性研究、加熱過程における石炭構造変化に関する研究、石炭の溶媒膨潤の動力学的研究、コンピュータを用いた石炭分子構造のシミュレーションなどの研究を行い、石炭架橋構造に関する多くの新たな知見が得られた。。その結果前述の非共有結合による架橋構造という構造概念は２年間の共同研究でますます確実なものになり、さらに討論を通じて新しいプロセスの設計についても斬新な構想がいくつか提出された。研究成果の詳細は平成６年３月に発行の本研究の成果報告書に記載されている。

またこの共同研究では研究成果の他に、日米両国の石炭研究者、技術者間の研究の交流が有り、特に今後さらに深刻化すると思われるエネルギー問題、環境問題に対処するために、研究協力者として日米双方の若手の研究者が数ヶ月間相手国で共に研究をし、互いに自由に意見を交換して双方の研究手法や文化の違いなどを認識する機会を得たことは非常に意義のあることであった。本研究のような文部省の国際学術研究は学術研究の国際化、国際レベルでの研究討論、日本の国際的な貢献、若手研究者の育成など大きな意味を持つ共同研究である。

この分野の研究者は世界各国において着実に増加する傾向にあり、今後のエネルギー源の担い手である石炭の画期的な無公害高効率利用プロセスの開発を最終ターゲットとしてこの共同研究をさらに発展させ、新たな石炭変換プロセスの設計・開発まで実現させたいと考えている。

最後に２年間の日米国際共同研究の実施にあたり、ご支援、ご援助いただいた文部省に深く感謝いたします。

日中国際共同研究（平成４年度～５年度）報告

飯野　雅・鷹觜利公

1. 研究の経緯

この共同研究の経緯は、昭和60年9月と昭和62年5月に野村正勝教授（阪大工）が中国を訪問し、中国政府は石炭を基幹エネルギーとして重工業を発展させており、石炭の有効利用を強力に推進していることを認識した。その後昭和63年5月に来日した中国石炭化学界の第一人者である郭樹才教授（本研究の中国側代表者）と野村教授が討議して詳細を取り決め、平成元年度から２年度まで国際学術共同研究「中国炭の有効利用に関する新統合プロセスの開発研究」を実施した。この研究では平成元年度は１０名の日本側研究者が中国において共同実験研究を実施し、平成２年度には中国側研究者７名を招聘し、一層濃密な共同研究を実施した。この共同研究を通じて、日本側の高い研究レベルや情報力と中国側の石炭利用に対する経験とが融合した結果、研究課題に対し多くの発見がなされ、大きな成果が挙げられた。しかしながら一方でその時点ではこれらの発見を実用化するには解決すべき点が未だ多く残されていた。石炭の有効利用研究の成否は、今後の中国に於ける重化学工業の発展の根幹に関わるため、中国側の日本に対する期待は極めて大きく、両国間の研究技術強力を更に進めることを中国側も熱望していた。特に今回は日本への影響が懸念される公害や地球環境汚染の問題についても対処しうるよう従来の個別の研究課題を修正することで合意に達した。

そこで、日中双方の研究代表者、分担者が前回の共同研究の成果をもとにして協議した結果、中国炭の利用プロセスの効率化とクリーン化に的を絞って共同研究を行うことが緊急の課題であるとの合意に達し、改めて申請を行ったところ、平成４年度～５年度の国際学術研究に採択され（代表・野村正勝教授）、「中国炭の有効利用に関する無公害・新統合プロセスの共同開発研究」という研究課題名で本共同研究が行われた。

2. 研究の組織

平成４年度～５年度の本研究の研究組織は次の通りである。

野村正勝	大阪大学・工学部・教授	総括・新しいコークス製造
乾　智行	京都大学・工学部・教授	CO2、COからのケミカルズ製造触媒
飯野　雅	東北大学・反応化学研究所・教授	溶媒抽出液化法
加部利明	東京農工大学・工学部・教授	深度脱硫・脱窒素触媒

諸岡成治	九州大学・工学部・教授	高効率前処理法
郭　樹才	大連理工大学・石炭化学研究所・教授	溶媒抽出液化法
程　懋圻	中国科学院・山西石炭化学研究所・教授	高効率前処理法
朱　起明	清華大学・化学系・教授	CO2、COからのケミカルズ製造触媒
沙　興中	華東化工学院・資源化学系・副教授	深度脱硫・脱窒素触媒
杜　宝生	東北内蒙古石炭公社・多種経営公社・副社長	石炭転換プロセス

3.　中国側研究者のプロフィール

郭樹才教授は中国コークス化学会副会長を勤めており、極めて卓抜した研究業績に加えて、温厚な人柄で人望も厚く、中国の石炭政策全体を指導する地位にある。研究分野は、石炭から半成コークス製造、溶媒抽出液化、構造解析、前処理など石炭化学全般にわたっている。特に半成コークス製造に関しては基礎研究から実プラントの製造まで一貫した研究業績を挙げ、現在、内蒙古に１万トン／日のプラントを建設している。また、ドイツのカールスルーエ大学のK.Hedden教授とコークスに関する共同研究を実施した経験を有している。

程　懋圻教授は、中国における科学研究のメッカである中国科学院において、石炭化学研究所の副所長を勤めており、中国政府の意向を反映した石炭化学研究を統括する立場にある。研究分野は、石炭化学工学から石炭化学まで広範囲に及ぶが、特に流動床急速熱分解による石炭のガス化、石炭前処理工学に優れた業績を挙げており、中国工業省や山西省等から数多くの賞を授与されている。また海外に於ても積極的に研究発表をしており、先進国の事情にも明るく、来日経験も有している。

朱起明教授は、Chinese Coal Conversion Associationの事務局長を勤めており、また J.Fuel Chem. and Technol.、Natural Gas Chemical Industry、Coal Chemical Industry等の雑誌の編集委員で中国触媒化学分野のニューリーダーの一人である。研究分野はC_1ケミストリーや炭化水素合成に関連した触媒全般、および特に代替ガソリン燃料として注目されている高級アルコールの合成、メタンの部分酸化反応、およびフィッシャー・トロプシュ反応に関する高性能触媒の開発、in situ FT-IRによる反応中間体の検出に顕著な業績を挙げている。

沙興中教授は、将来を嘱望されている中国若手石炭化学者の一人で、来日経験もある。研究分野は、石炭の熱分解反応や石炭－水スラリーに関するものが主で、石

炭の基礎的パラメータと反応性との関連性を明らかにしてきた。触媒を利用した石炭の前処理や改質にも興味を持っており、今後はこの分野に積極的に取り組む意向を示している。

杜宝生氏は、中国において石炭を利用した重化学工業会社を経営する実業家である。また、中国石炭転換化学協会の常務理事でもあり、中国炭から高付加価値製品を製造する将来技術開発を指導するとともに、上記協会を通じて学会活動にも積極的に参加している。

4. 研究の目的

中国石炭の統合的有効利用を図るため、日中両国の研究技術者が協力して新しい無公害プロセス（石炭の高効率前処理法、液化油の高性能深度脱硫・脱窒素触媒、低エネルギー消費型溶媒抽出法、二酸化炭素・一酸化炭素からのケミカルズを製造する高性能触媒、低エネルギー消費型コークス製造法）を開発することを目的とする。本プロセスは、石炭を重工業発展の基幹資源とする中国に大きく寄与するとともに、日本への影響が心配される中国に由来する環境汚染の問題の解決にも寄与する。さらに、両国の若手研究者が共同で実験を行うことにより、極めて深い相互理解関係を得ることが期待され、将来にわたる緊密な協力体制を確立することができるものと考えられる。

5. 研究の意義

中国政府は８千億トン埋蔵される石炭を基幹資源として重工業の発展に傾注しており、例えば、平頂山市（産出量中国第三位）では石炭を基盤とする大化学コンビナートを建設している。石炭の基盤的利用研究にも大きな力を注いでおり、拠点大学や中国科学院に石炭化学研究所を多く設けている。しかし、年間９億トン産出される中国石炭のうち、９割以上が燃料として直接燃焼されているのが現状で、煤塵や亜硫酸ガスなどによる公害がすでに深刻化している。酸性雨や二酸化炭素の問題も含め、中国の石炭化学者はこれらの公害問題の解決にも積極的に取り組む姿勢を示している。中国側は、石炭の有効を図るため、世界のトップレベルにある日本の技術協力を渇望しており、日中両国の石炭化学者が直接討議し、中国の実情を勘案しながら共同で実験を進めることは、中国の重工業の発展に大きく寄与するものと考えられる。

6. 研究内容の概要

平成４年度は野村正勝教授（研究代表者）、乾智行教授、飯野雅教授、加部利明教授、諸岡成治教授、および研究協力者として村田聡助手（阪大）、井上正志助教

授（京大）、鷹觜利公助手（東北大）、石原篤助手（東京農工大）、林潤一郎助手（九大）が、それぞれ派遣され、(1)石炭の高効率脱硫、脱灰処理法の開発（諸岡、林、程担当）、(2)液化油の深度脱硫・脱窒素触媒の開発（加部、石原、沙担当）、(3)低エネルギー消費型連続式溶媒抽出液化法の開発（飯野、鷹觜、郭担当）、(4)低エネルギー消費型連続式コークス製造法の開発（野村、村田、郭担当）、(5)二酸化炭素、一酸化炭素からケミカルズを製造する高性能触媒の開発（乾、井上、朱担当）、(6)統合プロセスとしての評価、設計（野村、諸岡、杜、郭担当）の共同実験研究が実施された。

平成５年度は４年度に実施した個別研究課題を担当している中国側研究機関から若手研究協力者を日本に招聘して、平成４年度の研究成果をふまえ、より濃密な共同実験研究を実施した。その後中国側研究分担者を日本に招聘し、研究成果の取りまとめ、評価を行うとともに、今後の長期にわたる研究協力の方針、並びにその方策を決定した。

以上２年間に渡り日中合わせて１９名の研究者の交流があり、国のレベルを越えた研究者相互の緊密な議論と共同研究が実現された。

7. 研究成果の要約

中国炭の有効利用は中国での高効率利用法の確立の問題に過ぎず、将来のアジア各国で用いる貴重なエネルギー源である。従って中国炭の統合的無公害有効利用プロセスの開発研究は、グローバルな意味をもつ重要なテーマである。本研究では統合プロセスの中で重要課題である個々のテーマに分けて共同実験を行い、多くの研究成果を得ることができた。特にその中でも液化油の深度脱硫・脱窒素触媒の開発、あるいは二酸化炭素、一酸化炭素からケミカルズを高効率に製造する触媒の開発研究では、中国炭のクリーン利用において一つの指針が得られ、今後のプロセス開発に重要な知見となった。なお研究成果の詳細は平成６年３月に発行の本研究の成果報告書に記載されている。

またこの共同研究では、前記のように日中両国の石炭研究者、技術者間の研究の交流が有り、互いに自由に意見を交換しあい、今後とも協力関係を続けていくことで双方の意見が一致したことは、本研究の大きな意義であった。本研究のような文部省の国際学術研究は学術研究の国際化、国際レベルでの研究討論、日本の国際的な貢献、若手研究者の育成など大きな意味を持つ共同研究である。特にこの研究課題では日本の石炭研究者、技術者の国際的な貢献として重要であり、この共同研究をさらに展開していきたいと考えている。

最後に２年間の日中国際共同研究の実施にあたり、ご支援、ご援助いただいた文部省に深く感謝いたします。

日本－カナダ共同学術研究に参加して

大塚　康夫

本共同研究（代表：京都大学工学部化学工学科・橋本健治教授）は、文部省科学研究費の援助を受けて、 1987度から4年間、「複合的変換プロセスによる石炭の有効利用」の課題で実施され、さらに1992度から、「環境負荷低減を目指した石炭高度利用技術の開発」のテーマで再開されたものである。これまで、両国あわせて通算100名にのぼる研究者が参加しており、 炭素資源反応研究センター長の富田彰教授は、本プロジェクトの開始当初より参画している。

筆者は、1993年度の研究分担者として、同年7月下旬より約1ヶ月半、カナダの首都オタワ郊外にあるCANMET（Canada Centre for Mineral and Energy Technology）のERL（Energy Research Laboratories）に滞在し、共同研究を実施した。

CANMETは、職員数約850名、年間予算約1億カナダドル（約80億円）のカナダ政府研究機関であり、エネルギー政策の立案、鉱物資源の採掘と無機材料開発、化石資源の採掘と利用技術、エネルギー効率化と代替エネルギー開発の四つの部門から構成される。その中でERLは、職員数約150名、年間予算約20億円で、石炭、ビチューメン、タールサンドなどの重質炭素資源の科学と利用に関する研究を進めている。現在ERLは、Synthetic Fuels（SFRL）、Combustion and Carbonization（CCRL）、Fuels Characterization （FCRL）の三つの独立したLaboratoryから成り、筆者は、CCRLのEd Furimsky博士と共同で研究を実施した。 博士はカナダを代表する石炭・重質油の研究者であり、 本プロジェクトだけでもすでに4名の日本側研究員を受け入れ、石炭の触媒ガス化や高温脱硫剤の研究に関し多くの成果を挙げている。

今回の滞在では、我々が進めている“石炭の事前脱窒素法”を発展させることを目的とした。この方法は、鉄を添加した石炭を単に加熱するだけで、石炭中の窒素の50～60％を無害なN_2ガスとして除去できるというものであり、高価な水素を必要とせず、高分散鉄微粒子が脱窒素作用を示すことも明らかとなっている。以前より鉄触媒ガス化の研究を進めていたFurimsky博士は、 1993年6月に当研究部を訪問した折り、この触媒脱窒素に強い関心を示した。そこで、カナダでの研究期間も限られていることを考慮して、渡航前に綿密な打ち合わせを行い、モデル炭素を用いて脱窒素反応のダイナミックスを明らかにすることに焦点を絞った。

渡航時の7月下旬は夏休み時期と重なるため、 研究所には誰もいないのではないかと心配したが、案に相違して、博士は勿論のこと、オタワ大学化学工学科の女子学生とテクニッシャンが待っていて、オタワ到着の翌々日から実験を始めることが

できた。この三人と一緒に、ポリアクリロニトリルからの炭素の製造、炭素の反応性とN_2の脱離挙動、金属鉄超微粒子の触媒作用に関する実験を進めた。女子学生は、4ヶ月間ERLに来ていた実習生であり、 彼女以外にも、カナダ各地の大学から少なくとも20名の学生が実習に参加していた。学生にとっては、大学院進学時の奨学金の取得に際し、実習先からの推薦状が重要となるので、まじめに研究に取り組んでいるものが多い。このような実習制度は、CANMETに限らず企業でも行なわれているが、予算削減で研究者を充分に確保できないERLでは、 短期間とはいえ学生は貴重な戦力になっているようであった。

オタワの夏は、日本の冷夏とは対照的に、連日好天に恵まれた。気温は30℃近くまであがるが、空気が乾いているので過ごしやすい。 ERLの敷地は広大で森に囲まれているため、昼休みにはジョッギングを楽しむ人が多い。周囲のほとんどの研究者は、朝8時（夏時間）頃から仕事を始めて、午後4時頃には（まだ日が高いと感じるのだが）家路につき、After Fourをエンジョイする。筆者は、Downtownのアパートからバスで通勤していたので、 5時半の最終バス！をよく利用していたが、乗客はいつも一人か多くても数人であった。今回の滞在日程では、7月下旬から9月上旬までの約50日間は、共同研究機関で研究に専念できるように配慮されていたので、月曜から金曜までは久しぶりに研究三昧の生活を送った。 滞在中には2週間足らずではあったが家族も加わり、 週末には、Patioでの食事、ショッピング、Biking、小旅行を楽しんだ。

日本の国立大学でも最近は、外国人が研究スタッフとして採用されるようになったが、ERLでは、 実に多種多様の人が働いており、東欧やアフリカ出身の研究者が、プロジェクトマネージャなどの重要なポストについている。よく知られているように、カナダの公用語は英語とフランス語であり、首都のオタワでは、交通標識、デパートの売場案内板、政府刊行物など、 公共のあらゆるものについて2カ国語の使用が徹底している。ところが、オタワ川の対岸のHullに渡ると、交通標識はフランス語のみとなる。つまり、Hullは、フランス大統領であったド・ゴールがカナダに来て「フランス万歳」と叫んだと言われるケベック州であり、英語の使用は禁止とのこと。さきの女子学生はケベック州出身でその名もFranceといい、おいしいフランス料理レストランはHullに集っていると言っていたのが思い出される。

1993年度は、筆者以外に、林順一（関西大）、前一廣（京都大）、船造俊孝（横浜国大）の3博士が、それぞれ、University of British Columbia、University of Waterloo、University of Sherbrookeに滞在して共同研究を行ない、カナダでの研究も最終段階に入った9月10日に、全員がCANMET/ERLに集まり、 Furimsky博士主宰の中間報告会に出席した。この会議には、三浦孝一助教授（京都大）、富田彰教授、カナダ側代表者のP. Silveston教授（University of Waterloo）をはじめ、 ERL所

東北大学ーペンシルベニア州立大学国際共同研究

富田　彰

1．研究課題

炭素の触媒ガス化反応を利用した環境・エネルギー問題への一つのアプローチ

A solution of pollution and energy problems by using catalytic gasification of carbon

2．研究代表者

日本側	東北大学反応化学研究所　教　授　富田　彰
アメリカ合衆国側	ペンシルベニア州立大学　助教授　Ljubisa R. Radovic

3．研究期間

平成３年～平成５年度

4．研究組織

氏　名	所　属・職	専門領域	役割分担
富田　彰	東北大･反応研･教授	工業物理化学	研究の総括
京谷　隆	東北大･反応研･助教授	炭素材料化学	炭素の触媒ガス化反応機構の解明
山下弘巳	東北大･反応研･助手	触媒化学	炭素を利用した新触媒の開発
L. R. Radovic	Pennsylvania State Univ., Associate Professor	炭素化学	炭素担持触媒の開発

5．研究の目的

環境の保全とエネルギーの安定確保はわれわれが来世紀に向けて取り組むべき最大課題の一つと考えられるが、本研究においては、炭素の触媒ガス化反応を巧みに利用することによって、これらの問題解決のための指針を与えることを目的とする。すなわち、酸性雨、温室効果などの原因となるNOxを処理するための新しい方法を開発するため、NOxの分解反応を選択的に促進する炭素系触媒の開発を行う。同時に炭素系資源のガス化によるクリーンエネルギー製造のための基礎研究として炭素のガス化反応を促進する触媒の開発を行い、両者の研究を有機的に関連づけ、触媒を用いた炭素のガス化反応を有効に利用する道を開拓する。

6．期待される研究成果

ディーゼルエンジンなどから排出されるNOxを効率的に除去することは緊急課題の一つであり、現在NOx分解法が盛んに研究されているが、分解によって生成した酸素種を触媒系から除去することが困難であり、隘路となっている。炭素は酸素種との親和性が強いので、炭素を担体とする触媒系を用いればNOxの分解反応は容易に起こり得る。共存する酸素ガスによる炭素の燃焼も同時に起こるので、NOxの分解反応を大いに促進するが、NOxと酸素ガスの反応には有効でないような金属触媒の開発が行われれば、有効なNOx除去法になることが期待される。そのような選択的な触媒を見いだすことが本研究の主題である。一方、エネルギー問題解決のための研究である石炭の触媒ガス化に関しては、高活性触媒を創出することが最重要課題であるが、そのためには炭素と触媒とガスの相互作用に関する深い理解が必要である。本研究ではとくにカルシウムを中心とする触媒を炭素上に高分散させた系の開発を行うが、安価で熱効率の高い石炭ガス化法開発の基礎を確立することが期待できる。

7．研究の意義

NOxは酸性雨だけでなく、温室効果による地球温暖化をももたらすので、その対策が強く望まれている。とくに、この問題は地球全体の問題であり国際的に協力を進めるべきであり、学問レベルにおいてもやはり国際協力関係を作っておく必要がある。また、石炭のガス化のための新しい触媒利用法も、開発規模が大きいので、国際協力による推進が強く望まれている分野である。

東北大学の「炭素の触媒ガス化」、「触媒を用いた小分子の転換反応」などの蓄積、ペンシルベニア州立大学の「触媒担体としての炭素利用」、「炭素の表面化学」などの研究は世界的に高レベルの研究と評価を受けており、双方がこれまで蓄積してきた得意の分野のノウハウを持ち寄り協力することにより、炭素を利用した新しい反応あるいは新しい触媒の設計のため共同研究を企画することには大きな意味がある。

8．共同研究を計画するに到った経緯

研究代表者が過去にペンシルベニア州立大学に留学していた関係でこれまでにも国際会議などにおいて頻繁な研究交流があった。とくに今回の分担者であるRadovic博士とは炭素質のガス化に対する触媒の作用、炭素触媒など多くの面で共通の関心を持っていた。1989年6月にペンシルベニア州立大学で開催された国際炭素学会に富田および京谷が出席し、その際Radovic博士と本共同研究について討議し、両者ともその意義を大いに認めるに至った。その後1年間両者の間で、対象とすべき研究課題についての入念な打ち合せを行い、本研究課題を計画した。

９．研究計画全体の概要

炭素を利用して、環境およびエネルギー問題の解決に寄与するような新しい反応系を確立するのが最終的な目的である。具体的には、前者に関しては、NOx / O_2混合ガスと金属触媒を担持した炭素との反応を行い、選択性に優れた触媒を用いることにより炭素の消費を抑えつつ、NOxを効率的に分解する方法の開発を試みた。後者に関しては、石炭ガス化の基礎である炭素とガスの反応に対する鉱物質あるいは添加触媒の作用を分子レベルで解明することを通じ、安価でしかも高性能な触媒を探索した。高分散したカルシウム触媒の役割を中心として研究を進め、とくに実際の利用にあたって問題となる触媒被毒現象を炭素表面の状態の把握を通じて行った。これらはいずれも、炭素－金属－ガスの３者間の相互作用に関する深い理解を必要とするものであり、本研究の学問的意義はこの相互作用の実態を明らかにすることにある。

１０．年度別研究実施内容

[平成３年度]

本研究課題はかなりの広がりを持つので、初年度ではまずNOxの反応を重点的に取り上げた。NOxの分解反応に選択的に作用するが酸素との反応には鈍感な金属触媒の探索を行い、炭素の消費を極力抑えつつ高転化率でNOxを除去できるような反応系を確立することを目指した。触媒系の設計には、これまでの炭素触媒の知見が蓄積されているペンシルベニア州立大学と緊密な連携をとりながら、東北大学における予備実験で数種類の触媒にしぼりこんだ。その後富田が大学院修士課程学生山田を伴い、カリフォルニア州サンタバーバラにて開催された国際炭素材料学会に出席し、同会議に出席していたRadovicと詳細な研究計画をたてた。その後山田はペンシルベニア州立大学に９月末までの３カ月間滞在し、ペンシルベニア州立大学で用いている過渡応答法、TPD/MS法などを利用して、NOxと触媒、あるいは炭素との相互作用を明らかにする研究に従事した。また、共同研究者である京谷は本学術共同プロジェクトとは別に博士研究員として１月よりRadovicの研究室に滞在しており、山田が研究を進めるにあたって好都合であった。

[平成４年度]

前年度の研究を継続し、より高性能の触媒系の探索を続けたる。また、炭素の反応性（とくにCa触媒の作用機構）を評価するためペンシルベニア州立大学で過渡応答法を用いた研究を進める。実際の研究に先立ち、富田、京谷、Radovicはドイツのエッセンで開催された国際会議 Carbon '92においてそれまでの研究の進捗状況を打ち合わせた。７月はじめから２カ月間山下が渡米し、ペンシルベニア州立大学で過渡応答法、TPD / MS法による実験を行い、ガス化反応に対するCaの触媒活性が水素の

存在により低下する原因を明らかにした。この結果のまとめが終了した１１月には富田およびRadovicがハワイで開催されたGordon会議で再会し、山下が得た結果について討議を行った。ハワイでの会議後、Radovicを日本へ招聘し、共同研究の一環として日本で進めている炭素とNOxの反応に関する実験結果、ならびに炭素ガス化のシミュレーションの実験結果について時間をかけて討議した。また、平成５年度の研究計画についての打ち合わせを行った。

[平成５年度]

６月中旬に京谷をバッファロで開催された米国炭素材料学会に派遣し、その帰途にペンシルベニア州立大学に立ち寄らせ、最終年度の計画を確立した。９月から３カ月T. Tao氏が来仙し、金属担持ゼオライト触媒上に生成した炭素のキャラクタリゼーションをEXAFS、XPS、表面積測定、TPDなどを駆使して行った。これは炭素析出によって低下した触媒活性を回復するためにガス化によって炭素を取り除く際に必要な情報を取得するためのものである。非常に精力的に実験を行い、あふれるばかりのデータを持帰り、現在整理に余念がないところである。各分野で得られた成果を評価するとともに、炭素－金属－ガス３者の相互作用に関する学問の上で得られた成果を総括し、87頁よりなる成果報告書を発刊した。

１１．派遣および招聘実績

[平成３年度]

[派遣]	富田　彰	６月２３日～　７月　４日　１３日間
[派遣]	山田　元	６月２３日～　９月２２日　９０日間

[平成４年度]

[派遣]	山下　弘巳	７月　１日～　８月３０日　６１日間
[招聘]	L. R. Radovic	１１月１５日～１１月２２日　８日間

[平成５年度]

[派遣]	京谷　隆	６月１３日～　６月２０日　８日間
[招聘]	T. Tao	９月　１日～１１月３０日　９０日間

１２．国外研究分担者のプロフィール

Radovic博士は、1951年Yugoslaviaに生まれ、1977年にBeoglade大学の化学工学科を卒業したのち、同地のBoris Kidric Institute of Nuclear Sciencesで２年間研究員をしている。Pennsylvania State Universityで1982年に博士号を取得後、ChileのConcepcion大学、Polytechnic Universityで勤めたあと、1986年より再びPennsylvania State Universityに戻り、1992年Associate Professorに昇格した。ACS, Carbon Conference, NATO Meetingなどのオーガナイザとしても活躍している。

NEDO国際共同研究

富田　彰

1．研究課題

クリーンコールを用いる先端発電システムの開発

2．研究組織および研究期間

研究代表者：富田　彰（東北大学：日本）

共同研究者：

大塚 康夫（東北大学：日本）
野村 正勝（大阪大学：日本）
Ian W. Smith（CSIRO：オーストラリア）
Geoff H. Taylor（オーストラリア国立大学：オーストラリア）
Edwin J. Hippo（南イリノイ大学：アメリカ）

研究期間：1993年4月～1996年3月

3．研究の概要

地球環境の危機が心配されているが、それとともに、遠くない将来に再びエネルギー問題が深刻になることも懸念されている。これらの両方の問題に対応するため、資源的に最も安心感のある石炭を、効率よく、しかもクリーンに利用することはわれわれに課せられた大きな課題である。例えば、石炭をガス化し、ガスタービンと蒸気タービンの両方で発電を行うガス化複合発電方式は、現在の微粉炭火力発電に比較して大幅な熱効率の増加が予想され、最も現実的な方法として期待されている。熱効率の増加は直接に炭酸ガスの低減にむすびつくため、エネルギー問題だけでなく環境問題に対しても大きな貢献となる。

ガス化複合発電に限らず、石炭の処理にあたって最も頭を悩ますのが灰の問題であり、硫黄・窒素化合物の排出である。本研究では発想を転換し、予め石炭より鉱物質やその他の環境汚染物質を除去しておき、転換処理の段階での負担をゼロとするようなシステムの開発を目的としている。

4．研究の具体的計画

(1) アルカリ、酸処理による鉱物質の除去。
(2) 有機硫黄の選択的酸化をともなう鉱物質・硫黄の同時除去。
(3) 高分散金属の作用による窒素化合物の選択的除去。
(4) コールクリーニング前後の鉱物質の挙動の解析。
(5) クリーンコールの反応性の解析。
(6) クリーンコールを用いた新しい燃焼・ガス化プロセスの構築。

研究論文および関連資料

Reprinted from ENERGY & FUELS, 1991, 5.

Insolubilization of Coal Soluble Constituents in Some Bituminous Coals by Refluxing with Pyridine

Toshimasa Takanohashi and Masashi Iino*

Institute for Chemical Reaction Science, Tohoku University, Katahira 2-1-1, Aoba-ku, Sendai 980, Japan

Received April 9, 1991. Revised Manuscript Received May 28, 1991

The solvent-treated coals were extracted with CS_2–*N*-methyl-2-pyrrolidinone (NMP) mixed solvent at room temperature to investigate the effect of the treatment on extractability. The refluxing with pyridine greatly decreased the extraction yield compared to that of the untreated coal. The treatment with pyridine at room temperature needed a longer time, i.e., 1 week, to detect the decrease in the extraction yields of coals. A similar treatment with CS_2–pyridine mixed solvent at room temperature, which is a better solvent than pyridine for coal molecules, for 1 day at room temperature, decreased the extraction yield to a great degree compared to that with pyridine. Fractionation of the soluble fractions by acetone and pyridine clarified that this decrease in the yields is due to the insolubilization of the heavy fraction, i.e., the pyridine-insoluble (E-PI) fraction in the extract. The swelling ratios of the E-PI fraction in benzene and methanol were decreased by this treatment, indicating the increase of cross-linking density. Spin concentrations of ESR spectra of the E-PI fractions were increased by refluxing with pyridine. Insolubilization mechanisms are discussed for the formation of covalent and/or noncovalent bonds between the heavy E-PI molecule and other heavy molecules (E-PI or residue) during the treatment.

Introduction

Coals have been considered to consist of covalently cross-linked network and relatively low molecular weight soluble constituents.[1-3] The thermal cleavage of the covalent bonds is a key step in the coal liquefaction process. Recently attention, however, has been directed to the significance and importance of noncovalent intra- and intermolecular interactions. The importance of hydrogen bonds in the coal structure has been established by many researchers.[4-6] As for other interactions, Mallya and Stock,[7] and Miyake and Stock[8] indicated that the diminution in stacking interactions between aromatic compounds for high-rank coals results in an increase in coal solubility. Quinga and Larsen[9] and Nishioka and Larsen[10] suggested that the formation of adducts between maleic anhydride and coals increased the pyridine extractability, due to the blocking noncovalent interactions. We found[11] that 40–65% of the extraction yields were obtained for some bituminous coals from extraction at room temperature with CS_2–*N*-methyl-2-pyrrolidinone (NMP) mixed solvent, which might cleave some noncovalent bonds between coal molecules, like other good solvents.

Nishioka and Larsen[10] reported a decrease in pyridine Soxhlet extraction yields after pretreatment in several solvents at 25–115 °C. They concluded that the decrease can be attributed to new noncovalent interactions between coal constituents formed when the treated coal became conformationally more stable than the raw coal, after the removal of treatment solvent. We preliminarily reported the similar decrease in the extraction yields with the CS_2–NMP mixed solvent by mild acetylation, methylation, and treatment with pyridine for some bituminous coals.[12] Our result differs from the result of Nishioka et al. in the effect of the kind of solvent and the effect of solvent removal after treatment. In the present study, the behaviors of this insolubilization of coals by treatment with solvents are studied and the mechanisms are discussed.

Experimental Section

Materials. The ultimate and proximate analyses of coals used are shown in Table I. Zao Zhuang (China), Shin-Yubari (Japan), and Miike (Japan) coals were ground <250 μm, and Upper Freeport (USA) coal which is from Argonne Premium Coal Sample Program was already ground <150 μm. Coal samples were dried in vacuo at 107 °C to constant weight (2–3 h). Reagent grade solvents were used without further purification.

Solvent Treatments. Three different solvent treatments were carried out: 2–4 g of samples were refluxed with 200 mL of pyridine, THF, or chlorobenzene, under nitrogen for 1 day; 2–4 g of samples were stirred in 200 mL of pyridine, THF, or CS_2–pyridine mixed solvent (1:1, by volume), under nitrogen at room temperature, with or without ultrasonic irradiation (38 kHz); 2–4 g of samples were kept for 1 week in pyridine vapor in a desiccator.

Extraction and Fractionation Procedures. Two to four grams of samples were extracted with 50–100 mL of CS_2–NMP mixed solvent (1:1 by volume) under ultrasonic irradiation (38 kHz) for 30 min at room temperature, and centrifuged at 14000 rpm (25400*g*), and then the supernatant was separated by decantation. This extraction procedure was repeated until the supernatant became almost colorless (usually 6–7 times). Filtration was carried out with a membrane paper of an average pore size of 0.8 μm. According to the procedure shown in Figure 1,

(1) Given, P. H.; Marzec, A.; Bartle, W. A.; Lynch, L. J.; Gerstein, B. C. *Fuel* **1986**, *65*, 155–163.
(2) Lucht, L. M.; Peppas, N. A. *Fuel* **1987**, *66*, 803–809.
(3) Green, T.; Kovac, J.; Brenner, D.; Larsen, J. W. In *Coal Structure*; Meyers, R. A., Ed.; Academic Press: New York, 1982; pp 199–282.
(4) Liotta, R.; Rose, K.; Hippo, E. *J. Org. Chem.* **1981**, *46*, 277–283.
(5) Patel, K. M.; Stenberg, V. I.; Baltisberger, R. J.; Woolsey, N. F.; Klabunde, K. J. *Fuel* **1980**, *59*, 449–450.
(6) Larsen, J. W.; Baskar, A. J. *Energy Fuels* **1987**, *1*, 230–232.
(7) Mallya, N.; Stock, L. M. *Fuel* **1986**, *65*, 736–738.
(8) Miyake, M.; Stock, L. M. *Energy Fuels* **1988**, *2*, 815–818.
(9) Quinga, E. M. Y.; Larsen, J. W. *Energy Fuels* **1987**, *1*, 300–304.
(10) Nishioka, M.; Larsen, J. W. *Energy Fuels* **1990**, *4*, 100–106.
(11) Iino, M.; Takanohashi, T.; Ohsuga, H.; Toda, K. *Fuel* **1988**, *67*, 1639–1647.
(12) Takanohashi, T.; Iino, M. *Energy Fuels* **1990**, *4*, 333–335.

0887-0624/91/2505-0708$02.50/0

Table I. Ultimate and Proximate Analyses of Coals

coal	ultimate analyses, wt %, daf					proximate analyses, wt %, db		
	C	H	N	S	O[b]	VM	ash	FC
Zao Zhuang	86.9	5.1	1.5	1.6	4.9	28.6	7.4	64.0
Shin-Yubari	86.6	6.0	2.0	0.8	4.6	38.3	6.2	55.5
Upper Freeport[a]	86.2	5.1	1.9	2.2	4.6	28.2	13.1	58.7
Miike	83.4	6.0	1.2	2.7	6.7	36.6	22.5	40.9

[a] Argonne Premium Coal Sample Program. [b] By difference.

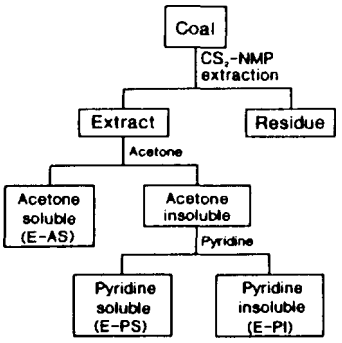

Figure 1. Solvent fractionation procedure of extracts obtained from CS_2–NMP mixed solvent extration.

the extract was fractionated with acetone and pyridine, respectively, under ultrasonic irradiation, into acetone-soluble (E-AS) fraction, and acetone-insoluble and pyridine-soluble (E-PS) fraction, and pyridine-insoluble (E-PI) fraction, which is the heaviest fraction of the extract obtained from the CS_2–NMP mixed solvent extraction. The residue and E-PS and E-PI fractions were washed with acetone, and the E-AS fraction was washed with acetone–water mixed solvent (2:8 by volume) which was found to be able to remove the retained solvent almost completely.[11] The extract fractions and the residue were dried in vacuo at 80 °C for 12 h. The extraction yield was calculated on dry ash-free (daf) basis by using the following equation, where the db means a dry basis.

$$\text{extraction yield (wt \%, daf)} = \frac{1 - (\text{residue (g)}/\text{coal feed (g)})}{1 - (\text{ash (wt \%, db)}/100)} \times 100$$

Swelling Measurement. The volumetric method by Hombach,[13] Liotta et al.,[14] and Green et al.[15] was used to measure the swelling ratio, Q, of the sample. The sample of 0.1 g was placed in an 8 mm outer diameter of glass tube and centrifuged for 30 min at 1500 rpm. The height of the sample layer was measured as h_1. About 1.0 mL of the solvent then was added and mixed with the sample using a spatula and ultrasonicated for 30 min. The content was again centrifuged and the height of the sample uptaking the solvent was measured as h_2. Q is defined as h_2/h_1. The mixing and centrifugation procedures were repeated until a constant height was attained (2–3 days).

ESR Measurement. About 20 mg of the sample (<250 μm) in a glass tube of 3 mm outer diameter was degassed for 2–3 h in vacuo, and then sealed. The ESR spectra were obtained on a Varian E-4 spectrometer system (100 kHz field modulation frequency, 9.52 GHz operating frequency) at room temperature. The resonant frequency of the sample cavity was set to yield a maximum detector current on microwave bridge controls in the spectrometer. The measuring condition was as follows: microwave power, 0.5 mW; centerfield value, 323 mT; scan range, 10 mT. Spin concentration was determined by using diphenylpicrylhydrazyl (DPPH) as a standard sample.

FT-IR Measurement. A 4-mg portion of the sample was ground <74 μm and diluted with 200 mg of KBr powder (<74 μm). The FT-IR spectra were measured by a diffuse reflectance method using a JEOL JIR-100 FT-IR spectrometer. The intensities of the spectra were calculated by the Kubelka–Munk function after 200 scan times.

Table II. Extraction Yields of Coals with CS_2–NMP Mixed Solvent at Room Temperature after Solvent Treatments

solvent treatment	coal			
	Zao Zhuang	Shin-Yubari	Upper Freeport	Miike
none	63.0	56.8	59.4	31.1
Py, 115 °C, 1 day	46.3	50.2	41.7	32.3
Py, 115 °C, 1 day[a]	43.5			
Py, 115 °C, 1 day[b]	45.5			
Py, room temp, 1 week	51.6		56.7	
Py, room temp, 1 day	64.1	53.9		
Py, room temp, 1 h[c]	62.9	51.4	62.5	
THF, 66 °C, 1 day	64.6	56.5		
THF, room temp, 1 day	63.4	57.0		33.5
THF, room temp, 1 h[c]	65.9	54.5		
chlorobenzene, 132 °C, 1 day	63.1			
CS_2–Py, room temp, 1 day	44.7			
Py vapor, 1 week	63.6			

[a] The extraction was done without removing pyridine. [b] The mixture of sample and solvent was thoroughly vacuumed before the treatment. [c] Sample was treated under ultrasonic irradiation.

Results and Discussion

Solubility. The effects of the treatments on the extraction yield with CS_2–NMP mixed solvent are summarized in Table II. When Zao Zhuang, Shin-Yubari, and Upper Freeport coals were treated with pyridine in refluxing (the treatment temperature reached near its bp (115 °C)), the extraction yields greatly decreased, i.e., from 63.0, 56.8, and 59.4% to 46.3%, 50.2, and 41.7%, respectively. The treatment with pyridine with stirring at room temperature for 1 day did not change the yields, but the treatment for longer time (1 week) decreased the extraction yields to a lesser degree than refluxing. Nishioka and Larsen[10] reported a decrease in pyridine extractability after the pretreatment, i.e., with chlorobenzene at 113 °C for 1 week, or with pyridine at 25 °C for 1 day, and also reported that the extraction yield did not decrease when the solvent was not removed after the treatment. They suggested that the solvent treatment swelled the coal molecules and enhanced their mobility, and after the solvent was removed, new noncovalent interactions were formed. However, in our case of CS_2–NMP solvent extraction, the extraction yield decreased even without the removal of the solvent used, i.e., without the evaporation and drying of the treated coal (column 3, Table II). Table II also shows that the treatments with chlorobenzene or THF, which is a poorer solvent than pyridine, had no effect on the extraction yields with the mixed solvent. The treatment with CS_2–pyridine mixed solvent, which is a better solvent than pyridine alone,[16] for only 1 day at room temperature, decreased the yield with CS_2–NMP extraction to a similar

(13) Hombach, H. P. *Fuel* **1980**, *59*, 465–470.
(14) Liotta, R.; Brown, G.; Isaacs, J. *Fuel* **1983**, *62*, 781–791.
(15) Green, T. K.; Larsen, J. W. *Fuel* **1984**, *63*, 1538–1543.
(16) Iino, M.; Li, Q.-T.; Matsuda, M. *Nenryou Kyoukai Shi* **1985**, *64*, 248–254.

Table III. Fractionation of Raw Coals, and the Samples after Treatment[a]

sample	extract fractions, wt %, db			total residue, wt %, db	extraction yield, wt %, daf
	E-AS	E-PS	E-PI		
Zao Zhuang Coal					
raw coal	6.7	24.3	26.0	41.7	63.0
treated coal	7.5	24.2	8.7	57.1	46.3
treated extract	0.3	0.9	5.0	62.8	40.2[b]
treated E-PI	0.0	4.0	2.4	60.7	42.4[b]
Upper Freeport Coal					
raw coal	6.1	18.3	24.9	48.4	59.4
treated coal	7.1	26.5	2.1	63.8	41.7
treated E-PI	0.0	3.8	6.9	62.5	43.2[b]

[a] Refluxing with pyridine, 1 day. [b] The yields on a raw coal basis.

degree as that for the refluxing in pyridine.

These results indicate that the treatment temperature and time, and the kind of solvents, are the important factors for the insolubilization behaviors. Pyridine at a high temperature or CS_2–pyridine mixed solvent even at room temperature increase the mobility of the coal molecules[17] and, moreover, remove a great amount of the extracted component from the coal to the solvent phase. Pyridine at room temperature could change the coal structure more slowly than that at high temperature. These results may be responsible for the insolubilization behavior observed here. When Zao Zhuang coal was treated with pyridine vapor for 1 week (Table II), the extraction yield did not decrease at all, although the treated coal increased 11.9 wt % by the absorption of pyridine. In this case, the increased mobility by this pyridine-vapor treatment is lower, and pyridine-soluble components are not removed from the coal, as compared with the case of the liquid-state pyridine (column 5, Table II).

The extract from the treated coals was fractionated with acetone and pyridine (Figure 1), and its fractionation distribution was compared with that for the extract from raw coals, and the result is shown in Table III. When the raw coal was refluxed with pyridine, the quantity of E-PI fraction, i.e., pyridine-insoluble fraction in the extract, exclusively decreased from 26.0% and 24.9% to 8.7% and 2.1%, for Zao Zhuang and Upper Freeport coals, respectively, and no decrease in E-AS and E-PS contents for both coals was observed, though a small increase in the E-PS content for the treated Upper Freeport coal can be also seen. Thus, the decrease in the extraction yield observed by the refluxing with pyridine is due to the decrease in the E-PI fraction. It is reasonable that Miike coal,[18] which has little E-PI fraction (0.1 wt %, dry raw coal basis), shows no decrease in extraction yield by the refluxing with pyridine, as shown in Table II. This suggests that this insolubilization is not observed for lower rank bituminous coals and subbituminous coals.

When the extract obtained from the CS_2–NMP mixed solvent extraction for Zao Zhuang coal was treated similarly, the E-PI content was found to decrease to the similar degree to that for the treated raw coal, as shown in Table III. Table III also shows a similar result was obtained when only the E-PI fraction was treated with pyridine.

During pyridine treatment, pyridine-soluble components are removed and pyridine-insoluble E-PI fraction is retained in the coal network. It seems likely that the noncovalent interactions such as hydrogen bondings, aromatic–aromatic interactions, and charge-transfer complexes, and/or physical entanglement may be formed between two E-PI molecules or the E-PI fraction with the coal network. Yokokawa[19] and Duber[20] suggested the occurrence of recombination of coal radicals during solvent treatment or extraction. So, the formation of covalent bonds by the recombination between coal radicals or the addition of the radicals to the aromatic rings may also be possible. The formation of the interactions and/or the bonds can lead to the decrease in the extraction yields as described above.

Table IV. Swelling Ratios of E-PI Fractions and Residues and Their Treated Samples[a]

solvent	Zao Zhuang coal		Upper Freeport coal	
	E-PI	treated E-PI	E-PI	treated E-PI
benzene	1.78	1.31	1.84	1.51
methanol	1.40	1.27	1.54	1.33

[a] Refluxing with pyridine, 1 day.

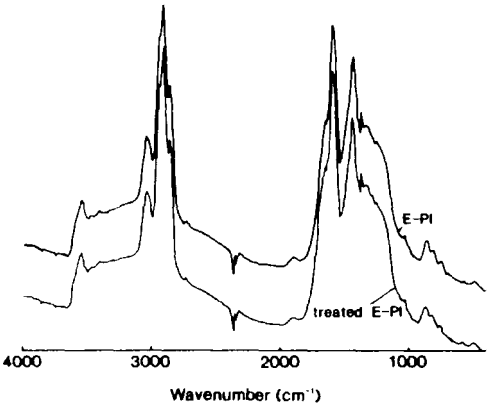

Figure 2. FT-IR spectra of the E-PI fraction from Upper Freeport coal, before and after refluxing with pyridine for 1 day.

Swelling Ratio. The formation of new noncovalent interactions and/or covalent bonds by the treatment with pyridine is expected to increase cross-linking density, resulting in a decrease in swelling ratio. Larsen and Mohammadi[17] found a decrease in swelling ratio after the solvent treatment, due to the formation of noncovalent interactions. The swelling ratios of E-PI fraction before and after the pyridine-refluxing were measured in benzene or methanol, as shown in Table IV. The treatment decreased the swelling ratios of E-PI fractions for both Zao Zhuang and Upper Freeport coals, indicating the formation of the new cross-linkages. Table IV also shows that the degree of the decrease in the swelling ratio of E-PI fractions in benzene is larger than that in methanol, suggesting that some noncovalently cross-linking sites, which could be released with benzene before treatment, were released by pyridine-refluxing, and then formed new strong noncovalent cross-linkages during the treatment. The swelling ratios before and after refluxing with pyridine for the residues obtained from CS_2–NMP extraction of Zao Zhuang and Upper Freeport coals were measured, and they did not change by the treatment.

FT-IR Measurement. FT-IR spectra for the E-PI fraction from Upper freeport coal, before and after the pyridine treatment, were measured to investigate structural changes and are shown in Figure 2. No detectable change by the treatment can be seen, except that the treated E-PI

(17) Larsen, J. W.; Mohammadi, M. *Energy Fuels* **1990**, *4*, 107–110.
(18) Iino, M.; Takanohashi, T.; Obara, S.; Tsueta, H.; Sanokawa, Y. *Fuel* **1989**, *68*, 1588–1593.
(19) Yokokawa, C. *Fuel* **1969**, *48*, 29–40.
(20) Duber, S.; Wieckowski, A. B. *Fuel* **1984**, *64*, 1641–1644.

Table V. Spin Concentrations[a] of E-PI Fractions and Residues and Their Treated Samples[b]

	E-PI	treated E-PI	residue	treated residue
Zao Zhuang coal	6.9	14.9	8.7	16.7
Upper Freeport coal	9.7	11.4	16.1	21.9

[a] 10^{18} spin/g daf basis. [b] Refluxing with pyridine, 1 day.

shows a very small shoulder at 1600–1750 cm^{-1}, which we could not assign.

ESR Measurement. Table V shows spin concentrations of the E-PI fractions and residues, before and after the treatment of each fraction. For all fractions, treatment with pyridine increased spin concentrations. At present the reason is not clear, but Fowler, Bartle, and Kandiyoti[21,22] found a similar increase in the spin concentration by heat treatment and attributed this to the desorption of absorbed oxygen and water.

Figure 3 shows the ESR spectra of the E-PI fractions and residues before and after treatment, for Zao Zhuang and Upper Freeport coals. For the E-PI fractions, there is no change in the shape of ESR spectra before and after the treatment. The spectra of the residue from Zao Zhuang coal is composed of two components, i.e., a broad and a narrow line. The treatment with pyridine showed no detectable narrow line. The origin of the narrow line is not clear at present. The disappearance of the narrow line may be related to the change of the mobility of coal segments by the pyridine treatment, although other explanations such as the change in chemical structure of the radicals have been suggested.[23,24]

Mechanisms for the Insolubilization of Coals. We reported[25] that addition of various compounds such as 7,7,8,8-tetracyanoquinodimethane (TCNQ), *p*-phenylenediamine, and anthracene increased the solubility of the E-PI fraction. We suggested that additives broke noncovalent interactions between coal molecules and made them extractable. However, in this case, the addition of TCNQ to the pyridine-treated Zao Zhuang coal did not increase the extraction yield at all.

Nishioka, Gebhard, and Silbernagel[26] suggested that a decrease in pyridine extractability for high-volatile bituminous coal by soaking in solvents is due to solvent-induced association by a charge-transfer interaction. In our case, however, no decrease was seen in the amount of pyridine-soluble fraction (E-PS). As a result, the following reasons may be considered for the insolubilization after the pyridine treatment. Some of coal soluble components were released and moved to the solvent phase from the coal, while the components retained inside the coal, i.e., mainly the E-PI fraction and residue, have many active (polar) sites, which before the treatment, might have interacted with the soluble components. So, the E-PI components retained in the coal could undergo any polymerization reaction (including the formation of noncovalent bonds) with other heavy molecules (E-PI or residue). We have also studied[27] the insolubilization behavior of extract fractions at 100–350 °C, in relation to a retrogressive reaction in coal liquefaction, and it will be reported elsewhere.

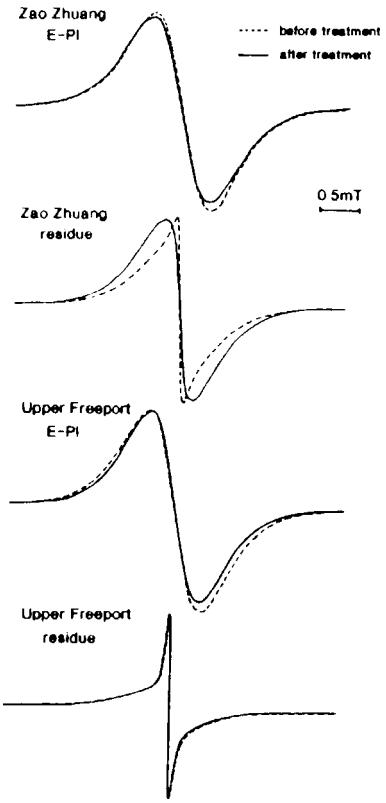

Figure 3. ESR spectra of the E-PI fractions and residues, before and after refluxing with pyridine for 1 day, for Zao Zhuang and Upper Freeport coals.

Registry No. E-PI, 110-86-1.

(21) Fowler, T. G.; Bartle, K. D.; Kandiyoti, R. *Fuel* **1987**, *66*, 1407–1412.
(22) Fowler, T. G.; Bartle, K. D.; Kandiyoti, R. *Fuel* **1988**, *67*, 1249–1254.
(23) Retcofsky, H. L.; Stark, J. M.; Friedel, R. A. *Anal. Chem.* **1968**, *40*, 1699–1704.
(24) Flowers II, R. A.; Gebhard L. A.; Larsen, J. W.; Silbernagel, B. G. *Energy Fuels* **1989**, *3*, 762–764.
(25) Sanokawa, Y.; Takanohashi, T.; Iino, M. *Fuel* **1990**, *69*, 1577–1578.
(26) Nishioka, M.; Gebhard, L. A.; Silbernagel, B. G. *Fuel* **1991**, *70*, 341–348.
(27) Shen, J.-L.; Takanohashi, T.; Iino, M., unpublished data.

On the solvent soluble constituents originally existing in Zao Zhuang coal

(*Received 22 April 1991*)

Dear Sir

Zao Zhuang coal (ZZ-1, Shan Tong province in China) was found to give a high extraction yield (63.0 wt%, daf) when it was exhaustively extracted with CS_2–*N*-methyl-2-pyrrolidinone (NMP) mixed solvent (1:1 v/v) at room temperature[1]. *Table 1* shows that another Zao Zhuang coal (ZZ-2), which was recently obtained, gave a much higher extraction yield (77.9 wt%, daf) with the mixed solvent under similar experimental conditions. The usual Soxhlet extraction of ZZ-2 coal with pyridine for 48 h gave an extraction yield of 36.3 wt%. *Table 1* also shows the ultimate, proximate and maceral analyses for the ZZ-1 and ZZ-2 coals. The maceral compositions were determined by microscopic analysis in an oil immersion using a reflected light according to Japanese Industrial Standard (JIS) 8816. Both coals are similar in elementary composition, volatile matter and fixed carbon content but differ in ash content and maceral composition. The higher extraction yield obtained for ZZ-2 coal may be attributed to the lower inertinite content, which is more difficult to extract than the other two macerals. *Table 2* shows the ultimate and proximate analyses of the CS_2–NMP mixed solvent extract [acetone insoluble (AI) fraction of the extract] and residue for ZZ-2 coal. The ash content was negligible for the extract. *Figure 1* shows the i.r. spectra of ZZ-2 coal, the AI fraction and the residue. The spectra are similar except there are no peaks due to mineral matter in the AI fraction.

Table 3 shows the results for solvent fractionation[1] of the extracts from the ZZ-1 and ZZ-2 coals. The pyridine insoluble (PI) fraction is a heavier fraction of the extract than a preasphaltene and can be obtained only by the use of the mixed solvent. The interesting solubilization behaviour of the PI fraction has been reported elsewhere[2]. *Table 3* shows that ZZ-2 coal has a similar acetone soluble content to ZZ-1 but a lower acetone insoluble and pyridine soluble (PS) content and higher PI content.

Coals are often considered to consist of solvent insoluble, covalently crosslinked networks and solvent soluble, low molecular weight substances trapped in the networks. Generally the quantity of the latter, i.e. the solvent soluble substances, is considered to be small, since even exhaustive Soxhlet extractions using pyridine, a good solvent for coal molecules, gave extraction yields of <40% (usually <30%) for bituminous coals[3]. There are several experimental results which suggest that for this mixed solvent extraction no solubilizing reactions such as covalent bond scissions in the coals between the solvents (CS_2 and NMP) and the coals occur[1]. So, the 79% extraction yield indicates that 79% of the extractable, solvent soluble substances exist originally in the coal. It is impossible to imagine that 80% of the solvent soluble substances are 'trapped' in the 20% of crosslinked networks.

Coals and their extraction residues are well known to swell upon exposure to a solvent due to their crosslinking structures. Recently extracts have also been reported[4,5] to swell with a solvent which does not dissolve the extract, suggesting that extracts also have a crosslinking network. This network may, however, consist of non-covalent crosslinks such as

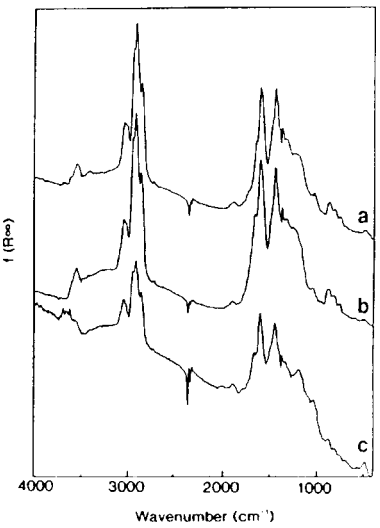

Figure 1 FT-i.r. spectra of: a, Zao Zhuang coal (ZZ-2 coal); b, its extract (AI fraction); c, the residue. $f(R_\infty)$ is the Kubelka – Munk function for the diffuse reflectance measurement

Table 2 Ultimate and proximate analyses of ZZ-2 coal, its extract and residue

	Ultimate analyses (wt%, daf)				Proximate analyses (wt%, dry basis)		
	C	H	N	S+O[b]	Volatile matter	Ash	Fixed carbon
ZZ-2 coal	87.8	5.2	1.4	5.6	26.4	13.1	60.5
Extract[a]	86.7	5.4	2.4	5.5	28.6	0.0	71.4
Residue	84.2	4.3	1.3	10.2	14.3	41.2	44.5

[a] Acetone insoluble fraction (acetone insoluble and pyridine soluble + pyridine insoluble fraction) of the extract
[b] By difference

Table 1 Properties and extraction yields of the two Zao Zhuang coals

Coal	Extraction yield (wt%, daf)[a]	Ultimate analyses (wt%, daf)				Proximate analyses (wt%, dry basis)			Maceral composition (vol%)		
		C	H	N	S+O[b]	Volatile matter	Ash	Fixed carbon	V[c]	I[d]	L[e]
ZZ-1	63.0	86.9	5.5	1.5	6.1	28.6	7.4	64.0	68.5	29.7	1.8
ZZ-2	77.9	87.8	5.2	1.4	5.6	26.4	13.1	60.5	78.3	19.3	2.4

[a] The coals were extracted with CS_2–NMP mixed solvent (1:1 v/v) exhaustively (five to six times under ultrasonic irradiation) at room temperature
[b] By difference
[c] Vitrinites
[d] Inertinites
[e] Liptinites

0016-2361/91/101236-02

Masashi Iino,
Toshimasa Takanohashi,
Tadashi Ohkawa
and Takayuki Yanagida
Institute for
Chemical Reaction Science,
Tohoku University,
Katahira 2-1-1,
Aoba-ku, Sendai 980, Japan

Table 3 Fractionation of the extracts

Coals	Extraction yield (wt%, daf)	Residue (wt%, dry basis)	Extract (wt%, dry basis)	Extract (wt%, dry basis)		
				AS[a]	PS[b]	PI[c]
ZZ-1	63.0	41.7	57.6	6.7	24.3	26.0
ZZ-2	77.9	32.3	67.5	6.6	17.7	43.2

[a] Acetone soluble fraction
[b] Acetone insoluble and pyridine soluble fraction
[c] Pyridine insoluble fraction

hydrogen bonds and π–π interactions, and the contribution of covalent bonds is probably small, since extracts are soluble in the solvent which extracted them and the network consisting of mainly covalent bonds should be insoluble in any solvent. It is not unlikely that extraction residues also have mainly non-covalent bonded crosslinks and few covalent ones, at least, for some bituminous coals. The nature of the crosslinks in coals is a key factor not only for the elucidation of coal structure, but also for the development of a new, effective coal conversion process. Further studies are needed in this area.

REFERENCES

1 Iino, M., Takanohashi, T., Obara, S. *et al. Fuel* 1988, **67**, 1639
2 Sanokawa, Y., Takanohashi, T. and Iino, M. *Fuel* 1990, **69**, 1577
3 Green, T., Kovac, J., Brenner, D. *et al.* in 'Coal Structure' (Ed. R. A. Meyer), Academic Press, New York, 1982, Ch. 6, p. 272
4 Aida, T. Report for the 17th meeting of the committee on Coal Utilization Technology of Japan Society for the Promotion of Science, 1987, p. 18
5 Green, T. K., Chamberlin, J. M. and Lopez-Froedge, L. *Am. Chem. Soc. Div. Fuel Chem. Prepr.* 1989, **34**(3), 759

Carbon Vol. 29, Nos. 4/5, pp. 541–546, 1991
Printed in Great Britain.

0008-6223/91 $3.00 + .00

MODIFICATION OF MESOPHASE FORMATION DURING THE CARBONIZATION OF ACENAPHTHYLENE BY THE ADDITION OF ACENAPHTHENE

OSAMU ITO, TOMOKI KAKUTA, and MASASHI IINO
Chemical Research Institute of Non-Aqueous Solution, Tohoku University, Katahira, Aoba-ku, Sendai, 980-Japan

(*Received* 17 *July* 1990; *accepted in revised form* 10 *October* 1990)

Abstract—The carbonization of acenaphthylene was affected by the addition of acenaphthene, which is the dihydride derivative of acenaphthylene. The addition of 10 to 20 wt% acenaphthene promoted the formation of the spherical mesophase compared with acenaphthylene alone in the heat-treatment temperature region of 500 to 540°C. Further addition of acenaphthene (30–40 wt%) reduced the mesophase formation and resulted in isotropic materials. The role of added aceaphthene in the carbonization of acenaphthylene was assessed employing spectroscopic measurements such as FT-IR, X-ray diffraction, FD mass spectrometer, and ESR, in addition to solvent separation and elemental analysis.

Key Words—Acenaphthylene, cocarbonization, mesophase.

1. INTRODUCTION

It is well known that mesophase pitch is an important precursor for further carbonaceous materials such as carbon fiber[1–3]. In the carbonization of aromatic hydrocarbons and pitches, hydrogenation treatment enhances the formation of the optical anisotropic textures including spherical mesophase. It was believed that the hydrogenation decreases the viscosity of the reaction system by the formation of the flexible naphthenic moiety[4–6]. For the aromatic hydrocarbons, the partially hydrogenated pyrene can be converted into the optical anisotropic textures, especially into spherical mesophase in high yield[7]. In the case of acenaphthylene, although acenaphthylene alone yields the mesophase spheres[8], hydrogenation of acenaphthylene pitches promotes the formation of the spherical mesophase[9]. Thus, it is important to clarify the relation between the degree of the hydrogenation and the property of the resultant carbonaceous materials. It is, however, difficult to determine quantitatively the degree of hydrogenation of intermediate pitches. In this study, we examined the carbonization of acenaphthylene (AN) by adding known amounts of acenaphthene (ANH) under various heat-treatment conditions (Fig. 1). ANH is also considered as one of the intermediates of carbonization of AN and plays an important role in mesophase formation[10].

In such reaction systems, we can control the amount of ANH and find out its role explicitly. We report that the addition of a small amount of ANH exhibits an excellent promotion effect on the formation of the mesophase of AN. The chemical structures of the carbonaceous materials and the reaction mechanism were examined by applying various spectroscopic methods.

2. EXPERIMENTAL

2.1 *Materials, heat treatments, and solvent extraction*

AN and ANH (reagent grade; Wako Chemical Co., Ltd.) were used without further purification. Benzene and pyridine used for the solvent separation of carbonaceous components were also reagent grade.

In a Pyrex tube (14 mm diameter and 50 cm long) a mixture of acenaphthylene and acenaphthene in various ratios (5 g) was heated under a flow of N_2 at atmospheric pressure with the heating rate of 10°C/min. During the heat treatment of the lower part (25 cm) of the reaction tube in a vertical furnace, reddish material began to reflux at the upper part. After maintaining the sample at the heat-treatment temperature (HTT) for a time, the reaction tube was gradually cooled down to room temperature.

The carbonaceous materials obtained were pulverized and separated with hot benzene into the soluble fraction (BS) and insoluble one (BI). After weighting both fractions, the BI fraction was separated with hot pyridine into pyridine soluble (BI-PS) and insoluble (PI) fractions.

2.2 *Microscopic observation and spectroscopic measurements*

The carbonaceous materials were potted in epoxy resin, polished, and observed with an Olympas BH-2 microscope with crossed Nicol polarizers. FT-IR spectra were measured with a JEOL J-100 FT-IR spectrometer equipped with a diffuse reflectance apparatus[11].

X-ray diffractions of the PI fractions (<60 mesh) were measured with a JEOL DX-GO-SR x-ray dif-

Fig. 1. Structure of starting compounds.

fractometer equipped with a JRX-12-VB rotating x-ray generator. Analyses of (002) and (11) bands yielded the average structural parameters such as interlayer distance, stacking number, and size of the layer[12].

Field desorption (FD) mass spectra were measured with a JEOL D-300. The PI fraction was attached to the carbon emitter after dissolving it in a mixed-solvent (N-methyl-2-pyrrolidinone-CS_2), which could dissolve the PI fraction and be evaporated more easily than quinoline.

ESR spectra were measured with a JEOL FE3X spectrometer at room temperature. The sample (20 mg) in a quartz sample tube connected with Pyrex tube was degassed and sealed off under vacuum. The spin concentration was obtained by comparing the double integration with that of a standard sample. Since the ESR intensity of the carbonaceous materials showed saturation phenomenon with microwave power, the spin concentrations were evaluated at powers before the onset of saturation. From the saturation phenomenon, we can evaluate the microwave power which results in maximum intensity (P_{max}), which is related to the spin-lattice relaxation time[13,14].

3. RESULTS AND DISCUSSION

3.1 *Microscopic observation*

In Table 1, microscopic observations are summarized; in Fig. 2, some photographs are shown. As shown in Fig. 2a, carbonization of AN alone at 500°C tends to yield fine anisotropic optical texture with many pores; we referred to this texture as fine flow. On addition of 10 wt% ANH to AN at 500°C (Fig. 2b), stick-like mesophase was formed. On addition of 20 wt% ANH, corolla-like mesophase begins to form (Fig. 2c). These shapes suggest that both the carbonization reaction and the orientation of the carbonaceous materials seem to be incomplete because of high viscosity of the reaction system at such a low temperature. With an increase in HTT up to 540°C, the AN pitch produced by adding 20 wt% ANH exhibits spherical mesophase (Fig. 2d). This indicates that the viscosity of the carbonaceous material becomes sufficiently low for the formation of mesophase spheres. By the heat treatment of the spherical mesophase at a higher temperature (580°C), it changed into bulk flow optical texture (Fig. 2e). On prolonged heat treatment of the spherical mesophase at 540°C, the spherical mesophase also changed into the bulk flow texture. Further addition of 30 wt% ANH gives rise to a needle-like texture (Fig. 2f), suggesting that the carbonization of AN was retarded by excess ANH. On addition of more than 40% ANH, the most part was isotropic.

In the case of carbonization of AN containing 20 wt% ANH, it can be clearly shown that the carbonization steps proceed from the spherical mesophase to the bulk flow texture when HTT and HT-time

Table 1. Optical texture

ANH(%)	HTT(°C)	HT-time(h)	Optical texture	Fig. 1
0	500	2	Fine flow (ffl)†	a
10	500	2	Stick-like (st)	b
20	500	2	Spherical mesophase (sm(co))‡	c
30	500	2	Isotropic (iso)	
40	500	2	iso	
0	500	4	ffl	
20	500	4	sm(co)	
40	500	4	iso	
0	540	1	ffl	
10	540	1	ffl	
20	540	1	sm	d
30	540	1	Needle-like (nd)	
40	540	1	iso	
0	540	2	ffl	
10	540	2	Bulk flow (bfl)	e
20	540	2	bfl	
30	540	2	nd	f
40	540	2	iso	
0	580	1	ffl	
10	580	1	ffl	
20	580	1	bfl	
30	580	1	iso	
40	580	1	iso	

†Abbreviations given in parentheses.
‡Corolla-like shape is abbreviated as sm(co).

Table 2. Elemental analysis for some PI fractions

Carbonaceous material†	C(%)	H/C
ANH00-500-4-ffl	94.6	0.41
ANH20-500-4-sm	93.6	0.55
ANH40-500-4-iso	95.3	0.54
ANH00-540-1-ffl	95.2	0.36
ANH20-540-1-sm	94.1	0.48
ANH40-540-1-iso	93.1	0.49
ANH00-540-2-ffl	94.7	0.42
ANH20-540-2-bfl	94.7	0.46
ANH40-540-2-iso	94.3	0.53
ANH00-580-1-ffl	94.9	0.35
ANH20-580-1-bfl	94.0	0.43
ANH40-580-1-iso	93.8	0.53

†Designated as follows: (ANH; wt%)-(HTT; °C)-(HT-time; h)-(optical texture).

when ANH is not added. The high H/C value of isotropic material suggests that the aromatization reaction of AN is retarded by excess ANH. The moderate H/C value indicates that the carbonization of spherical mesophase is a stage intermediate between the isotropic material and flow texture. A change from the spherical mesophase to flow texture by prolonged heat treatment (ANH 20 wt% at 540°C) occurs without appreciable change in the H/C value, suggesting that this change is caused by the phase change with only small chemical changes.

The H/C values of decacyclene and zethrene, which are well-known intermediates of the carbonization of AN, are 0.50 and 0.58, respectively[15,16]; the H/C values of zethrene dimer and trimer are 0.42 and 0.36, respectively. Thus, it is presumed that the former compounds are contained in carbonaceous materials produced at low HTT with high ANH content. The latter compounds are included in the products obtained at high HTT with less ANH.

3.4 *FD-mass spectral data*

The FD mass spectra are shown in Fig. 4. Figure 4a is the spectrum for the PI fraction of the isotropic material with excess ANH. A main peak at m/e = 450 is due to decacyclene. At higher molecular weight region than m/e = 450, weak peaks appear. In the FD mass spectrum for the spherical mesophase (Fig. 4b), the peaks at higher molecular weights than the decacyclene peak increase. Some of the strong peaks are attributed as follows: $m/e \cong 600$ and 900 are zethrene dimer and trimer, respectively. The peak at $m/e \cong 750$ is due to adducts such as decacyclene-zethrene or 5 pentamer of AN. Since the PI fractions showing flow textures are insoluble in any solvent, the FD mass spectrum was not measured.

3.5 *FT-IR measurements*

The diffuse reflectance spectra of the carbonaceous materials are shown in Fig. 5. Before the solvent separation of the carbonaceous material exhibiting spherical mesophase, the sharp IR bands characteristic of low molecular weight compounds appeared as shown in Fig. 5a, which seems to be a mixture of starting compounds, polymer, decacyclene, and highly condensed aromatic hydrocarbons[17]. The PI fraction of the isotropic material with excess ANH (Fig. 5b) may also show the sharp IR bands; the polymers connecting the low molecular weight compounds with C—C single bonds may be included. The bands at 3030 and 900 to 600 cm^{-1} which are attributed to the aromatic C—H[18] decrease in the order of isotropic < spherical mesophase < flow texture. The broad absorption band in the near-IR region is attributed to the aromatic hydrocarbons with large size[11]. With the decrease in the aromatic C—H bands, the broad near-IR band increases on going from isotropic material to spherical mesophase (Fig. 5c). In the PI fraction showing the flow texture (Fig. 5d), the aromatic C—H bands decrease with the further broadening of the near-IR band, suggesting that the further carbonization to coke occurs. The IR band of the aliphatic C—H groups would be expected in 2950 to 2850 cm^{-1} and 1500 to 1400 cm^{-1}, in which the latter is superimposed with other bands. The weak band at 2900 cm^{-1} implies that a very small amount of aliphatic C—H

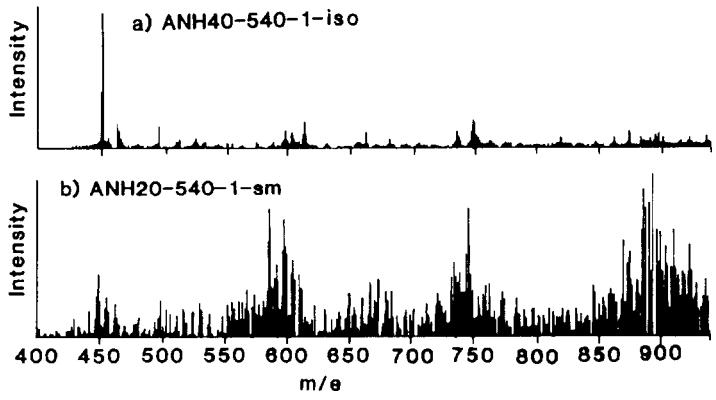

Fig. 4. FD mass spectra of PI fractions.

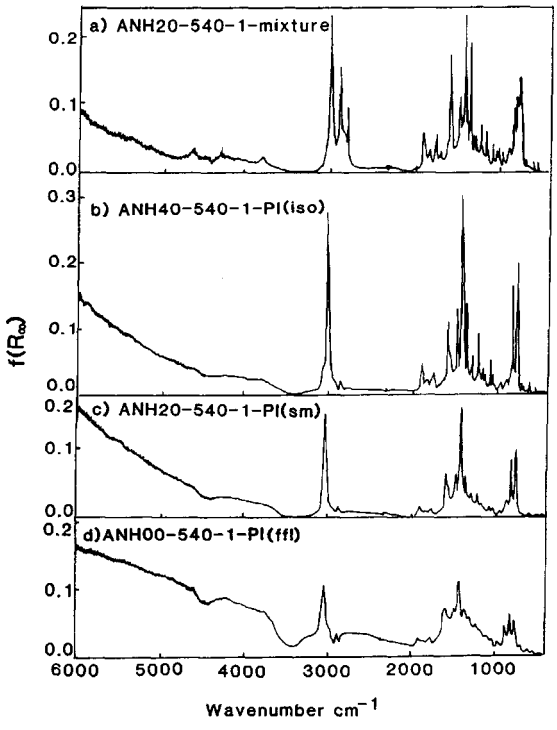

Fig. 5. FT-IR spectra measured with diffuse reflectance method in the region of near-IR and IR (1 mg sample/150 mg KBr).

is involved in the spherical mesophase even though ANH is added.

In Fig. 5a, the peaks at 2919 and 2837 cm^{-1} are characteristic of ANH; considerable amounts of added ANH remain in the reaction system after heat treatment at 540°C. The ANH peaks were observed by the heat treatment of AN alone at 540°C, when HT-time was shorter than 1 hour. This suggests that ANH is produced from AN as indicated by Lewis and Edstron [10]. It is presumed that the presence of appropriate amount of ANH in the reaction system may play an important role in the mesophase formation of the carbonaceous materials from AN (i.e., at moderate HTT, ANH affords an appropriately viscous reaction system in addition to the role of the hydrogen donor).

3.6 *X-ray diffraction*

From x-ray diffraction of the PI fractions, the average distance between the stacked layers (d), thickness of each stack (L_c), number of layers per stack (n), the size of the layer (L_a), and the ring number of the layer (m) were evaluated[12]; they are summarized in Table 3. Although there may be a large estimated error in the analysis of the (11)-band, the L_a and m values seem to be invariant for the carbonaceous materials exhibiting different optical textures. On the other hand, the L_c and n values differ among the kinds of the carbonaceous materials; the spherical mesophases have smaller L_c and n values than those of flow optical textures.

3.7 *ESR parameters*

The carbonaceous material produced from AN with and without ANH showed the symmetric single ESR signal at $g = 2.00$, indicating the existence of carbon radicals; in Fig. 6, four typical spectra are shown. By addition of ANH, a broadening of the ESR signal was observed; at ANH = 30 wt%, the ESR signal was composed of two signals. The spin concentration and linewidth are summarized in Table 4, in which the P_{max} values are also listed.

At HTT = 540°C, the spin concentration is highest, excepting isotropic material. At low HTT such as 500 and 540°C, the spin concentration decreases by the addition of ANH. The linewidth tends to increase with the hydrogen content in Table 2, indicating that the linewidth is determined by the hyperfine interaction; this implies that the linewidth reflects the hydrogen content near the radical center. For each HTT, the linewidth increases with the ANH content. This is an evidence that ANH is a main source of hydrogen atoms during the carbonization reaction of AN.

The P_{max} value is decreased by addition of 10 to 20 wt% ANH compared with that of AN. By further addition of ANH more than 30 wt%, the P_{max} value is increased. This suggests that the mobility of the molecules in the carbonaceous material produced by the presence of appropriate amount of ANH is increased[14]. On addition of excess of ANH, the mobility of the molecules in the carbonaceous materials decreases. From these findings, the spherical

Table 3. X-ray diffraction data for some representative PI samples

	Stack thickness	Distance		Size	
Samples	L_c, A	d, A	n†	L_a, A	m‡
ANH00-500-2-ffl	31.4	3.45	9.1	13.8	24
ANH00-540-1-ffl	25.5	3.45	7.3	15.0	27
ANH20-540-1-sm	29.1	3.48	8.4	15.1	27
ANH00-540-2-ffl	28.1	3.46	8.1	15.3	25
ANH20-540-2-bfl	40.8	3.47	11.8	14.2	25
ANH20-580-1-bfl	40.8	3.45	11.8	14.2	25

†n; number of layers per stack.
‡m; ring number.

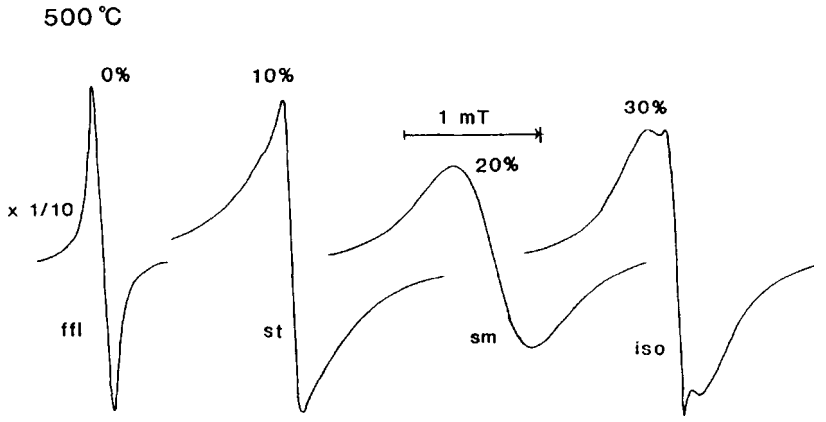

Fig. 6. Typical ESR signals for PI fraction obtained at HTT = 500°C.

mesophase and bulk-flow optical texture can be presumed to consist of loosely stacked aromatic hydrocarbons, which is probably caused by the formation of hydroaromatic moieties in the presence of appropriate amounts of hydrogen generated from ANH.

4. CONCLUSIONS

We examined the effect of the addition of ANH on the carbonization of AN under various conditions. It was found that addition of 10 to 20 wt% ANH led to a significant improvement of the formation of spherical mesophase. Carbonization of AN alone yielded fine flow texture, suggesting that the carbonization proceeds rapidly without passing through the spherical mesophase stage. On addition of 20 wt% ANH, the carbonaceous materials exhibited the spherical mesophase and flow optical texture. The chemical and spectroscopic observations suggest that the carbonization of AN is appropriately controlled by the addition of ANH.

Table 4. ESR parameters

Samples	Spin con.† × 10^{-19}/g	Linewidth‡ *mT*	P_{max}§ *mW*
ANH00-500-2-ffl	1.3	0.09	14
ANH10-500-2-st	0.34	0.14	10
ANH20-500-2-sm	0.21	0.49	8
ANH30-500-2-iso	0.47	0.35	—‖
ANH00-540-1-ffl	30	0.20	10
ANH10-540-1-ffl	13	0.34	—‖
ANH20-540-1-sm	17	0.36	7
ANH30-540-1-iso	1.5	0.50	17
ANH00-580-1-ffl	3.3	0.09	8
ANH10-580-1-ffl	3.8	0.24	7
ANH20-580-1-bfl	6.1	0.21	13
ANH30-580-1-iso	3.0	0.10	10

†Total spin concentration.
‡The broader linewidth is cited when dual signals were observed.
§P_{max} for the broader signal is cited for dual signals.
‖The saturation was not observed.

Acknowledgment—We are grateful to Professor S. Suzuki and Dr. N. Tsuchiya of Tohoku University for their useful suggestions to the microscopic observations and x-ray diffraction measurements.

REFERENCES

1. S. Otani, *Mol. Cryst. Liq. Cryst.* **63**, 249 (1981).
2. L. S. Singer, *Fuel* **60**, 839 (1981).
3. H. Marsh, C. S. Latham and E. M. Gray, *Carbon* **23**, 555 (1985).
4. I. Mochida and H. Marsh, *Fuel* **58**, 790 (1979).
5. T. Obara, T. Yokono, K. Miyazawa and Y. Sanada, *Carbon* **19**, 263 (1981).
6. G. Bhatia, E. Fitzer and D. Kompalik, *Carbon* **24**, 489 (1986).
7. I. Mochida, Y. Sone and Y. Korai, *Carbon* **23**, 175 (1985).
8. I. Mochida and H. Marsh, *Fuel* **58**, 626 (1979).
9. Y. Yamada, M. Shiraishi, T. Furuta, T. Yamakawa and Y. Sanada, *Bull. Chem. Soc. Jpn.* **57**, 3027 (1984).
10. I. C. Lewis and T. Edstron, *J. Org. Chem.* **28**, 2050 (1963).
11. O. Ito, H. Seki and M. Iino, *Fuel* **67**, 573 (1988).
12. T. F. Yen, J. G. Erdman and S. S. Pollack, *Anal. Chem.* **33**, 1587 (1961).
13. O. Ito, H. Seki and M. Iino, *Bull. Chem. Soc. Jpn.* **60**, 1967 (1987).
14. O. Ito, T. Kauta and M. Iino, *Carbon* **27**, 869 (1989).
15. L. S. Singer and I. C. Lewis, *Carbon* **2**, 115 (1964).
16. E. Fitzer, K. Muller and W. Schaefer, In *Chemistry and Physics of Carbon* (Edited by P. L. Walker, Jr. and P. A. Thrower), Vol. 7, p. 237, Marcel Dekker, New York (1970).
17. M. Nakamizo and K. Tamai, *Carbon* **23**, 193 (1984).
18. P. Painter, M. Starsinic and M. Coleman, *Fourier Transfer Infrared Spectra; Chemical Application*, Vol. 4, p. 169, Academic Press, New York (1985).

Reprinted from ENERGY & FUELS, 1992, 6.

Thermal Behavior of Coals at Temperatures as Low as 100–350 °C: Heat Treatment of THF-Insoluble Extract from CS_2–NMP Mixed Solvent Extraction of Zao Zhuang Coal

Jian-Li Shen, Toshimasa Takanohashi, and Masashi Iino*

Institute for Chemical Reaction Science, Tohoku University, Katahira 2-1-1, Aoba-ku, Sendai 980, Japan

Received July 7, 1992. Revised Manuscript Received September 16, 1992

Heat treatment of THF-insoluble, CS_2–*N*-methyl-2-pyrrolidinone (NMP) mixed solvent (1:1 by volume) soluble fraction (TIMS) of the extract, which was obtained from the extraction of Zao Zhuang coal with the same mixed solvent at room temperature, was carried out in several organic solvents at 100–350 °C under N_2 atmosphere. Retrogressive reaction of TIMS, i.e., its conversion to the mixed solvent-insoluble fraction (MI), was observed in tetralin (TET), naphthalene (NAP), and 9,10-dihydrophenanthrene (DHP) at temperatures as low as 100 and 175 °C, while MI formation at 175 °C was suppressed by adding 9,10-dihydroanthracene (DHA) or 1,4,5,8,9,10-hexahydroanthracene (HHA), which are much stronger hydrogen donors than TET, NAP, or DHP. Moreover, by these treatments, the THF-soluble fraction (TS), the lighter fraction than TIMS, was formed from TIMS. The quantity of hydrogen transferred from the solvents to TIMS and/or TIMS moieties was found to be well correlated with the quantity of MI formed. By a similar heat treatment in DHA at 175 °C, Zao Zhuang raw coal was found to undergo dissolution reactions, i.e., the increase of TS and the decrease of MI, compared with those originally existing in the raw coal. The mechanism of the MI formation and its suppression during the heat treatments of TIMS at low temperatures is discussed.

Introduction

CS_2–*N*-methyl-2-pyrrolidinone (NMP) mixed solvent (1:1 by volume) gave high extraction yields (40–65%, daf) at room temperature for many bituminous coals.[1,2] No significant occurrence of reactions of the solvents with the coals, which would result in an increase of the extraction yields, is indicated, suggesting that the extracts obtained originally existed in the coals.[2] It was also found[3] that the extracts obtained with the CS_2–NMP mixed solvent include a considerable amount of the heavy fraction which is not soluble in THF or pyridine but is soluble in the mixed solvent.[3]

We have used the mixed solvent as an extraction solvent for the dissolution reaction products of the bituminous coals at 300–450 °C in tetralin (TET) or naphthalene (NAP) without a catalyst.[4] The extracts obtained after the dissolution reaction were fractionated into THF-insoluble, mixed solvent-soluble fraction (TIMS), preasphaltene, asphaltene, and oil by using THF, benzene, and *n*-hexane, respectively. The change of the yields of each fractions with experimental conditions showed that retrogressive reactions occur most readily for the heaviest fraction, i.e., TIMS, which can be obtained only by the use of the mixed solvent.

Berkowitz, Calderon, and Liron[5] reported that substantial retrogressive reactions (reversions of toluene-soluble to toluene-insoluble matter) occur during heating to, as well as cooling from, 400 °C in the dissolution experiments of Canadian subbituminous coals in TET at 400 °C under nitrogen atmosphere. They also found the occurrence of dissolution reaction at temperatures as low as 250 °C and discussed the mechanisms from the possibilities of homolysis of weak bonds, preasphaltene–asphaltene equilibria, and partial dispersal of physically entangled molecules.

In this study, the heat treatments of TIMS from Zao Zhuang coal, which gave 50% (daf, based on the raw coal) of TIMS by the extraction with the mixed solvent, were carried out at low temperatures of 100–350 °C in various solvent systems including TET, NAP, 9,10-dihydrophenanthrene (DHP), 9,10-dihydroanthracene (DHA), 1,4,5,8,9,10-hexahydroanthracene (HHA), anthracene (ANT), and NMP. TIMS was found to be converted to the heavier fraction (the mixed solvent-insoluble fraction (MI), the residue) or the lighter fraction (THF-soluble fraction (TS)), depending on the solvent system used. The mechanism for these conversions is discussed.

Experimental Section

Materials. Zao Zhuang coal (China) was ground to −60 mesh (−250 μm) and dried in vacuo at 107 °C to constant weight (2–3 h). Its ultimate and proximate analyses are given in Table I. TIMS was obtained as follows: Zao Zhuang coal was extracted exhaustively with the CS_2–NMP mixed solvent (1:1 by volume) at room temperature. The extraction yield (daf) was 65%. The extract obtained was washed with an acetone–water mixed solvent (2:8 by volume) and fractionated into TIMS (77% of the extract, 50% (daf) of the raw coal) and THF-soluble fraction (TS) with THF at room temperature under ultrasonic irradiation (38 kHz), by the procedure described elsewhere.[2,4] The ultimate analysis

(1) Iino, M.; Kumagai, J.; Ito, O. *J. Fuel Soc. Jpn.* **1985**, *64*, 210–212.
(2) Iino, M.; Takanohashi, T.; Ohsuga, H.; Toda, K. *Fuel* **1988**, *67*, 1639–1647.
(3) Iino, M.; Takanohashi, T.; Obara, S.; Tsueta, H.; Sanokawa, Y. *Fuel* **1989**, *68*, 1588–1593.
(4) Wei, X.-Y.; Shen, J.-L.; Takanohashi, T.; Iino, M. *Energy Fuels* **1989**, *3*, 575–579.
(5) Berkowitz, N.; Calderon, J.; Liron, A. *Fuel* **1988**, *67*, 626–631, 1017–1019, 1139–1142.

0887-0624/92/2506-0854$03.00/0

Table I. Ultimate and Proximate Analyses of Zao Zhuang Coal and Its TIMS Fraction

	ultimate analysis (wt %, daf)					proximate analysis (wt %, db)		
	C	H	N	S	O[a]	VM	ash	FC
raw coal	86.9	5.1	1.5	1.6	4.9	28.6	7.4	64.0
TIMS	86.3	5.4	1.9	1.8	4.6		0.0	

[a] By difference.

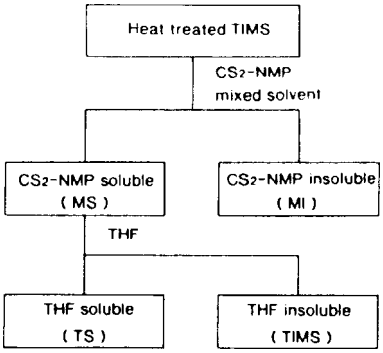

Figure 1. Fractionation procedure of the heat-treated TIMS.

of TIMS is also shown in Table I. Reagent grade solvents were used without further purification.

Heat Treatment and Solvent Fractionation. Heat treatment of TIMS was carried out at 100, 175, 250, 300, and 350 °C for 1 h in a solvent or a solvent mixture, under N_2 atmosphere, by using a 100-mL magnetically stirred autoclave. Then, 1 g of TIMS, 5 g of a solvent, and 5 MPa of N_2 were charged, and after the heat treatment the mixture was fractionated into the mixed solvent-insoluble fraction (MI) and -soluble fraction (MS) and then further into TIMS and TS (and the solvent), at room temperature with the mixed solvent and THF under ultrasonic irradiation, as shown in Figure 1. The MI and TIMS obtained were washed with acetone and the acetone–water mixed solvent (2:8 by volume) respectively and were dried in vacuo at 80 °C and weighed. The conversion (wt %) into TS was calculated by the difference, i.e., 100 − MI − TIMS.

Analyses of the Heat-Treated Products. FT-IR spectra of TIMS and other fractions after the heat treatment were measured by the diffuse reflectance method. ^1H NMR spectra were measured in CS_2–pyridine-d_5 mixed solvent (1:1 by volume). ESR spectra were obtained on a Varian E-4 spectrometer at room temperature, and the spin concentrations were determined by using diphenylpicrylhydrazyl (DPPH) as a standard sample. The quantities of NAP, ANT, and phenanthrene, which were formed from the corresponding hydrogenated solvents, were determined by GC analysis, assuming that the area ratios of non-hydrogenated solvent/hydrogenated solvent equal are to their weight ratios.

Results

Heat Treatment of TIMS in TET, NAP, and Their Mixtures with DHA and HHA. Figures 2 and 3 show the fraction distributions after the heat treatments of TIMS in TET and NAP at 100–350 °C. The raw TIMS was found to include a small amount of TS (3.6%) and MI (0.4%) due to the incomplete solvent fractionation, as shown in Figure 2. The formation of MI, a heavier fraction than TIMS, was observed at 100–350 °C in NAP and at 100–250 °C in TET. TS, a lighter fraction than TIMS, was also formed by these treatments. The plots (Figure 4) of the yield of MI vs the heat treatment temperature for the both solvents show that TET gave the yields similar to those for NAP at 100–250 °C but zero yield at 300–350 °C.

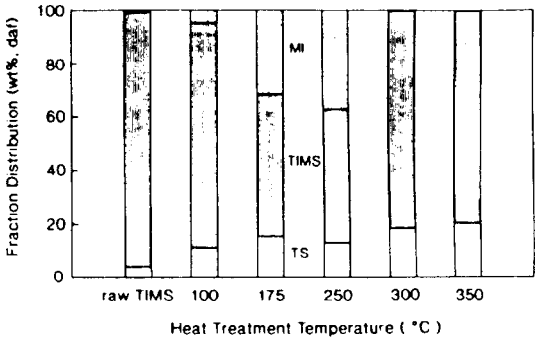

Figure 2. Fraction distribution after the heat treatments of TIMS in TET.

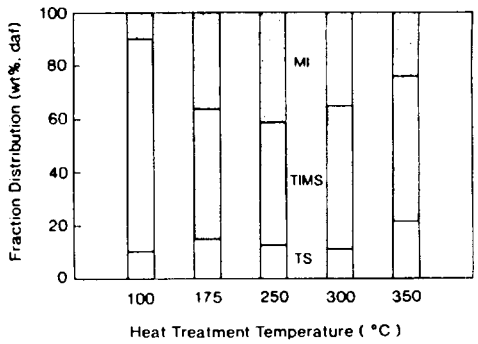

Figure 3. Fraction distribution after the heat treatments of TIMS in NAP.

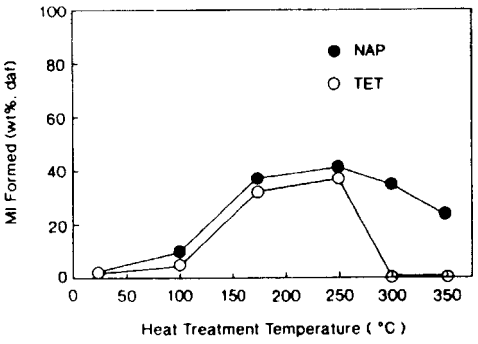

Figure 4. Plot of MI weight percent (based on TIMS used) formed versus heat treatment temperatures in NAP (●) and TET (○).

Figure 5 shows the fraction distributions after heat treatment of TIMS in mixtures of TET with DHA, HHA, and DHP. As the weight ratio of DHA increased, the quantity of MI formed at 175 °C decreased, and HHA was more efficent than DHA but DHP was inefficient. DHA is also efficient for the suppression of MI formation at 250 °C. Figure 6 shows the results for the mixed solvents of NAP with HHA at 175 °C. Like the case of TET–DHA mixed solvents, the quantity of MI formed decreased as HHA increased. NAP–HHA, 10:1 mixed solvent gave similar MI yield as the corresponding TET–HHA mixed solvent.

Heat Treatment of TIMS in TET–ANT Mixtures and Other Solvents. The results for the heat treatments of TIMS in 1:1 TET–ANT mixed solvent are shown in Figure 7, together with those for TET alone. The mixed solvent gave lower yield of MI at 250 °C but higher yield

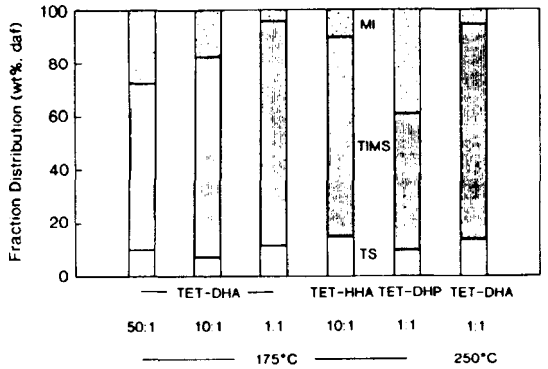

Figure 5. Fraction distribution after the heat treatments of TIMS in the mixtures of TET with DHA, HHA, and DHP mixed solvents. Solvents, their weight ratios (TET:solvent), and the heat treatment temperatures are shown below the abscissa.

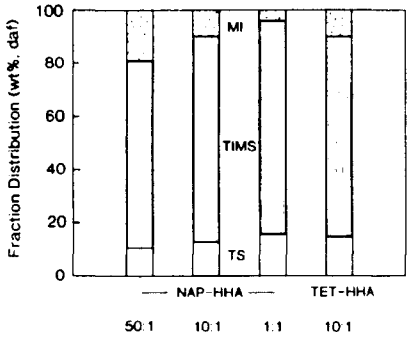

Figure 6. Fraction distribution after the heat treatments of TIMS at 175 °C in the mixtures of NAP or TET with HHA mixed solvents. Solvents and their weight ratios (NAP or TET: HHA), are shown below the abscissa.

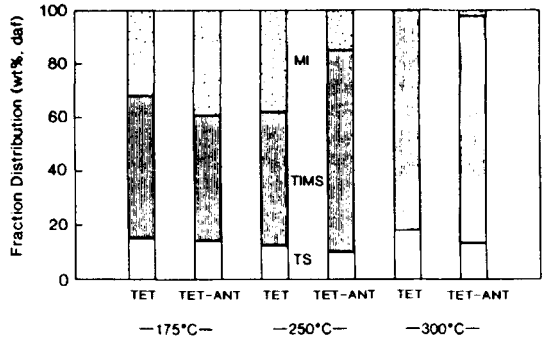

Figure 7. Fraction distribution after the heat treatments of TIMS in TET and TET-ANT mixed solvent (1:1 by weight). Solvents and the heat treatment temperatures are shown below the abscissa.

at 175 °C. Figure 8 shows the results for the heat treatments of TIMS in TET, NAP, ANT, DHA, HHA, DHP, and NMP at 175 °C. DHA, HHA, and NMP gave little MI, but DHP gave much more MI than TET and NAP.

Heat Treatment of Zao Zhuang Raw Coal, MI, and TS. Figure 9 shows the fraction distribution after the heat treatments of Zao Zhuang coal, together with that for the raw coal, which was obtained from the fractionation of the extract from the extraction of the raw coal with the CS_2-NMP mixed solvent at room temperature. Figure 9 shows that TET gave higher yields of MI and TS, and

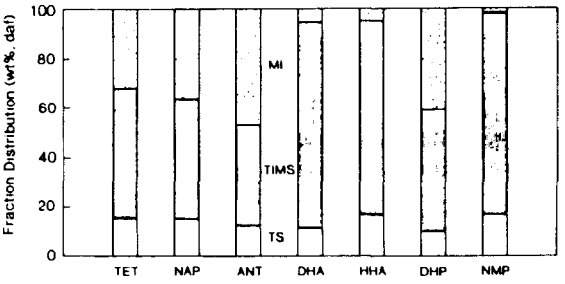

Figure 8. Fraction distribution after the heat treatments of TIMS at 175 °C in TET, NAP, ANT, DHA, HHA, DHP, and NMP.

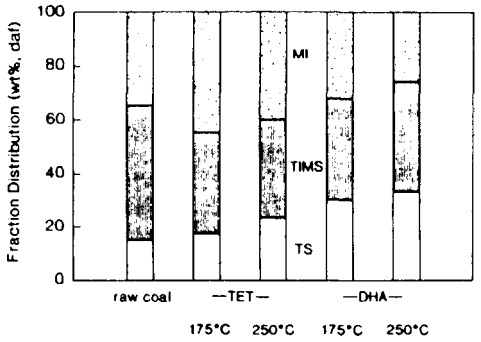

Figure 9. Fraction distribution before and after the heat treatments of Zao Zhuang raw coal in TET and DHA. Solvents and the heat treatment temperatures are shown below the abscissa.

DHA gave lower yields of MI and higher yields of TS at 175 and 250 °C, than those for the raw coal. The heat treatments of MI, in NAP, DHA, and HHA at 175 °C, gave 3.6, 5.0, and 5.7% of TIMS and 4.7, 10.1, and 10.5% of TS, for NAP, DHA, and HHA, respectively, while the heat treatments of TS in NAP and DHA at 175 °C recovered 99.5 and 100% of TS for NAP and DHA, respectively.

IR Spectra of MI and TIMS after the Heat Treatment. IR spectra of raw TIMS (a) and MI formed by the heat treatment of TIMS in TET at 250 °C (b), 175 °C (c), and 100 °C (d) are shown in Figure 10. Little difference between TIMS and MI formed was observed. Other IR spectra such as MI formed and TIMS by the heat treatments of TIMS in NAP, TET-DHA, and TET-ANT also show little difference, as compared with the raw TIMS.

Hydrogen Transferred from the Solvents to TIMS. The quantities of hydrogens transferred from DHA and DHP to TIMS (and/or its moieties formed during the heat treatment) were determined from the GC analysis of the ANT and phenanthrene formed, respectively. For HHA it was determined from the quantity of tetrahydroanthracene which was identified as a main product by GC/MS analysis of the the mixture after heat treatment. For the TET-ANT mixture at 250 °C, the hydrogen shuttling mechanism in Figure 11 (see Discussion) was assumed and the quantity of hydrogen transferred from the mixture to TIMS was determined from the difference of NAP and DHA formed from TET and ANT, respectively. The quantities of hydrogen transferred were well correlated to those of MI formed during the heat treatments at 175–300 °C in various solvent systems used here, as shown in Figure 11.

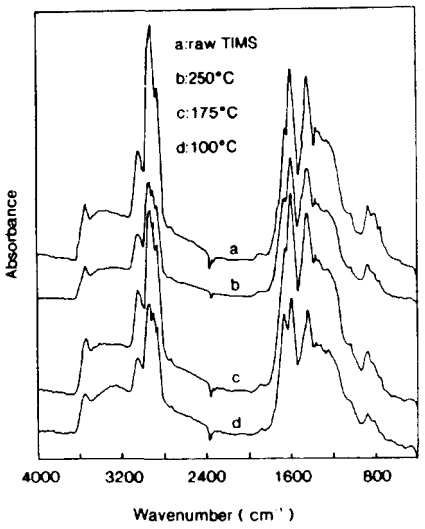

Figure 10. FT-IR spectra of raw TIMS and MI formed by the heat treatments of TIMS in TET.

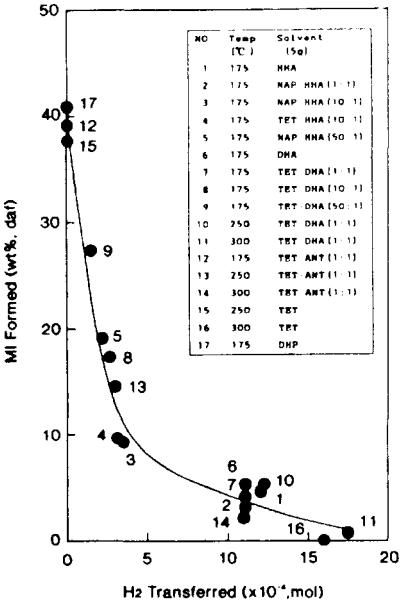

Figure 11. Plot of MI formed versus H_2 transferred during the heat treatments of TIMS.

Discussion

Solvent Effects on the Heat Treatments of TIMS. The results obtained at temperatures above 300 °C in Figure 4 were reasonably explained by the fact that TET has more donatable hydrogen than NAP to the coal radicals formed by the breaking of covalent bonds. However, Figure 4 also shows that even at temperatures below 250 °C some retrogressive reactions of TIMS to MI occur and little difference between TET and NAP was observed. However, when we use DHA and HHA, which have much more donatable hydrogen than TET,[6-9] as the solvent, MI formation was suppressed (Figures 5 and 6). DHP, which

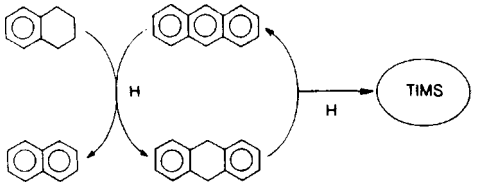

Figure 12. Hydrogen shuttling mechanism in the heat treatment of TIMS in TET-ANT mixed solvent.

is known[7] to be less hydrogen donating than DHA, gave no suppression of MI formation. The relative reactivities of the hydrogen abstraction from TET, DHP, and DHA by benzyl[8] (170 °C) and diphenylmethyl[9] (275 °C) radicals were reported to be 1:1.5:33 and 1:1.9:39, respectively, in agreement with the order of the suppression of MI formation observed here. Figure 11 clearly shows that the degree of the suppression of MI formation during the heat treatments at 175–300 °C is well correlated with the quantity of hydrogens transferred to TIMS and/or its moieties from the solvents systems widely used here.

In Figure 11 the data with TET–ANT mixture are included, in which the quantities of hydrogen transferred were estimated from the difference of NAP and DHA formed from TET and ANT, resepctively, assuming the hydrogen shuttling mechanism shown in Figure 12. The formation of NAP or DHA was not observed when TIMS was treated in TET or ANT alone, respectively, at temperatures below 250 °C.

Figure 8 shows that NMP is also effective for the suppression of MI formation from TIMS. Since NMP does not seem to be a strong hydrogen-donating solvent, a different mechanism from that above described may be considered. The detailed study on this treatment is being done.

Heat Treatment of Zao Zhuang Coal in DHA. Figure 9 indicates that Zao Zhuang raw coal undergoes dissolution reactions in DHA at temperature as low as 175 °C. The formation of ANT indicates the occurrence of the hydrogen transfer from DHA to Zao Zhuang coal, resulting in the increase of TS and the decrease of TIMS and MI. The heat treatment of MI in DHA at 175 °C also resulted in the formation of lighter fractions, TIMS and TS. This low-temperature dissolution of bituminous coals is also being studied.

Mechanism of Insolubilization and Dissolution Reaction of TIMS by the Heat Treatment at 175 °C. The insolubilization behavior of pyridine-insoluble fraction (PI) of the extracts from the extraction of some bituminous coals with CS_2–NMP mixed solvent (1:1 by volume) was observed[10] when we tried to redissolve this fraction in the CS_2–NMP mixed solvent. The effectiveness of the addition of the compounds such as *p*-phenylenediamine, 7,7,8,8-tetracyanoquinodimethane, and LiBr for the redissolution of the PI indicates that this insolubilization may be attributed to the association of PI molecules.[10] The THF-insoluble fraction of the extracts from Zao Zhuang coal, i.e., TIMS used here, which is a lighter fraction than PI, however, is completely soluble in the mixed solvent, unlike PI, suggesting that the insolubilization found here may proceed by a different mechanism from that for the PI.

(6) Bedell, M. W.; Curtis, C. W. *Energy Fuels* **1991**, *5*, 469–476.
(7) Poutsma, M. L. *Energy Fuels* **1990**, *4*, 113–131.
(8) Bockrath, B.; Bittner, E.; McGrew, J. *J. Am. Chem. Soc.* **1984**, *106*, 135–138.
(9) Manka, M. J.; Brown, R. L.; Stein, S. E. *Int. J. Chem. Kinet.* **1987**, *19*, 943–957.
(10) Sanokawa, Y.; Takanohashi, T.; Iino, M. *Fuel* **1990**, *69*, 1577–1578.

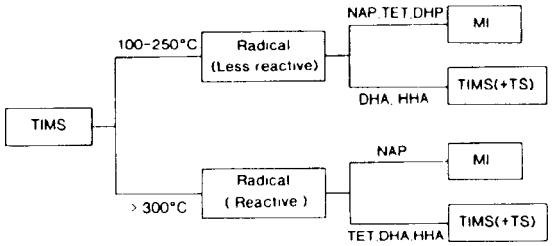

Figure 13. Reaction scheme for the heat treatment of TIMS in several solvents at 100–350 °C.

The result that hydrogen donatability of the solvent correlates with the suppression of the insolubilization of TIMS at temperatures below 250 °C (Figure 11) suggests the participation of coal radicals in this phenomenon. The radicals considered here are not so reactive as those formed by the breakings of covalent bonds at temperatures above 350 °C, which are the intermediates in the usual coal liquefaction, since Figure 4 indicates little difference in MI formation between TET and NAP at temperatures below 250 °C, unlike the case of the usual liquefaction. Two kinds of the radicals are conceivable. One is from thermally very weak bonds existing in coals that are broken to form radicals even at these low temperatures. For example, the dimer of some ring-substituted diphenylmethyl radicals is known to be in equilibrium with the radicals even at room temperature.[11] The radical formation through molecular disproportionation (hydrogen transfer) between polyaromatic moieties is also conceivable.[12] Another possibility is that the radicals originally existing in coals become reactive at temperatures above 100 °C to be able to undergo the insolubilization reaction and abstract hydrogens from DHA and HHA, but not from TET and DHP. Fowler, Bartle, and Kandiyoti found in the in situ ESR measurement of a bituminous coal that spin concentration increased from room temperature up to 180 °C and then decreased between 180 and 300 °C.[13] They attributed[13] the decrease of the spin concentration to the recombination of free radicals brought about by thermally activated mobility.

The reaction scheme for the heat treatment of TIMS at 100–350 °C in several solvents is summarized in Figure 13. When there is no strong hydrogen-donating solvent, the radicals assumed above may undergo coupling reactions with each other and/or addition reactions to aromatic rings of other TIMS molecules, resulting in MI formation from TIMS. Table II shows the spin concentrations of MI, TIMS, and TS from the extraction of the raw Zao Zhuang coal and from the heat treatment of TIMS at 175 °C in the several solvents. MI formed in the heat treatment of TIMS in DHA and HHA has smaller spin concentrations than those in TET and DHP, suggesting that the former gave hydrogens to the radicals and decreased the radical concentrations. It is also noticed that total spin concentrations after the heat treatment of TIMS all decreased compared with that of the raw TIMS. A simple calculation shows that the number of the spins (radicals) capped with a hydrogen, which are estimated by assuming that every hydrogen transferred from the solvent (Figure 11) capped one of the radicals, are 1.35×10^{21} and 1.45×10^{21} for the treatment in DHA and HHA at 175 °C, respectively, while the corresponding numbers of the radicals, which are estimated from the decrease of the radical concentration (ESR, Table II) by the treatment, are quite small, i.e., 3.9×10^{18} and 6.2×10^{18}, respectively. This suggests the possibilities of the occurrence of the hydrogen transfer to the radical newly formed during the heat treatment (the first mechanism) and/or that of the hydrogen transfer through nonradical intermediates. The fact that TS, a lighter fraction than TIMS, does not increase in DHA and HHA as much as MI increases in TET (Figures 5, 6, and 8) suggests that the first mechanism, i.e., radical formation by the weak bond breaking, is less likely, since the bond breaking should accompany the formation of TS, together with the suppression of MI formation. So, at present it is uncertain which mechanism explains this phenomenon.

Table II. Spin Concentrations[a] of the Extract Fractions from the Zao Zhuang Raw Coal and after the Heat Treatment of TIMS in Several Solvents

		heat treatment (175 °C, 1 h)			
	raw coal[b]	TET	DHP	DHA	HHA
MI	4.45 (33.8)	2.17 (31.9)	2.15 (40.7)	1.83 (5.1)	1.70 (4.4)
TIMS	2.05 (51.0)	1.95 (52.9)	1.77 (49.9)	1.87 (83.5)	1.71 (78.9)
TS	0.18 (15.2)	0.37 (15.2)	[c]	[c]	[c]
total[b]	2.57	1.78	1.76[d]	1.66[d]	1.43[d]

[a] 10^{19} spin/g daf basis. The values in parentheses are wt %, daf based on the raw coal or TIMS. [b] The average value for three extractions. [c] TS could not be isolated due to the high boiling point of the solvent used. [d] Total spin concentrations were determined from MI and TIMS alone, since the contributions of TS to it are very small.

Conclusion

TIMS was found to undergo retrogressive reaction to MI by heat treatment in TET, NAP, and DHP at temperatures as low as 175 °C. The MI formation was suppressed by adding a strong hydrogen-donating solvent such as DHA and HHA. The Zao Zhuang raw coal was also found to undergo dissolution reaction in the presence of DHA and HHA at 175 °C. The quantities of hydrogen transferred were well correlated to those of MI formed, suggesting the participation of coal radicals in this heat treatment. The nature of coal radicals and the mechanism of this behavior were discussed.

Acknowledgment. We thank Dr. Yoshiki Sato of the National Institute for Resources and Environment for his useful discussion and measurement for GC/MS analysis of the products.

Registry No. NMP, 872-50-4; TET, 119-64-2; DHP, 776-35-2; DHA, 613-31-0; AHA, 5910-28-1; CS_2, 75-15-0; naphthalene, 91-20-3; anthracene, 120-12-7.

(11) Lankamp, H.; Nauta, W. Th.; MacLean, C. *Tetrahedron Lett.* **1968**, 249–254.
(12) Billmers, R.; Griffith, L. L.; Stein, S. E. *Prepr. Pap.—Am. Chem. Soc., Div. Fuel Chem.* **1985**, *30* (4), 283–290.
(13) Fowler, T. G.; Bartle, K. D.; Kandiyoti, R. *Fuel* **1987**, *66*, 1407–1412.

Reprinted from ENERGY & FUELS, 1992, 6.

Swelling of the Extracts and Residues from Carbon Disulfide–*N*-Methyl-2-pyrrolidinone Mixed Solvent Extraction

Mikihiko Fujiwara, Hironori Ohsuga, Toshimasa Takanohashi, and Masashi Iino*

Institute for Chemical Reaction Science, Tohoku University, Katahira 2-1-1, Aoba-ku, Sendai 980, Japan

Received October 23, 1991. Revised Manuscript Received August 10, 1992

Solvent swellings of the raw coals, their extracts and residues, which were obtained by carbon disulfide–*N*-methyl-2-pyrrolidinone mixed solvent extractions of some bituminous coals at room temperature, were studied. The swelling ratios (Q) of the raw coals were generally lower than those of the corresponding extracts and residues, like the results of Larsen et al. for the swelling of two bituminous raw coals and their residues. Swelling ratios of PS (pyridine-soluble and acetone-insoluble extract fraction), PI (pyridine-insoluble extract fraction), and residue in four solvents were in the order of cyclohexane < methanol < benzene < THF for three bituminous coals. For Illinois No. 6 coal, which has a higher oxygen content than the coals above, swelling ratios in methanol are higher than those in benzene. Large synergistic effect for the swelling ratios of PI in benzene–methanol mixed solvent was observed. These results were discussed from the points of the nature of cross-link bonds and cross-link density of raw coals, extracts and residues.

Introduction

Many studies on coal swelling in solvents have been carried out to elucidate cross-link density, but the studies concerning the nature of cross-link bonds are rather few. Recently, Painter et al.[1-3] indicated that the Flory–Rehner equation or its revised version may be not applicable for coals which have strong inter- or intramolecular interactions such as hydrogen bonds and proposed a new model to evaluate cross-link density. For the nature of cross-link bonds, Larsen et al.[4] have found that acetylation of hydroxyl groups increases the swelling ratios (Q), suggesting hydrogen bonds play a role in cross-link structures of coals. The contribution of other noncovalent bonds such as aromatic–aromatic (π–π)[5] and dipole (ion)–dipole (ion) interactions may be possible, though no studies seem to be reported about their contribution to coal swelling. Painter et al.[2] suggested that noncovalent bonds such as hydrogen bonds are dynamic, constantly breaking and reforming in the presence of solvents, and do not therefore prevent the network from reaching an equilibrium swollen state. They also suggested that the phase behavior of coal–solvent systems, which include phase separation, is a crucial factor that has not been addressed in previous studies of the swelling of coals. So, the nature and structure of cross-links, especially the role of noncovalent bonds, do not seem to be fully elucidated.

One approach to the clarification of this problem is to study the swelling of solvent-soluble constituents, i.e., coal extracts, since it is more likely for them to have cross-links by noncovalent bonds than solvent insoluble residues, which are considered to have covalent cross-links.

Aida[6] found that the swelling degrees of pyridine extract of Illinois No. 6 coal (IL) with nonpolar solvents showed a similar tendency of solvent effect as the corresponding extraction residue. Green et al.[7] also reported that the O-methylated extract swelled more than the underivatized extract for Illinois No. 6 coal, like the results for the swelling of raw coals and extraction residues. However, no systematic swelling study on raw coals, their extracts, and their residues has been carried out.

In this study, swelling behaviors of the raw coals, their extracts, and their residues in several organic solvents, which were obtained from the extraction with carbon disulfide–*N*-methyl-2-pyrrolidinone (NMP) mixed solvents, were investigated. The mixed solvents gave high extraction yields at room temperature, and pyridine-insoluble extract fraction which is heavier than preasphaltene.[8] Although we could not offer a clear interpretation concerning the nature of cross-links, several findings about swelling behavior of coals are shown.

Experimental Section

Materials. The coals were ground to <250 μm (–60 mesh) and dried in vacuo at 107 °C to constant weight (2–3 h). The ultimate and proximate analyses are shown in Table I.

Extraction of Coals and Fractionation of the Extracts. Extraction and fractionation procedures are shown in Figure 1. The coals were extracted exhaustively with CS_2–NMP mixed solvent (1:1 by volume) at room temperature and fractionated with acetone into acetone-soluble (AS) and acetone-insoluble (AI) fractions, and then AI was fractionated with pyridine into

(1) Painter, P. C.; Graf, J.; Coleman, M. M. *Energy Fuels* **1990**, *4*, 379–383.
(2) Painter, P. C.; Park, Y.; Sobkowiak, M.; Coleman, M. M. *Energy Fuels* **1990**, *4*, 384–393.
(3) Painter, P. C.; Graf, J.; Coleman, M. M. *Energy Fuels* **1990**, *4*, 393–397.
(4) Larsen, J. W.; Green, T. K.; Kovac, J. *J. Org. Chem.* **1985**, *50*, 4729–4735.
(5) Nishioka, M.; Larsen, J. W. *Energy Fuels* **1990**, *4*, 100–106.
(6) Aida, T. Report for the 17th Meeting of the Committee on Coal Utilization Technology, Japan Society for the Promotion of Science, 1987; pp 18–25.
(7) Green, T. K.; Chamberlin, J. M.; Lopez-Froedge, L. *Prepr. Pap.—Am. Chem. Soc., Div. Fuel Chem.* **1989**, *34* (3), 759–768.
(8) Iino, M.; Takanohashi, T.; Ohsuga, H.; Toda, K. *Fuel* **1988**, *67*, 1639–1647.

0887-0624/92/2506-0859$03.00/0

Table I. Ultimate and Proximate Analyses of Coals

coal (abbrev)	ultimate anal, wt % (daf) C	H	N	S	O[a]	proximate anal, wt % (db) VM	ash	FC
Zao Zhuang (ZZ)	86.9	5.1	1.5	1.6	4.9	28.6	7.4	64.0
Shin-Yubari (SY)	86.6	6.0	2.0	0.8	4.6	38.3	6.2	55.5
Lower Kittanning (LK)[b]	82.3	5.2	1.7	3.9	6.9	31.4	11.6	57.0
Illinois No. 6 (IL)[c]	80.0	5.0	1.6	2.9	10.5	38.9	10.4	50.7

[a] By difference. [b,c] The Pennsylvania State University Coal Sample Bank, PSOC 815 and PSOC 1354, respectively.

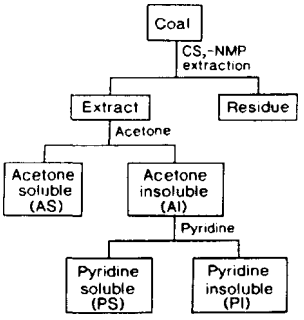

Figure 1. Extraction and fractionation procedures.

Table II. Extraction of Coals with CS_2–NMP Mixed Solvent and Fractionation of Their Extracts

coal	extraction yield, wt % (daf)	residue, wt % (db)	extract, wt % (db) AS	PS	PI
ZZ	63.0	41.7	6.7	24.3	26.0
SY	56.8	46.7	5.5	30.0	16.1
LK	46.2	59.0	5.8	25.4	8.6
IL	16.7	85.1	4.7	11.7	0.1

acetone-insoluble and pyridine-soluble (PS) fractions, and pyridine-insoluble (PI) fraction, respectively, according to the methods described before.[9] Since a part of the PI fraction was found recently to be insoluble in the CS_2–NMP mixed solvent, probably due to self-association,[10] the symbol was changed from MS (the mixed solvent soluble fraction) used before[9] to PI.

The yields (db) of the extract fractions and residues are shown in Table II.

The residues from the various extraction yields were obtained by changing the solvent composition of CS_2–NMP mixed solvents.

A 5.0-g sample of raw coal was acetylated with 5 mL of acetic anhydride in 60 mL of pyridine under reflux for 20 h. IR spectra of acetylated coals showed the large peak of acetyl group at 1764 cm^{-1}.

Swelling Measurement. The swelling ratio (Q) was measured by the volumetric method of Green and Larsen.[11] A 0.1-g sample of coals, extracts or residues was placed in a 8 mm o.d. Pyrex tube and centrifuged for 30 min at 1500 rpm. The height of the sample layer was measured as h_1. About 1.0 mL of the solvent was added and mixed thoroughly with the sample using a spatula. The sample was again centrifuged and the height of the sample layer (h_2) was measured. Swelling ratio (Q) is defined as h_2/h_1. The mixing and centrifugation were repeated until a constant height was attained. Larsen et al.[12] recently reported that high solvent:sample ratios must be used for accurate measurement of swelling ratio, since the permeability of solvent into a coal sample is changed by dissolving extractable substances retained in the sample, even if the sample is exhaustively preextracted with a swelling solvent. Although the solvent:sample ratio of 10 used here is within the range of their recommendation, the swellings of the raw coals and PS in THF, which gave considerable amount of extractable substances in the solvents, possibly gave a little lower swelling ratio than a true ratio due to the effect described above.

(9) Takanohashi, T.; Iino, M. *Energy Fuels* **1990**, *4*, 452–455.
(10) Sanokawa, Y.; Takanohashi, T.; Iino, M. *Fuel* **1990**, *69*, 1577–1578.
(11) Green, T. K.; Larsen, J. W. *Fuel* **1984**, *63*, 935–938.
(12) Larsen, J. W.; Cheng, J. C.; Pan, C.-S. *Energy Fuels* **1991**, *5*, 57–59.

Table III. Swelling Ratios (Q) of Shin-Yubari Coal, Its Extracts and Residues

	raw coal	extract (AI)	residue	extract (AS + AI) + residue[a]	extract (AI) + residue[a]
swelling ratio (Q)	1.12	1.47	1.53	1.42	1.45

[a] Mixing well AS, AI, and residue or AI and residue in a mortar in the same ratio as that in the raw coal.

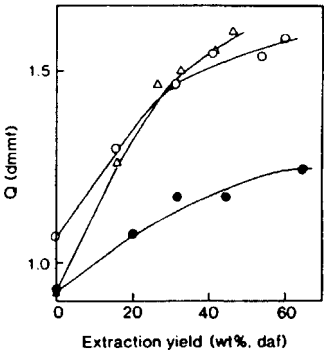

Figure 2. Swelling ratios (Q) of the extraction residues in benzene vs the extraction yields for ZZ (●), SY (○), and LK (△) coals.

Results

Swelling of the Raw Coals, Extracts, and Residues in Several Solvents. Table III shows the swelling ratio (Q) of SY coal, its extract (AI fraction in Figure 1), and residue in benzene. The yields of the AI and residue are 47.2 and 47.1 wt % based on the raw coal (db), respectively. Table III shows that the swelling ratios of the AI and residue are considerably higher than that for the raw coal. Table III also shows that Q of the recovered "raw" coal, which was obtained by remixing the whole extract (AS + AI) and residue well in a mortar to -200 mesh particle size, was not restored to that of the raw coal and gave similar values as the AI or residue. The mixture of the AI + residue gave also a similar value as AI, residue or the recovered "raw" coal (Table III). The mixture of AI + residue, which was obtained by the evaporation of the solvents from the well-mixed suspension of AI + residue in the CS_2–NMP mixed solvent, also gave a similar value as those described above and a higher value than that for the raw coal.

Figure 2 shows the plots of swelling ratio of the extraction residues in benzene vs the extraction yield for three coals, which was varied by changing the solvent composition of CS_2–NMP mixed solvents. For all the coals used here the swelling ratios increased with the increase of the extraction yield.

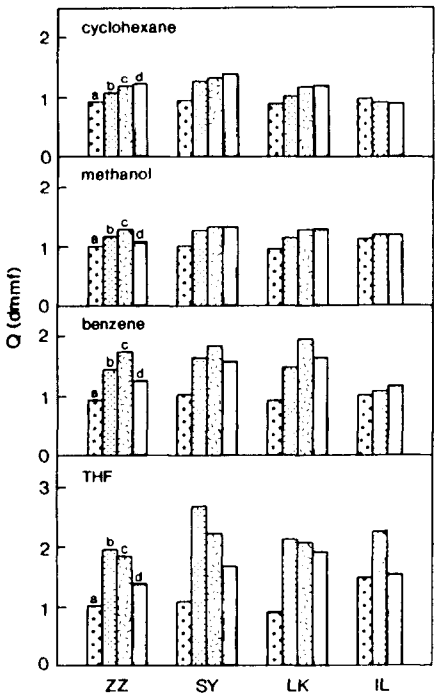

Figure 3. Swelling ratios (Q) of the raw coals (a), PS (b), PI (c), and residues (d) in several solvents.

Table IV. Swelling Ratios (Q) for the Raw and Their Acetylated Coals

		swelling ratio (Q)	
coal	solvent	raw coal	acetylated coal
ZZ	cyclohexane	0.94	1.00
	methanol	1.00	1.25
	benzene	0.92	1.34
SY	cyclohexane	0.95	1.11
	methanol	1.00	1.15
	benzene	1.07	1.39

Figure 3 shows the swelling ratios of the raw coals, PS, PI, and residue in several solvents. Elementary and proximate analyses of these constituents including the raw coals showed[13] that PI had higher oxygen % and lower H/C atomic ratio than the corresponding AS and PS. The solvents used for the swelling measurements are cyclohexane, methanol, benzene, and THF, in the order of increasing affinity to bituminous coal molecules. In fact, the extractions yields of bituminous coals with these solvents are generally in this order.

Figure 3 shows that the raw coals gave the lowest swelling ratio among them, except for IL coal in cyclohexane. For PS, PI, and residue it can be generally said from Figure 3 that the stronger affinity to coal molecules the solvent has, the greater the increase in swelling ratios in this solvent. For IL coal, the swelling ratios in methanol are higher than those in benzene.

Figure 3 also shows that the differences of the swelling ratios between PI and residue are smaller than those between PI and the raw coal.

Swelling of the Acetylated Coals. Table IV shows that the acetylated ZZ and SY coals gave higher swelling ratios than the corresponding raw coals for all solvents used. THF could not be used here due to its high solubility for the acetylated coals. The swelling ratio of PI and residue of the acetylated coals gave no general tendency.

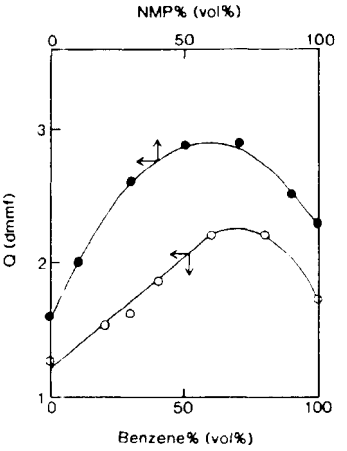

Figure 4. The effect of solvent composition of methanol–benzene (○) and CS_2–NMP (●) mixed solvents on swelling ratios (Q) for the PI (○) and residue (●) of ZZ coal, respectively.

Effect of Solvent Composition of Mixed Solvent on Swelling. Figure 4 shows the effect of solvent composition on swelling ratios for PI of ZZ coal (ZZ-PI) in benzene–methanol mixed solvent and for the residue of ZZ coal (ZZ-residue) in CS_2–NMP mixed solvent. Swelling ratio has the maximum at around 70% of benzene for ZZ-PI and 60% of NMP for ZZ-residue, and both mixed solvents show large synergistic effect.

Discussion

Swelling Behaviors of the Raw Coals, Extracts, and Residues. Coals have several kinds of noncovalent interactions, which varies depending on coal rank. Although it is suggested[2] that noncovalent bonds by these interactions are too weak to form cross-links, it may be possible to consider that cross-links are formed through aggregation of chains by several cooperative noncovalent bonds such as dipole–dipole, π–π, and hydrogen bonds interaction, etc., as considered in physical gels in a sol–gel chemistry of synthetic and biological macromolecules.[14] PI and PS swell in cyclohexane, methanol, benzene, and THF. The cross-link structure of the extracts may consist of mainly noncovalent bonds and the contribution of covalent bonds to cross-links may be small, since extracts are generally soluble in the solvent (in this case CS_2–NMP mixed solvent) which extracted them and the cross-linked polymer consisting of covalent bonds should be insoluble in any solvent, when cross-link structures are three-dimensionally developed.

Although we do not know what kind of cross-links (aggregates) coal extracts have, it may be reasonable to consider that the decrease of the cooperative noncovalent bonds may decrease the cross-link density and so increase Q. The lower swelling ratio of the raw coals than those of the corresponding extracts and residues suggests the higher cross-link density of the raw coals. Larsen et al.[4] have already found that the pyridine-extracted residue gave higher Q than the raw coal and suggested destruction

(13) Iino, M.; Takanohashi, T.; Obara, S.; Tsueta, H.; Sanokawa, Y. *Fuel* **1989**, *68*, 1588–1593.

(14) Ross-Murphy, S. B. *Prepr. Pap—First Symp. Polym. Gels, Tsukuba* **1989**, 15–18.

of coal–coal hydrogen bonds during the extraction. So, the noncovalent interactions between the extracts and residues make an important contribution to cross-link formation in the raw coal. The interaction between extracts of relatively low molecular weight and residues of high molecular weight seems to be more sterically favorable than that between the immobile residues themselves. The interactions between the extracts and residue were not recovered by their remixing, probably due to insufficient permeation of the extracts into the pores of the residue. A similar insufficient recovery by the remixing of the extract and residue was observed for the caking property of the coals.[15] Another possible reason for the low swelling ratios for the raw coals is that penetration of a swelling solvent is very slow, resulting in the apparent constant swelling ratios near 1. At present, no evidence distinguishing between the two explanations was obtained.

Although the increase in the swelling ratio of the acetylated coals can be explained by the decrease of cross-links due to the loss of hydrogen bonds, the situation is more complex. The blank experiments of acetylation, i.e., only refluxing in pyridine, increased the swelling ratio of ZZ coal in benzene from 0.92 to 1.44, which is a similar value as the swelling ratio (1.34) for the acetylated coal in benzene. This increase by pyridine refluxing may be caused by the release of pyridine-soluble constituents from the coal, like the case of the separation of the extract and the residue described above. So, the net effect of the acetylation could not be evaluated in this study. Refluxing in pyridine also changes the extraction yields and were discussed elsewhere.[16]

Solvent Effect of Swelling. Swelling ratio is determined by the balance of the elastisity of the cross-link network and the permeability of the solvent into the network. Solvents which have greater affinities to coal molecules give greater permeabilities, resulting in the greater swelling ratios. Among the solvents used here the order of the affinity for bituminous coals may be cyclohexane < methanol < benzene < THF. The order of the swelling ratios in the four solvents for the PI, PS, and residues are in the above order, except those for IL coal, in which methanol gave higher swelling ratios than benzene. This can be explained by the fact that IL coal has a higher oxygen content, and therefore higher hydroxyl groups, than the other coals (Table I).

Nelson et al.[17] have reported that swellings of raw coals of various carbon % in benzene have a maximum at 75 carbon % and the difference between those in benzene and methanol (methanol > benzene) is larger at lower carbon %, in agreement with the result here. These results suggest that methanol and benzene have an affinity to diffeent interaction sites of coals, i.e., hydroxyl groups (hydrogen bonds) for methanol and aromatic rings (π–π interaction) for benzene. Synergistic effect obtained with methanol–benzene mixed solvents (Figure 4) can be explained by this consideration.

We have already shown the strong synergistic effect on swelling of the residue of SY coal in CS_2–NMP mixed solvents.[8] The results for the residue of LK coals here is an another example with CS_2–NMP mixed solvents. The reasons for this strong synergistic effect were discussed in relation with the extraction mechanism in the previous paper.[8]

Registry No. NMP, 872-50-4; THF, 109-99-9; CS_2, 75-15-0; CH_3OH, 67-56-1; cyclohexane, 110-82-7; benzene, 71-43-2.

(15) Seki, H.; Ito, O.; Iino, M. *Fuel* **1989**, *68*, 837–842.
(16) Takanohashi, T.; Iino, M. *Energy Fuels* **1991**, *5*, 708–711.
(17) Nelson, J. R.; Mahajan, O. P.; Walker, Jr., P. L. *Fuel* **1980**, *59*, 831–837.

Kinetics of Ring-Opening Radical Polymerization of Vinyloxiranes

OSAMU ITO, TATSUSHI ISHIZUKA, MASASHI IINO, and MINORU MATSUDA

Institute for Chemical Reaction Science, Tohoku University, Katahira, Aoba-ku, Sendai, 980 Japan

TAKESHI ENDO and TSUTOMU YOKOZAWA

Research Laboratory of Resources Utilization, Tokyo Institute of Technology, Nagatsuda, Midori-ku, Yokohama, 227 Japan

Abstract

Ring-opening radical polymerization has been followed by the flash photolysis method. As an initiator radical, the arylthiyl radical ($ArS^{\cdot}$) was used; the addition reaction rate constants of $ArS^{\cdot}$ to vinyl monomer containing epoxy-ring such as vinyloxiranes ($CH_2=CHCROCH_2$) have been determined at first. The rate constant of ring opening reaction of the adduct radical ($ArSCH_2C^{\cdot}HCROCH_2$) changing to $ArSCH_2CH=CROCH_2^{\cdot}$ were determined in the form of the relative values, which were converted to the absolute values. The ring-opening reaction rate constants were ca. $10^6\ s^{-1}$, which indicates that the ring-opening rates are faster than usual radical propagation rates. The rate constants for vinyl monomer with 5-member ring (1,4-epoxy-1,4-dihydronaphthalene) were similarly evaluated.

Introduction

Some vinyl monomers such as vinyl cyclopropanes and vinyloxiranes undergo radical ring-opening polymerization to afford polymers containing the functional groups in the backbone [1–5]. ESR study using stopped flow method revealed that the radical attacks at C=C of vinyloxirane followed by the C—C or C—O cleavage of oxirane ring [6]. The kinetic data for the ring-opening radical polymerization, however, have not been reported, because of the difficulty in the analysis of kinetics.

(1)
$$CH_2=CHCHX(CH_2)_n \xrightarrow{Y^{\cdot}} [YCH_2C^{\cdot}HCHX(CH_2)_n \xrightarrow{k_0} YCH_2CH=CHX(CH_2)_n^{\cdot}] \longrightarrow \cdots \rightarrow \text{-}(CH_2CH=CHX(CH_2)_n)_m\text{-}$$

In our previous articles, the absolute rate constants of the addition reaction of the arylthiyl radicals ($ArS^{\cdot}$) to various vinyl monomers have been determined by the flash photolysis method [7–9]. Since the addition reaction mode of $ArS^{\cdot}$ is reversible, the kinetic behavior characteristic to the reversible reaction system was observed; i.e., the third material which is only reactive to the adduct radical has to be added to accelerate the decay of $ArS^{\cdot}$. As the carbon radical scavenger, we found that oxygen was most appropriate since $ArS^{\cdot}$ is quite unreactive to oxygen. Similar observation was

International Journal of Chemical Kinetics, Vol. 23, 853–860 (1991)

CCC 0538-8066/91/100853-08$04.00

reported in the ESR measurements of the addition reaction of the thiyl radical to styrene by Gilbert et al. [10].

In this study, we try to determine the rate constants for the ring-opening reactions of the propagating radicals during the polymerization of vinyloxiranes initiated by the addition reaction of ArS· using the flash photolysis method. The vinyl monomers used in this study are as follows;

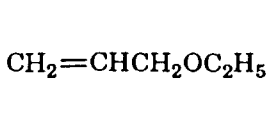

allyl ethyl ether (AEE)

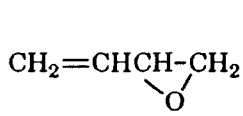

vinyloxirane (VO)

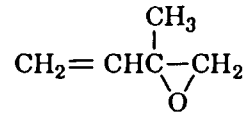

2-methyl-2-vinyloxirane (MVO)

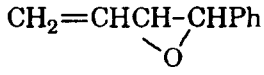

2-phenyl-3-vinyloxirane (PVO)

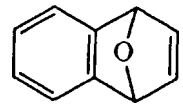

1, 4-epoxy-1, 4-dihydronaphthalene (EPN)

Experimental

Vinyl monomers used in this study were commercially available except PVO which was prepared by the method described in the literature [4]. As a radical source, $(p\text{-}BrC_6H_4S)_2$ was used. Oxygen concentration in cyclohexane solvent was controlled by varying the partial pressure of oxygen after degassing up to 10^{-1} Pa.

The flash photolysis apparatus was of standard design equipped with two xenon flash photolysis lamps (Xenon Corp. N-815C; half duration of 8 μs and input energy of 50 J). All the measurements were performed at 23°C.

Results and Discussion

Insert of Figure 1 shows the transient absorption spectrum observed after the flash photolysis of $(p\text{-}BrC_6H_4S)_2$. The absorption peak at 520 nm was attributed to $p\text{-}BrC_6H_4S\cdot$ (abbreviated as ArS·), since similar absorption band was observed by the flash photolysis of $p\text{-}BrC_6H_4SH$. Figure 1 shows the first-order plot of the decay of ArS·. The decay rate of ArS· in the presence of oxygen is similar to that in degassed solution, suggesting low reactivity of ArS· to oxygen. On addition of ordinal vinyl monomer such as ally ethyl ether ($CH_2=CHCH_2OC_2H_5$) to the degassed solution, the decay of ArS· was not accelerated, which indicates the reversible mode of the addition reaction of ArS· to this vinyl monomer. Only when oxygen was added to the solution containing the vinyl monomer, the decay of ArS· was accelerated; oxygen selectively scavenges the carbon centered radical ($ArSCH_2C\cdot HCH_2OR$), which results in the shift of the equilibrium to the peroxide radical side.

(2) $$ArS\text{-}SAr \underset{k_r}{\overset{h\nu}{\rightleftharpoons}} 2ArS\cdot$$

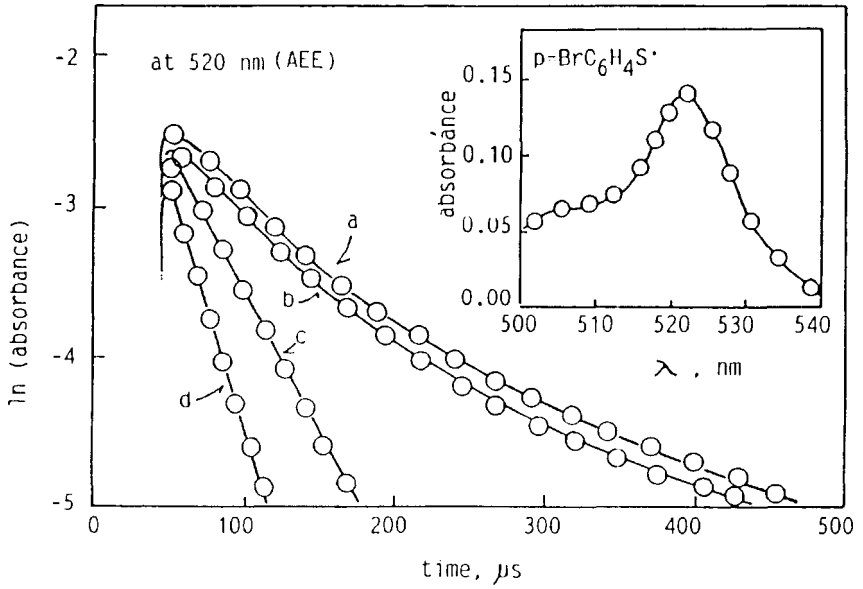

Figure 1. First-order plot for decay of p-$BrC_6H_4S^{\cdot}$: (a) in cyclohexane; (b) in degassed solution in presence of $CH_2{=}CHCH_2OC_2H_5$ (1.5 M); (c) 4 mM of oxygen was added to solution b; and (d) $[O_2]$ = 11 mM was added to solution b. Insert: Transient absorption spectrum of p-$BrC_6H_4S^{\cdot}$ produced by flash photolysis of 5×10^{-4} M of (p-$BrC_6H_4S)_2$; the absorbance immediately after flash is depicted.

(3) $$ArS^{\cdot} + CH_2{=}CHCH_2OR \underset{k_{-1}}{\overset{k_1}{\rightleftharpoons}} ArSCH_2C^{\cdot}HCH_2OR$$

$$ArSCH_2C^{\cdot}HCH_2OR \xrightarrow[k_2]{+[O_2]} ArSCH_2\underset{\displaystyle OO^{\cdot}}{\underset{|}{C}}HCH_2OR$$

In reaction (3), the anti-Markownikoff addition reaction mode of $ArS^{\cdot}$ has been confirmed in the literature [7–9]. On assuming the steady state concentration about the intermediate adduct radical ($ArSCH_2C^{\cdot}HCH_2OR$), the first-order rate constant (k_{first}) was expressed as eq. (4) for AEE is in excess and with the assumption that $ArS^{\cdot}$ does not recombine significantly compared with its reaction with olefin;

(4) $$[AEE]/k_{first} = 1/k_1 + k_{-1}/k_1k_2[O_2]$$

In the lower part of Figure 2, eq. (4) is plotted for AEE; from the intercept and slope, the rate constants were evaluated as follows, respectively; $k_1 = 3.1 \times 10^4\ M^{-1}\ s^{-1}$ and $k_{-1}/k_2 = 1.3 \times 10^{-3}$ M. By substituting the reported value $k_2 = 4 \times 10^9\ M^{-1}\ s^{-1}$ in the literature [11], k_{-1} and the equilibrium constant K ($= k_1/k_{-1}$) can be calculated. The rate parameters are summarized in Table 1.

In the case of VO, the decay of $ArS^{\cdot}$ was accelerated even in the degassed solution as shown in Figure 3. This indicates that the adduct radical changes into other radical which leads to the shift of the equilibrium even though the selective radical scavenger such as oxygen is absent. By the addition of oxygen to the solution, the decay rate of $ArS^{\cdot}$ was further increased; the addition step of $ArS^{\cdot}$ to VO is partially reversible. The reactions can be shown in reactions (5)–(8); the attack of $ArS^{\cdot}$ to the terminal carbon of C=C in VO was confirmed by Stogryn and Gianni [12]. Although the hydrogen in the epoxy ring at the allylic position seems to be reactive, the

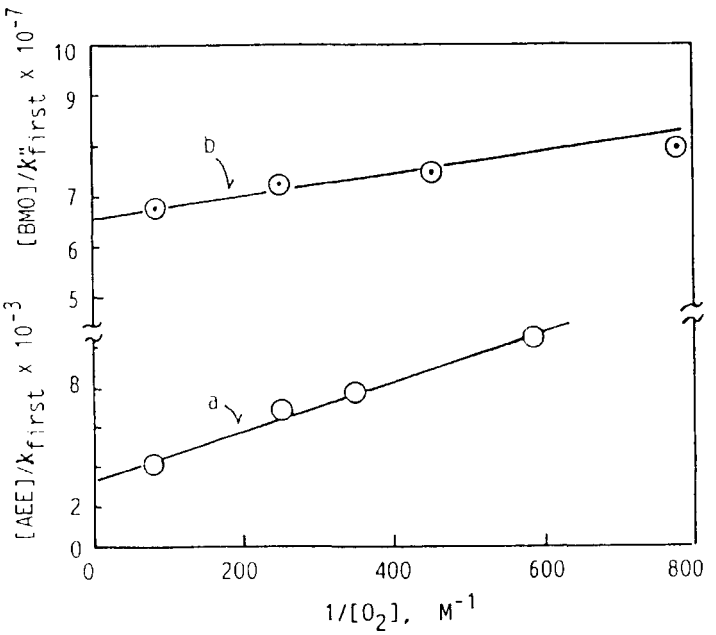

Figure 2. (a) Plot of eq. (4) for reaction of p-$BrC_6H_4S^{\cdot}$ with $CH_2{=}CHCH_2OC_2H_5$ and (b) Plot of eq. (11) for reaction of p-$BrC_6H_4S^{\cdot}$ with $CH_2{=}CHCHOCH_2$.

TABLE I. Rate constants obtained in cyclohexane at 23°C.

monomer	k_1 / $M^{-1}\,s^{-1}$	k_{-1} / s^{-1}	K^a	k_0/k_2 / M	$k_0{}^a$ / s^{-1}
AEE	3.1×10^4	5.1×10^6	6.7×10^{-3}		
VO	1.5×10^6	3.1×10^5	4.8	9.0×10^{-4}	3.6×10^6
MVO	4.3×10^5	1.1×10^6	3.9×10^{-1}	1.1×10^{-3}	4.4×10^6
EPN	5.7×10^6	1.7×10^5	3.4	6.5×10^{-4}	2.6×10^6

[a] $k_2 = 4 \times 10^9\ M^{-1}\,s^{-1}$.

product arisen from the hydrogen abstraction reaction was not found [12]. Low reactivity of $ArS^{\cdot}$ to hydrogen abstraction was confirmed in various methods [8]. Thus, the reactions are presumed as follows;

(5) $$ArS^{\cdot} + CH_2{=}CHCH{-}CH_2 \underset{k_{-1}}{\overset{k_1}{\rightleftarrows}} ArSCH_2C^{\cdot}HCH{-}CH_2$$ (O bridges CH–CH$_2$ in both)

(6) $$ArSCH_2C^{\cdot}HCH{-}CH_2 \overset{k_0}{\rightleftarrows} ArSCH_2CH{=}CHOCH_2^{\cdot}$$ (O bridges CH–CH$_2$)

(7) $$ArSCH_2C^{\cdot}HCH{-}CH_2 \overset{k_0'}{\rightleftarrows} ArSCH_2CH{=}CHCH_2O^{\cdot}$$ (O bridges CH–CH$_2$)

(8) $$ArSCH_2C^{\cdot}HCH{-}CH_2 \xrightarrow[+[O_2]]{k_2} ArSCH_2C(OO^{\cdot})HCH{-}CH_2$$ (O bridges CH–CH$_2$)

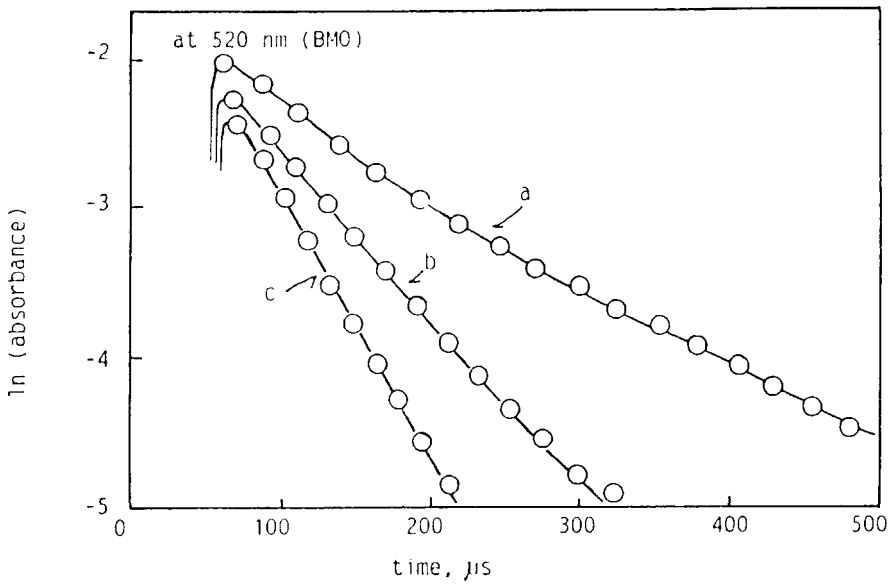

Figure 3. First-order plot for decay of p-$BrC_6H_4S^{\cdot}$: (a) without monomer; (b) degassed solution in the presence of $CH_2{=}CHCHOCH_2$ (25 mM); and (c) 4 mM of O_2 was added to solution b.

In the case of cyclopropenylmethyl radical, the reverse rate constant of the ring opening reaction is smaller than that of the forward reaction by a factor of 10^5 [13,14]. Thus, the reverse processes of reaction (6) and (7) are not taken into consideration in the following treatment. Although both reaction paths (6) and (7) were presumed by ESR study [6], the analysis of the polymer structure indicates that reaction path (6) is predominant [4]. In the absence of oxygen, k'_{first} was expressed as follows;

$$k'_{first} = \{k_1 - k_1k_{-1}/(k_0 + k_{-1})\}[VO] \quad (9)$$

In the presence of oxygen, reaction (8) may become predominant, since the spin trapping reagent traps the radical before the bond cleavage [6]. In this case, the first-order rate constant (k''_{first}) can be described as follows;

$$k''_{first} = \{k_1 - k_1k_{-1}/(k_0 + k_{-1} + k_2[O_2])\}[VO] \quad (10)$$

Since the decay of $ArS^{\cdot}$ was accelerated by the addition of oxygen more than that in the degassed system, $k_0 < k_2[O_2]$. Thus, eq. (10) reduces to a form identical to eq. (4). From the plot of the upper part in Figure 2, k_1 and k_{-1}/k_2 are evaluated for VO to be 1.5×10^6 M^{-1} s^{-1} and 7.8×10^{-5} M, respectively.

In Figure 4, eqs. (9) and (10) are plotted. From the ratio of eqs. (4) for VO to the reverse of eq. (9), the following equation can be derived;

$$([VO]/k''_{first}) - 1/k_1)/([VO]/k'_{first}) - 1/k_1) = k_0/k_2[O_2] \quad (11)$$

By substituting the slopes in Figure 4 and the observed k_1 value, the ratio of k_0/k_2 can be calculated from eq. (11). The rate parameters thus evaluated are summarized in Table I; relative values are converted to the absolute values for k_0 by replacing reported k_2. The k_0 value of 3.6×10^6 s^{-1} for VO satisfies the assumption of $k_0 < k_2[O_2]$ for aerated cyclohexane solution ($[O_2]$ = 2.1 mM).

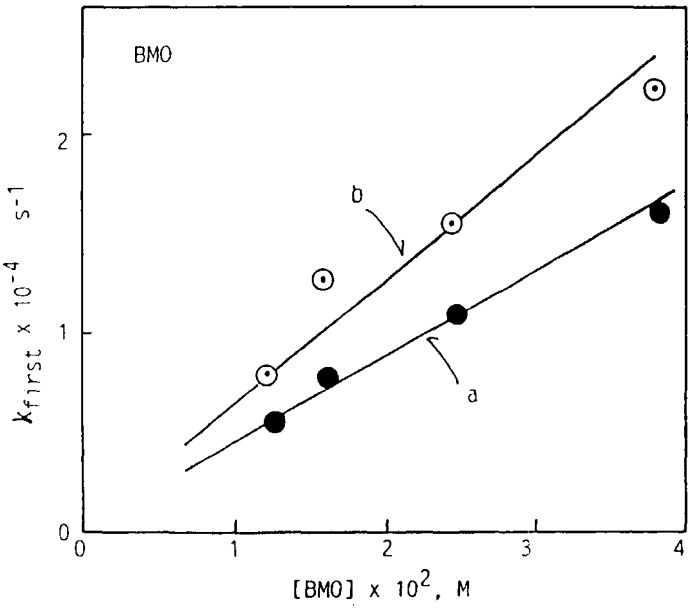

Figure 4. Plot of eqs. (9) and (10) for reaction of p-$BrC_6H_4S^{\cdot}$ with $CH_2{=}CHCHOCH_2$.

In the same manner, the rate constants for MVO and EPN were evaluated; they are also listed in Table I. The k_0 value of MVO is similar to that of VO. These k_0 values are smaller than that of cyclopropylmethyl radical by a factor of ca.100 [13,14]. The activation energy of the ring-opening process (mainly reaction (6)) can be estimated to be ca. 10 kcal/mol, assuming the frequency factor of 10^{13} s^{-1} [13]. This activation energy is smaller than that of dissociation of oxirane (ca. 57 kcal/mol) [15]. The former reaction accompanying by the double bond formation has extremely lower barrier than the latter biradical formation reaction.

The k_0 of EPN is slightly smaller than those of VO and MVO; since the former is bicyclo-derivative, it is not clear that the cleavage of the 3-member ring is easier than that of 5-member ring. In the case of EPN, two cleavage paths yielding the alkoxy and phenyl radical are possible (eq. (12)). We, however, did not succeed in the detection of the alkoxy and phenyl radicals by the flash photolysis method, because of their high reactivities in solution.

(12)

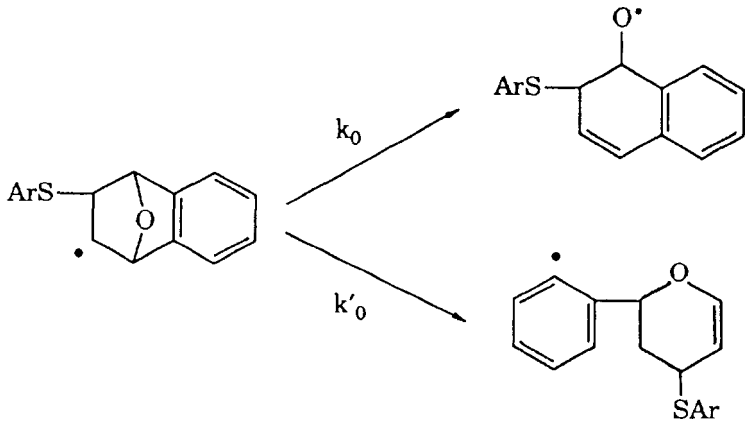

Compared with the k_1 value of AEE, k_1 of VO is larger by a factor of 50. Although both the monomers belong to the nonconjugated monomer, the p_z orbital of the radical center in $ArSCH_2C{\cdot}HCHOCH_2$ may be conjugated with the orbitals of the epoxy ring. The k_1 value of EPN is quite large compared with those of other nonconjugated olefins; this seems to be characteristic to bicyclo-olefins [16]. In Table I, a tendency that the larger the K value, the larger the k_1 value is seen.

Figure 5 shows the decay of ArS· in the presence of PVO; the decay rate of ArS· in degassed solution is faster than that in oxygen-containing solution. In the ring-opening polymerization of PVO, the C—C cleavage occurs producing benzyl radical (reaction 13) [4].

(13) $$ArSCH_2C{\cdot}HCH(O)CHPh \xrightarrow{k_0} ArSCH_2CH{=}CHOC{\cdot}HPh$$

For the reaction in degassed solution, if the C—C bond partially breaks forming the resonance-stabilized benzyl radical in the transition state, the rate of the addition reaction becomes faster than those of VO and MVO [17]. On the other hand, when oxygen is present, oxygen may trap the delocalized radical ($ArSCH_2C{\cdot}HCHOCHPh$) before the C—C cleavage (reaction 14); thus, the reaction rate of the addition process may be slowed down. The method of analysis for the decay curves derived in this study can not be applied to PVO.

(14) $$ArSCH_2C{\cdot}HCH(O)CHPh \xrightarrow{k_2} ArSCH_2C(OO{\cdot})HCH(O)CHPh$$

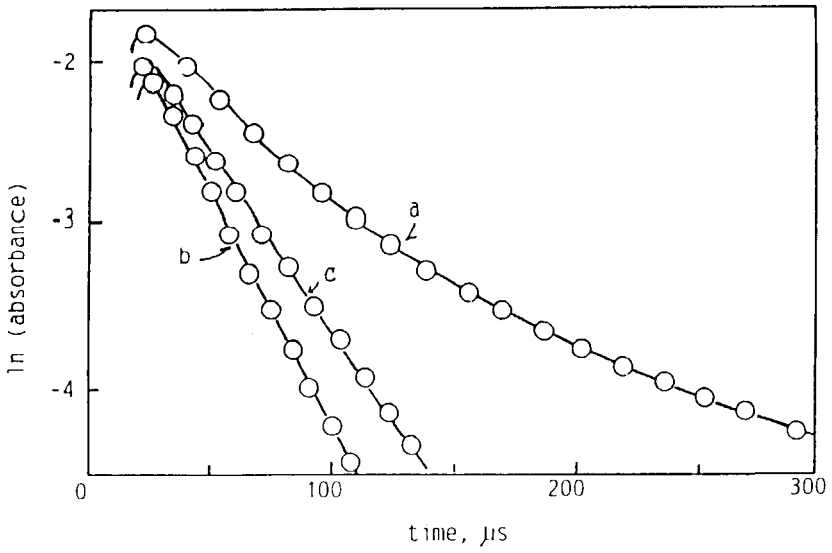

Figure 5. First-order plot for decay of p-BrC_6H_4S·: (a) without monomer; (b) degassed solution in the presence of $CH_2{=}CHCHOCHPh$ (140 mM); and (c) 11 mM of O_2 was added to solution b.

In general, the radical-propagating rate constants for nonconjugated vinyl monomers are $10^2 - 10^3$ M^{-1} s^{-1} [18]. Even in bulk polymerization, which contains ca. 10 M of vinyl monomer, the ring-opening reaction occurs prior to the propagation of the radical polymerization by attacking other vinyl monomer.

Acknowledgment

The authors would like to express our thanks to Mr. Hidenao Saito for his useful suggestions. This research was partially supported by Grant-in-Aide (No. 63550676) for Scientific Research from the Japanese Ministry of Education, Science, and Culture.

Bibliography

[1] K. Murata, *J. Polym. Sci. Polym. Chem. Ed.*, **10,** 367 (1972).
[2] Sh. M. Novruzov, K.A. Gulieva, R.A. Dzhalilov, and E.M. Voroshilovskaya, *Azerb. Khim. Zh.*, **1881,** 66 (1981).
[3] T. Endo and N. Kan, *J. Polym. Sci. Polym. Chem.*, **23,** 1931 (1985).
[4] I. Cho and J.-B. Kim, *J. Polym. Sci. Polym. Lett. Ed.*, **27,** 333 (1989).
[5] T. Endo, M. Watanabe, K. Suga, and T. Yokozawa, *J. Polym. Chem. Ed.*, **27,** 1435 (1989).
[6] A.J. Dobbs, B.C. Gilbert, H.A.H. Laue, and R.O.C. Norman, *J. Chem. Soc. Perkin II,* **1976,** 1044 (1976).
[7] O. Ito and M. Matsuda, *J. Am. Chem. Soc.*, **101,** 1815 (1979).
[8] O. Ito and M. Matsuda, in *Chemical Kinetics of Small Organic Radicals,* Z.A. Alfassi, Ed., CRC Press, 1998, Boca Raton, Vol. 3, p. 133.
[9] O. Ito and M. Matsuda, *J. Polymer Sci. Polymer Chem.*, **28,** 1947 (1990).
[10] B.C. Gilbert, P.A. Kelsall, M.D.G. Sexton, G.D.G. McConnacchie, and M.C.R. Symon, *J. Chem. Soc., Perkin Trans. II,* **1984,** 629 (1984).
[11] B. Millard, K.U. Ingold, and J.C. Scaiano, *J. Am. Chem. Soc.*, **105,** 5095 (1983).
[12] E.L. Stogryn and M.H. Gianni, *Tetrahedron Lett.*, **34,** 3025 (1970).
[13] B. Maillard, D. Forrest, and K.U. Ingold, *J. Am. Chem. Soc.*, **98,** 702 (1976).
[14] A. Effio, D. Griller, K.U. Ingold, A.L.F. Beckwith, and A.K. Serelis, *J. Am. Chem. Soc.*, **102,** 1734 (1988).
[15] M.E. O'Neal and S.W. Benson, *J. Phys. Chem.*, **72,** 1866 (1968).
[16] O. Ito and M. Matsuda, *J. Org. Chem.*, **49,** 17 (1984).
[17] A.J. Castellino and T.C. Bruice, *J. Am. Chem. Soc.*, **110,** 1313 (1988).
[18] J.L. Yong, in *Polymer Handbook,* Wiley, New York, 1975, p. 2–45.

Received July 31, 1990
Accepted February 20, 1991

Effect of maceral composition on the extraction of bituminous coals with carbon disulphide–*N*-methyl-2-pyrrolidinone mixed solvent at room temperature

Toshimasa Takanohashi, Tadashi Ohkawa, Takayuki Yanagida and Masashi Iino

Institute for Chemical Reaction Science, Tohoku University, 2-1-1 Katahira, Aoba-ku, Sendai 980, Japan

(Received 12 May 1992)

The residues obtained from the extraction with carbon disulphide *N*-methyl-2-pyrrolidinone mixed solvent at room temperature were optically examined and their maceral composition was determined. At low extraction yields, below 30 wt% (daf), a significant amount of semifusinite and pseudovitrinite were extracted. The solvents penetrated the vitrinite particles, softening and extracting them. Pseudovitrinite, an intermediate component between vitrinite and semifusinite, was fragmented like the vitrinite by the penetration of the solvents. Semifusinite was also fragmented and extracted. Fusinite, macrinite, and micrinite were hardly extracted with the mixed solvent. Above 50 wt% (daf) extraction yield, vitrinite was preferentially extracted, but even at 74.1 wt% (daf) extraction yield, some vitrinite components remained in the residue.

(Keywords: solvent extraction; macerals; bituminous coals)

Coals consist of three optically different maceral groups: exinite, vitrinite, and inertinite, the chemical and physical properties of which are significantly different. Therefore, the maceral composition of coal is recognized to be very important in coal utilization such as coking and liquefaction.

It is generally considered that inertinites are chemically inert to reactions such as liquefaction, exhibiting no fusibility, low volatile matter, high reflectance and high aromaticity[1], although their properties also depend on coal rank. Shibaoka *et al.* reported that hydrogenation of inertinites in Australian coals became significant only above 400 C without added catalyst[2], and that a significant amount of oil was obtained at 450 C[3], whereas virtrinites started to dissolve above 300 C[4]. Inertinite seems to be neither swollen nor dissolved significantly in tetralin at low temperatures (e.g. <330 C).

Inertinites and vitrinites consist of several maceral components distinguished optically. The chemical reactivities of individual maceral components are not fully understood. Schapiro and Gray[5] regarded one-third of the semifusinite, one of the components of inertinite, as reactive in coking. Mochida *et al.*[6] reported that the major portion of semifusinite could be fully liquefied, although its reactivity depended on the kind of coal. Mochida *et al.*[7] examined the correlation of inertinite reactivity with microscopic characteristics and concluded that each maceral component had a different condition appropriate for liquefaction. Maceral components in the vitrinite group also show different reactivities for liquefaction[8].

The present authors reported[9,10] that carbon disulphide–*N*-methyl-2-pyrrolidinone (CS_2–NMP) mixed solvent gave very high extraction yields (45–66 wt% daf) for many bituminous coals at room temperature, probably without any cleavage of covalent bonds. The effect of coal rank on the extraction and the extraction mechanism were discussed[9]. For solvent extraction of coals under mild conditions, the penetration of the solvent into the coal as well as the solubility of the coal components are important factors in obtaining a high extraction yield[9]. Zao Zhuang coal (China), which showed a high extraction yield (66 wt%), contained 28.4 vol% of inertinites[11]. It is therefore worth while to clarify the solubility of macerals in this particular solvent.

In this study, bituminous coals were extracted with the CS_2–NMP mixed solvent at room temperature to determine the extractability of individual macerals, which were identified microscopically before and after extraction.

EXPERIMENTAL

Coals

Five bituminous coals were ground to <850 μm and dried *in vacuo* at 107 C. Their ultimate and proximate analyses are shown in *Table 1*. The two kinds of Zao Zhuang coal were obtained from the same seam.

Extraction procedure

A coal sample (4 g) was added to 100 ml of the CS_2–NMP solvent (at various mixture ratios) in a flask

0016-2361/93/010051-05

Table 1 Ultimate and proximate analyses and vitrinite reflectances of coals

Coal	Country	Ultimate analysis (wt% daf)				Proximate analysis (wt% db)			$R_{o,max}$ (%)
		C	H	N	S+O[a]	VM	Ash	FC	
Sewell 'B'[b]	USA	88.4	5.3	1.4	4.9	30.8	4.6	64.6	0.86
Zao Zhuang I	China	87.8	5.2	1.4	5.6	26.4	13.1	60.5	0.87
Zao Zhuang II	China	86.9	5.5	1.5	6.1	28.6	7.4	64.0	0.86
Shin-Yubari	Japan	86.7	6.2	2.0	5.1	38.3	6.2	55.5	0.86
Lower Kittanning[c]	USA	82.3	5.2	1.7	10.8	31.5	12.1	56.4	0.83

[a]By difference
[b]PSOC726
[c]PSOC815

Table 2 Maceral group compositions and extraction yields of coals

Coal	Maceral group composition (vol%)				Extraction yield (wt% daf)
	Vitrinite	Exinite	Inertinite[a]	Mineral matter	
Sewell 'B'	64.8	9.5	23.1	2.6	37.1
Zao Zhuang I	70.1	0.5	21.4	8.0	78.8
Zao Zhuang II	59.4	1.1	35.0	4.5	66.8
Shin-Yubari	95.2	0.6	0.6	3.6	59.8
Lower Kittanning	87.5	1.5	3.3	7.7	46.8

[a]Including pseudovitrinite

and extracted with magnetic stirring for 60 min at room temperature under atmospheric pressure. After centrifuguation at 14 000 rev min^{-1} (25 400 *g*) for 40 min, the supernatant was immediately filtered through a membrane paper with an average pore size of 0.8 μm. The retained solid was again extracted with fresh mixed solvent in the same way. This extraction procedure was repeated twice. The residue was washed three times with acetone for 15 min to remove CS_2 and NMP retained in the coal, and dried *in vacuo* at 90°C for 12 h. The extract was washed with acetone–water (2:8 v/v) after evaporation. The yield of residue plus extract was 98–102 wt% of the raw coal.

Coal was also extracted under ultrasonic irradiation for 30 min at room temperature, after which the residue was treated by the same procedure as above.

The coals (<850 μm) were also extracted in a Soxhlet extractor with pyridine for 48 h under nitrogen. The residues were washed thoroughly with acetone.

The extraction yield was calculated on a dry ash-free basis according to the equation

$$\text{Extraction yield (wt\% daf)} = \frac{1 - \text{residue (g)/coalfeed (g)}}{1 - \text{ash (wt\% db)}/100} \times 100$$

Microscopic analysis

Microscopic analysis was carried out in oil immersion by reflected light according to the Japanese Industrial Standard (JIS 8816). About 4 g of the coal sample (250–850 μm) was mounted in epoxy resin. The block was cured at 60°C for 3 h and was polished with abrasive papers and then with 1.0, 0.3 and 0.06 μm alumina on silk. The maceral composition was determined with a polarizing microscope, using more than 500 counts. The mineral matter content (vol%) was calculated from the ash content (wt%) and total sulphur content (wt%) by the Parr equation[12].

RESULTS AND DISCUSSION

Maceral composition and extraction yield

Table 2 shows the maceral group composition and the extraction yield with 1:1 (v/v) CS_2–NMP mixed solvent for five raw bituminous coals. Since pseudovitrinite is considered to be an intermediate between vitrinite and semifusinite[1], pseudovitrinite is here included in the inertinite group. Shin-Yubari coal, with a high vitrinite content of 95.2 vol% and little inertinite, gave a high extraction yield of 59.8 wt% (daf). Zao Zhuang I and Zao Zhuang II coals, with relatively high inertinite contents, nevertheless showed higher extraction yields than Shin-Yubari coal. Zao Zhuang I gave a higher extraction yield than Zao Zhuang II, which had a similar ultimate analysis, volatile matter and fixed carbon but a higher inertinite content than Zao Zhuang I. No correlation was found between the maceral group composition and the extraction yield with the mixed solvent at room temperature.

Table 3 shows the maceral analyses of Zao Zhuang I and II coals. Telocollinite (>90 vol%) dominates the vitrinite group in both coals. For Zao Zhuang I, the macrinite + micrinite content is relatively low, whereas the pseudovitrinite is high compared with Zao Zhuang II. Both coals have similar semifusinite and fusinite contents. The exinite group consisted almost entirely of sporinite.

Table 3 Maceral compositions of maceral groups

Coal	Vitrinite (vol% dmmf)			Inertinite and pseudovitrinite (vol% dmmf)			
	Telocollinite	Telinite	Degradinite	Pseudovitrinite	Semifusinite	Fusinite	Macrinite + micrinite
Zao Zhuang I	96.0	4.0	0.0	41.1	40.0	5.1	13.1
Zao Zhuang II	90.7	8.4	0.9	28.0	40.3	2.7	29.0

Table 4 Maceral group composition of extraction residues

Coal	Mixed solvent volume ratio CS_2:NMP	Extraction yield (wt% daf)	Maceral group composition (vol% dmmf)		
			Vitrinite	Exinite	Inertinite[a]
Zao Zhuang I	raw coal	0.0	76.2	0.5	23.3
	90:10	11.0	73.9	0.6	25.5
	80:20	28.5	73.5	0.6	25.9
	65:35	59.1	64.4	0.6	35.0
	50:50	74.1	59.9	0.0	40.2
Sewell 'B'	raw coal	0.0	66.5	9.7	23.8
	50:50	28.3	67.0	11.0	22.0

[a]Including pseudovitrinite

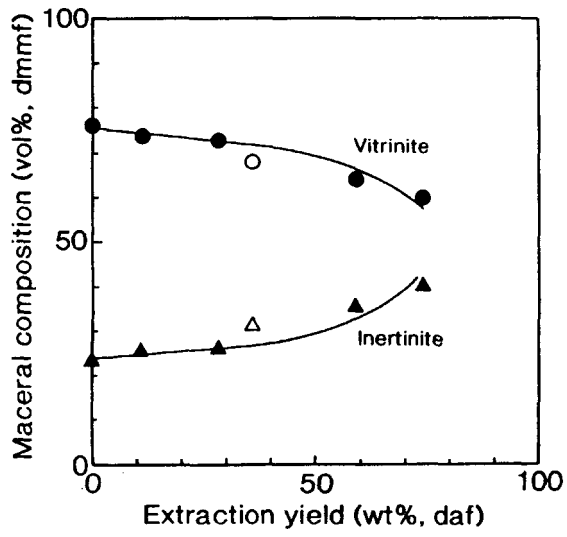

Figure 1 Contents of vitrinite and inertinite (including pseudovitrinite) in extracted residues versus extraction yield: ●, ▲, CS_2–NMP; ○, △, pyridine

Maceral compositions of the extracted residues

Table 4 shows the extraction yields with various volume ratios of the mixed solvent, as well as the maceral compositions of the extracted residues. The extraction yield can vary with the volume ratio[9]. The inertinite (including pseudovitrinite) content did not increase in the residue after the extraction of 28.5 and 28.3 wt% from Zao Zhuang I and Sewell 'B' coals respectively, suggesting that the extraction rates for the reactive and inert macerals were similar at such extraction yields. Preliminary experiments on the extraction of maceral concentrates prepared by the sink–float method also showed that significant amounts of semifusinite and pseudovitrinite were extracted with the mixed solvent.

When the extraction yield increased to 59.1 wt%, inertinite was found to be concentrated in the residue from Zao Zhuang I coal. *Figure 1* shows the contents of inertinite (including pseudovitrinite) and vitrinite in the extracted residues versus the extraction yield. Above 59 wt%, vitrinite was somewhat preferentially extracted. However, even at 74.1 wt% extraction yield, some vitrinite still remained in the residue, indicating that there is a significant difference in extractability among vitrinite components.

When the residue from Soxhlet extraction with pyridine was optically analysed, the result was similar to that obtained with the mixed solvent, as shown in *Figure 1*.

Microscopic observation

Photomicrographs of the extracted residues from Zao Zhuang I coal at various extraction yields are shown in *Figure 2*. At 11.0 wt% extraction yield, no significant change was found in the maceral components, except that the edges of vitrinite and pseudovitrinite particles became somewhat dark. As the extraction yield increased to 28.5 wt%, the dark regions spread inside the particles, and some cracks appeared, indicating that the solvents gradually penetrate[4] vitrinites and pseudovitrinite. Some semifusinite grains were fragmented, whereas there was no change in fusinite, macrinite and micrinite.

At 59.1 wt% extraction yield, most of the unextracted vitrinite (telocollinite) particles were finely fragmented, although breakage may have occurred in the fragile vitrinites when the epoxy resin block was cured. This observed difference of extractability in vitrinites may be attributed not to differences in their maceral components, but to the heterogeneity of the chemical structure in telocollinite, such as the cross-link density and the

Table 5 Compositions of inertinite in Zao Zhuang I coal and its extraction residues

Extraction yield (wt% daf)	Inertinite[a] (vol% dmmf)	Composition (vol% dmmf)			
		Pseudovitrinite	Semifusinite	Fusinite	Macrinite + micrinite
0.0	23.3	41.1	40.0	5.1	13.8
11.0	25.5	37.9	41.5	8.0	12.6
28.5	25.9	36.3	39.4	7.0	16.8
59.1	35.0	23.0	40.2	14.5	22.1
74.1	40.2	14.9	43.1	17.8	24.2
36.3[b]	30.8	23.7	49.4	6.8	20.0

[a]Including pseudovitrinite
[b]Soxhlet extraction with pyridine

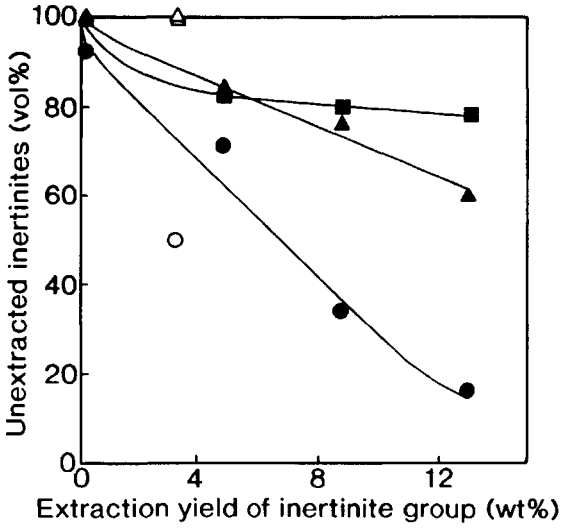

Figure 3 Contents of unextracted inertinite macerals and pseudovitrinite versus coal extraction yield: ●, ○, pseudovitrinite; ▲, △, semifusinite; ▼, ▽, fusinite; ■, □, macrinite + micrinite; ●, ▲, ▼, ■, CS_2–NMP; ○, △, ▽, □, pyridine

analysis of the inertinite macerals in the Zao Zhuang I coal and its residues. As the extraction yield increased, pseudovitrinite in the residue decreased, semifusinite did not change, and fusinite and macrinite + micrinite gradually increased, indicating that a significant amount of pseudovitrinite and semifusinite was extracted with the mixed solvent.

Figure 3 plots the contents of inertinites and pseudovitrinite in the residues against the extraction yield. Most of the fusinite, macrinite and micrinite was unextracted. In contrast, pseudovitrinite and semifusinite were extracted with the CS_2–NMP mixed solvent, to the extent of 80 and 50 wt% respectively at an extraction yield of 13 wt% of the inertinite. Such extractability of semifusinite exceeds that expected according to Scharpiro and Gray[5]. This high extractability of semifusinite and pseudovitrinite may be the reason for the high extraction yield with the CS_2–NMP mixed solvent. Pyridine extracted more pseudovitrinite than did CS_2–NMP at the same extraction yield, as shown in *Figure 3*.

CONCLUSIONS

There was a difference in extractability with carbon disulphide–*N*-methyl-2-pyrrolidinone mixed solvent at room temperature among the maceral components. At low extraction yields (<30 wt% daf), pseudovitrinite and semifusinite were extracted to a similar extent to vitrinites. Pseudovitrinite became dark and fragile on solvent extraction, similar to the behaviour of vitrinites. Fusinite, macrinite and micrinite were little penetrated by the solvent and only slightly extracted. At high extraction yields (>50 wt% daf), vitrinites were somewhat preferentially extracted. At 74.1 wt% extraction yield for Zao Zhuang I coal, 80 wt% of pseudovitrinite and 50 wt% of semifusinite were extracted with the CS_2–NMP mixed solvent even at room temperature, whereas some vitrinite still remained in the residue, although it was almost completely fragmented by the penetration of the solvents.

It is known that extractability also depends considerably on coal rank. Coal extractability therefore needs to be considered in terms of maceral composition (coal origin) and with rank (coalification).

ACKNOWLEDGEMENTS

The authors thank Dr Keizo Fujii of the Geological Survey of Japan for his direction and discussion on the maceral analysis, and Takeo Yamada, Yukio Enda and Toru Yamashita of Idemitsu Kosan Co. Ltd for their support in the maceral separation.

REFERENCES

1 Stach, E., Mackowsky, M.-T., Teichmuller, M., Taylor, G. H., Chandra, D. and Teichmuller, R. 'Stach's Textbook of Coal Petrology', Gebrüder Borntraeger, Berlin, 1982, pp. 127, 423
2 Shibaoka, M., Heng, S. and Okada, K. *Fuel* 1985, **64**, 600
3 Heng, S. and Shibaoka, M. *Fuel* 1983, **62**, 610
4 Shibaoka, M. *Fuel* 1985, **64**, 606
5 Schapiro, N. and Gray, R. J. *J. Inst. Fuel* 1964, **37**, 234
6 Mochida, I., Iwamoto, K., Tahara, T., Korai, Y., Fujitsu, H. and Takeshita, K. *Fuel* 1982, **61**, 603
7 Mochida, I., Kishino, M., Sakanishi, K., Korai, Y. and Takahashi, R. *Energy Fuels* 1987, **1**, 343
8 Fujii, K. and Shoda, K. *J. Jpn. Ass. Pet. Technol.* 1983, **48**, 321
9 Iino, M., Takanohashi, T., Ohsuga, H. and Toda, K. *Fuel* 1988, **67**, 1639
10 Iino, M., Takanohashi, T., Obara, S., Tseuta, H. and Sanokawa, Y. *Fuel* 1989, **68**, 1588
11 Iino, M., Takanohashi, T., Ohkawa, T. and Yanagida, T. *Fuel* 1991, **70**, 1236
12 Kimura, H. *J. Fuel Soc. Japan* 1979, **58**, 75

Effects of additives and oxygen on extraction yield with CS_2–NMP mixed solvent for Argonne premium coal samples

Tatsushi Ishizuka, Toshimasa Takanohashi, Osamu Ito and Masashi Iino
Institute for Chemical Reaction Science, Tohoku University, Katahira 2-1-1, Aoba-ku, Sendai 980, Japan
(Received 17 August 1992)

Addition of tetracyanoethylene or *p*-phenylenediamine to CS_2–NMP mixed solvent markedly increased the extraction yield for Upper Freeport coal (86 wt% C). The presence of atmospheric oxygen during extraction decreased the yield. The pyridine-insoluble fraction of the extract was most affected. No such large effects were observed for other coals. The mechanisms responsible are discussed.

(Keywords: oxygen; extraction yield; carbon disulfide)

Carbon disulfide (CS_2)–*N*-methyl-2-pyrrolidone (NMP) mixed solvent (1:1 by volume) has been found to give high extraction yields (40–65 wt% daf) for many bituminous coals at room temperature[1,2]. When the extracts were fractionated with pyridine to yield pyridine-insoluble (mixed-solvent-soluble) (PI) and pyridine-soluble (PS) fractions, part of the PI fraction was found to become insoluble in the CS_2–NMP mixed solvent[3]. It was also found[3] that the addition of compounds such as 7,7,8,8-tetracyanoquinodimethane (TCNQ), tetracyanoethylene (TCNE) and *p*-phenylenediamine (PDA) to PI suppressed its precipitation, probably because the association between PI molecules was broken by the additives.

This communication reports the effect of these additives on the mixed solvent extraction of the Argonne premium coal samples, analyses of which[4] are listed in *Table 1*. The extractions were carried out exhaustively, without special protection from exposure to air, at room temperature under ultrasonic irradiation (38 kHz), as described previously[2]. Usually 1 g of coal was extracted for 30 min in 65 ml of the mixed solvent containing 10–25 mg of additive per g of coal (0.15–0.38 mg per ml of solvent). Further extractions (usually two or three) of the residue were performed using the same quantities of the mixed solvent and additive until the supernatant became almost colourless. The extraction yield (daf) was determined from the weight of the residue. The recovery of residue + extract was 96.5–100.5 wt%.

Table 2 shows that a very high extraction yield, 84.6 wt% (daf), was obtained from Upper Freeport (UF) coal on addition of a small amount (10 mg g^{-1}) of TCNE, an increase of ~20 wt% over the yield without TCNE. PDA was also found to be effective. The extraction yields did not increase when the amount of TCNE increased from 10 to 25 mg g^{-1}. The other coals gave no clear increase of the yield upon addition of TCNE.

Table 2 also shows that the addition of TCNE mainly increased the PI fraction, which is heavier than PS. FT-i.r. spectra of the extracts and residues showed that even after washing with acetone, a new peak due to the CN group appeared at 2198 cm^{-1} for PI, PS and residue. Corresponding peaks for TCNE itself appeared at 2262 and 2227 cm^{-1}. This shift may be ascribed to the formation of π–π complexes (including charge-transfer complexes with aromatic rings in coal) and/or Diels–Alder adducts of TCNE and aromatic rings in the coal molecules. E.s.r. measurements showed that the spin concentrations of PI, PS and residue increased, but the line shape was not detectably changed, in the extraction with TCNE.

These effects of TCNE and PDA can be explained by the formation of π–π complexes, as in the solubilization behaviour of PI described previously[3]. It seems unlikely that adduct formation is a main cause, since PDA, which does not form Diels–Alder adducts with aromatics, increased the extraction yields. In addition to the increase in solubility[3] of the coal molecules in the mixed solvent, weakening of the stacking of the aromatic rings in coal may also be responsible for the increase in yield. TCNE is known to undergo Diels–Alder addition reactions with aromatics such as anthracene[5].

In relation to the effect of the additives above, the effect of oxygen was also investigated. *Table 3* shows that UF coal gave a distinctly higher extraction yield, 63.7–69.7 wt% (daf), when the whole extraction procedure was performed under nitrogen in a glove box than that (60.1–62.6 wt% daf) obtained by the usual procedure in air. The fraction distributions of the extracts show that it was mainly the PI that increased, compared with extraction in air. As with TCNE addition, coals other than UF did not show a yield increase. The extraction

Table 1 Analyses of coals

Coal	Ultimate analysis (wt% daf)				Proximate analysis (wt% db)			Maceral analysis (vol% mmf)[b]		
	C	H	N	S + O[a]	VM	Ash	FC	Liptinite	Vitrinite	Inertinite
Pocahontas No. 3	89.7	4.5	1.1	4.7	17.6	4.8	77.6	1	89	10
Upper Freeport	86.2	5.1	1.9	6.8	28.2	13.1	58.7	1	91	8
Pittsburgh No. 8	82.6	5.5	2.1	9.8	38.3	8.7	53.0	7	85	8
Illinois No. 6	76.9	5.5	1.9	15.7	38.6	15.0	46.4	5	85	10

[a] By difference
[b] Ref. 4

0016-2361/93/04/0579-02

Table 2 Effect of additives on extraction of Argonne premium samples with CS_2–NMP mixed solvent

Coal	C(wt% daf)	Additive (mg g^{-1} coal)	Extraction yield (wt% daf)	Fraction distribution of extract	
				PI (wt% db)	PS (wt% db)
Pocahontas No. 3	89.7	none	2.8[b]	–	–
		TCNE (25)	1.9	–	–
Upper Freeport	86.2	none	59.4	19.9	32.9
		TCNE (10)	84.6	–	–
		TCNE (25)	84.6	39.0	31.9
		TCNE (25)[a]	84.1	–	–
		PDA (25)	78.7	–	–
Pittsburgh No. 8	82.6	none	39.0[b]	–	–
		TCNE (25)	42.6	–	–

[a] Extraction three times with magnetic stirring for 120 min, without ultrasonic irradiation
[b] Data from Ref. 6

Table 3 Effect of atmosphere on extraction of Argonne premium samples with CS_2–NMP mixed solvent

Coal	C(wt% daf)	Atmosphere	Extraction yield (wt% daf)	Fraction distribution of extract	
				PI(wt% db)	PS(wt% db)
Pocahontas No. 3	89.7	N_2	1.9	0.1	2.0
		Air[a]	2.8	0.5	2.2
Upper Freeport	86.2	N_2	68.9	32.3	31.3
		N_2	69.7	39.6	28.7
		N_2	66.2	35.4	24.9
		N_2	63.7	34.7	23.4
		Air	62.6	26.1	28.8
		Air	60.7	27.5	27.3
		Air	60.1	19.9	32.9
		Air	60.5	26.5	24.5
Pittsburgh No. 8	82.6	N_2	36.7	0.3	39.7
		Air[a]	39.0	0.4	35.2
Illinois No. 6	76.9	N_2	31.2	0.2	29.7
		Air[a]	33.1	0.1	27.6

[a] Data from Ref. 6

yields of weathered UF coal exposed to air for 1, 3, 5 and 7 days were reported[6] to be almost unchanged, compared with the original coal; only after 6 months did the yield decrease detectably from ~60 wt% (daf) for the raw coal to 51.8 wt% (daf). Since the extraction procedure, including solvent washing, usually takes 1–2 days, oxidation does not seem to be responsible for the decrease in yield when air is present. Possible reasons are insolubilization by association of coal molecules accelerated by oxygen and/or a decrease in affinity of the solvent for the coal as a result of adsorption of oxygen on the coal surface.

The result without ultrasonic irradiation in *Table 2* shows that such irradiation only accelerates the extraction rate and does not increase the yield, suggesting that it does not break any covalent bonds in coals. These results show that UF coal contains ~85 wt% of extractable, solvent-soluble material, suggesting that this coal does not possess much covalently cross-linked network. The fact that UF coal gives a very high extraction yield, agrees with the speculation[7] that coals of ~86 wt% C (daf), such as UF coal (*Table 1*), have a minimum cross-link density. Therefore the coal structure model[8] widely accepted, which consists of covalently cross-linked network with a relatively small amount of extractable components, does not seem to be applicable to this coal.

REFERENCES

1 Iino, M., Kumagai, J. and Ito, O. *J. Fuel Soc. Japan* 1985, **64**, 210
2 Iino, M., Takanohashi, T., Ohsuga, H. and Toda, K. *Fuel* 1988, **67**, 1589
3 Sanokawa, Y., Takanohashi, T. and Iino, M. *Fuel* 1990, **69**, 1577
4 Vorres, K. S. 'Users' Handbook for the Argonne Premium Coal Sample Program', Argonne National Laboratory, Argonne, IL, 1989
5 Middleton, W. J., Heckert, R. E., Little, E. L. and Krespan, C. G. *J. Am. Chem. Soc.* 1958, **80**, 2783
6 Takanohashi, T. and Iino, M. *Energy Fuels* 1990, **4**, 452
7 Green, T., Kovac, J., Brenner, D. and Larsen, J. W. In 'Coal Structure' (ed. R. A. Mayers), Academic Press, New York, 1982, p. 268
8 Given, P. H., Marzec, A., Barton, W. A., Lynch, L. J. and Gernstein, B. C. *Fuel* 1986, **65**, 155

論　文

液化残渣の構造と水素供与能

(キーワード　液化残渣，溶媒抽出，重質成分，水素供与能)

— 1993. 7 .15 受理 —

東北大学　鷹觜　利公，劉　　宏濤
沈　　建立，飯野　　雅

1．緒　言

現在開発が進められているNEDOLプロセスでは，プロセスのスケールアップおよびその長時間運転がいくつかの炭種で実現され，大きな成果を挙げているものの，その一方で多量に排出される液化残渣の処理の問題が指摘されている。この液化残渣の処理方法には大きく分けて二つの選択がある。一つは排出される液化残渣の利用法を探索し，その付加価値を高め利用するプロセスの導入であり，もう一方は現在の液化反応の運転条件の最適化により，排出される残渣の量それ自身を減少させる方法である。単純に考えると後者の対策が，新たな設備の必要も無くより効率的に思える。しかしながら現実問題として，現段階ではその最適条件の検索は難しい。それは液化反応プロセスが大規模であり運転条件の操作が容易でないこと，あるいは単位操作ごとの石炭のハンドリングが難しく，運転条件によっては閉塞などの新たな問題が発生するためである。従って最適な運転条件の問題とも関連して，現在のプロセスで排出される液化残渣の性状，反応性について明らかにしていくことが，液化残渣の処理方法の探索において必要であると考えられる。

NEDOLプロセスに限らず，液化残渣の性状と利用法に関してこれまでいくつか報告されている。古田ら[1)2)]は0.1t/dayのBSUプラントからの液化残渣を溶媒分別して，各成分の構造解析を行ない，さらにそれらの熱処理によるガス生成挙動や炭素化挙動について報告している。その結果，重質な成分であるトルエン不溶-THF可溶成分でも単位構造の平均芳香族環数は3環程度であると述べている。液化残渣のハンドリングに関して，その粒子の付着力の強さのために，閉塞などの問題が起こることが指摘されている。この点に関して川島ら[3)]海保ら[4)]はPDU液化プラントから排出される液化残渣を試料として，その液化残渣と原炭の付着力の違いを明確にし[4)]，また液化残渣を酸化処理することによりその付着力が低下し，ガス化反応性が向上することを報告している[3)]。また鵜野ら[5)]は液化残渣に残存する揮発成分に注目し，利用法の一つとして液化残渣の熱分解プロセスを想定し，その基礎実験結果を検討している。その結果，750℃の急速熱分解（3sec）では，熱分解油収率25％，ガス収率5％が得られ，液化プロセスとの組み合わせにより，トータルのオイル収率の向上が期待できると述べている。

液化残渣の一つの処理法として，排出される残渣の一部を反応器へ戻す，いわゆるボトムリサイクル法が考えられる。この処理においては，残渣に残存する揮発分量のほかに，残渣の水素供与能・受容能の性状が関与する。すなわち液化残渣と原炭の間に効率的な水素の交換が達成されれば，液化収率の向上が期待される。この点に関して二タ村ら[6)]は，*trans*-スチルベン，ビベンジルを用い，その水素化分解に及ぼす液化残渣の添加効果から，液化残渣の水素供与能について評価している。その結果，液化残渣が不飽和結合の水素化，およびアリールメチルラジカルの安定化に対して有効な水素供与体として働いていることを見いだしている。液化残渣のこのような高い水素供与能は，単にボトムリサイクル法に限らず，液化残渣自身の付加価値を高め，その有効な利用法につながる重要な性状である。

本研究ではNEDOL液化プロセスから排出される液化残渣を，溶媒抽出と分別によりいくつかのフラクションに分け，特にその中の重質可溶成分に注目して構造解析を行なった。さらにこの液化残渣と瀝青炭

反応化学研究所　仙台市青葉区片平2丁目1－1

（原炭）との共熱処理を行ない，その生成物分布をもとに液化残渣から石炭への水素供与能の評価を試みた。

2．実　験

2.1　試　料

ワンドアン（WN）炭，イリノイ（IL）炭，ワイオミング（WY）炭を450℃で液化した際に生成した液化残渣（それぞれWN-LR，IL-LR，WY-LRで示す）を試料とした。またIL炭とWY炭についてはそれらの原炭（IL-OR，WY-OR）も用いた。

2.2　溶媒抽出および分別

250㎜以下に粉砕した試料2 gを二硫化炭素-*N*-メチル-2-ピロリジノン混合溶媒（容積比1：1）50mℓと加え，超音波（38kHz）照射下，室温で30min抽出した。この混合溶媒は瀝青炭に対して高い抽出率を与え，特に石炭中の重質成分の抽出に有効であることが分かっている[7)8)]。抽出後高速遠心分離（25400 g）をかけ，それから平均径0.8μmのメンブレンフィルターを用いて濾過し抽出液を得た。この一連の抽出操作を3回繰り返して行なった。抽出残渣から溶媒を除去するために，アセトンで超音波洗浄（15min）を3回繰り返した。その後80℃で真空乾燥を行なった。抽出率は乾燥後の抽出残渣の重量をもとに無水無灰基準で計算した。一方抽出液は，エバポレーターで順次混合溶媒を除き，それからFig.1に示すようにアセトンとピリジンを用いて，アセトン可溶分（AS），アセトン不溶-ピリジン可溶分（PS），ピリジン不溶分（PI）にそれぞれ分別した。

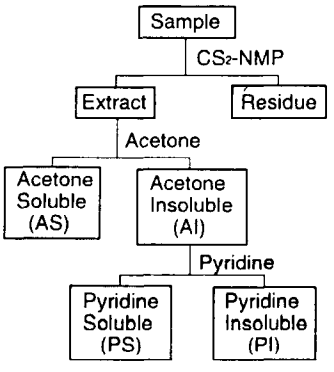

Fig. 1　Fractionation procedure of extract

以降抽出残渣についてはERで示し，例えばイリノイ炭液化残渣の抽出残渣はIL-LR-ERで表わすことにする。

2.3　FT-IR測定

液化残渣の抽出から得られる各抽出物フラクションと残渣，および原炭の抽出で得られる各フラクションついてFT-IRスペクトルを測定した。装置はJEOL JIR-100を使用し，拡散反射法で行なった。

2.4　共熱処理

著者ら[9)10)]は，瀝青炭を100-250℃でテトラリンまたはナフタレン中で熱処理すると，石炭中の重質成分の一部が不溶化し，また同様の処理を9,10-ジヒドロアントラセンなどの強い水素供与性溶媒中で行なうとその不溶化反応が抑制され，さらに一部で軽質化反応が起こることを見いだしている。そこでアルゴンヌ標準試料炭であるアッパーフリーポート炭とワイオミング液化残渣の共熱処理を行ない，液化残渣から石炭への水素供与能について検討した。熱処理は100mℓの撹拌式オートクレーブを用い，窒素雰囲気下反応温度250℃，反応時間1 hrで行なった。反応生成物をCS_2-NMP混合溶媒とTHSを用いて溶媒分別し，各成分の挙動を見た。

3．結果と考察

3.1　溶媒抽出と分別

Table 1に原炭とその液化残渣のCS_2-NMP混合溶媒抽出率，および溶媒分別の結果を示す。原炭の抽出率はIL-ORとWY-ORでそれぞれ23.9%，16.5%であるのに対して，それぞれの液化残渣の抽出率は

Table 1　Extraction and fractionation of raw coals and the liquefaction residues

Sample	Residue (wt%, db)	Extraction yield (wt%, daf)	Extract (wt%, daf)			Recovery (wt%, db)
			AS	PS	PI	
IL-OR	78.4	23.9	9.5	14.3	0.1	99.0
IL-LR	42.4	86.1	61.7	23.8	0.6	98.0
WY-OR	84.4	16.5	14.0	2.4	0.1	95.2
WY-LR	33.1	91.1	53.3	31.9	5.9	100.7
WN-LR	37.0	90.1	64.3	21.3	4.5	97.3
WN-LR	37.3[a)]	89.7[a)]	-	-	-	-

a) Quinolin extraction

Table 2 Ultimate analysis of Wyoming raw coal and its liquefaction residue, and their extract fractions and extraction residue

Fraction	C	H	N	S	O[a)]	ash	H/C	O/C
	(wt%, daf)					(wt%, db)	(-)	(-)
WY-OR	64.7	5.2	0.9	0.8	28.4	5.2	0.97	0.33
WY-OR-RE	69.5	5.3	1.8	0.9	22.5	5.8	0.91	0.24
WY-OR-PS	72.6	6.3	1.6	2.2	17.3	0.0	1.04	0.18
WY-OR-AS	70.6	7.4	3.6	3.5	14.9	0.0	1.26	0.16
WY-LR	88.1	5.3	2.0	2.0	2.6	26.6	0.73	0.022
WY-LR-RE	-	-	-	-	-	75.3	-	-
WY-LR-PS	86.5	4.6	1.8	1.9	5.2	0.0	0.64	0.045
WY-LR-AS	88.9	6.0	1.6	1.3	2.2	0.0	0.81	0.019

a) By difference

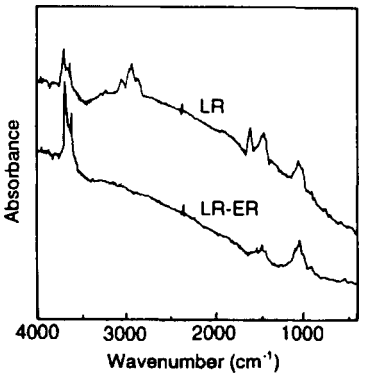

Fig. 2 FT-IR spectra of the Wandoan coal liquefaction-residue (LR) and its extraction-residue (LR-ER)

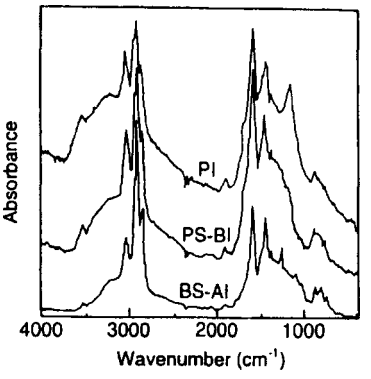

Fig. 3 FT-IR spectra of the extract fractions obtained from the extraction of Wandoan coal liquefaction-residue

86.1%，91.1%と高いことが分かる。またワンドアン炭液化残渣（WN-LR）に対して同様な室温抽出をキノリンで行なった結果も表に示しているが，混合溶媒（90.1%）とほぼ同程度の抽出率（89.7%）が得られた。キノリンはそれ自身粘度が高く，通常の原炭の抽出では抽出速度が遅く，また抽出能も混合溶媒に比べてかなり低い溶媒である。溶媒分別の結果を見ると，比較的軽質なアセトン可溶（AS）成分がイリノイ，ワイオミング，ワンドアン炭の液化残渣中にそれぞれ61.7wt%，53.3wt%，64.3wt%と多く含まれていることが分かる。原炭のフラクション分布を見ると，もともと含まれるAS成分の量は約10～14wt%程度と少ないことから，液化残渣中に含まれる成分は，液化反応による分解生成物であると言える。また本実験での最重質成分であるPI成分の量は各残渣で少なく，結果的に抽出物のほとんどがピリジン可溶の成分（AS+PS）であった。

以上の溶媒抽出・分別の結果から，液化反応においてかなり低分子化反応が進んでおり，すでに石炭の架橋結合の大部分が切断され，排出される液化残渣中にはかなりの量の液化中間生成物が含まれていることを示している。一方で各石炭の液化残渣中の抽出残渣成分である約10%の有機質成分については，化学的に不活性と言われているフジニット成分などの未反応成分であると考えられる。例えばワンドアン炭中にはフジニットが15.0vol%含まれていることが分かっている[11]。

3.2 構造解析

Table 2にワイオミング炭の各フラクションの元素分析値を示している。液化残渣WY-LRのH/C値は0.73であり，これは原炭WY-OR（0.97）やその抽出残渣WY-OR-ER（0.91）に比べてかなり低い。また酸素含量が液化により大幅に減少していることが分かる。灰分量に注目すると，液化残渣中には原炭に含ま

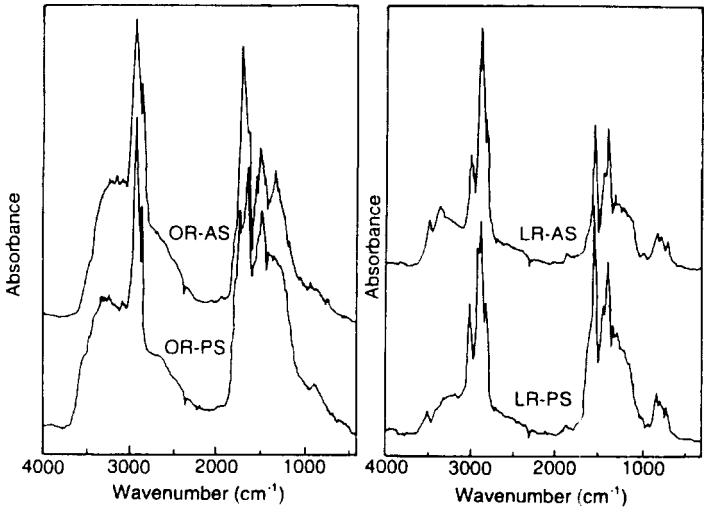

Fig. 4 FT-IR spectra of the extract fractions obtained from the extractions of raw Wyoming coal and its liquefaction residue

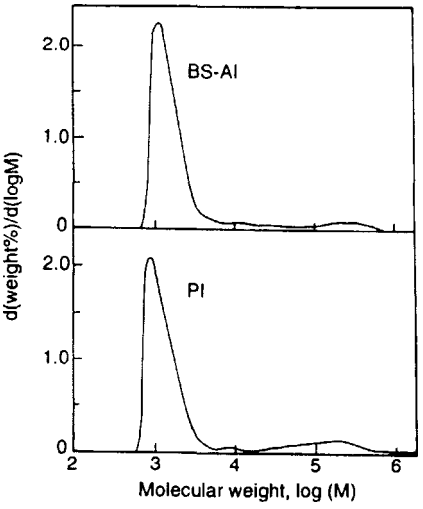

Fig. 5 Molecular weight distribution of the extract fractions from the extraction of Wandoan coal liquefaction-residue

れていた灰分のほかに，液化反応で使用した触媒が残存しているため26.6%と高い値となっている。表から分かるように，溶媒抽出後 AS，PS 成分中には灰分が検知されず，抽出残渣にすべて濃縮されている。従って液化残渣を有効利用する際に，こうした単純な室温抽出により，液化残渣中の多量の有機質成分から（灰分＋残存触媒）を効率的に除去できることが示唆された。また原炭抽出および液化残渣抽出からそれぞれ得られる OR-PS，OR-AS および LR-PS，LR-AS を比較すると，液化残渣から得られた方が O/C，H/C 値ともそれぞれかなり低い値となっており，同石炭からの同じフラクション成分とはいえ，液化反応により芳香族性が増加した重質な成分になっていることを表わしている。他に窒素，硫黄含量には大きな違いは見られなかった。以上の傾向はイリノイ炭でも同様に確認された。

Fig.2にワンドアン炭液化残渣（LR）とその抽出残渣（LR-ER）の FT-IR スペクトルを示す。これらの試料中には前述のようにかなりの鉱物質成分が含まれるため，スペクトルは鮮明ではない。液化残渣中に2900cm^{-1}付近の脂肪族 C-H に起因するピーク，あるいは3030cm^{-1}付近の芳香族 C-H に起因するピークが見られる。Fig.3にはそのワンドアン炭液化残渣からの抽出物フラクション中の重質成分の FT-IR スペクトルを示す。違いを明確にするため，PS 成分についてはベンゼンでさらに溶媒分別を行ない，ベンゼン可溶-アセトン不溶（BS-AI）成分とベンゼン不溶-ピリジン可溶（PS-BI）成分に分けて測定を行なった。BS-AI，PS-BI，PI とフラクションの重質化に伴ない，2900cm^{-1}のピークに対する3030cm^{-1}のピーク強度比が増加しており，この順に芳香族性が増加していることを示している。また3300cm^{-1}～3400cm^{-1}の水酸基に由来するピークもこの順に増加しており，重質成分中に水酸基が多いことを示している。原炭の抽出から得られた抽出物フラクションのキャラクタリゼーションでも同様の傾向が得られている[12]。

次に原炭および液化残渣の抽出から得られた各フラクションの FT-IR スペクトルを Fig.4に示す。両ス

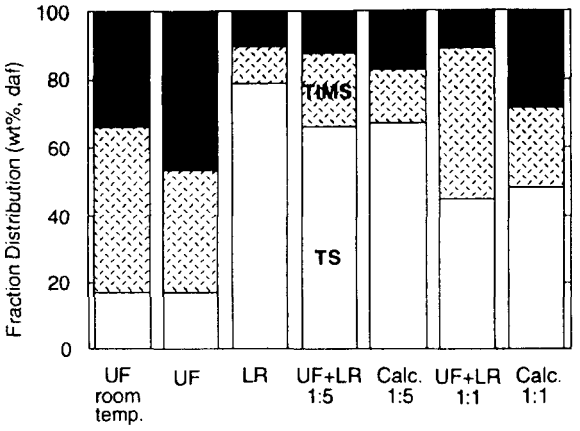

Fig. 6 Fraction distribution after the heat treatment of Wyoming coal liquefaction-residue (LR) with Upper Freeport (UF) raw coal at 250℃ : MI ; the CS_2-NMP mixed solvent insoluble, TIMS ; THF insoluble and the mixed solvent soluble, TS ; THF soluble fractions

ペクトルを比較すると大きな違いが見られ，原炭由来の成分に比較して液化残渣由来の抽出物成分では，3300～3400cm^{-1}付近のピークが大きく減少し，逆に1600cm^{-1}，3030cm^{-1}付近の芳香族由来の吸収が相対的に増加しているのが分かる。従って液化反応により構造内の水酸基を含む酸素官能基が分解脱離され，また芳香環が発達した成分が液化残渣中に多く含まれていることを示している。以上の結果は元素分析の結果と一致している。

Fig.5にはワンドアン炭液化残渣中のBS-AI成分とPI成分のサイズ排除クロマトグラフィーで求めた分子量分布を示す。移動相にはCS_2-NMP混合溶媒を用い，分子量換算には標準ポリスチレンの校正曲線を用いた。いずれの成分でも分布は二相に分かれており，大部分は数千の分子量からなるのに対して，少量の高分子量（数10万）成分を含んでいる。またより重質な成分であるPI成分に高分子量成分が多いことが分かる。元素分析，FT-IRの結果から重質成分には極性成分が相対的に多いことが分かっており，ここで見られた高分子量域のピークがそうした極性成分同士の会合，あるいは移動相溶媒との相互作用に起因することも考えられ，実際この成分が高分子量成分であるかどうかについては明らかでない。

3.3 共熱処理

液化残渣中には元素分析で示したように，いまだ多くの水素が残存しており，その水素を有効に利用することが望ましい。そこでモデル化合物の水素化分解で液化残渣自身に高い水素供与能が認められたという二タ村らの報告[6]に基づき，液化残渣の石炭への水素供与能について検討を試みた。Fig.6にアッパーフリーポート炭（UF）とワイオミング炭液化残渣（WY-LR）の共熱処理を250℃で行なった結果を示している。UF炭だけの熱処理では（溶媒：1-メチルナフタレン），室温での溶媒分別の結果に比較して，可溶成分収率（TIMS＋TS）が減少しているのが分かる。この不溶化機構については他で詳しく検討を行なっている[10]。またこのWY-LRだけを熱処理した時（溶媒：1-メチルナフタレン），ほぼ室温と同様の混合溶媒可溶成分収率が得られている。一方でこれらを1：1で混合した後共熱処理した場合（UF＋LR），それぞれの単独の熱処理から計算される分布（Calc.）に比較して，17%の可溶成分収率（TIMS＋TS）の増加が確認された。各生成物分布から考察したところ，液化残渣中の成分も共熱処理により変化していることが考えられ，UF炭基準の収率変化を決定することはできなかった。一方でUF炭を同様の熱処理条件の下，9,10-ジヒドロアントラセンや液化循環溶剤中で行なうと，この共処理で見られたように，石炭の不溶化反応が抑制され，軽質成分が増加することが確認されている[10]。従ってこの共熱処理では，液化残渣から瀝青炭への水素供与がこうした比較的低温で起きていることを示唆している。

4．結　論

本研究で試料として用いた3炭種からの液化残渣中には，53%～64%のかなりの量のアセトン可溶成分（アスファルテン程度）が含まれており，さらにピリジン可溶成分（プレアスファルテン程度）まで含めると約85%の可溶成分収率が得られた。ただし原炭由来の各成分との構造解析の比較では，液化残渣由来の成分ではH/C値，O/C値が低く，FT-IR測定からも芳香族性の高い成分であることが明らかとなった。液化残渣と瀝青炭との250℃の共熱処理の結果，こうした低温にもかかわらず，全体として軽質化反応が進行することが確認された。これは液化残渣からの水素供与が関連していることが考えられ，こうした比較的低温で，液化残渣が高い水素供与能をもつことが示唆された。

以上の結果をまとめると，液化残渣のボトムリサイクルにより，それ自身の分解でオイル成分を向上させるのは，液化残渣の芳香族性の発達から容易ではないと考えられるものの，循環溶剤として考えた場合，石

炭未反応分や中間生成物への水素源として有用であることが示唆された。また低温で高い水素供与能を有することから，別の低温改質処理プロセスの水素源として有効であることが期待される。

（謝　辞）

本研究は新エネルギー・産業技術開発機構（NEDO）の委託研究の一環として実施されたものであり，試料を提供して下さいました日本コールオイル㈱，また発表の機会を与えて下さいましたNEDOに感謝いたします。

文　献

1) 古田　毅，丸山勝久，山口　潔，白石　稔，伊牟田和敏，第25回石炭科学会議発表論文集，p.167 (1988)
2) 古田　毅，丸山勝久，山田能生，白石　稔，第26回石炭科学会議発表論文集，p.244 (1989)
3) 川島裕之，山下安正，海保　守，小林光雄，牧野三則，山田　理，第25回石炭科学会議発表論文集，p.199 (1988)
4) 海保　守，牧野三則，小林光雄，山田　理，山下安正，川島裕之，岩田博行，第27回石炭科学会議発表論文集，p.214 (1990)
5) 鵜野健夫，佐々木正樹，小水流広行，奥原捷晃，和田幸一，第28回石炭科学会議発表論文集，p.125 (1991)
6) 二タ村森，本多総一郎，大川晃次郎，第29回石炭科学会議発表論文集，p.36 (1992)
7) Iino, M., Takanohashi, T., Ohsuga, H. and Toda K., *Fuel*, 67, 1639 (1988)
8) Takanohashi, T. and M. Iino, *Energy Fuels*, 4, 452 (1990)
9) Wei, X.-Y., Shen, J.-L., Takanohashi, T. and Iino, M., *Energy Fuels*, 3, 575 (1989)
10) Shen, J.-L., Takanohashi, T. and Iino, M., *Energy Fuels*, 6, 854 (1992)
11) 鵜野健夫，奥原捷晃，和田幸一，第28回石炭科学会議発表論文集，p.121 (1991)
12) Iino, M., Takanohashi, T., Obara, H. and Tsueta, H., *Fuel*, 68, 1588 (1989)

Structures and Hydrogen Donating Abilities of Liquefaction Residues

Toshimasa TAKANOHASHI, Hong-Tao LIU, Shen-Jian LI and Masashi IINO

(Institute for Chemical Reaction Science, Tohoku University)

SYNOPSIS：— The liquefaction residues discharged from the NEDOL process, were extracted with carbon disulfide - *N*-methyl-2-pyrrolidinone mixed solvent at room temperature. The extraction yields were 86.1%, 91.1%, 90.1% for Illinois, Wyoming, Wandoan coal liquefaction-residues, respectively. The fractionation of the extract showed that the amount of acetone-soluble fraction was 53%-64%. From ultimate analysis and FT-IR measurements, the extract fractions had a higher aromaticity and a lower content of oxygen (especially hydroxyl group) than those for the corresponding raw coals. Heat treatment of the liquefaction residue with a bituminous coal was carried out at 250℃ to evaluate the hydrogen donating ability of the liquefaction residue to the bituminous coal. The content of soluble fraction increased by the heat treatment with the bituminous coal, compared to that calculated from the heat treatment of each component alone, indicating that the liquefaction residue donated hydrogens to the raw coal moiety even at temperature as low as 250℃.

Key Words

Liquefaction residue, Solvent extraction, Heavy fraction, Hydrogen donating ability

Reprinted from ENERGY & FUELS, 1993, 7.

Effect of TCNE Addition on the Extraction of Coals and Solubility of Coal Extracts

Hong-Tao Liu, Tatsushi Ishizuka, Toshimasa Takanohashi, and Masashi Iino*

Institute for Chemical Reaction Science, Tohoku University, Katahira 2-1-1, Aoba-Ku, Sendai 980, Japan

*Received June 8, 1993. Revised Manuscript Received August 25, 1993**

The effect of TCNE addition on the extraction of coals of different rank with carbon disulfide–*N*-methyl-2-pyrrolidinone (CS_2–NMP) mixed solvent (1:1 by volume) was investigated. TCNE increases considerably the extraction yields for some coals among the coals examined. TCNE seems to be effective for the coals that have much of heavy extract fraction, i.e., pyridine-insoluble extract fraction (E-PI). The effect of TCNE addition on the solubility of E-PI and other lighter extract fractions, and characterization of the solubilized fraction fractions by TCNE, suggest that the extraction yield enhancement by TCNE described above may be attributed to the suppression of association between coal molecules.

Introduction

A previous study[1] showed that the pyridine-insoluble extract fraction (E-PI), which was obtained from the extraction of Zao Zhuang (ZZ) coal with carbon disulfide–*N*-methyl-2-pyrrolidinone (CS_2–NMP) mixed solvent (1:1 by volume) at room temperature, was found to become partly insoluble in the CS_2–NMP mixed solvent, and the addition of the separated lighter fractions or other compounds such as tetracyanoethylene (TCNE) and *p*-phenylenediamine (PDA) recovered its solubility in the mixed solvent. Our recent work[2] shows that the addition of TCNE and PDA increases the yield of the extraction with the CS_2–NMP mixed solvent for Upper Freeport (UF, Argonne premium sample) coal, but not for other Argonne coals such as Pocahontas No. 3 and Pittsburgh No. 8 coals.

In this study, the effect of TCNE addition on the extraction of coals and the solubility of the extracts is investigated in detail for UF and other coals of different rank and mechanistic interpretations for the effect of TCNE are given.

Experimental Section

Materials. The coals were ground to <250 μm (−60 mesh), except for Argonne Premium Coal Samples, which were already ground to <150 μm (−100 mesh). All the coals were then dried in vacua at 107 °C to constant weight (2–3 h). The ultimate and proximate analyses are shown in Table I. TCNE (95% purity) and the solvents were used without further purification.

Extraction and Fractionation Procedures. Extraction and fractionation procedure are shown in Figure 1. The coals were exhaustively extracted (usually 6 times) with CS_2–NMP mixed solvent (1:1 by volume) at room temperature according to the method described before.[3] TCNE was added to a slurry of a coal in the CS_2–NMP mixed solvent just before the extraction was carried out under ultrasonic irradiation (38 kHz). The residue was washed with acetone under ultrasonic irradiation three times. The extraction yield (wt %, daf) was determined from the weight of the residue.[3] Fractionation of the extracts with acetone and pyridine gives acetone-soluble (E-AS), acetone-insoluble and pyridine-soluble (E-PS), and pyridine-insoluble (E-PI) fractions, respectively. E-PS and E-PI were washed with acetone and E-AS was washed with acetone–water mixed solvent (2:8 by volume) three times, respectively. The previous study[4] without TCNE showed that the recovery (E-AS + E-PS + E-PI + residue) for UF coal is 97.7%, indicating little retention of NMP and CS_2 in the extract and residue. FT-IR spectra (Figure 3) also showed little retention of TCNE in the residue, from which the extraction yield was determined.

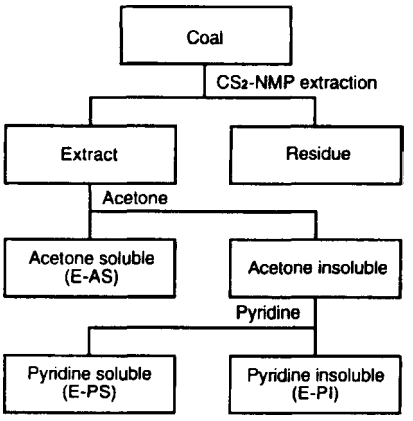

Figure 1. Solvent fractionation procedure of extracts obtained from CS_2–NMP mixed solvent extraction.

Treatment of the Extract Fractions with TCNE. A 400-mg portion of the extract fraction (E-PI or E-PS) was treated with 40 mg of TCNE in 50 mL of the CS_2–NMP mixed solvent for 30 min at room temperature under ultrasonic irradiation (38 kHz). The mixed solvent insoluble part (E-MI) was washed with acetone after centrifugation and filtration. The soluble part was fractionated with acetone and pyridine, after the evaporation of CS_2 and NMP, into E-AS, E-PS, and pyridine-insoluble and the mixed solvent soluble fraction (E-MS). The treatment of E-PI and E-PS without TCNE was also carried out and the fraction distribution was determined. FT-IR spectra of the samples were obtained by a diffuse reflectance method using a JEOL JIR-100 spectrometer.

* Abstract published in *Advance ACS Abstracts*, October 1, 1993.

(1) Sanokawa, Y.; Takanohashi, T.; Iino, M. *Fuel* **1990**, *69*, 1577–1578.

(2) Ishizuka, T.; Takanohashi, T.; Ito, O.; Iino, M. *Fuel* **1993**, *72*, 579–580.

(3) Takanohashi, T.; Iino, M. *Energy Fuels* **1991**, *5*, 708–711.

(4) Iino, M.; Takanohashi, T.; Ohsuga, H.; Toda, K. *Fuel* **1988**, *67*, 1639–1647.

0887-0624/93/2507-1108$04.00/0

Table I. Ultimate and Proximate Analyses of Coals

coal	symbol	specification	ultimate analyses (wt %, daf) C	H	N	O + S[a]	proximate analyses (wt %, db) VM	ash	FC
Pocahontas No. 3	PC	Argonne	89.7	4.5	1.1	4.7	17.6	4.8	77.6
Sewell B	SW	PSOC726	88.4	5.3	1.4	4.9	30.8	4.6	64.6
Upper Freeport	UF	Argonne	86.2	6.8	1.9	6.8	28.2	13.1	58.7
Upper Freeport	UFPSOC	PSOC1441	85.0	5.6	1.7	7.7	32.5	13.1	54.0
Lower Kittanning	LK	PSOC815	84.0	5.6	1.7	8.7	31.5	9.0	56.4
Pittsburgh No. 8	PITT	Argonne	82.6	5.5	2.1	9.8	38.3	8.7	53.0
Stigler	SG	PSOC1376P	77.8	4.8	1.5	15.9	30.7	11.7	57.6
Illinois No. 6	IL	Argonne	76.9	5.5	1.9	15.7	38.6	15.0	46.4

[a] By difference.

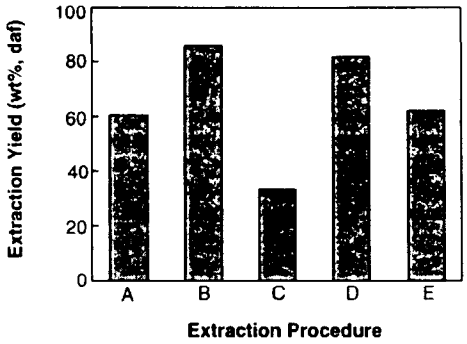

Figure 2. Extraction yield with CS_2–NMP mixed solvent for UF coal: (A) exhaustive extraction without TCNE; (B) exhaustive extraction with TCNE (0.1 g/g of coal); (C) extraction without TCNE one time; (D) extraction with TCNE (0.1 g/g of coal) one time; (E) exhaustive extraction without TCNE and subsequent extraction with TCNE (0.1 g/g of coal) one time.

Table II. Effect of TCNE Addition on Extraction of UF Coal with CS_2–NMP Mixed Solvent and Fraction Distribution of the Extracts

TCNE (g/g of coal)	extraction yield (wt %, daf)	extract fraction (wt %, db) E-PI	E-PS
none	59.4	19.9	32.9
0.010	84.6	–	–
0.025	85.0	47.0	28.5
0.025	84.6	39.0	31.9
0.100	83.2	–	–

Results and Discussion

Effect of TCNE Addition on the Extraction of UF Coal. Table II shows the yields of the exhaustive extraction of UF coal (1 g) in the mixed solvent (65 mL) without and with TCNE (0.01–0.1 g). It indicates that the addition of only 0.01 g/g of coal of TCNE increases the extraction yield from 59.4 to 84.6% and that increasing TCNE to 0.1 g/g of coal causes no increase of the extraction yield. The fraction distribution before and after TCNE addition shows that the increases in yield are due to the increase of the heavy extract fraction, i.e., E-PI, not those of E-AS and E-PS.

Figure 2 shows the yields for exhaustive extraction without (A) and with (B) TCNE (0.1 g/g of coal), single extraction without (C) and with (D) TCNE, and single extraction with TCNE after exhaustive extraction without TCNE (E). Figure 2 shows that single extraction with TCNE gives similar yield as that for the exhaustive one (B and D) and TCNE addition after the exhaustive extraction without TCNE gives no increase in yield (A and E).

Figure 3 shows the plots of the yield for single extraction with TCNE vs TCNE concentration. It shows that 0.05–

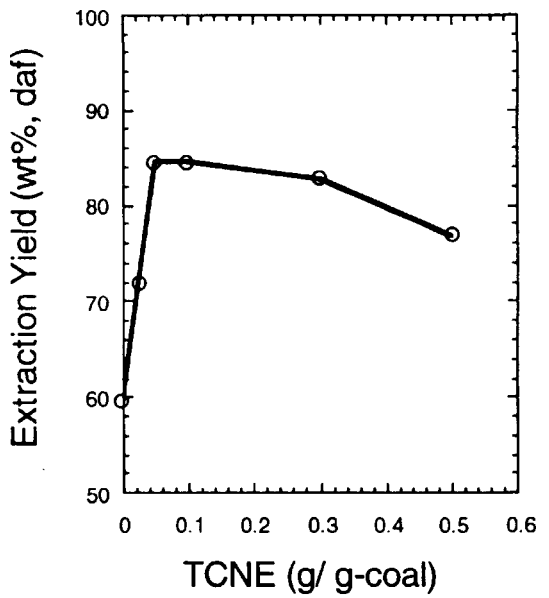

Figure 3. Plot of extraction yield vs amount of TCNE used in the extraction.

0.1 g/g of coal of TCNE gives similar high extraction yield, but the use of more TCNE than 0.1 g/g of coal unexpectedly decreases the yield. The reason is not clear at present, though the change of association state or the occurrence of some side reactions between coal molecules with TCNE may be conceivable.

Effect of TCNE Addition on the Extraction of Various Coals. Table III shows the effect of TCNE addition on the exhaustive extraction of various coals together with the fraction distribution of the extracts obtained from the extraction without TCNE. It shows that the effectiveness of TCNE does not depend on coal rank (percent carbon), and seems to depend on whether a coal has much of E-PI, i.e., the heaviest fraction of the extract or not. TCNE is not effective for the coals which have little E-PI.

Effect of TCNE Addition on the Extraction with Various Solvents. Table IV shows the results for the extraction of UF coal with pyridine and CS_2–pyridine mixed solvent (1:1 by volume) at room temperature, together with the result for the CS_2–NMP mixed solvent. Table IV shows that TCNE is not so effective for the extraction with pyridine and the CS_2-pyridine mixed solvent. This is not unexplainable since the extraction yields for the both solvents are low and the extracts mainly consist of E-AS and E-PS and have little E-PI which is responsible for the increase of the extraction yield.

Table III. Effect of TCNE Addition on Extraction of Various Coals with CS_2–NMP Mixed Solvent

coal	C, % (daf)	amount of TCNE (g/g coal)	extraction yield (wt %, daf)	extract fraction (wt %, db) E-PI	E-PS	E-AS
PC	89.7	none	2.8	0.5	1.5	0.7
		0.025	1.9	–	–	–
SW	88.4	none	37.9	11.4	18.6	5.9
		0.100	47.9	–	–	–
UF	86.2	none	60.4	24.4	24.3	7.6
		0.025	85.0	–	–	–
UFPSOC	85.0	none	44.2	6.9	23.2	8.8
		0.100	50.1	–	–	–
LK	84.0	none	46.2	8.6	25.4	5.8
		0.100	61.5	–	–	–
PITT	82.6	none	39.0	0.4	27.1	8.1
		0.025	42.6	–	–	–
SG	77.8	none	37.5	10.4	14.0	6.5
		0.100	52.3	–	–	–
IL	76.9	none	33.1	0.1	18.7	8.9
		0.100	33.1	–	–	–

Table IV. Effect of TCNE Addition on Extraction of UF Coal with Various Solvents

solvent	extraction yield (wt %, daf) without TCNE	with TCNE[a]
pyridine	2.8	4.0
pyridine–CS_2[b]	27.7	28.9
CS_2–NMP[b]	60.4	83.2

[a] TCNE/coal = 0.1 g/g coal. [b] 1:1 by volume.

Table V. Effect of TCNE Addition on the Solubility of E-PS and E-PI Fractions of UF Coal in the CS_2–NMP Mixed Solvent

fraction	additive	fraction distribution (wt %, db) E-MI	E-MS	E-PS	E-AS
E-PS	none	0.8	0.4	88.2	10.6
	TCNE[a]	0.3	0.3	83.2	16.2
E-PI	none	47.6	38.8	13.4	0.2
	TCNE[a]	1.1	83.6	14.1	1.2

[a] TCNE/coal = 0.1 g/g of extract.

Treatment of the Extract Fractions with TCNE. Table V shows the fraction distribution of E-AS, E-PS, and E-MS (the CS_2–NMP mixed solvent soluble and pyridine-insoluble fraction) and E-MI (the CS_2–NMP mixed solvent insoluble fraction of the extract, not extraction residue in Figure 1), when E-PS and E-PI were treated with TCNE in the mixed solvent, together with the results without TCNE. Table V shows that the raw E-PS contains about 10% of E-As and E-MS, probably due to a change of association state by drying at 90 °C and redissolution in the CS_2–NMP mixed solvent. Table V shows that TCNE addition to E-PS increases slightly E-AS, while the raw E-PI contains a large amount of E-MI (about 50%) due to the formation of insoluble aggregates by association during solvent fractionation, since in this case the addition of the separated E-AS and E-PS to E-PI recovers E-PI's solubility in the CS_2–NMP mixed solvent to over 90%, as described in Introduction. Table V shows that TCNE addition to E-PI decreases E-MI almost to zero, and increases E-MS, suggesting that TCNE addition changes the fraction distribution to lighter fractions. The result, that TCNE is effective for E-PI and not for E-PS, is agreement with that for the effect of TCNE addition on the extraction yields of various coals described above.

FT-IR Spectra of TCNE-Treated Samples. Figure 4 shows IR spectra of each fractions from the extraction of UF coal with TCNE, together with that of the raw coal.

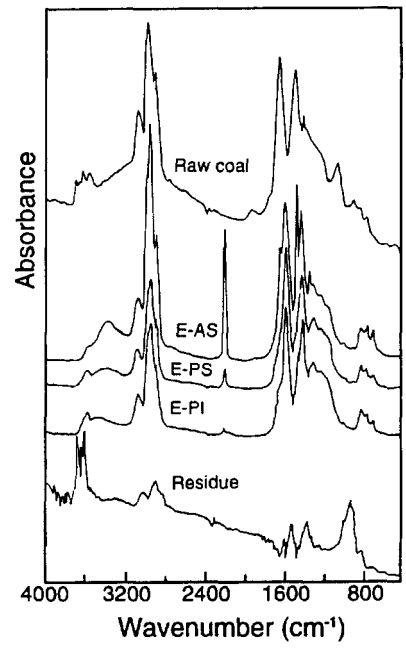

Figure 4. FT-IR spectra of UF raw coal and the fractions from the extraction with CS_2–NMP mixed solvent with TCNE.

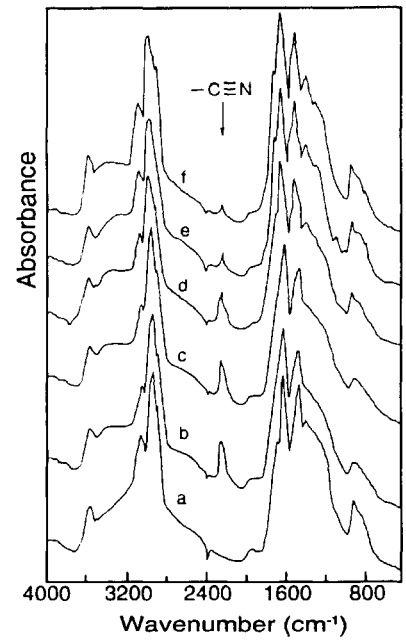

Figure 5. FT-IR spectra of CS_2–NMP mixed solvent insoluble E-PI (a) and soluble E-PI (b–f) after treatment of E-PI with TCNE. (b) Washing with acetone; (c–f) washing of the E-PI-b with benzene (c), THF (d), DMSO (e) and pyridine (f), respectively.

Figure 4 shows that TCNE-treated samples show the peak at 2200 cm^{-1} due to –CN group of TCNE, and the peak for the lighter fractions is much more intense than that for the heavier fractions. Figure 5 shows FT-IR spectra of the CS_2–NMP mixed solvent insoluble (a) and soluble E-PI (b–f) after TCNE treatment. (b, washing with acetone; c–f, washing of the soluble E-PI-b with benzene (c), THF (d), DMSO (e) and pyridine (f), respectively).

Figure 5 shows that TCNE is retained in the soluble E-PI-b not in insoluble E-PI-a. Figure 5 also shows that TCNE retained in E-PI-b was removed by the further washing with better solvents than acetone for coal. The order of the degree of the TCNE removal, i.e., acetone ≈ benzene < THF < DMSO < pyridine, agrees with that of the extraction yields obtained in the extraction of two bituminous coals (75.4 and 86.7% C, daf, respectively) with these solvents.[4,5]

The result that TCNE can be removed by solvent washing suggests that TCNE is retained by adsorption to E-PI, not by covalent bonds with E-PI by some chemical reactions such as Diels-Alder reactions.[6]

Mechanism for the Increase of Extraction Yield and Solubility by TCNE Addition. The previous section indicated that TCNE is strongly retained in the extracts and not in the residues. TCNE is also retained in the soluble fraction of E-PI, not in the insoluble fraction of E-PI, suggesting that E-PI becomes more soluble in the CS_2–NMP mixed solvent when it forms some aggregates with TCNE. In fact, the solubilized fraction of E-PI by TCNE addition becomes again partly insoluble in the CS_2–NMP mixed solvent after the removal of TCNE by washing with acetone.

Coal molecules are known to associate readily between themselves.[7,8] The associates, especially those between molecules of heavy components, are considered to be less soluble than separate "free" molecules. This may be the reason why E-PI becomes insoluble in the CS_2–NMP mixed solvent, after the removal of lighter fractions of E-AS and E-PS with solvent fractionation. The solubility increase on TCNE addition may be also due to the breaking of such associates by the formation of new associates of TCNE and coal molecules, which are, in turn, more soluble in the mixed solvent, since TCNE is readily soluble in the mixed solvent. The increase for the extraction yield by TCNE addition can be also explained by the suppression of the formation of associates between various coal molecules in raw coal by the formation of associates between TCNE and coal molecule. Hydrogen bonding, charge transfer, and dipole (ion)–dipole (ion) interaction, and aromatic (π)–aromatic (π) interaction by London dispersion forces, may be responsible for the formation of the associates. TCNE is known to be one of the strongest electron acceptors which easily forms a charge-transfer complex with electron donors, and charge-transfer interaction between coal and electron acceptors was suggested to exist.[9,10] But at present it is not clear whether it is a predominant interaction or not.

(5) Iino, M.; Matsuda, M. *Bull. Chem. Soc. Jpn.* **1984**, *57*, 3290–3294.
(6) Middleton, W. J.; Heckert, R. E.; Little, E. L.; Krespan, C. G. *J. Am. Chem. Soc.* **1958**, *80*, 2783–2788.
(7) Sternberg, H. W.; Raymond, R.; Schweighardt, F. K. *Science* **1975**, *188*, 49–51.
(8) Stenberg, V. I.; Baltisberger, R. J.; Patel, K. M.; Raman, K.; Woolsey, N. F. *Coal Science*; Gorbaty, M. L., Larsen, J. W., Wender, I., Eds.; Academic Press: New York, 1983; pp 125–171.
(9) Noshioka, M.; Gebhard, L. A.; Silbernagel, B. G. *Fuel* **1991**, *70*, 341–348.
(10) Nishioka, M. *Fuel* **1992**, *71*, 941–948.

総　説

石炭構造－溶媒抽出からのアプローチ

（キーワード　室温抽出、混合溶媒、化学構造、分子間相互作用、分子集合体）

—1991.6.17受理—

東北大学　鷹觜　利公、飯野　　雅

1．緒　言

石油の代替エネルギーとして石炭のガス化、液化、熱分解プロセスの開発研究が活発に行われている。その過程で必ず問題になるのが石炭の化学構造である。石炭は固体でハンドリングが難しく、溶媒に対して難溶であるため、化学構造などの基礎的研究が立ち遅れている。その上石炭は炭種によりその性質がかなり異なることも、このような石炭研究を進めていく上で障害となっている。

これまでの石炭構造のイメージとして、水酸基、アルキル基のついた数環の多環芳香族を基本構造とし、それがメチレン鎖、エーテル結合でつながれた三次元網目構造の中に少量の抽出可能の低分子量化合物がトラップされた構造をもつと考えられてきた[1)~3)]。

最近我々は、ある混合溶媒系が室温で、石炭によっては50%以上の抽出率を与えることを見いだした。これは上述の石炭構造に対するイメージでは説明がつかない結果である。また、得られた抽出物の性状の研究からも、石炭分子の構成や分子間相互作用の寄与などについての興味ある結果が得られている。

この総説では、最近の石炭構造に関する新しい考え方について、主として我々が行っている石炭の溶媒抽出研究から述べてみたい。

2．石炭の溶媒抽出

反応化学研究所　仙台市青葉区片平２丁目１-１

2.1　分解を伴わない単独溶媒抽出

石炭の溶媒抽出は古くから行われているが、抽出条件を見ると300℃以上の熱分解、もしくはアルカリを用いた化学的分解を含む抽出が多く見られる。これは、ある程度の抽出量を得るには共有結合の解裂が必要と考えられていたためである。

Table 1　Extraction yields of a high volatile bituminous coal with various organic solvents at room temperature[4)]

Solvent	Extraction Yield (wt%, daf)
n-Hexane	0.0
water	0.0
Formamide	0.0
Acetonitrile	0.0
Nitromethane	0.0
Isopropanol	0.0
Acetic acid	0.9
Methanol	0.1
Benzene	0.1
Ethanol	0.2
Chloroform	0.35
Dioxane	1.3
Acetone	1.7
Tetrahydrofuran	8.0
Diethyl ether	11.4
Pyridine	12.5
Dimethylsulfoxide	12.8
Dimethylformamide	15.2
Ethylenediamine	22.4

しかし構造研究では、できるだけ試料が分解や反応を起こさない条件が要求されるため、ここでは温和な条件で行われた研究に限定して述べる。

Marzec ら[4]は、瀝青炭（C%；80.7%、daf）に対して室温で撹拌抽出を行い、Table 1 の抽出率を得ている。ヘキサン、ベンゼンなどでは0.1%以下と低く、一方ピリジンで12.5%、DMSO で12.8%、DMF で15.2%と高い抽出率となっている。また、エチレンジアミンでは22.4%と高い値となっているが、溶媒の残留、可溶化反応の可能性がある（Marzec らは、他の文献から *N*-メチル-2-ピロリジノンで抽出率35.0%というデータをこの表に載せているが、これは Soxhlet 抽出（約200℃）の結果であるので、ここでは除いた）。Dryden[5]は種々の溶媒に対して抽出を行い、良溶媒の条件として非共有電子対を有する窒素、酸素原子を含んでいることを挙げている。この条件は溶媒抽出で良溶媒の選択に一つの指標となっている。

良溶媒であるピリジンでソックスレー抽出(約115℃)を行った場合、その抽出率は瀝青炭に対して高いもので30-35%が得られる。ピリジンは石炭の抽出溶媒としてかなりの良溶媒であることが分かっており、これまではこのピリジン抽出量が石炭中の溶媒可溶成分量と考えられていたようである。

石炭の溶媒抽出機構についても現在よく分かっていない。石炭の溶解性を Hildebrand の溶解度パラメータで整理しようという試み[6][7]、また抽出が石炭分子への溶媒の置換反応と考え、溶媒のドナー数、アクセプター数で整理する試み[4]などが見られるが、何れもあまり良い相関は得られていない。詳細はここでは割愛させていただく。

2.2　石炭の混合溶媒抽出

2.2.1　二硫化炭素—*N*-メチル-2-ピロリジノン混合溶媒抽出

石炭の混合溶媒抽出に関する研究は比較的少ない。我々は最近、二硫化炭素（CS_2）と *N*-メチル-2-ピロリジノン（NMP）溶媒の容積比１：１の混合溶媒が、瀝青炭に対して室温で、40-66（wt%、daf）の高い抽出率を与えることを見いだした[8][9]。Table 2 に各種有機溶媒と CS_2 の混合溶媒による抽出率と、単独溶媒での抽出率の比較を示した。表から CS_2、NMP 単独溶媒では抽出率はそれぞれ0.8%、9.3%であるが、それらの混合溶媒で抽出率は55.9%と大きく増加しており、相乗効果が大きいことが分かる。またこの傾向は NMP に限らずピリジン、DMF、DMA などでも

Table 2　Extraction yields of Shin-Yubari coal (C%: 86.7%, daf) with various mixed solvents of an organic solvent with CS_2, and with the organic solvent alone at room temperature

Organic solvent	Extraction yield(wt%, daf)	
	Mixed solvent with CS_2	Single solvent
Carbon disulfide	-	0.8
Carbon tetrachloride	0.4	0.4
Benzene	0.5	0.5
Acetone	2.6	0.4
Methanol	3.5	0.1
Tetrahydrofuran	4.2	0.9
Triethylphosphate	10.6	0.8
Phenol	18.9	2.5
Dimethylsulfoxide	35.0	1.7
Pyridine	37.8	3.0
Dimethylformamide (DMF)	40.4	2.6
Dimethylacetoamide (DMA)	47.0	2.6
N-Methyl-2-pyrrolidinone (NMP)	55.9	9.3

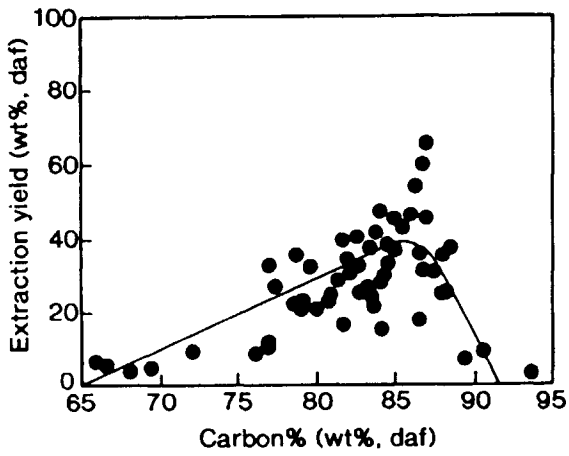

Fig. 1 Plot of the extraction yield with CS_2-NMP mixed solvent *versus* carbon% of coals

見られる。さらに、混合溶媒での抽出では、単独溶媒に比べその抽出速度も大きく増加することが分かっている。

この溶媒抽出では、室温という温和な条件であること、抽出物と残渣の収率の和が98-102%であること、元素分析の各元素の収支バランスが抽出前後で合うこと、およびFT-i.r.の結果から、溶媒と石炭間での反応は起こっておらず、また溶媒の残存もほとんどないことが分かっている[9]。

Fig. 1に石炭の炭素%に対するCS_2-NMP混合溶媒抽出率の結果を示す[9]。ここで抽出率は超音波で室温抽出(30分)、遠心分離、ろ過の一連の操作を3回繰り返した後の残渣の重量から求めた値である。炭素%とともに86%辺りまで抽出率は増加し、炭素%86～87%付近で最大を示し、中国のZao Zhuang（棗庄）炭で65.6%、日本の新夕張炭で60.6%、アメリカのUpper Freeport炭(Argonne Premium Coal Sample)で54.0%という高い抽出率が得られている。それから炭素%が88%以上で急激に抽出率は減少している。ピリジンソックスレー抽出でも同じ傾向が見られている[3]。この混合溶媒での高い抽出率は、石炭中にこれまで考えられていたよりもかなり多くの溶媒可溶成分量が存在することを示唆している。

炭素%が85～87%付近の石炭ではこの抽出率のほか、タール生成量[10]、流動性[11]、^{1}H-NMRのスピン格子緩和時間[12]らも最大値を示すことから、この付近の石炭の特徴や反応性（抽出特性も含む）が石炭の構造と関係していることが予想される。これに対する明確な解答はまだ得られていないようであるが、抽出率が最大を示すひとつの考え方として、石炭化作用で石炭骨格の解裂反応による分子サイズの減少と、置換基の脱離反応による水素結合の減少により、低ランクの石炭に比べて抽出されやすく、また、より高ランクの石炭では、芳香族化縮合反応が進行することにより逆に抽出率が減少するため、この85～87炭素%の石炭で抽出率が最大を示すものと考えている。後で述べるように、石炭ランクの違いによる種々の分子間相互作用の分布やその強さなどもこの抽出率に影響することが考えられる。また、Greenら[3]は石炭の高分子構造の違い、すなわちこのランクの石炭で架橋密度が最小となることを指摘している。

2.2.2 混合溶媒抽出機構

我々は上記の混合溶媒による相乗効果の理由に

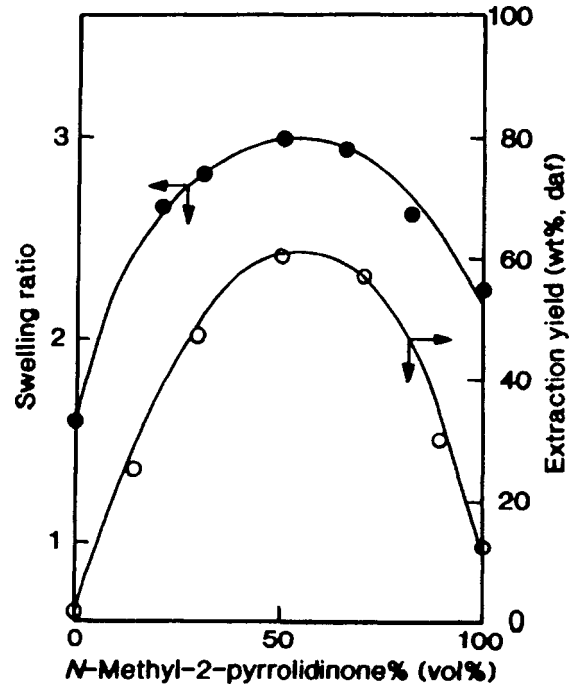

Fig. 2 Swelling ratio (●) and extraction yield (○) *versus* *N*-methyl-2-pyrrolidinone% in CS_2-NMP mixed solvent, for Shin-Yubari coal
Swelling ratio was measured for the residue from the extraction with the 1:1 mixed solvent

Table 3 The extraction yields with NMP and pyridine, and the quantities of NMP and pyridine soluble fraction in coals

Solvent	Coal	Extraction yield[a] (wt%, daf)	Soluble fraction in the coal[b] (wt%, daf)
NMP	Zao Zhuang	33.6	40.0
	Shin-Yubari	35.9	53.7
Pyridine	Zao Zhuang	12.5	30.8
	Shin-Yubari	15.7	36.7

[a]Exhaustive extraction with NMP and pyridine at room temperature

[b]The quantity of the NMP and pyridine soluble fraction in the extract from the extraction with the 1:1 CS_2-NMP mixed solvent

ついて詳しく検討した[9]。Fig. 2 には CS_2 と NMP の容積比を変化させた時の、新夕張炭(C%; 86.7%、daf)の抽出率と抽出残渣炭の膨潤度（容積法から）を示している。混合比1：1において抽出率の最大を示し、また膨潤度の結果も同じ傾向を示している。膨潤度の増加は石炭と溶媒間の親和性の良さを示し、また物理的には溶媒中で膨れることによる非共有結合性相互作用の解放、および抽出物の拡散抵抗の減少が、抽出率の増加に大きく影響しているものと考えている。Table 3 は、NMP とピリジン溶媒による室温抽出率と、混合溶媒抽出物中の NMP とピリジン可溶成分量の比較を示している。表は、例えばピリジン抽出では12-16%の抽出率を示すが、実際に石炭中には31-37%のピリジン可溶分が存在することを示しており、抽出において溶媒の浸透性が重要な要素であることを示唆している。相田ら[13]は独自の膨潤測定装置を試作して膨潤速度を測定し、石炭内部に溶媒が入り込む際の溶媒の立体的嵩高さが、膨潤速度に顕著に影響することを見いだしている。

また、我々は単独溶媒と混合溶媒の溶解性を検討した。その結果、モデル化合物を用いた実験から CS_2 は脂肪族炭化水素に、NMP は芳香族炭化水素に対してそれぞれ高い溶解性を持つことが分かり、これが両者の構造を有する石炭分子に対する混合溶媒の溶解性の増加の原因と考えられる。

さらに混合溶媒ではその単独溶媒に比べ、溶媒の粘性が低下することが分かっている。溶媒の粘性の低下により、石炭内から溶媒相への石炭分子の拡散のしやすさと、それによるポア内での石炭マトリックスへの再結合反応の抑制が抽出率増加のひとつの理由として考えられる。

3．石炭の溶媒抽出から見た石炭構造

3.1 溶媒抽出物、抽出残渣炭の性状と石炭構造

3.1.1 石炭の構成

Table 4 に瀝青炭の原炭、抽出物、残渣炭の工業分析値を示している[14]。灰分量を見ると原炭の灰分がすべて残渣炭に濃縮されているのがわかる。興味深いのは揮発分の量である。抽出物成分に揮発分が濃縮されるであろうという予想と異なり、daf ベースで揮発分は抽出物と残渣炭に僅かの差が見られるだけであった（新夕張炭では逆転)。また抽出物と残渣炭の元素分析の結果から、残渣炭は抽出物に比べて H/C が低く、O/C が高い値を示したが、その差は小さいことが分かった[14][15]。FT-i.r. のスペクトルも両者の違いに大きな差は見られなかった。これらの結果は、両者の単位構造にはほとんど差はなく、抽出物の石炭分子と残渣炭の分子がこれまで考えられていたような不連続ではなく、連続的な分布を構成していることを示唆している。この点に関して Nishioka ら[16]は最近石炭の単一相モデルを提案した。これは石炭が低分子とネットワークからなるとする従来の二相モデルに対して、抽出物と残渣は連続的な混合物であり、単に両者は分子量、会合状態の差であるという考えである。ほかに林ら[17]は、熱分解反応に伴う石炭の溶媒可溶分の生成機構とその分子量分布の変化から、石炭を連続的な混合

Table 4 Proximate analysis of raw coals, their extracts and residues

	Yield (wt%, db)	Moisture	VM[b]	Ash	FC[b]
		(wt%)			
Zao Zhuang					
Raw coal	-	0.6	28.4(30.8)	7.4	63.6(69.2)
Extract[a]	48.9	1.1	32.6(32.9)	0.0	66.3(67.1)
Residue	45.5	1.0	22.1(27.2)	17.8	60.1(72.8)
Shin-Yubari					
Raw coal	-	0.9	38.0(40.9)	6.1	55.0(59.1)
Extract[a]	44.7	1.3	35.5(36.0)	0.0	63.2(64.0)
Residue	46.6	1.3	32.7(37.8)	12.2	53.8(62.2)
Upper Freeport					
Raw coal	-	2.3	27.6(32.5)	12.8	57.3(67.5)
Extract[a]	43.2	2.5	27.4(28.1)	0.0	70.1(71.9)
Residue	48.4	2.4	18.1(25.3)	26.0	53.5(74.7)

[a]Acetone insoluble fraction in extract

[b]The values in parentheses are calculated on daf base

物と考えている。最近我々はCS_2-NMP混合溶媒の室温抽出で77.9（wt%、daf）（溶媒可溶成分量）というさらに高い抽出率を示す石炭を見いだした[18]。石炭の構成として、以上の結果は従来の二相モデルでは説明が困難であり、少なくともあるランクの石炭は、広範囲の分子量分布を持つ石炭分子の集合体であるということが言える。

3.1.2 溶媒抽出物の化学構造

瀝青炭をCS_2-NMP混合溶媒で抽出後、アセトン、ピリジンで、アセトン可溶分AS（通常のオイル成分に相当する）、アセトン不溶、ピリジン可溶分PS（アスファルテン＋プレアスファルテン）、ピリジン不溶分PI（プレアスファルテンより重質な抽出物）に分別した。Table 5に各抽出物フラクションについて、修正Brown-Ladner式[19]を用いて計算したときの構造パラメータの値を示す。ただしここでのPI'成分は、全体のPI成分中のCS_2と*N,N*-ジメチルアセトアミド混合溶媒可溶分（PIの約30%）についての結果である。表から、芳香族指数f_aはAS<PS<PI'と重質化に伴い増加しているが、芳香族環縮合度H_{aru}/C_{ar}はフラクション間で大きな差は見られず、環数にして3～4環という結果を得ている。これはIwataら[20]が同程度のランクの石炭の温和な分解

Table 5 Structural parameters of extract fractions

	Zao Zhuang			Shin-Yubari			Upper Freeport		
	AS	PS	PI'[c]	AS	PS	PI'[c]	AS	PS	PI'[c]
f_a	0.68	0.74	0.82	0.65	0.70	0.76	0.71	0.78	0.79
n	1.9	1.6	2.0	1.9	1.9	1.9	1.4	1.5	1.4
H_{aru}/C_{ar}	0.68	0.66	0.69	0.85	0.63	0.71	0.69	0.72	0.71
R_a[a]	3.3	3.6	3.1	1.7	4.1	2.9	3.1	2.7	2.9
R_n[b]	1.2	1.7	0.8	0.7	1.7	0.8	1.0	1.1	1.3
σ	0.47	0.59	0.40	0.49	0.65	0.44	0.39	0.48	0.51

[a]Number of aromatic rings per structural unit

[b]Number of naphthenic rings per structural unit

[c]CS_2-*N, N*-Dimethylacetoamide mixed solvent (1:1 by volume) soluble portion (about 30%) of PI fraction

生成物から求めた結果と良く一致している。

上で述べたように、本溶媒抽出法では石炭と溶媒間の反応は考えられないので、ここで得られる抽出物の化学構造はそのまま原炭中の構造を反映していると言える。現在、抽出残渣の化学構造についても研究を進めている。

3.2　石炭構造における分子間相互作用

3.2.1　抽出物の分子間相互作用

石炭はフェノール性水酸基を有しているので、水素結合について多くの研究が行われている[21]。水酸基のアルキル化[22]、シリル化[23]等による抽出率の増加が報告されている。水素結合以外に、芳香環同士の相互作用[24]、電荷移動相互作用[25]、イオン（双極子）-イオン（双極子）相互作用[26]などが考えられる。

我々はこの分子間相互作用に関して興味深い結果を得ている[27)28)]。混合溶媒抽出から得られたPI成分（ピリジン不溶分）は抽出物の一部であるので混合溶媒に可溶の筈であるが、実際の再溶解実験では、Table 6に示すように槽庄炭で55.1%、新夕張炭で66.9%が溶解するだけであった[27]。抽出物全体では再溶解ですべて溶解することから、分別した抽出物フラクションであるPS、AS成分をPI成分に再添加したところ90%以上が溶解した。そこでいろいろな化合物を添加したところ、LiBr、*p*-フェニレンジアミン、テトラシアノキノジメタン(TCNQ)などがPI成分の溶解性を増加させた（Table 6)。この理由として、上述の石炭の分子間相互作用による会合体が添加物の攻撃により解離され、同時に石炭分子と添加物との間で会合体を形成することにより、溶媒への溶解性が向上したものと考えている。

抽出物における分子間相互作用の寄与は、溶媒膨潤の結果からも認められる。抽出物の膨潤は他でも報告されているが[29)30)]、抽出物のような溶媒可溶成分が抽出物を溶解しない貧溶媒で膨潤するのは、抽出物が前述の水素結合などの非共有結合性相互作用により架橋していることを示してい

Table 6　Effect of additives on the solubility of PI fraction from Shin-Yubari (SY) and Zao Zhuang (ZZ) coal extraction

Additive	Additive/PI weight ratio	Soluble wt% of PI
PI of ZZ coal[a]		
None	-	55.1
ZZ-(AS+PS)	1.19[b]	91.6
ZZ-AS	0.50	68.0
ZZ-PS	0.50	76.6
LiBr	0.25	87.5
Anthracene	1.00	78.1
p-Phenylenediamine	0.022	93.8
TCNQ	0.025	99.7
PI of SY coal[a]		
None	-	66.9
SY-(AS+PS)	2.20[b]	97.4
SY-AS	0.51	71.4
SY-PS	0.51	91.2
LiBr	1.00	95.1
TCNQ	0.025	99.8

[a] The yield (daf) of PI fraction is 16.1% and 26.0% for Shin Yubari or Zao Zhuang coal, respectively

[b] The weight ratio was used to give the same composition of AS, PS and PI as that of the extract before fractionation

る。真田ら[31]は、添加物による石炭のESRスピン濃度の変化から、石炭中の分子間相互作用について検討しているが、詳細は本特集の真田先生らの総説を参照されたい。

3.2.2 石炭構造における分子間相互作用の寄与

一般に高ランク炭ほど芳香環同士の相互作用が多く、低ランク炭ほど酸素官能基が関与した水素結合が多く存在すると推定される。Krichkoら[32]は、炭素%85～86%の石炭では、これらの相互作用による会合の程度が最も小さいと考えている。2.2.1で述べたように、これは石炭化作用による酸素官能基の減少と、ランク上昇に伴う芳香族化から説明される。実際高ランク炭に対して、芳香環-芳香環相互作用を解裂する目的でのアルキル化反応[24]や無水マレイン酸と芳香環とのディールス・アルダー反応[33]によりその抽出率が大きく増加する。また低ランク炭に対しては、最近水酸化テトラブチルアンモニウム溶液が石炭を大きく膨潤させることが分かり[34]、その後の溶媒抽出で多量の抽出物が得られることが報告されている[35]。

このように石炭ランクによって石炭中には様々の分子間相互作用の存在が予想される。Shinn[36]は詳細なデータをもとにかなり正確に石炭構造モデルを組み立てたが、そのモデルで欠けていたのがこの分子間相互作用の寄与である。分子間相互作用は石炭の三次元分子集合体を形成する上で重要な意味を持ち、石炭の溶媒抽出のほかいろいろな反応性に影響を及ぼしていることが考えられる。

4．これからの石炭構造研究と石炭の利用

最近の科学機器分析の性能の向上、あるいは膨潤理論などの高分子化学の手法の利用により、石炭構造についてこれまでにはない新しい石炭の見方、考え方が見られるようになってきた。石炭中にもともと存在する溶媒可溶成分量を見ても、石炭によっては従来考えられたよりも多量存在することが示唆され、過酷な条件下で反応を進めると、逆にこれらの成分が重質化反応を起こしている可能性がある[37][38]。また分子間相互作用による結合は、かなり弱いものから、共有結合エネルギーに近いものまでがあると考えられ、どのような処理、反応においても、同時に進行する石炭構造変化[39]を常に頭に入れておく必要がある。

石炭液化を例にしても、こうした石炭構造の分子レベルでの研究でその構造が明らかにされていくことにより、より効率的な新しい石炭の変換法の可能性があるように思われる。

石炭はこれまで「複雑で不均質な固体」というイメージであったが、最近我々は「石炭はもともとデリケートで反応性の高い分子の集合体」ではないかと考えている。そうした見方でこれからも石炭構造の研究を進めていきたい。

文　献

1) Given, P.H., Marzec, A., Bartle, W.A., Lynch L.J. and Gerstein, B.C., *Fuel*, **65**, 155 (1986)
2) Lucht, L.M. and Peppas, N. A., *Fuel*, **66**, 803 (1987)
3) Green, T., Kovac, J., Brenner, D. and Larsen, J. W., In, *Coal Structure*, Meyers, R. A., Ed., Academic Press: New York, p.199, p.272 (1982)
4) Marzec, A., Juzwa, M., Betlej, K. and Sobkowiak, M., *Fuel Proc. Tech.*, **2**, 35 (1979)
5) Dryden, I. G. C., *Fuel*, **30**, 39, 145, 217 (1951)
6) van Krevelen, D. W., *Fuel*, **45**, 229 (1966)
7) Larsen, J. W., Green, T. K. and Kovac, J., *J. Org. Chem.*, **50**, 4729 (1985)
8) 飯野　雅、熊谷　淳、伊藤　攻、燃協誌、**64**, 210 (1985)
9) Iino, M., Takanohashi, T., Ohsuga, H. and Toda, K., *Fuel*, **67**, 1639 (1988)
10) Solomon, P.R. and Carangelo, R. M., "Characterization of Wyoming Subbituminous Coals and Liquid Products by FTIR Spectroscopy." EPRI Rep. No. AP2115 (1981)
11) Sanada, Y. and Honda, H., *Fuel*, **45**, 295 (1966)
12) Yokono, T. and Sanada, Y., *Fuel*, **57**, 334 (1978)
13) Aida, T, Fuku, K., Fujii, M., Yoshihara, M., Maeshima, T. and Squires, T. G., *Energy Fuels*, **5**, 79 (1991)
14) Iino, M., Takanohashi, T., Obara, S., Tsueta, H. and Sanokawa, Y., *Fuel*, **68**, 1588 (1989)

15) Takanohashi, T and Iino, M., *Energy Fuels* **4**, 452 (1990)
16) Nishioka, M. and Larsen, J. W., *Energy Fuels* **4** 70 (1990)
17) 林　潤一郎、安藤　亮、草壁　克己、諸岡　成治、燃協誌、**69**, 446 (1990)
18) Iino, M., Takanohashi, T., Ohkawa, T. and Yanagida, T., *Fuel*, in press
19) Kanda, N., Itoh, H., Yokoyama, S. and Ouchi, K., *Fuel*, **57**, 676 (1978)
20) Iwata, K., Mondragon, F., Itoh H. and Ouchi, K., *Fuel*, **63**, 1528 (1984)
21) For example, Larsen, J. W. and Baskar, A. J., *Energy Fuels*, **1**, 230 (1987)
22) Liotta, R., Rose, K. and Hippo, E., *J. Org. Chem.*, **46**, 277 (1981)
23) Patel, K.M., Stenberg, V. I., Baltisberger, R. J., Woosley, N. F. and Klabunde, K. J., *Fuel*, **59**, 449 (1980)
24) For example, Miyake, M. and Stock, L. M., *Energy Fuels*, **2**, 815 (1988)
25) Nishioka, M., Gebhard, L. A. and Silbernagel, B. G., *Fuel*, **70**, 341 (1991)
26) 持田　勲、油布　淳、坂西欣也、趙　興哲、大隅　修、平野　龍夫、燃協誌、**68**, 244 (1989)
27) Sanokawa, Y., Takanohashi, T. and Iino, M., *Fuel*, **69**, 1577 (1990)
28) Takanohashi, T. and Iino M., *Energy Fuels*, in press
29) Aida, T., 日本学術振興会石炭利用技術第148委員会第17回研究会資料, p.18 (1987)
30) Green, T. K., Chamberlin, J. M. and Lopez-Froedge, L., *Prepr. ACS Div. Fuel Chem.*, **34**, 759 (1989)
31) Sanada, Y., Proceeding of the 3rd China-Japan Symposium on Coal and C_1 Chemistry, p.7 (1990)
32) Krichko, A. A. and Gagarin, S. G., *Fuel*, **69**, 885 (1990)
33) Quinga, E. M. Y. and Larsen, J. W., *Energy Fuels*, **1**, 300 (1987)
34) 相田　哲夫、第45回北海道石炭研究会資料、p.11 (1989)
35) Matturro, M. G., Liotta, R. and Reynolds, R. P., *Energy Fuels*, **4**, 346 (1990)
36) Shinn, J. H., *Fuel*, **63**, 1187 (1984)
37) Wei, X.-Y., Shen, J.-L., Takanohashi, T. and Iino, M., *Energy Fuels*, **3**, 575 (1989)
38) Shen, J.-L., Takanohashi, T. and Iino, M., Proc., 1991 Intern. Conf. Coal Sci., Newcastle (1991)
39) Takanohashi, T. and Iino, M., *Energy Fuels*, **4**, 333 (1990)

Coal Structure: Approach from Solvent Extraction of Coals

Toshimasa TAKANOHASHI and Masashi IINO

(Institute for Chemical Reaction Science, Tohoku University)

SYNOPSIS : — Coal structure is reviewed based on the results from solvent extractions of coals, especially on those with Carbon disulfide-*N*-Methyl-2-pyrrolidinone mixed solvent extraction. It has been widely suggested that coals consist of covalently three-dimensional macromolecular networks and a small amount of relatively low molecular-weight molecules. However, recently, several results which can not be explained by the above concept, have been reported. First, the very high extraction yields obtained for some bituminous coals suggest that a considerable amount of solvent soluble molecules exist originally in coals. Next, there are many evidences which indicate that noncovalent intermolecular interactions such as hydrogen bondings, aromatic-aromatic, charge transfer, and dipole-dipole interactions play important roles for the formation of coal macromolecular structures. It is suggested that coals seem to be comprised of "aggregate" of coal molecules having a continuous molecular weight distribution.

Key Words

Coal structure, Room-temperature-extraction, Mixed solvent, Noncovalent interaction, Molecular aggregate

[総合論文]

石炭の溶媒抽出と膨潤

飯野 雅

東北大学反応化学研究所，980 仙台市青葉区片平 2-1-1

（平成 3 年 5 月 15 日受理）

石炭の溶媒抽出と膨潤について我々の研究結果を中心にして概説した。

石炭の溶媒抽出について，抽出率と溶媒の種類および良溶媒のピリジンを用いた時の抽出率と炭種の関係，溶媒パラメーターと抽出率との相関，抽出機構について述べた。次いで，我々の研究室で見い出された室温抽出で極めて高い抽出率を与える CS_2-*N*-メチル-2-ピロリジノン（NMP）混合溶媒抽出の特徴，炭種との関係および混合溶媒の相乗効果が大きい原因などについて述べた。また，この混合溶媒で得られた抽出物の興味ある不溶化および試薬の添加による可溶化現象が，水素結合などの非共有結合による会合のためと推定されることを述べた。さらに，コークス製造における軟化溶融問題，液化反応における液化率の評価など，上記の混合溶媒抽出に関連した石炭工業への応用例を紹介した。

石炭の膨潤については，膨潤の一般的様相，架橋構造との関連および CS_2-NMP 混合溶媒抽出物の膨潤について述べた。抽出物の膨潤挙動から，石炭の架橋構造に対する水素結合などの非共有結合の寄与の重要性を指摘した。

最後に，抽出と膨潤の共通項である石炭-溶媒相互作用について考察した。

1. 緒 言

石炭は発電およびコークス（タール，ガス）の製造に多量に使用されており，またガス化，液化，熱分解プロセスの開発研究も活発になされているが，化学構造などの基礎的な面ではいまだ不明な点が多い。

石炭の化学構造は従来，アルキル基，水酸基などの置換基をもつ多環芳香環（平均縮合度は，最近の固体 NMR を用いての研究[1]で炭素％が 80％程度のれき青炭で 3～4 環と報告されている）がメチレン鎖などで結ばれた溶媒不溶の架橋構造と，それにトラップされている少量の溶媒可溶（抽出可能）の低分子成分から成ると考えられてきた。良溶媒を用いても低い抽出率しか得られないことがこのような構造イメージをもつ一因になっているが，我々は最近，室温抽出で高い抽出率を与える混合溶媒を見い出し，この溶媒を用いての抽出，得られた抽出物の性状について研究している。

本総説では，石炭の溶媒抽出と膨潤およびそれらと密接に関連している石炭と溶媒との相互作用について我々の研究を中心にして述べてみたい。

2. 石炭の溶媒抽出

2. 1 単独溶媒による抽出

2. 1. 1 種々の溶媒による抽出

石炭の溶媒抽出は古くから行われているが，その中には熱分解（約 300°C 以上）や加水分解などの反応を伴う抽出が多い。ここでは，このような反応を伴う抽出は除外し，抽出のみが起こっている場合に限定して述べる。

Table 1 にれき青炭（炭素％：80.7％，daf）の室温での種々の溶媒による抽出率を示した[2]。ヘキサン，メタノール，ベンゼンは貧溶媒で抽出率は 0.1％ 以下であり，一方ピリジン，DMF などは 12～15％ と良溶媒である。表にはエチレンジアミンでさらに高い抽出率が得られているが，溶媒の残留および石炭可溶化反応が起こっている可能性がある。Dryden[3]は数多くの溶媒と石炭を用いて抽出を詳細に検討しており，塩基性の含窒素溶媒および含酸素溶媒が良溶媒であり，その中でも塩基性が強いほど高い抽出率を与えることを見い出している。また，ピリジンのオルト位にかさ高い置換基を導入すると抽出率が減少する[4]。**Fig. 1** にピリジンによる各種石炭のソックスレー抽出（ピリジンの沸点（115°C）近くの温度で数日間抽出）した時の抽出率と石炭の炭素％との関係の一例を示す[5]。石炭化の度合が進むほど一般に炭素％は高くなるが，炭素％が 85％ あたりで抽出率が最大になっている。他の報告も含めて 40％ を越える抽出率を与える石炭は極めてまれである。

Table 1 Extraction of a High Volatile Bituminous Coal with Various Organic Solvents at Room Temperature[2]

Solvent	Extraction yield [wt%, daf]
Hexane	0.0
Water	0.0
Formamide	0.0
Acetonitrile	0.0
Nitromethane	0.0
Isopropyl alcohol	0.0
Acetic acid	0.9
Methanol	0.1
Benzene	0.1
Ethanol	0.2
Chloroform	0.35
Dioxane	1.3
Acetone	1.7
Tetrahydrofuran	8.0
Diethyl ether	11.4
Pyridine	12.5
Dimethylsulfoxide	12.8
Dimethylformamide	15.2
Ethylenediamine	22.4

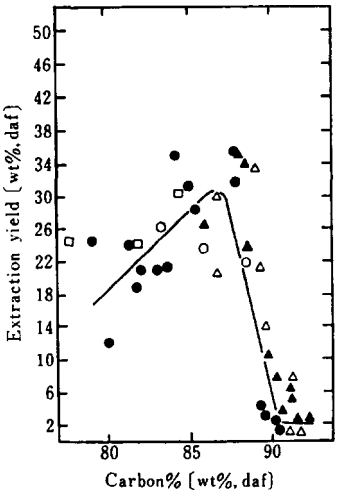

●, ▲, ○, □ and △ are the results obtained by five different research groups[5].

Fig. 1 Relation between Pyridine Extraction Yield and Carbon Content of Coals

2. 1. 2 抽出機構

抽出率を溶媒の Hildebrand の溶解度パラメーターで解釈しようとする試みは多くなされている。van Krevelen[6]は石炭の溶解度パラメーターを推算し，その値に近い溶媒が高い抽出率を与えることを示した。しかし，石炭には水素結合などの強い相互作用が存在しており，そのような相互作用を持たないことを基礎としている溶解度パラメーターの取り扱いには注意が必要である。

Marzec ら[2]は，抽出成分は架橋構造に電荷移動相互作用で結合しており，抽出は溶媒による置換反応と考え，抽出率を溶媒の電子供与性と受容性で解釈することを試みているが，あまり良い相関は得られていない。Dryden[3]は，種々の溶媒による抽出率がその時の石炭の膨潤度と相関していることを見い出している。これは後述するように抽出と膨潤（架橋高分子は溶解しないで，膨潤する）が石炭-溶媒相互作用という共通の因子を持っているためであるが，そのほかに膨潤そのものによる抽出速度の加速と抽出率の増加も考えられる。

石炭の抽出は，石炭中の抽出成分量が少なく溶媒が石炭内部へ浸透しにくいため，速度は極めて遅い。また，溶媒が抽出物および残さに強く吸着し，取り除くことが困難な場合が多い。

2. 2 混合溶媒抽出

2. 2. 1 二硫化炭素-*N*-メチル-2-ピロリジノン混合溶媒抽出

石炭の混合溶媒抽出の研究は比較的少ない。褐炭をアルコール-ベンゼン混合溶媒で抽出し，ワックスを得る研究は古くから行われているが抽出率は低い。

我々は，上記のアルコール-ベンゼン混合溶媒抽出の機構[7]についての研究中に，二硫化炭素（CS_2）とピリジンとの混合溶媒がれき青炭の室温抽出で高い抽出率を与えることを見い出した[8]。その後，CS_2-*N*-メチル-2-ピロリジノン（NMP）混合溶媒がさらに高い抽出率を与えることが分かり[9]，現在，この混合溶媒を用いて以下に述べるような種々の研究を行っている。

Table 2 Extraction of Shin-Yubari Coal with Various Mixed Solvents of CS_2 with an Organic Solvent and with an Organic Solvent Alone

Organic solvent	Extraction yield [wt%, daf]	
	Mixed solvent with CS_2[a),b)]	Organic solvent[b)]
Carbon tetrachloride	0.4(99.9)	0.4(99.9)
Benzene	0.5(100.4)	0.5(100.4)
Acetone	2.6(101.1)	0.4(101.3)
Methanol	3.5(101.1)	0.1(100.1)
Tetrahydrofuran	4.2(101.1)	0.9(101.3)
Triethyl phosphate	10.6(98.7)	0.8(98.5)
Phenol	18.9(100.0)	2.5(101.8)
Dimethylsulfoxide	35.0(99.6)	1.7(101.4)
Pyridine	37.8(100.0)	3.0(101.4)
Dimethylformamide	40.4(99.3)	2.6(101.5)
Dimethylacetoamide	47.0(102.1)	2.6(101.8)
N-Methyl-2-pyrolidinone (NMP)	55.9(102.3)	9.3(100.1)

a) The extraction yield with 1 : 1 (by volume) mixed solvent at room temperature.
b) The values in parentheses are the recovery wt% (db), *i. e.*, [(extract + residue)(g)/coal (g)] × 100.

Table 2 は，CS_2 と種々の有機溶媒との混合溶媒（体積比 1 : 1）で 60 mesh 以下に粉砕した新夕張炭（炭素%: 86.7%）を磁気かくはん下，1 時間の室温抽出を 3 回行った時の総抽出率を示す[10]。NMP の時に 55.9% と最も高く，ジメチルアセトアミド，DMF，ピリジンも 37.8～47.0% の高い抽出率を与えた。一方，四塩化炭素，ベンゼン，アセトンなどは 3% 以下の抽出率であり，**Table 2** に示したそれぞれの有機溶媒単独の時の抽出率の傾向と一致している。

世界各国の褐炭から無煙炭までの石炭を CS_2-NMP 混合溶媒（体積比 1 : 1，以下同じ）で徹底的に抽出（室温，超音波照射下，6～7 回抽出）した時の抽出率と石炭の炭素%とのプロットを **Fig. 2** に示す[10]。抽出率が全般に高くなっているが，**Fig. 1** のピリジン溶媒によるソックスレー抽出と同じ傾向を示した。検討したれき青炭 49 種中 29 種で 30～66% の高い抽出率が得られた。

衝圧炭（中国，Zao Zhuang（ZZ）炭）の抽出率について，同じ徹底的抽出の条件下で CS_2-NMP 混合溶媒，NMP およびピリジン単独溶媒のそれぞれを比較すると，65.6%，33.6%，12.5% の抽出率が得られ，また CS_2 単独溶媒での抽出率は極めて低く 3% を越えない。NMP はれき青炭に対する最も優れた溶媒であるが，これに単独では貧溶媒である CS_2 を加えるとなぜ抽出率が大幅に増大するのかについて検討した。その結果，混合溶媒は NMP 単独溶媒よりも（1）石炭抽出物をよく溶かす，（2）石炭を大きく膨潤させる，（3）溶媒の粘性が小さいということがわかった。（1）は CS_2，NMP がそれぞれ飽和炭化水素，芳香族炭化水素への親和性が大きいことが両者の構造を有する石炭抽出物に対する混合溶媒の有効性の原因であると考えられる。（2）については水素結合，π-π 相互作用などの非共有結合で会合あるいは石炭マトリックス（石炭架橋構造）に結合している抽出可能な成分が，それらの結合の切断と

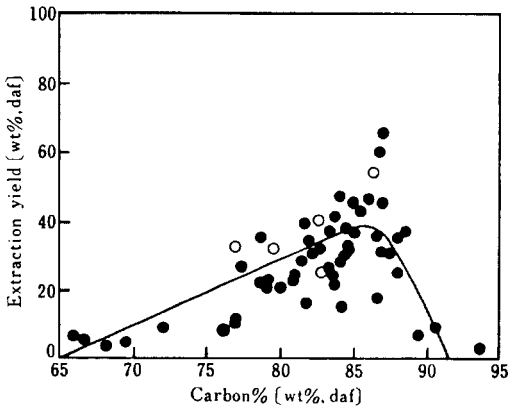

○, Argonne premium coal sample[10].

Fig. 2 Plot of Extraction Yield with CS_2-NMP Mixed Solvent (1 : 1 by volume) *vs.* Carbon Content of the Coals

膨潤により，抽出されやすくなったと考えられる。(3)は抽出物の石炭の細孔内から外部の溶媒相への拡散が混合溶媒中では速く，そのため細孔内での種々の不溶化反応が抑制され，抽出率が増加したと考えている[10]。

最後に，マスバランス，原炭，抽出物および残さの IR スペクトルと元素分析値，抽出物の性状などの検討結果および室温という温和な条件下の抽出であることから，この混合溶媒における石炭中の共有結合の切断のような可溶化反応は起こっていないと思われる[10]。

2. 2. 2 CS_2-NMP 混合溶媒抽出物の溶解性

CS_2-NMP 混合溶媒で高い抽出率を与えた数種の石炭を選び，得られた抽出物と残さの化学構造と性状について研究している[11),12)]。抽出物の化学構造の研究はもとの石炭の構造を知る上で極めて重要であるが，ここでは最近見い出した抽出物の溶解性についての興味ある現象について述べる[13)]。

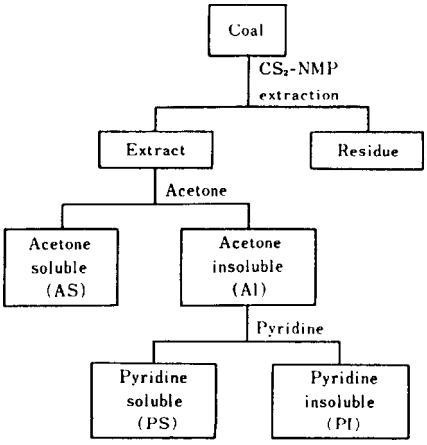

Fig. 3 Fractionation Procedure for Extracts with CS_2-NMP Mixed Solvent (1 : 1 by volume)

Fig. 3 に示したような手順で抽出および溶媒分別し，抽出物をアセトン可溶分（AS），アセトン不溶，ピリジン可溶分（PS）およびピリジン不溶分（PI）に分別した。5 種のれき青炭での結果を **Fig. 4** に示す。ここで PI は抽出物であるので抽出溶媒の CS_2-NMP 混合溶媒に可溶のはずであるが，実際には新夕張炭で 66.9%，霞庄炭で 55.1% しか溶解しなかった（**Table 3**）。そこで分別した AS と PS を再び加えたところ，**Table 3** に示したように新夕張炭，霞庄炭それぞれの PI の 97.4%，91.6% が溶解するようになった。ここで溶解性は，400 mg の PI を 50 ml の混合溶媒に室温，超音波照射下，30 分間溶解させた時の溶解量とした。

Table 3 には AS，PS 以外の種々の添加物を加えた時の結果

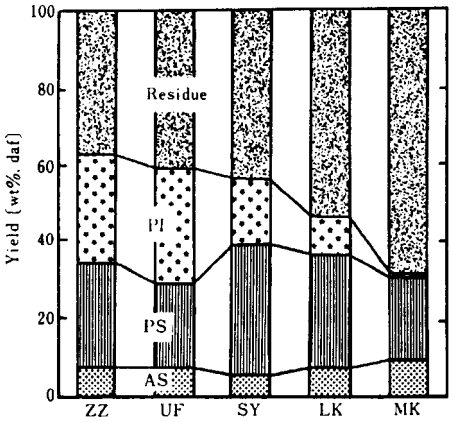

Fig. 4 Fraction Distribution for Zao Zhuang (ZZ), Upper Freeport (UF), Shin-Yubari (SY), Lower Kittaning (LK) and Miike (MK) Coals[11]

Table 3 Effect of Additives on Solubility of PI Fraction from Shin-Yubari (SY) and Zao Zhuang (ZZ) Coal Extraction

Additive	Additive/ PI fraction (wt ratio)	Soluble (wt% of) PI fraction
PI fraction of SY coal[a)]		
None	—	66.9
SY-(AS+PS)	2.20[b)]	97.4
SY-AS	0.51	71.4
SY-PS	0.51	91.2
LiBr	1.00	95.1
TCNQ	0.025	99.8
PI fraction of ZZ coal[a)]		
None	—	55.1
ZZ-(AS+PS)	1.19[b)]	91.6
ZZ-AS	0.50	68.0
ZZ-PS	0.50	76.6
LiBr	0.25	87.5
Anthracene	1.00	78.1
Chloranil	0.026	64.7
p-Phenylenediamine	0.022	93.8
Tetracyanoethylene	0.022	97.7
TCNQ	0.025	99.7

a) The yields (daf) of PI fraction are 16.1% and 26.0% for SY and ZZ coals, respectively.
b) The wt ratio was used to give the same composition of AS, PS and PI as that of the extract before the fractionation.

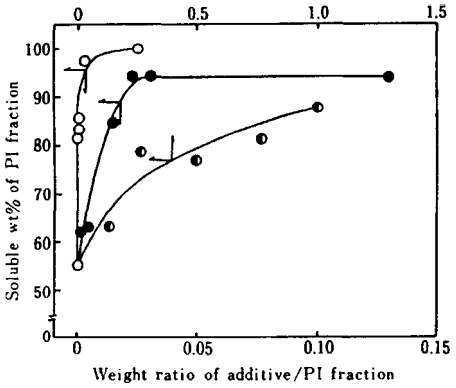

○, TCNQ; ●, *p*-phenylenediamine; ◐, PS fraction of Zao Zhuang coal[13].

Fig. 5 Plot of the Content of the Soluble PI Fraction of Zao Zhuang Coal *vs.* Wt Ratio of Additive to PI Fraction

も示しているが，LiBr，アントラセン，*p*-フェニレンジアミン，テトラシアノエチレン，テトラシアノキノジメタン（TCNQ）などが PI の溶解性を増大させることが分かった。特に，*p*-フェニレンジアミン，テトラシアノエチレン，TCNQ は効果的な添加剤であり，400 mg の褐炭炭の PI に対してわずか 1.1 mg の TCNQ，8.8 mg の *p*-フェニレンジアミンの添加で，溶解性は 55.1% からそれぞれ 97.3%，93.8% へ増加した。**Fig. 5** には PI 成分量 TCNQ，*p*-フェニレンジアミンおよび褐炭炭の PS 成分の添加量の比と PI 溶解性とのプロットを示した。三者の添加物の効果には大きな相違があることが分かる。

PI 成分の不溶化の原因は酸化などによる化学構造の変化によるものでなく，会合のような可逆的なものであることが上記の結果から示唆されている。石炭分子間には水素結合（フェノール性水酸基他），芳香環-芳香環（π-π）相互作用，双極子（イオン）-双極子（イオン）相互作用，電荷移動相互作用などが働いている。不溶化はこれらの相互作用により，もともと難溶の PI 成分が会合した結果起こったと推定される。この会合体に上記の相互作用のいずれかあるいはいくつかを持ち，混合溶媒に溶け易い添加物を加えると PI 同士の会合が解け，新たな可溶性の会合体あるいはフリーの PI が生成するため可溶化したのであろうと推定される（**Fig. 6**）。

Fig. 7a は CS_2-NMP 混合溶媒を Size Exclusion Chromatography（SEC）の溶媒に用いて，褐炭炭の AS，PS，PI の SEC（ポリスチレンゲルのカラム）を測定したものである。AS，PS，PI の順により高分子側にピークを持つ。**Fig. 7b**，c は SEC 溶媒に 10 mM の LiBr とアントラセンを加えた CS_2-NMP 混合溶媒を用いた時の結果である。AS は **Fig. 7a** と変わらないが，PS と PI，特に PI のピークが低分子側にシフトしているように見える。添加物により会合が解けた結果と解釈され，上記の可溶化機構を支持している。

Table 3 で種々の添加物が PI の可溶化に効果があることが分かった。それらが石炭分子（PI）とどのような分子間相互

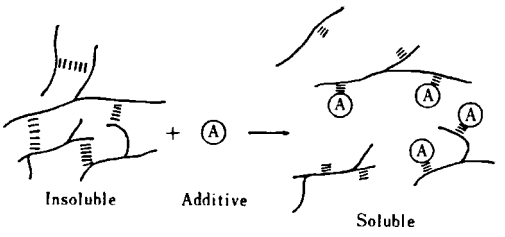

Fig. 6 Mechanism for Promoting Solubility of PI Fraction by Additives

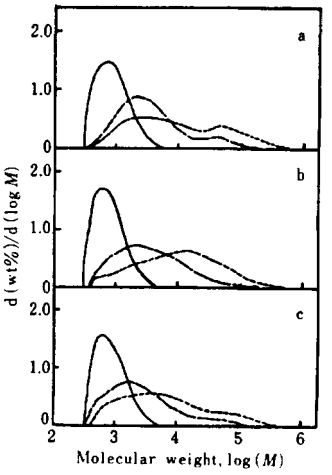

Fig. 7 SEC Analysis of AS (——), PS (-·-·-), and PI (·····) Fractions of Zao Zhuang Coal in the Absence (a) and Presence of Additives (b, LiBr; c, anthracene)

作用を持つのか考えてみる。アントラセンのような芳香族化合物は π-π 相互作用で，また LiBr は双極子（イオン）-双極子（イオン）相互作用，水素結合で PI の会合を解くものと推定される。*p*-フェニレンジアミン，フェノールは水素結合，TCNQ，テトラシアノエチレンは電荷移動相互作用を（石炭の芳香環には電子供与性のアルキル基，エーテル基がついているので）示唆している。しかし，TCNQ と同程度の電子受容性のクロラニルがあまり効果がなく，TCNQ は反応が起こっている可能性があり，この点について現在検討している。真田ら[14]は，TCNQ，I_2 を石炭に加えて ESR を測定すると，スピン密度が大きく変化することを見い出している。

上記のような現象は他にも見つかっており，Sternberg[15]らは石炭液化物を酸を用いて中性，酸性成分と塩基性成分へ分離することにより，酸塩基相互作用による会合が消失し溶解性が増大することを見い出している。宍戸ら[16]もコールタールピッチの超臨界ガス抽出物で重質成分の溶解性に軽質成分の存在が重要な役割を果たしていることを報告している。また，このような現象は石油系重質油でも起こっているものと思われる。石炭系との相違点など比較してみることは興味深い。

2. 2. 3 CS_2-NMP 混合溶媒抽出の石炭工業への利用

コークスを製造するためには 500°C 近辺で軟化溶融する石炭（原料炭）を用いなければいけない。軟化溶融するためには石炭中にもともと含まれている低分子成分である，いわゆる「粘結成分」が不可欠であると言われているが，反論もある。我々は CS_2-NMP 混合溶媒抽出率を溶媒混合比を変え，変化させた時の抽出残さの軟化溶融性（ギーセラー最高流動度など）を測定した。その結果，低分子成分である抽出物を取り除くことにより流動性が顕著に減少していくことが分かった。炭種により減少の仕方がかなり異なるが，コークス製造には低分子成分の存在が不可欠であることを確かめた。

石炭直接液化の液化率は石炭からオイル，アスファルテン，プレアスファルテンへの変換率で求められている。したがって，これらがもともと原炭中に含まれている時には差し引くことが必要であるが，実際にはその量が無視し得るとしている。すでに示した **Fig. 4** で AS はオイルに，PS はアスファルテン＋プレアスファルテンに，PI はプレアスファルテンにより重質な溶媒可溶分に相当する。少なくともこれらの石炭においては決して無視し得る量ではないことが分かる。実際にテトラリンまたはナフタレン中，350～450°C で液化反応を行い，液化率の評価にはこれらのもともと原炭中に存在している溶媒可溶成分量を補正することが必要であることを示した[17]。このほか，混合溶媒抽出物を用い，液化反応で並行して起こる重質反応（チャーの生成）の機構についても研究している。また，混合溶媒抽出，抽出残さの熱分解，ガス化を組み合わせた新しい石炭変換プロセスの開発および抽出物の工業的利用に関する研究も行っている。

3. 石炭の膨潤

3. 1 石炭の膨潤と架橋構造

石炭を溶媒蒸気で満たしたデシケーター中に入れておくと膨潤する。石炭が架橋構造を有しているためである。

膨潤度（Q）は，膨潤前の石炭の体積（細孔を除いた真の体積）に対する膨潤後の溶媒を取り込んだ石炭の体積との比で表される。一般には平衡に達した値の膨潤度が測定されている。測定としては，溶媒蒸気を用いる重量法と溶媒に一定粒度の石炭を浸し，膨潤による石炭粒子塔の高さの増加分から求める容積法とがあるが，最近は後者の方が良く用いられている。また，測定溶媒で石炭を徹底的に抽出して得られた残さを用いなければ正しい膨潤値は得られない[18]。

Fig. 8 は，Larsen ら[19]によるイリノイ No. 6 炭（炭素%: 79.8%）のピリジン抽出残さを種々の有機溶媒に浸した時の膨潤値と溶媒の溶解度パラメーターとのプロット（**Fig. 8**）である。図中の番号 1 から 11 はペンタン，ベンゼン，CS_2 などの非極性溶媒である。DMSO，THF，ピリジンなどの極性溶媒は非極性溶媒の値と比べて高い膨潤値を示している。

抽出残さの膨潤値より，架橋高分子に対する Flory-Rehner 式（Eq.（1））を用いて架橋の程度を表す架橋点間の平均分子量 $\bar{M}c$ を求めることが可能である。

$$\bar{M}c=\rho_c V_s V^{1/3}/[-\ln(1-V)-V-\chi V^2] \qquad (1)$$

ここで V_s は溶媒のモル体積，V は膨潤平衡時の石炭の体積分率（膨潤度（Q）の逆数），ρ_c は石炭の真の密度，χ は石炭と溶媒間の Flory の相互作用パラメーターである。実際に Eq.（1）あるいは改良した Kovac 式[20]を用いて $\bar{M}c$ を求めた文献がかなりある。しかし，石炭の架橋構造，膨潤機構がいまだ不明であるので，これらの式が石炭に適用できるという確証は得られていない。最近，Painter ら[21)～23)]は，強い相互作用である水素結合を会合モデルで，また膨潤を disinterspersion（空間的に入り組んでいる架橋構造がその鎖があまり伸びずにほどけること）プロセスとして取り扱い，イリノイ No. 6 炭（炭素%: 79.8%）の架橋点間の平均分子量として炭素数で 30～60 個程度の小さい値を報告している。

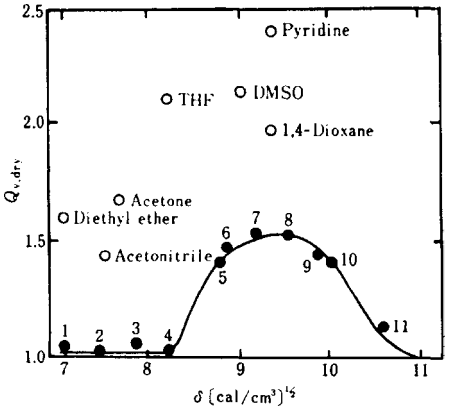

Fig. 8 Plot of Swelling Ratio (Q) for Pyridine-extracted Illinois No. 6 Coal *vs.* Hildebrand Solubility Parameter of Nonpolar Solvents (●) and Nonpolar Solubility Parameter of Polar Solvents (○)[19]

Brenner[24),25)]は，イリノイ No. 6 炭の厚さが 15 μm で 0.5 mm 四方程度の大きさの均質な薄片を製作した。これをプロピルアミンに浸し，膨潤を顕微鏡で観察し，膨潤後，プロピルアミンを蒸発させるとほぼ元の大きさに戻ることおよび溶媒で膨潤した状態の薄片はゴム弾性を示すことを見い出している。

相田ら[26]は膨潤の速度を測定する装置を製作し，種々の有機溶媒による石炭の膨潤速度および平衡膨潤値を求めている。溶媒の立体的かさ高さが膨潤速度に大きな影響を与えることを明らかにしている。また，混合溶媒による膨潤も多く行われている[27]。

3. 2 CS_2-NMP 混合溶媒抽出物の膨潤

先の **Fig. 7** はイリノイ No. 6 炭のピリジン抽出残さの膨潤値を示したものであるが，相田ら[28]は同じ石炭のピリジン抽出物の方を同じ 1～11（**Fig. 8**）の非極性溶媒（これらの溶媒は抽出物をほとんど溶解しない）で膨潤させたところ，ほとんど同じような膨潤値が得られたことを報告している。

我々も抽出物の膨潤挙動を研究しており，CS_2-NMP 混合溶媒抽出物，残さおよび原炭の膨潤値を測定している。膨潤溶媒および炭種によって挙動が異なるが，抽出物も残さと同程度に膨潤することを見い出している。膨潤現象は架橋構造に由来しているが，抽出物のような溶媒可溶物が膨潤するのは架橋構造が共有結合ではなく主として前述の水素結合などの非共有結合で構成されていることを示唆している。石炭構造は緒言で述べ

たように架橋構造とそこにトラップされている少量の溶媒可溶成分から成ると考えられてきた。しかし，抽出物の膨潤挙動，化学構造（芳香族性 f_a，平均縮合度など）は抽出残さとそう異なっておらず，構造は抽出物から残さへと連続的に変化していくように見える。最近入手した褐炭（中国）の CS_2-NMP 混合溶媒による室温抽出で 78%（daf）という高い抽出率を得ており，この量は架橋構造にトラップされた少量の成分というイメージには合わない。したがって，少なくともある種のれき青炭では架橋構造が主に水素結合などの分子間相互作用で形成されている可能性がある。この石炭構造に関しては他の総説[29]を参照されたい。

3.3 膨潤の石炭工業への利用

膨潤した石炭の液化反応性が向上することがいくつか報告されている[30]。石炭液化プロセスにおける石炭粒子の膨潤とスラリーの粘度との関係について詳細に検討されている[31]。また，熱分解による架橋構造の発達の程度を膨潤値から見積もることも行われている[32),33]。

最近，橋本らは溶媒で膨潤させた石炭を迅速に熱分解する方法を開発し，タール収率が大きく増大することを見い出している[34]。

4. 石炭と溶媒との相互作用

石炭は種々の縮合度の多環芳香環にアルキル基，水酸基，カルボキシル基などの官能基がついた構造単位がメチレン，エーテル，エステルなどの結合で結びつけられた構造をしていると推定されている。したがって，石炭内部での分子間あるいは分子内相互作用および石炭と溶媒の相互作用としては水素結合，芳香環-芳香環（π-π）相互作用，双極子(イオン)-双極子(イオン）相互作用，電荷移動相互作用が考えられている。石炭内でこれらの寄与はどの程度であるのか，またそれらが石炭化度でどのように変化するのかはいまだよく分かっていない。

上記の相互作用をもつ溶媒は石炭分子との親和性がよく，溶解性（抽出率）が高い。一方，膨潤は溶媒が濃度こう配と石炭との親和性で石炭内部へ溶解しようとする力とこれに対抗する架橋構造からの弾性（これは架橋密度に依存する）とのつり合いで決まる。したがって，親和性のある溶媒は溶け込む傾向が大きく膨潤値は大きくなる。**Fig. 9** で CS_2-NMP 混合溶媒抽出率と膨潤値はよく相関している。この相関は Dryden[3] によっても見い出されている。

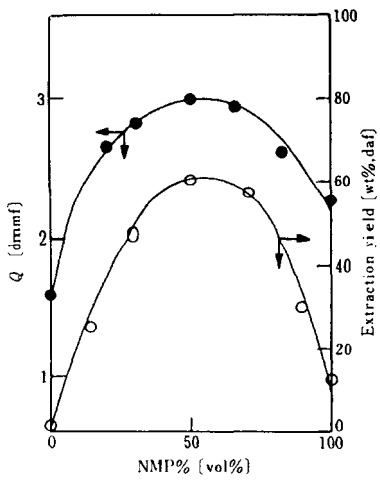

Fig. 9 Plot of Extraction Yield (○) or Swelling Ratio (Q, ●) *vs.* NMP Content in CS_2-NMP Mixed Solvents[10]

Painter ら[21)~23)]は相互作用力が強い水素結合を会合モデルに取り入れることにより，双極子-双極子や π-π 相互作用などの弱い相互作用から切り離して取り扱い，イリノイ No. 6 炭について水素結合を含まない Flory の χ パラメーターを種々の溶媒で求めた。さらに，ピリジンで膨潤させた石炭は通常の温度で相分離とゲルの崩壊が起こることを予想した。また，彼らは前述したように膨潤が前述の disinterspersion プロセスで起こると仮定して，イリノイ No. 6 炭の架橋点間の平均分子量は炭素数が 30～60 個程度の小さい値になることを推算した。これらの予想および推算値に対する実験的証拠はまだ報告されていない。

5. 結　　言

以上，石炭の溶媒抽出および膨潤について我々の研究結果を中心に述べた。石炭の化学構造および石炭-溶媒相互作用はいまだ不明な点が多く，現在，少しづつ解明されつつある段階である。これらは石炭の新しい高効率の利用プロセス開発にもつながる重要な問題であり，今後，ますます明らかにされることを期待している。

References

1) Solum, M. S., Pugmire, R. J., Grant, D. M., *Energy and Fuels*, **3**, 187 (1989).
2) Marzec, A., Juzwa, M., Betlej, K., Sobkowiak, M., *Fuel Proc. Tech.*, **2**, 35 (1979).
3) Dryden, I. G. C., *Fuel*, **30**, 39, 145, 217 (1951).
4) Halleux, A., Tschamler, H., *Fuel*, **38**, 291 (1959).
5) Green, T., Kovac, J., Brenner, D., Larsen, J. W., "Coal Structure", ed. by Meyer, R. A., Academic Press, New York (1982), p. 272.
6) van Krevelen, D. W., *Fuel*, **45**, 229 (1966).
7) Iino, M., Matsuda, M., *Bull. Chem. Soc. Jpn.*, **57**, 3290 (1984).
8) Iino, M., Matsuda, M., *Fuel*, **62**, 744 (1983).
9) Iino, M., Kumagai, J., Ito, O., *Nenryo Kyokaishi*, **64**, 210 (1985).
10) Iino, M., Takanohashi, T., Ohsuga, H., Toda, K., *Fuel*, **67**, 1639 (1988).
11) Iino, M., Takanohashi, T., Obara, S., Tsueta, H., Sanokawa, Y., *Fuel*, **68**, 1588 (1989).
12) Takanohashi, T., Iino, M., *Energy and Fuels*, **4**, 452 (1990).
13) Sanokawa, Y., Takanohashi, T., Iino, M., *Fuel*, **69**, 1577 (1990).
14) Sanada, Y., Proceeding of the 3rd China-Japan Symposium on Coal and C_1 Chemistry, 1990, p. 7.
15) Sternberg, H. W., Raymond, R., Schweighardt, F. K., *Science*, **188**, 49 (1975).
16) Shishido, M., Yamada, S., Arai, K., Saito, S., *Fuel*, **69**,

1490 (1990).
17) Wei, X.-Y., Shen, J.-L., Takanohashi, T., Iino, M., *Energy and Fuels*, **3**, 575 (1989).
18) Larsen, J. W., Cheng, J. C., Pan, C.-S., *Energy and Fuels*, **5**, 57 (1991).
19) Larsen, J. W., Green, T. K., Kovac, J., *J. Org. Chem.*, **50**, 4729 (1985).
20) Kovac, J., *Macromolecules*, **11**, 362 (1978).
21) Painter, P. C., Graf, J., Coleman, M. M., *Energy and Fuels*, **4**, 379 (1990).
22) Painter, P. C., Park, Y., Sobkowiak, M., Coleman, M. M., *Energy and Fuels*, **4**, 384 (1990).
23) Painter, P. C., Graf, J., Coleman, M. M., *Energy and Fuels*, **4**, 393 (1990).
24) Brenner, D., *Prepr. Am. Chem. Soc. Div. Fuel Chem.*, **30**, (1), 83 (1985).
25) Brenner, D., *Prepr. Am. Chem. Soc. Div. Fuel Chem.*, **31**, (1), 17 (1986).
26) Aida, T., Fuku, K., Fujii, M., Yoshihara, M., Maeshima, T., Squires, T. G., *Energy and Fuels*, **5**, 79 (1991).
27) For example, Amemiya, K., Kodama, M., Esumi, K., Meguro, K., Honda, H., *Energy and Fuels*, **3**, 55 (1989).
28) Aida, T., The report for the 17th meeting of the committee on Coal Utilization Technology of Japan Society for the Promotion of Science, 1987, p. 18.
日本学術振興会石炭利用技術第 148 委員会第 17 回研究会資料, 1987, p. 18.
29) Takanohashi, T., Iino, M., *Nenryo Kyokaishi*, **70**, 802 (1991).
30) For example, Fujii, Y., Akezuma, M., Esumi, K., Meguro, K., Honda, H., *Fuel*, **65**, 1616 (1986).
31) Deng, C.-R., Nio, T., Sanada, Y., Chiba, T., *Fuel*, **68**, 1134 (1989).
32) For example, Suuberg, E. M., Lee, D., Larsen, J. W., *Fuel*, **64**, 1668 (1985).
33) Solomon, P. R., Serio, M. A., Despande, G. V., Kroo, E., *Energy and Fuels*, **4**, 42 (1990).
34) Miura, K., Mae, K., Asaoka, S., Yoshimura, T., Hashimoto, K., *Energy and Fuels*, **5**, 340 (1991).

Summary

Extraction and Swelling of Coal

Masashi IINO

Institute for Chemical Reaction Science, Tohoku University, 2-1-1 Katahira, Aoba-ku, Sendai 980

Extraction and swelling of are reviewed, putting emphasis on the results obtained at our laboratory.

First, the effects of the kinds of coals and solvents on the extraction yields and the extraction mechanisms, proposed so far, are reviewed. Secondly, the mechanism of the extraction with CS_2-*N*-methyl-2-pyrrolidinone (NMP) mixed solvent, which was found at our laboratory to give very high extraction yields at room temperature, are discussed. The interesting behavior of rendering insoluble the extracts obtained with CS_2-NMP mixed solvent is attributed to their association by non-covalent interaction such as hydrogen-bonding and π-π interaction. Examples of the utilization of this mixed solvent to the basic studies of carbonization and liquefaction are also indicated.

Swelling behavior of coals with different solvents, and the swelling of coal extracts, are discussed on the basis of cross-linking structures of coals, indicating that non-covalent interactions between coal molecules play important roles for the cross-linking structures.

Finally, the nature of the interaction between coal molecules and solvents are discussed.

Keywords

Coal, Solvent extraction, Coal swelling, Coal solvent interaction

“地下深く眠る石炭” その不思議な構造

—石炭の非共有結合構造—

On Marvelous Structure of Coal Lying Underground
—Noncovalent Bond Structure of Coals—

Toshimasa TAKANOHASHI
鷹觜利公

石炭の化学構造については現在でも不明な点が多い。今後の石炭利用は環境に適応した省エネルギー利用が必要条件とされ，石炭自身の付加価値を高めたクリーンな高効率利用が求められている。そのためにもさらに石炭の化学的・物理的特性を理解するとともに，その構造を解明していくことが新たな利用法への重要な鍵となっている。

石炭は数環の芳香環を基本骨格に持つことはわかっているが，それらがどのように結合し，全体の構造を形成しているのかについては明らかでない。本稿では，最近の石炭研究の分野で注目されている石炭の非共有結合構造について紹介し，こうした石炭自身の構造特性を利用した新たな石炭高効率変換プロセスの可能性について触れてみたい。

はじめに

エネルギー危機もグローバルな問題

石炭と聞くと黒い，混合物である，環境に悪いといういわゆる“3K”のイメージがある。しかし一方で，安価である，安定した供給が可能である，安心できる埋蔵量をもつという“3A (Advantage)”の要素も兼ね備えている。将来，需要と供給のアンバランスから原油価格が急騰するのは必至であるにもかかわらず，その代替資源・エネルギーの確保は不十分であると思われる。グローバルな問題とは決して地球温暖化に限ったものではなく，エネルギー確保，人口増加などの諸要素が相互に関連した問題であることを十分認識する必要がある。

石炭構造の解明は有効利用への近道である！

さて石炭の有効利用を考える場合，環境問題の観点からも，クリーンな省エネルギー利用が必要条件である。そのためには相手となる石炭がどのような化学構造を有しているのかを知ることが，その有効利用への近道であると考えられる。一例を挙げると，酸性雨のもとになる硫黄・窒素酸化物を取り除く脱硫・脱硝プロセスにおいて，もともと石炭構造内で硫黄，窒素がいかなる形態で存在しているのかを解明することが重要である。近年の分析装置の高性能化ならびに分析技術の向上により，これまでブラックボックスであった石炭の構造に対してもメスが入れられつつある。

特に最近の研究報告から，石炭構造における，水素結合[1]やπ電子間相互作用[2]などの非共有結合の役割が注目されており，そうした二次的結合を制御することによる新たな高効率利用プロセスの開発が期待されている。本稿では，自然が創り上げた石炭の不思議な構造の一面を紹介したい。

石炭構造はどのように考えられ，また利用されてきたか？

石炭を約 400 ℃ 以上で加熱すると共有結合の解裂反応が進行し，水素供与性溶媒下では生成ラジカルへ水素が移行し，オイルの前駆体である重質炭化水素化合物が得られる。いわゆる基本的な石炭液化反応機構である。またこうした熱的解裂からの生成物の構造解析も数多く行なわれており，主に図1の単位構造に相当する脂肪族側鎖・極性置換基が数個ついた芳香族炭化水素化合物が検知されている。したがってこれらの事実から想像される石炭の高分子構造としては，図1に示すように，単位構造クラスターがメチレン鎖等でつながれた三次元網目構造が考えられてきた。また石炭の利用法にしても，これまでは苛酷な条件下における結合の熱的解裂に基づいた方法が考えられてきた。

Magic Solvent の登場！

石炭中の溶媒抽出可能な成分量は？

石炭の溶媒抽出に関する研究はその簡易さにより古くから行なわれている。その抽出率はピリジンなどを溶媒とすることにより数%～20% の値を与え，そこで得られた抽出成分は，図1に示した三次元網目間に存在する低分子量の成分に相当すると考えられてきた。

一方で筆者らの研究室では，石炭の抽出溶媒に二硫化炭素と *N*-メチル-2-ピロリジノン (CS_2-NMP) の容積比1：1の混合溶媒を用いることに

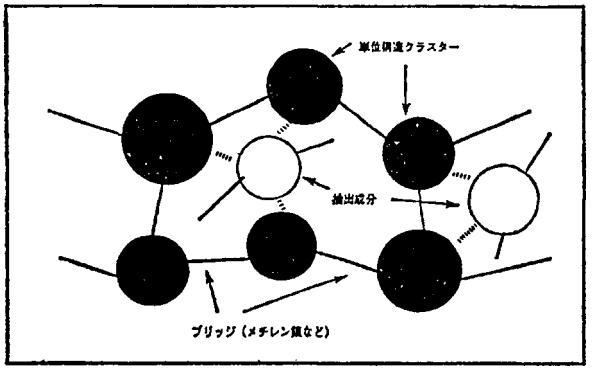

図1　これまで提案された石炭の三次元網目構造。

表1　二硫化炭素-*N*-メチル-2-ピロリジノン混合溶媒抽出率

石　炭	抽出率 (wt%, daf)	アセトン可溶分 (wt%, db)	ピリジン可溶分 (wt%, db)	ピリジン不溶分 (wt%, db)
Zao Zhuang I	77.9	6.6	17.7	43.2
Zao Zhuang II	63.0	6.7	24.3	26.0
Upper Freeport	59.4	6.1	18.3	24.9
Shin-Yubari	56.8	5.5	30.0	16.1

より，表1に示すように，数種の石炭に対して室温で 50～80 wt% (石炭中に含まれる水分，灰分を除いた有機質成分に対する重量%) の非常に高い抽出率を与えることを見いだした[3~5]。抽出が温和な条件で行なわれること，抽出前後の石炭のFT-i.r. 吸収に溶媒の吸収や新たなピークが見られないこと，また抽出による回収率がほぼ 100% である等の理由により，この抽出では，石炭中の共有結合の解裂は起きていないことがわかった[4]。したがってこの結果は，石炭内に元々これだけの量の抽出可能成分が含まれていることを示しており，こうした高抽出率を与える石炭の構造は，少なくとも図1に示したような三次元網目構造のイメージでは説明のつかない結果であった[6]。いわゆるこの "Magic Solvent" ともいうべき混合溶媒の登場により，これまで考えられてきた石炭構造の概念に大きな疑問を投げかけた。

石炭分子間をつなぐ非共有結合

抽出物の一部が同じ溶媒に溶けなくなる訳？

溶媒抽出物をアセトンでアセトン可溶分 (AS) とアセトン不溶分 (AI) に溶媒分別する。さらにこの AI をピリジンでアセトン不溶-ピリジン可溶分 (PS) とピリジン不溶分 (PI) の各フラクションに分ける[7]。この AS, AI, PS, PI をそれぞれ抽出溶媒である CS_2-NMP 混合溶媒に再溶解させたところ，AS, AI, PS はすべて溶解するが，最も重質な成分である PI ではその約 40～50% が不溶となることがわかった。すなわち分別で溶媒可溶分中の軽質な成分を取り除くことにより，残った重質成分の一部が不溶化してしまうという現象を見いだした[8]。

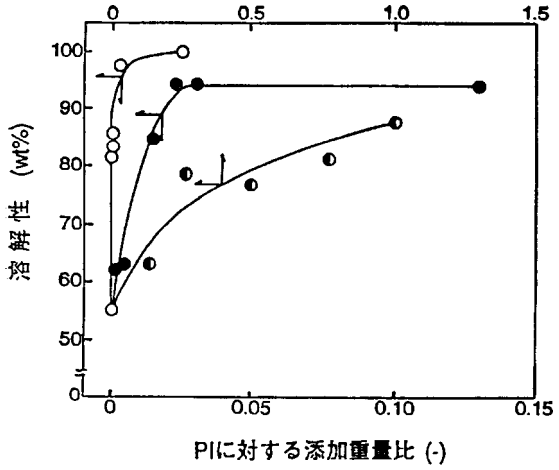

図 2　重質可溶成分 (PI) の溶解性に及ぼす添加物効果。
○：TCNQ, ●：*p*-フェニレンジアミン,
◐：PS 成分

微量の添加物による溶解性の向上

この再溶解実験の際に，図2に示すように，テトラシアノキノジメタン (TCNQ)，*p*-フェニレンジアミンなどの添加物を極微量加えることにより，前述の不溶化が抑制されることが見いだされた[8]。またこのほかにも，臭化リチウム，アントラセンでも同様な添加効果が見られた。したがって図3に示すように，溶媒分別による不溶化は，石炭中に存在する水素結合，π電子間相互作用，電荷移動相互作用等の非共有結合による PI 成分間の会合によるものであり，種々の添加物による不溶化の抑制は，添加物の会合サイトへの攻撃による会合の解放と考えている。

表 2　混合溶媒の室温抽出におけるテトラシアノエチレン (TCNE) の添加効果

石　炭	室温抽出率 (wt%, daf)	添加量 (g/1g-coal)	添加した時の抽出率 (wt%, daf)
Upper Freeport	59.4	0.025	85.0
Lower Kittanning	46.8	0.100	61.5
Sewell B	37.1	0.100	47.9
Pittsburgh No.8	39.0	0.025	42.6

室温抽出での添加物の効果

石炭抽出物間で会合が存在するという結果から，筆者らは，原炭の抽出においてもそうした石炭分子間の会合により，一部抽出可能成分が抽出残渣となっているのではないかと考えた。そこで抽出時に添加物を加えてみたところ，表2に示すように数種の石炭において無添加 (CS_2-NMP だけ) の抽出に比べて，大きな抽出率の増加が確認された[9]。特に石炭標準試料の一つである Upper Freeport 炭では室温にもかかわらず 85% の抽出率が得られた。

非共有結合による物理的架橋の存在

石炭が有機溶媒中で膨潤することはよく知られている[10]。また弾性などの高分子物性を示すことなどから，石炭中に架橋が存在することを示している。この架橋構造についても従来は共有結合架橋が考えられてきたが，前述の室温における高い抽出率の結果から，こうした共有結合による架橋ゲル構造にも疑問がもたれた。興味深いのは，抽出物中の重質成分である PI, PS 成分もそれらを

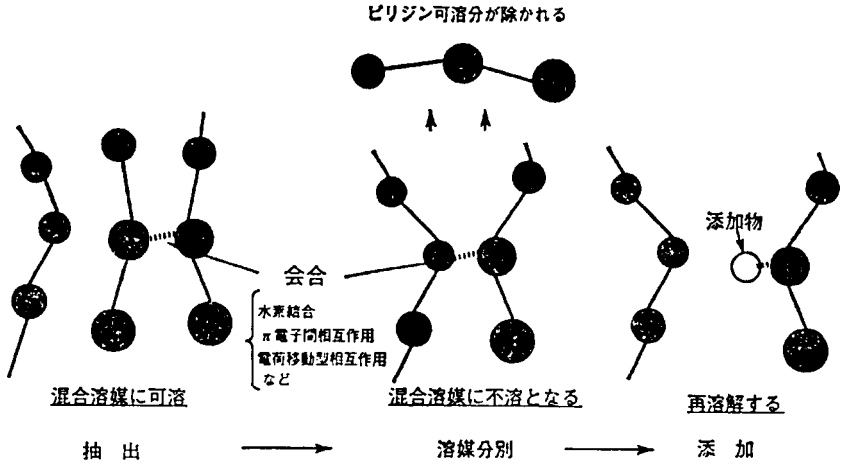

図 3　石炭分子間の会合に及ぼす添加物の効果。

総　説

石炭架橋への溶媒の浸透

（キーワード　溶媒抽出，溶媒膨潤，非共有結合，分子会合，架橋構造）

— 1993. 2.25 受理 —

東北大学　鷹觜　利公、飯野　　雅

1．緒　言

エネルギー消費予測によれば，来る21世紀初頭には現在の石油供給のピークが過ぎ，エネルギー源としての石炭の占める割合が今以上に高くなるという。一方では地球環境汚染に関連して，化石燃料の利用に不安感が増している現在，石炭を高効率に利用する技術開発に取り組み，エネルギー源，化学原料源としての石炭の有用性を唱えていく必要がある。

石炭の反応性はその反応条件に大きく依存する。例えば同じ反応温度でも昇温速度の違いにより生成物分布が異なる。これは石炭が不均質な成分からなるということに加えて，石炭構造の複雑さ，特に三次元架橋構造特性が大きく関連している。一方最近の分析技術の多様化，高性能化にともない，石炭構造研究が盛んに行われ，こうした石炭構造に基づいた反応性の評価が重要であるという認識が高まりつつある。

我々の研究室では以前から石炭構造研究の手法として溶媒抽出，溶媒膨潤の研究を進めている[1)-4)]。すでに溶媒の関与した石炭特有の現象が見い出されており，これが石炭のハンドリング法や前処理技術への応用として期待されている。本総説では，溶媒の浸透によって起こる様々の現象を石炭構造変化という観点から述べ，溶媒浸透に影響するいくつかの因子について考えてみたい。

2．溶媒処理による石炭構造の変化

2.1　溶媒中での石炭構造変化

石炭構造は異方性をもち，エネルギー的に不安定な歪んだ構造をしていると言われる[5)~7)]。従って原炭を溶媒中に浸すとこの歪み構造の緩和が起こり，石炭は急激に膨れ，石炭可溶成分の多くが溶媒相へ抽出される。それから石炭架橋と溶媒の間で，比較的ゆっくりと平衡膨潤状態に達する。一方膨潤状態では石炭分子の動き易さが増加するために，原炭とは異なる種々の強さの会合体が形成される[3)]。

2.2　溶媒除去による石炭構造の安定化

石炭の溶媒膨潤状態から徐々に溶媒を除いていくとどのような変化が起きるであろうか。溶媒除去とともに石炭構造は収縮していくが，一度歪み状態から緩和された構造はもとの構造には戻らず，水素結合，ファンデルワールス相互作用，芳香環相互作用等を介してより安定な構造に落ちつくと言われている[8)9)]。従ってこのいわゆる溶媒処理炭は原炭とは異なったより安定な分子配向性を示し，溶媒抽出率も処理炭では一般に減少することが報告されている[3)8)]。脱灰，アルキル化等の処理も含めて溶媒下で反応を行う際には，こうした新たな会合体生成を含めた石炭分子の再配向による構造変化の影響を加味しなければ，その反応の真の効果が評価されないので注意が必要である[1)10)11)]。

溶媒処理による石炭改質を液化反応[12)]・熱分解反応[13)]に利用する試みも最近数多く報告されている。詳細は本特集号の他の総説を参考していただきたいが，上でも述べたように単なる溶媒処理→溶媒除去の過程では，石炭構造のポテンシャルエネルギーは低い状態に移行すると考えられる

反応化学研究所　仙台市青葉区片平２丁目１－１

ので，その処理方法にも工夫が必要であろう。またこうした溶媒処理を繰り返すと，2度目以降では初めの処理で見られた急激な構造緩和は起こらず，短時間で初回と同程度の平衡膨潤状態になることがCodyらの研究[7]から分かっている。

3．　石炭の分子会合

3.1　種々の非共有結合

石炭分子は構造内の芳香環や極性置換基の分子間相互作用により分子会合を形成していると考えられている[2)14)~18)]。Larsenらはピリジンで石炭を処理することにより石炭分子間の水素結合が解裂し，溶解性や膨潤値が増加することを報告している[19)~21)]。Miyake, Stockらは高ランクの石炭のC-アルキル化反応をそのアルキル鎖長を変えて行ない，鎖の長さに対応して処理後の溶媒抽出率が大幅に増加することを見いだしている[22)]。これはアルキル鎖が長いほど，芳香環のπ-π相互作用を弱めているためと考えられている。Nishiokaらは高揮発性瀝青炭をクロロベンゼンなどの溶媒で処理することにより，その後のピリジン抽出率が減少することを報告し[8)17)]，UVやFT-i.r.測定からこれが電荷移動型相互作用による会合であると述べている[17)]。またLarsenらは石炭分子とテトラシアノキノジメタン(TCNQ)を混合することにより，TCNQのシアノ基のFT-i.r.吸収ピークが低波数側へシフトし，石炭分子とTCNQの間で電荷の移動が起きていると考えている[23)]。また佐々木，真田らはヨウ素，TCNQを添加した石炭のESR測定から，電荷移動型相互作用による非共有結合構造について述べている[15)]。

3.2　石炭構造における非共有結合の役割

石炭にはこのようにいくつかの非共有結合が関与した会合が存在し，その種類，量は石炭ランクに大きく依存する。そこでNishiokaはランクの異なる石炭に対してその処理方法を変え，いくつかの処理を段階的に行なう多段抽出法を検討している[24)]。すなわちイオン性相互作用の処理として塩酸洗浄を，電荷移動型相互作用の解放として無水マレイン酸(電子供与体)処理を，またπ-π相互作用の解放にはMallya, Stockらの C-ブチル化法[25)]をそれぞれ適用し，Table 1に示す組み合わせで各石炭の多段抽出の効果を見ている。その結果ピリジンでの単独抽出に比べて，多段抽出により各石炭とも抽出率の増加が見られる。しかしNishiokaはこのような処理の組み合わせでは一部の会合が解放されるに過ぎず，まだ多くの会合により抽出されない可溶成分が石炭に存在すると考えている。その理由として2.で述べたように，溶媒処理だけで新たな強い会合が生成する可能性があること，また各相互作用はこの多段階処理だけでは完全には解放されないこと，さらに石炭中には高分子鎖の物理的な絡み合いが存在することを挙げている。Nishiokaは石炭全体が一つの分子量分布をもった分子の集まりからなり[26)]，それらが上述のいろいろな分子間相互作用から会合体を形成していると考え，従来の高分子網目成分と低分子量成分からなるとするtwo phase概念に対して，mono phaseモデルを提案している[16)18)]。

我々の研究室では瀝青炭の溶媒抽出に二硫化炭素とN-メチル-2-ピロリジノン(NMP)の混合溶媒が特に強力な溶媒系であることを見いだ

Table 1　Multistep extraction of coals[a)]

Coal	C% (daf)	Multistep extraction[b),c)]	Single step extraction	Multistep extraction
North Dakota	72.9	2N HCl→Py-Sox.→Bu_4NOH/H_2O/Py→Py-Sox.	15	38
Wyodak Anderson	75.0	2N HCl→Py-Sox.→Bu_4NOH/H_2O/Py→Py-Sox.	24	44
Illinois No.6	77.7	Py-Sox.→O-methyl.→Py-Sox.→MA/PhOH→Py-Sox.	42	50
Pittsburgh No.8	83.2	Py-Sox.→MA/PhOH→Py-Sox.→O-butyl.→Py-Sox.	42	54
Upper Freeport	85.5	MA/PhOH→Py-Sox.	45	73

a) Ref. 24

b) "Py–Sox." refers to Soxhlet extraction with pyridine

c) "MA/PhOH" refers to soaking in the presence of maleic anhydride in phenol

Table 2 Effect of addition of TCNE on extraction with CS_2-NMP mixed solvent

Coal	Specification	C%(daf)	Amount of additive (g/1 g coal)	Extraction yield wt%(daf)
Pocahontas No.3	Argonne	89.7	none	2.8
			0.025	1.9
Upper Freeport	Argonne	86.2	none	60.4
			0.025	85.0
Pittsburgh No.8	Argonne	82.6	none	39.0
			0.025	42.6
Illinois No.6	Argonne	76.9	none	33.1
			0.100	33.1
Sewell 'B'	PSOC726	88.4	none	37.9
			0.100	47.9
Upper Freeport	PSOC1441	85.0	none	44.2
			0.100	50.1
Lower Kittanning	PSOC815	84.0	none	46.2
			0.100	61.5
Stigler	PSOC1376P	77.8	none	37.5
			0.100	52.3

し[27)28)]，室温で40-79%(daf)の高抽出率を得ている[27)29)]。さらに最近この抽出系に強い電子受容体であるテトラシアノエチレン(TCNE)を極少量加えて[2)]抽出を行ってみたところ，Table 2に示すように，いくつかの石炭で添加なしの場合に比べて大きな抽出率の向上が認められている[30)]。この室温抽出では，共有結合の解裂などの可溶化反応は起きていないと考えられる。従ってUpper Freeport炭で得られる85%の抽出率の結果を考えると，このランクの一部の石炭は少なくとも従来のtwo phaseモデルでは説明されず，石炭の大部分が分子の会合体から形成されていると考えられる[31)32)]。

4．溶媒の浸透現象

4.1 石炭と溶媒の相溶性

石炭の有機質成分は少なくとも部分的に高分子架橋構造からなると考えられている[21)33)]。従って溶媒中で石炭は膨潤し，その網目の体積は，溶媒により広がろうとする力とその網目の弾性により縮もうとする力の平衡から決まり，もとの体積に対する体積変化が膨潤値で表される。ただし石炭にはもともと抽出可能成分が存在し，それらが溶媒相に溶け出すという現象，すなわち溶媒抽出が膨潤と同時に起きている。石炭の溶媒抽出，溶媒膨潤の程度はその石炭の抽出可能成分量や架橋特性に依存するが，そのほかに石炭とその溶媒との相溶性が大きく関連することが知られている[34)35)]。この相溶性の指標の一つとして溶解度パラメータがあり，溶媒種を変えた膨潤測定[20)36)]，またはグループ寄与法[37)]から石炭の溶解度パラメータが評価されている。最近，Painterらは膨潤測定から求めた石炭の溶解度パラメータを，グループ寄与法から求めた値と比較し，水素結合に会合モデルを取り入れることにより，石炭と溶媒間の相互作用について検討している[38)]。

4.2 非共有結合による物理的架橋の存在

石炭高分子内への溶媒の浸透には，3.で述べたように溶媒による石炭分子会合の解放が関連している。Green, Larsenら[19)]はピリジン-クロロベンゼン混合溶媒系の膨潤値とその時の各溶媒の石炭内への吸収量を測定している。その結果ピリジンを少量加えると膨潤値が大きく増加し，同時にクロロベンゼンの吸収量も増加することを見いだしている。これはピリジンによる非共有結合架橋の解裂でクロロベンゼンの浸透が促進されているためと考えられている。Amemiyaら[39)]は石炭をテトラヒドロキノン(THQ)-アルコール系の混合溶

媒で膨潤処理することにより，アルコールで大きく膨潤した石炭内部に多くのTHQが吸収され，結果としてその後の液化収率が向上することを報告している。また我々が用いているCS_2-NMP混合溶媒系でも，混合溶媒による相乗効果が膨潤値と溶媒抽出率で認められている[4)28)]。

また良溶媒で得られた(溶解する)抽出物が貧溶媒で膨潤するという現象が見られており[4)40)41)]，これは石炭分子の会合が架橋点として働いていることを示唆している。ただしこの抽出物の膨潤現象については相分離から説明されるという解釈もあり[42)]，今後抽出物の高分子特性について詳しい検討を行う考えである。

4.3　溶媒浸透に及ぼす抽出成分の影響

溶媒の石炭架橋への浸透ではその石炭にもともと存在する抽出可能成分の存在が影響する。Fig.1はBruceton原炭とピリジン抽出残渣炭のメタノール／*N*,*N*-ジメチルアニリン混合溶媒の溶解度パラメータに対する膨潤値を示している[19)]。原炭では混合溶媒による相乗効果が見られるのに対し，抽出残渣炭では*N*,*N*-ジメチルアニリン単独の場合に最も高い膨潤値が得られている。この結果に対してGreen, Larsenらは二つの理由を考えている。第一に原炭の場合にはその可溶成分が溶媒に溶け出し，溶媒成分の化学ポテンシャルが変化することが考えられる。この点に関しては最近膨潤測定時の石炭と溶媒比の影響が報告されている[43)]。また第二の理由として，原炭と抽出残渣炭の架橋密度の違いを挙げている。

原炭(4種の瀝青炭)の膨潤に関して，我々はベンゼン，シクロヘキサン，メタノール，THFで測定を行っており，いずれの石炭，溶媒中でもほとんど膨潤しないという結果が得られている[4)]。そこで抽出成分の影響を見るために，CS_2-NMP混合溶媒比を変えて，異なる抽出率の抽出残渣を試料としてベンゼン膨潤値を測定した(Fig.2)[4)]。Fig.2から3種の石炭とも抽出率の増加にともない平衡膨潤値が増加していることが分かる。従って原炭では，抽出可能成分と残渣成分が非共有結合を介した比較的架橋密度の高い構造であるのに対して，そこから抽出成分を除いた抽出残渣炭では，その量に応じて架橋間平均分子量が大きくなり，膨潤値が高くなると考えられる。

このように石炭は比較的架橋密度の高い構造と考えられ，溶媒の浸透には物理的因子として溶媒の嵩高さが影響する。相田らはブチルアミン誘導体とメタノールの混合溶媒系の組成比を変えた膨潤値を求めている(Fig.3)[44)]。比較的立体障害の小さい*n*-ブチルアミンでは組成比に対して直線性を示すのに対して，立体障害の大きい*t*-ブチ

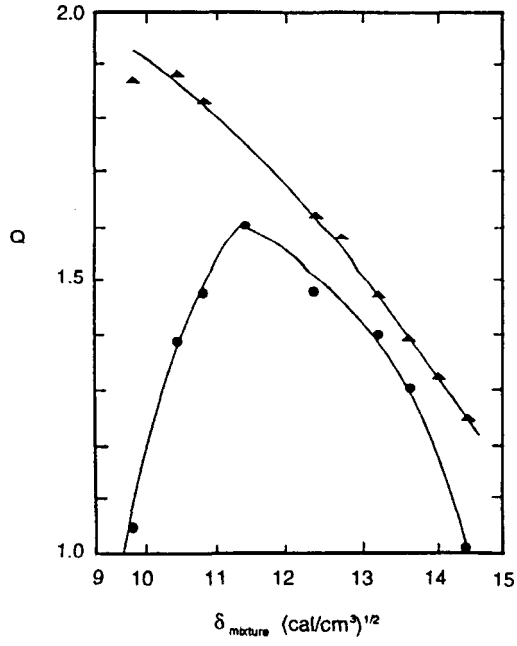

Fig. 1　Plot of d of solvent mixture versus Q for the methanol — *N*, *N*-dimethyaniline mixtures : ▲, pyridine-extracted ; ●, unextracted[19)]

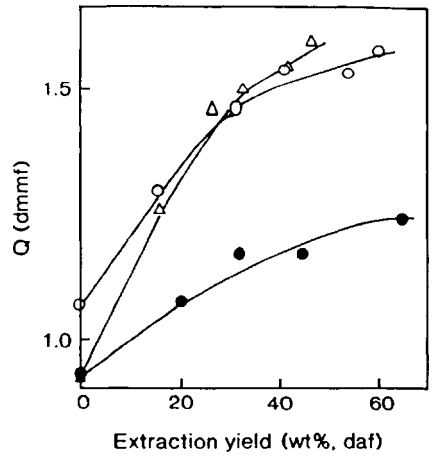

Fig. 2　Swelling ratios(Q) of the extraction residues in benzene versus the extraction yields for Zao Zhuang(●), Shin-Yubari(○), Lower Kittanning(△)coals

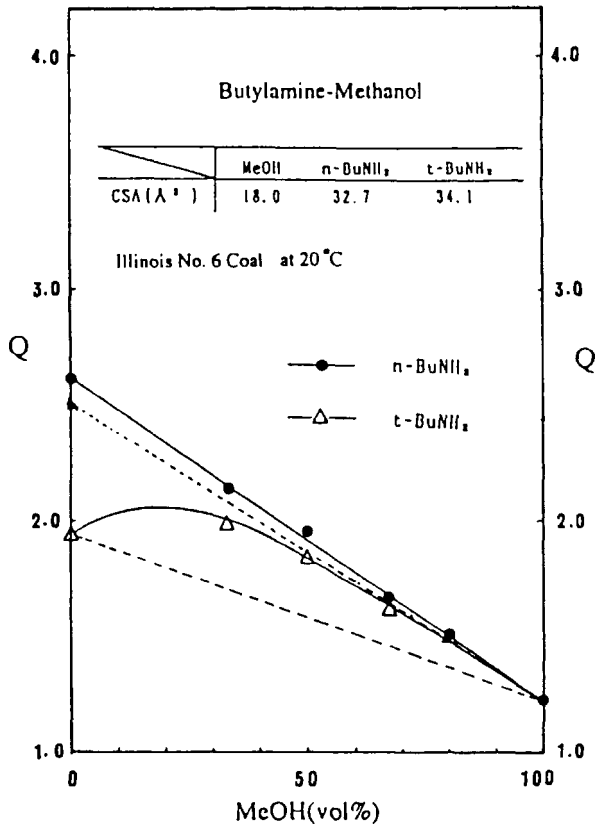

Fig. 3 Swelling ratios of Illinois No. 6 coal in binary solvents[44]

ルアミンではメタノールの濃度が低くなるに従い，膨潤値が減少することが分かる。この結果とFig.1の結果から，原炭では溶媒と石炭の立体障害が溶媒の浸透性に大きく影響することを示している。相田らはこうした立体障害も考慮に入れた新たな石炭相溶性パラメータを提案している[44]。

4.4 架橋間平均分子量

Flory-Rehner の高分子理論が石炭架橋構造解明に取り入れられたのは古く，すでに Sanada, Honda[34] Kirov ら[35]によって行われている。溶媒膨潤値から Flory-Rehner 式に基づき架橋間平均分子量の推算が行われている[20)45)46)]。推算された架橋間平均分子量は石炭ランクに大きく依存し，こうした高分子特性の違いが各石炭の反応性に影響すると述べている。一方でこの推算法では，石炭への適用性，また石炭と溶媒間の相互作用パラメータ値の妥当性に問題が残っている。

我々は溶媒抽出残渣を細かく粉砕し，それを空カラムに充填した逆クロマトグラフィーを行い，

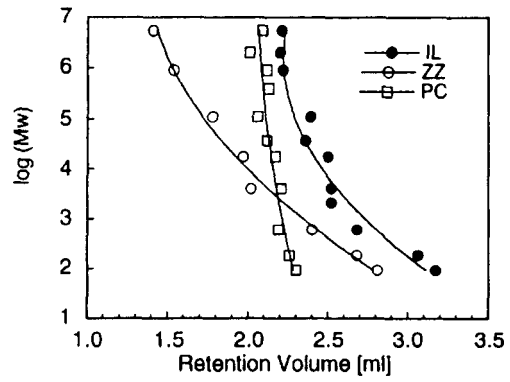

Fig. 4 Retention volume of standard polystyrene using columns packed with the residues from the CS_2-NMP mixed solvent extraction : ●, Illinois No. 6 (IL, extr. yield=16.7%) ; ○, Zao Zhuang (ZZ, extr. yield=63.0%) ; □, Pocahontas No. 3 (PC, extr. yield=2.8%) coals

石炭架橋構造に関して直接的に情報を得ることを試みている[47]。Fig.4に CS_2-NMP 混合溶媒抽出残渣炭のポリスチレン標準サンプルの溶出曲線を示す。Illinois No.6炭の溶出曲線を見ると，10^2から10^5までは分子量の増加にともない保持容量が減少しており，それ以上では保持容量に変化が見られていない。この結果はポリスチレンが，分子サイズによる排除クロマトグラフィーの機構で溶出分離されている可能性があるものの，石炭ーポリスチレン間の吸着，または孔隙構造の影響なども考えられ，現在分離機構に関して詳しい検討を行っている。またこの手法を用いて石炭と有機化合物との相互作用に関する研究も進めている。

4.5 溶媒浸透の速度論

石炭の溶媒浸透を現象論で見た場合，これまで述べたように石炭構造は大きく変化する。従って石炭架橋への溶媒の浸透速度は，こうした構造変化による高分子鎖の緩和過程と，溶媒自身の拡散過程に支配される。Ritger, Peppas[48]は石炭の薄片を用いてピリジン吸収量の時間変化を求めている。その結果150-1500mmの薄片の範囲では，その浸透が溶媒の関与した緩和過程に支配されると述べている。Hsieh, Duda ら[46)49)]も同様な溶媒の吸収速度を調べており，その現象が通常の高分子架橋への拡散支配では説明できず，溶媒の存在による構造変化が大きく影響していると報告している。Green ら[50]は石炭のベンゼン吸収速度に及ぼす

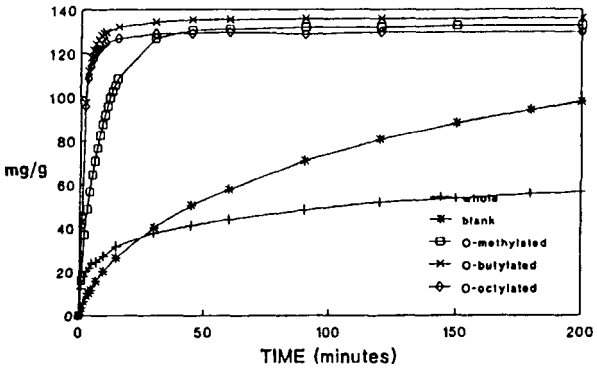

Fig. 5　Sorption of benzene by O-alkylated Illnois No. 6 coals at 30℃[50]

O-アルキル化の影響を調べ，Fig.5に示すように，アルキル化による水素結合の解裂により吸収速度が高くなることを示している。

5．結　言

以上溶媒の浸透現象とそれにともなう石炭の高分子構造変化について述べた。ここで紹介したほかにもNMR-imaging法を用いた溶媒浸透時の石炭分子の画像解析法が提案され[51]，新たなアプローチ法として注目される。また膨潤による孔隙構造の変化を小角中性子散乱測定から評価する方法が報告されている[52]。膨潤以外の高分子化学的手法も石炭高分子構造の解明に取り入れられており，Brenner[53]は均質な石炭薄片を作製し，石炭の粘弾性挙動について述べている。またHall, Larsen[54]は石炭と溶媒をある容量比で混合することにより，安定な石炭-NMPゲルと石炭-ピリジンゲルが作られることを見いだし，それらのゲルの特性について報告している。

以上，本総説で述べた現象は主に室温での溶媒中の石炭構造変化であり，これをさらに温和な加熱下である100-250℃で行うと，一般に石炭高分子の構造変化は大きくなる[55]。従って，こうした低い温度での石炭の構造変化を，逆に石炭利用プロセスに応用することが期待されている。具体的には膨潤状態での石炭変換反応の実施，あるいは石炭分子鎖の再配向や会合状態の制御による石炭改質反応(前処理)の導入などが考えられる。さらに，石炭の高分子構造特性に関する理解を深め，高効率利用プロセスの開発に結びつけていきたいと考えている。

文　献

1) Takanohashi, T. and Iino, M., *Energy Fuels*, **4**, 333 (1990)
2) Sanokawa, Y., Takanohashi, T. and Iino, M., *Fuel*, **69**, 1577 (1990)
3) Takanohashi, T. and Iino, M., *Energy Fuels*, **5**, 708 (1991)
4) Fujiwara, M., Ohsuga, H., Takanohashi, T. and Iino, M., *Energy Fuels*, **6**, 859 (1992)
5) Brenner, D., *Fuel*, **62**, 1347 (1983)
6) Brenner, D., *Fuel*, **63**, 1347 (1984)
7) Cody, G. D. Jr., Larsen, J. W. and Siskin, M., *Energy Fuels*, **2**, 340 (1988)
8) Nishioka, M. and Larsen, J. W., *Energy Fuels*, **4**, 100 (1990)
9) Larsen, J. W. and Mahammadi, M., *Energy Fuels*, **4**, 107 (1990)
10) Larsen, J. W., Pan, C.-S. and Susan, S., *Energy Fuels*, **3**, 557 (1989)
11) Larsen, J. W., Azik, M. and Korda, A., *Energy Fuels*, **6**, 109 (1992)
12) 例えば，Joseph, J. T., *Fuel*, **70**, 139 (1991)
13) Miura, K., Mae, K., Yoshimura, T., Masuda, K. and Hashimoto, K., *Energy Fuels*, **5**, 803 (1991)
14) Krichko, A. A. and Gagarin, S. G., *Fuel*, **69**, 885 (1990)
15) 佐々木正秀，真田雄三，燃協誌，**70**，790 (1991)
16) Nishioka, M. and Gorbaty, M. L., *Energy Fuels*, **4**, 70 (1990)
17) Nishioka, M., Gebhard, L. A. and Silbernagel, B. G., *Fuel*, **70**, 341 (1991)
18) Nishioka, M., *Fuel*, **71**, 941 (1992)
19) Green, T. K. and Larsen, J. W., *Fuel*, **63**, 1538 (1984)
20) Larsen, J. W., Green, T. K. and Kovac, J., *J. Org. Chem.*, **50**, 4729 (1986)
21) Larsen, J. W., Lee, D. and Shawver, S. E., *Fuel Proc. Tech.*, **12**, 51 (1986)
22) Miyake, M. and Stock, L. M., *Energy Fuels*, **2**, 815 (1988)
23) Larsen, J. W., Flowers II, R. A., Hall, P., Silbernagel, B. G. and Gebhard, L. A., 1991 In-

ter. Conf. Coal Sci. Proc., p. 1 (1991)
24) Nishioka, M., *Fuel*, 70, 1413 (1991)
25) Mallya, N. and Stock, L. M., *Fuel*, 65, 736 (1986)
26) 林潤一郎, 安藤 亮, 草壁克己, 諸岡成治, 燃協誌, 69, 446 (1990)
27) 飯野 雅, 熊谷 淳, 伊藤 攻, 燃協誌, 64, 210 (1985)
28) Iino, M., Takanohashi, T., Ohsuga, H. and Toda, K., *Fuel*, 67, 1639 (1988)
29) Iino, M., Takanohashi, T., Ohkawa, T. and Yanagida, T., *Fuel*, 70, 1236 (1991)
30) Ishizuka, T., Takanohashi, T., Ito, O. and Iino, M., *Fuel*, 72, 579 (1993)
31) 鷹觜利公, 飯野 雅, 燃協誌, 70, 802 (1991)
32) 飯野 雅, 石油誌, 35, 26 (1992)
33) Green, T., Kovac, J., Brener, D. and Larsen, J. W., In, *Coal Structure*, Meyers, R. A., Ed., Academic Press: New York, p. 199 (1982)
34) Sanada, Y. and Honda, H., *Fuel*, 45, 295 (1966)
35) Kirov, N. Y., Oshea, J. M. and Sergeant, G. D., *Fuel*, 47, 415 (1968)
36) Hombach, H. P., *Fuel*, 59, 465 (1980)
37) van Krevelen, D. W., *Fuel*, 45, 229 (1966)
38) Painter, P. C., Graf, J. and Coleman, M. M., *Energy Fuels*, 4, 379 (1990)
39) Amemiya, K., Kodama, M., Esumi, K., Meguro, K. and Honda, H., *Energy Fuels*, 3, 55 (1989)
40) 相田哲夫, 日本学術振興会石炭利用技術第148委員会第17回研究会資料, p. 18 (1987)
41) Green, T. K., Chamberlin, J. M. and Lopez -Froedge, L., *Prep. Pap.-Am. Chem. Soc., Div. Fuel Chem.*, 34, 759 (1989)
42) Painter, P. C., *Energy Fuels* ,6, 863 (1992)
43) Larsen, J. W., Cheng, J. C. and Pan, C.-S., *Energy Fuels*, 5, 57 (1991)
44) 相田哲夫, 鈴木衆策, 山脇信光, 藤井政幸, 吉原正邦, 第1回日本エネルギー学会大会講演要旨集, p. 80 (1992)
45) Lucht, L. M. and Peppas, N. A., *Fuel*, 66, 803 (1987)
46) Painter, P. C., Park Y., Sobkowiak, M. and Coleman, M. M., *Energy Fuels*, 4, 384 (1990)
47) 金子博之, 鷹觜利公, 飯野 雅, 第28回石炭科学会議論文集, p. 265 (1991)
48) Ritger, P. L. and Peppas, N. A., *Fuel*, 66, 1379 (1987)
49) Hsieh, S. T. and Duda, J. L., *Fuel*, 66, 170 (1987)
50) Green, T. K., Ball, J. E. and Conkright, K., *Energy Fuels*, 5, 610 (1991)
51) French, D. C., Dieckman, S. L. and Botto, R. E., *Energy Fuels*, 7, 90 (1993)
52) Winans, R. E. and Thiyagarajan, P., *Energy Fuels*, 2, 356 (1988)
53) Brenner, D., *Prep. Pap.-Am. Chem. Soc., Div. Fuel Chem.*, 31, 17 (1986)
54) Hall, P. J. and Larsen, J. W., *Energy Fuels*, 7, 47 (1993)
55) Yun, Y. and Suuberg, E. M., *Energy Fuels*, 6, 328 (1992)

Accessibility of Solvent to Coal Cross-links

Toshimasa TAKANOHASHI and Masashi IINO

(Institute for Chemical Reaction Science, Tohoku University)

SYNOPSIS : — The contact of solvent with a coal macromolecular network may induce relaxation of the strained structure, solvent extraction, and solvent swelling. Several factors influencing accessibility of solvent to coal network, are discussed. First, chemical affinity of coal with solvent is discussed from solubility parameter of coals estimated. Next, the disruption of non-covalent bonds such as hydrogen bonding, π - π interaction, and charge transfer interaction etc., by attack of solvent may increase extraction yields and swelling ratios. While, the formation of association of coal molecules through the non-covalent bonds may occur due to relaxation of macromolecular structure in solvent, resulting in a decrease in extraction yields and swelling ratios. Finally, physical factors such as steric bulkiness of solvent, and existence of extractable substances in coal cross-links influence accessibility of solvent to coal cross-links. The nature of coal cross-links is also discussed. The fact that coals are comprised of association of a considerable amount of extractable molecules suggests the existence of physical (non-covalent) cross-links in coal network.

Key Words

Solvent extraction, Solvent swelling, Non-covalent bonds, Association of coal molecules, Cross-link structure

Reprinted from I&EC RESEARCH, 1991, 30.

Steam Gasification of Low-Rank Coals with a Chlorine-Free Iron Catalyst from Ferric Chloride

Yasuo Ohtsuka* and Kenji Asami

Research Center for Carbonaceous Resources, Institute for Chemical Reaction Science, Tohoku University, Sendai 980, Japan

A novel method for converting $FeCl_3$ to an active, Cl-free Fe catalyst for coal gasification has been studied. Fe cations alone can be incorporated into low-rank coals from an aqueous solution of $FeCl_3$ by using NH_3/NH_4Cl solution. Some Fe cations are exchanged with the protons in carboxyl groups. The Cl-free Fe results in a finely dispersed catalyst, which shows a high activity for gasification with steam at around 950 K. The degree of rate enhancement by the Cl-free catalyst depends on char conversion, Fe loading, and temperature. The chemical form of the Fe catalyst on devolatilization and during gasification is Fe_3O_4. The catalytic activity is discussed in terms of the dispersion of Fe_3O_4 particles.

Introduction

Cheap Fe is one of the most promising catalysts for coal gasification. We have found that the activity of Fe catalyst strongly depends on the kind of precursor salts: iron nitrate and ammonium oxalate are quite effective for the low-temperature gasification of brown coal with steam as well as with H_2, whereas the chloride and the sulfate are not effective (Ohtsuka et al., 1987a). Since iron chloride and sulfate are readily available as acid wastes from steel pickling and titanium oxide production plants, they would be most desirable as raw materials for Fe catalyst. Under some circumstances, these compounds were converted to active catalysts (Kasaoka et al., 1979; Hüttinger and Schleicher, 1981; Adler and Hüttinger, 1984). In these cases, however, Cl- or S-containing compounds inevitably evolve during gasification, and they may cause some serious problems such as corrosion on various parts of materials and increased capacity of desulfurization. Therefore, it would be necessary to develop a new method to convert iron chloride and sulfate to active catalysts without such pollutants.

In the present work, a novel method to prepare a Cl-free Fe catalyst from an aqueous solution of $FeCl_3$ is presented, and the catalytic effectiveness for the steam gasification of low-rank coals is examined in detail. Cl ions from $FeCl_3$ are completely removed in the step of catalyst addition. The Cl-free catalyst is much more effective than the $FeCl_3$ simply impregnated on coal. The effect of some factors on the rate enhancement by the Cl-free catalyst are clarified.

Experimental Section

Coal Sample. In order to incorporate Fe ions alone into coal, low-rank coals with large amounts of oxygen-containing groups as cation exchangeable sites were selected as coal samples. A Japanese Sarobetsu peat and an Australian Loy Yang brown coal, abbreviated as SA and LY, respectively, were used. They were crushed and sieved to 74–150 μm. Their proximate and ultimate analyses are shown in Table I.

Catalyst Preparation. The preparation was carried out in the following manner, where the ion-exchange method for preparing exchanged alkali-metal catalysts for NaCl and KCl solutions (Takarada et al., 1987, 1989) was modified in order to prevent $FeCl_3$ from being precipitated as iron hydroxides in a high-pH region. The mixture of coal particles and $FeCl_3$ solution was stirred at room temperature, and a buffer solution of NH_3/NH_4Cl was added dropwise into the mixture. The pH of the mixture changed gradually from the initial value of about 2 to the alkaline region. The final pH was kept at a constant value of 8–9. After a sufficient amount of buffer solution was added, the solution was filtered off, and the coal was washed with deionized water repeatedly to remove the Cl ions. Fe loading was varied by changing the initial concentration of $FeCl_3$; for example, 0.2 N $FeCl_3$ solution was used for the loading of 5% Fe. As a reference, $FeCl_3$ was impregnated on coal; the coal was soaked in the aqueous solution for 30 min, and then water was evaporated in vacuo at 340 K.

Determination of Iron and Chlorine. The amount of Fe incorporated was determined by atomic absorption spectroscopy (Japan Jarrell Ash Co., AA-855) after extraction of the metal from the coal with hot HCl for 2 h. The Cl content in the coal was determined by a standard Eschka method (ISO 587-1981 (E)). Fe loading or Cl content is expressed as weight percent in the dried sample.

Steam Gasification. The experiments were conducted with a thermobalance (Shinku-Riko, TGD-5000) at a temperature range of 873–1073 K. About 20 mg of a dried sample was mounted on quartz wool in a quartz cell with holes for the passage of steam, heated in a H_2O (80 kPa)/N_2 stream at a rate of 300 K/min, and soaked for 2 h at a constant temperature. The reaction consisted of the coal devolatilization and following char gasification stages. The effectiveness of Fe catalyst in the latter stage will be discussed in this paper. Char conversion is used as an index for the reactivity of char, being expressed as weight percent on a dry ash free, catalyst-free basis. The specific rate of char as another index means the gasification rate per unit weight of residual char. Since the presence of metal catalysts shows no significant effect on the surface area of the chars from Australian brown coals (Tomita et al., 1985; Ohtsuka, 1990), the specific rate can be used to show the effect of iron catalyst. Gas products during the gasification of SA peat at 973 K were analyzed at char conversion of around 30% by gas chromatograph.

Characterization. Fourier transform infrared (FT-IR) spectra of original and Fe-loaded coals were measured by a JEOL JIR-100 spectrometer equipped with a diffuse-reflectance apparatus. For the semiquantitative analysis, care was taken to keep the content of catalyst-free coal constant among all the samples. X-ray diffraction (XRD) analysis of Fe catalyst was carried out by a Shimadzu XD-3A diffractometer with Mn-filtered Fe Kα radiation (40 kV, 25 mA). The samples for XRD measurements were prepared in pure N_2 or in H_2O/N_2 at 973 K in the same

* To whom correspondence should be addressed.

0888-5885/91/2630-1921$02.50/0

Table I. Proximate and Ultimate Analysis of Coals

coal (code)	proximate anal., wt % (dry)			ultimate anal., wt % (daf)				
	ash	VM[a]	FC[a]	C	H	N	S	O (by diff)
Sarobetsu (SA)	2.9	66.4	30.7	56.9	5.9	1.5	0.3	35.4
Loy Yang (LY)	0.5	52.4	47.1	66.7	4.6	0.5	0.3	27.9

[a] VM, volatile matter; FC, fixed carbon.

Table II. Iron and Chlorine Contents for SA Peat and LY Coal

coal	catalyst solution	content, wt %	
		Fe	Cl
SA	none	0	0.08
	$FeCl_3$/buffer[a]	1	0.01
	$FeCl_3$/buffer[a]	5	0.01
	$FeCl_3$/buffer[a]	15	0.02
	$FeCl_3$ alone[b]	8	14
LY	none	0	0.01
	$FeCl_3$/buffer[a]	1	0.02
	$FeCl_3$/buffer[a]	5	nd[c]
	$FeCl_3$/buffer[a]	9	0.04
	$FeCl_3$/buffer[a]	14	0.01
	$FeCl_3$ alone[b]	8	13

[a] NH_3/NH_4Cl buffer solution. [b] Impregnation method. [c] Not determined.

manner as the gasification runs. The crystallite size of Fe species was determined by the Debye–Shörrer method.

Results

Iron Loading and Residual Chlorine. Table II shows the Fe and Cl contents in all the samples used in the gasification runs. When $FeCl_3$ was loaded by using the buffer solution, a large amount of Fe up to 15 wt % was incorporated into SA peat and LY coal. On the other hand, the Cl content was almost the same as the amount of Cl inherently present in the original coal. Thus, Cl ions from $FeCl_3$ were completely removed by water washing, and the Cl-free Fe catalyst was prepared. When $FeCl_3$ was impregnated without the buffer solution, however, a considerable amount of Cl, corresponding to the amount of Fe loaded, was retained on both coals (Table II). Most of the Cl existed in the form of $FeCl_3$.

FT-IR Spectra. Figure 1 illustrates the FT-IR spectra of LY coal with different loadings of Cl-free Fe catalysts. The strong, carboxylic C=O stretching band near 1700 cm^{-1} was observed in the original coal. The intensity of the absorption peak was lowered in the presence of Fe and decreased with increasing Fe loading up to 9 wt %. Both LY coal soaked in the buffer solution without $FeCl_3$ and impregnated with $FeCl_3$ coal showed the same spectra as the original coal. These findings show that the ion exchange between Fe^{3+} and H^+ in COOH groups takes place with the Cl-free catalysts. The carboxylate anions formed by the ion exchange have the absorption band near 1600 cm^{-1}. Since the C=C bonds inherently present in coal also exhibited the strong absorption in this region (Figure 1), however, the intensity of the peak from carboxylate anions could not be determined.

Gasification Profile. Figures 2 and 3 show the profiles for steam gasification of SA peat and LY coal, respectively, at 973 K. With a Cl-free Fe catalyst, a small amount of Fe of 1 wt % promoted the gasification of each coal; char conversions after 90 min for SA peat and LY coal increased from 48 and 26% without catalyst to 66 and 46% at 1 wt % Fe, respectively. The dependence of gasification reactivity on the Fe loading was somewhat different between both coals: the reactivity of SA peat increased with an increase in the loading and the conversion at 15 wt % Fe reached around 90% within 60 min, whereas the reactivity

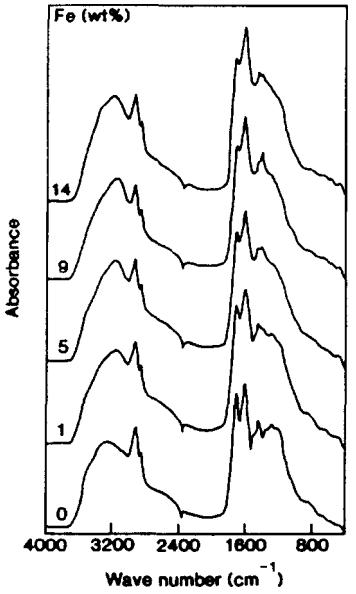

Figure 1. FT-IR spectra of LY coal with a Cl-free Fe catalyst.

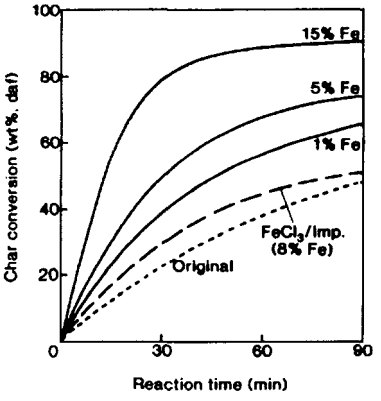

Figure 2. Steam gasification of SA peat at 973 K.

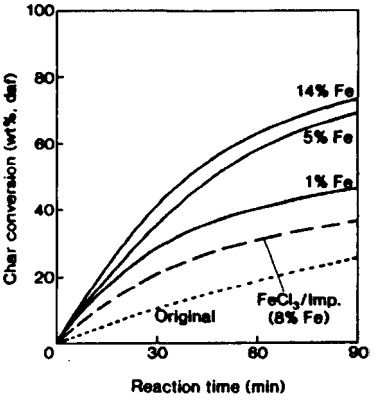

Figure 3. Steam gasification of LY coal at 973 K.

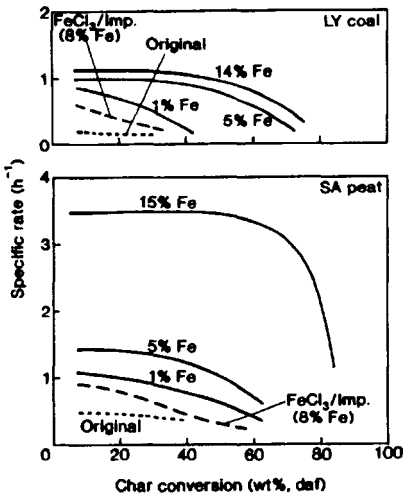

Figure 4. Profiles for specific gasification rates of SA peat and LY coal with Fe catalysts at 973 K.

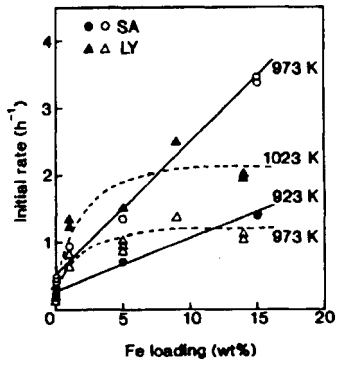

Figure 5. Effect of Fe loading on initial gasification rates of SA peat and LY coal.

of LY coal leveled off beyond 5 wt % Fe. Reactivities of $FeCl_3$-impregnated coals were quite small in spite of a high loading of 8 wt %, being much lower than those of the coals with the Cl-free Fe of 1 wt %.

Specific Rate versus Conversion. Figure 4 illustrates the relationship at 973 K between the specific gasification rate and the char conversion. The rates for $FeCl_3$-impregnated SA peat and LY coal with 8 wt % Fe were low and decreased with increasing conversion, showing the rapid deactivation of the impregnated catalyst. With the Cl-free iron catalyst, on the other hand, the rates at the comparable loading were larger and kept constant until a higher level of conversion. The larger rate observed for SA peat with 15 wt % Fe was constant up to the conversion of 60%, although the rate dropped after 60%. Thus, the initial activity of the Cl-free catalyst was retained until the latter stage of gasification.

Effect of Iron Loading on Initial Rate. The initial rate for the Cl-free catalyst as a function of Fe loading is summarized in Figure 5. The initial rate denotes the average specific rate in the char conversion range of 10–20%, and it is given from Figure 4. The rates at 923 and 973 K with SA peat increased linearly with an increase in the loading up to 15 wt %, whereas the rates at 973 and 1023 K with LY coal leveled off beyond 5 wt %. The rates at 973 K for SA peat and LY coal with the largest loadings, 15 and 14 wt %, were about 8 and 6 times those for the original coals, respectively.

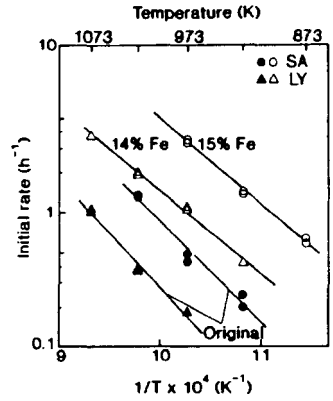

Figure 6. Arrhenius plots for gasification with and without a Cl-free Fe catalyst.

Table III. Product Gas Composition during Steam Gasification of SA Peat at 973 K

Fe, wt %	product, mol % H_2	CO	CO_2	CH_4	C_2[a]	char conv, wt % (daf)
0	64.7	3.6	30.4	1.1	0.2	31
15	68.6	0.7	30.3	0.4	tr[b]	34

[a] C_2H_4 and C_2H_6. [b] Trace amount.

Temperature Dependence of Initial Rate. Figure 6 illustrates the Arrhenius plots for noncatalyzed and iron-catalyzed gasification. The apparent activation energies with and without the Cl-free catalyst were 120 and 140 kJ/mol for SA peat and 120 and 160 kJ/mol for LY coal, respectively, showing the chemical reaction control in every case. The presence of the Fe catalyst lowered slightly the activation energies for both coals. Figure 6 also shows the degree of lowering in the gasification temperature by catalyst addition. The temperatures required for obtaining the reaction rate of 1 h^{-1} for SA peat and LY coal are 1010 and 1080 K without catalyst and 900 and 970 K in the presence of Fe, respectively. Thus, the presence of a Cl-free Fe catalyst lowered the gasification temperature by 110 K in both cases.

Product Gas. Table III shows an example for the composition of product gas during the gasification of SA peat at 973 K. The product gas from the original peat consisted mainly of H_2 and CO_2. When the gas with the Cl-free catalyst was determined at a comparable level of char conversion, the composition was quite similar to that without Fe, although the proportion of CO and CH_4 was a little lower with catalyst. These observations point out that the following stoichiometric reaction takes place predominantly irrespective of the presence of Fe.

$$C + 2H_2O = 2H_2 + CO_2$$

The Ni-catalyzed gasification of brown coal with steam under the same conditions as in this study gave almost the same gas composition as the present Fe-catalyzed gasification (Tomita et al., 1983). It is suggested that the gas-phase equilibrium controls the gas composition under the conditions of excess amount of steam.

Chemical Form of Iron Species. Figure 7 illustrates the XRD patterns for some samples prepared from LY coal with Cl-free Fe of 9 wt %. No crystalline Fe species could be detected without any heat treatment (Figure 7a). Metallic Fe and iron carbides appeared with the sample heated in pure N_2 at 973 K. On the other hand, when the coal was devolatilized in steam at the same temperature,

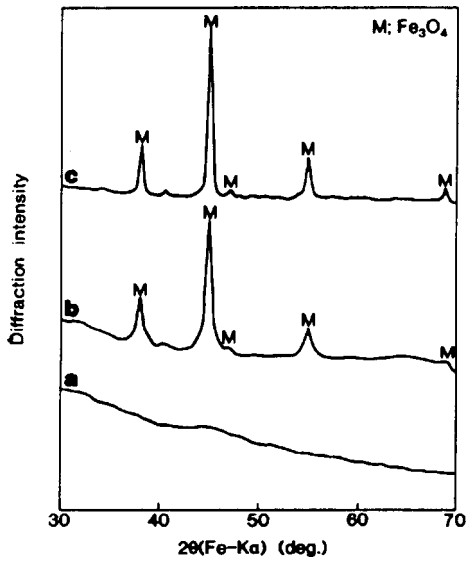

Figure 7. XRD profiles of samples derived from LY coal with Cl-free Fe of 9%: (a) untreated; (b) devolatilized in steam at 973 K; (c) gasified in steam at 973 K (31% conversion).

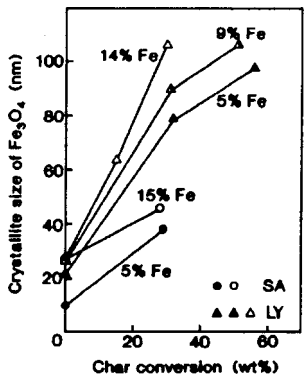

Figure 8. Change in average size of Fe_3O_4 crystallites with char conversion at 973 K.

the XRD lines due to Fe_3O_4 alone were detectable (Figure 7b). The intensity of the diffraction lines was rather weak in spite of a high Fe content of about 18 wt % at this stage. In contrast, the strong and sharp peaks of Fe_3O_4 were observed on devolatilization of the $FeCl_3$-impregnated coal. Figure 7c reveals that the chemical form of a Cl-free Fe catalyst during gasification is Fe_3O_4. Thus, Fe_3O_4 was the stable bulk species in an oxidizing atmosphere, as confirmed by an in situ XRD technique (Ohtsuka et al., 1986) and by Mössbauer spectroscopy (Furimsky et al., 1988).

Catalyst Dispersion. Figure 8 shows the change in the average crystalline size of Fe_3O_4 during gasification. The average size of Fe_3O_4 at char conversion of zero, that is, on devolatilization, was very small, 10–30 nm, regardless of both the Fe loading and the coal type. For impregnated $FeCl_3$, on the other hand, Fe_3O_4 crystallites were too large (>100 nm) to be determined by the line-broadening method. Thus, Fe_3O_4 particles prepared from Cl-free Fe were found to be very highly dispersed on the devolatilized char prior to gasification. As the reaction proceeded, catalyst agglomeration occurred because of the consumption of char, and the size of Fe_3O_4 increased with increasing conversion (Figure 8). When the agglomeration behavior was compared between both coals at the highest loadings, the growth of Fe_3O_4 crystallites proceeded more readily for LY coal. Fe_3O_4 particles on LY char agglomerated more easily at higher loadings.

Discussion

Chlorine-Free Iron. Low-rank coals like peat and brown coal used in this study contain large amounts of carboxyl and phenolic groups, which act as cation-exchange sites. Some of the inherent Fe in these coals exists as cations in association mainly with carboxyl groups (Schafer, 1977). When Fe cations alone are externally introduced to low-rank coals, therefore, ion-exchange techniques are used. According to Schafer (1972), they are first demineralized by HCl washing and the resultant acid-form coals are exchanged with Na ions, which are subsequently exchanged with Fe cations. However, the rate enhancement of lignite char by such exchanged Fe was not so significant (Hippo et al., 1979). The residual Cl in the demineralization step may cause catalyst deactivation (Hengel and Walker, 1984; Ohtsuka, 1989). Fe cations are also incorporated by ion exchange with inherent cations of alkali or alkaline-earth metals (Hatswell et al., 1980), but the exchanged amount is very small.

In the present method, a pH-adjusting agent of NH_3/NH_4Cl solution was used, and large amounts of Fe of 14–15 wt % were incorporated without introduction of Cl ions (Table II). The FT-IR spectra of Fe-loaded LY coal showed that Fe^{3+} ions in $FeCl_3$ are exchanged with H^+ in the carboxyl groups, and the extent of exchange increases as the ion loading is increased (Figure 1). It is not clear whether the exchange proceeds through the equimolar (one Fe^{3+} to one COOH) or equivalent (one Fe^{3+} to three COOH) mechanism. If the former is predominant, the amount of exchanged Fe may be about 12 and 10 wt % with SA peat and LY coal, respectively. However, the content of Cl-free Fe exceeded these values, reaching 14–15 wt % (Table II). Since it is suggested that the amount of hydroxy-bridged Fe increases as the pH of the ion-exchange process is increased (Dack et al., 1985), some Fe at higher loadings may exist in the form of iron hydroxides like $Fe(OH)_3$ and FeOOH. No XRD lines due to these species were observed on LY coal with Cl-free Fe of 9 wt % (Figure 7a), implying that, even if present, they are in the amorphous or finely dispersed state. Thus, the present method realizes the incorporation of a large amount of Cl-free Fe into low-rank coals from a cheap $FeCl_3$ solution.

Rate Enhancement. A Cl-free Fe catalyst, even at a low loading of 1 wt %, promoted the gasification of SA peat and LY coal with steam at a low temperature of 973 K (Figure 2). Initial gasification rates of SA peat and LY coal increased as the Fe loading was increased, though the rate for LY coal reached a plateau at around 5 wt % (Figure 5). In both coals the rates at the largest loadings were 6–8 times those without catalyst. On the other hand, the rates of $FeCl_3$-impregnated coals were small in spite of high loadings of 8 wt %. A larger rate enhancement by the Cl-free catalyst would be ascribed to a higher degree of catalyst dispersion on devolatilization; the average size of Fe_3O_4 crystallites was as small as <30 nm even for the samples with the largest loadings (Figure 8), whereas Fe_3O_4 particles derived from the impregnated $FeCl_3$ were too large to be determined. The presence of Cl may deteriorate catalyst dispersion (Ohtsuka et al., 1987a; Ohtsuka, 1989).

As is seen in Figure 6, the presence of the Cl-free catalyst made possible the lowering in the gasification temperature by 110 K in both coals. From the observations in the gasification of an Australian Yallourn brown coal with other catalysts, the degree of the lowering by the present catalyst is comparable to that by an exchanged Na catalyst

(Takarada et al., 1989), but is smaller than those by impregnated Ni, Ca, and exchanged K catalysts (Tomita et al., 1983; Ohtsuka and Tomita, 1986; Takarada et al., 1989). However, a Cl-free Fe catalyst has some advantages over these other catalysts: $FeCl_3$ as a raw material is much more inexpensive than Ni, and Fe catalyst also exhibits a high catalytic activity toward hydrogasification, but on the contrary K and Ca catalysts are inactive in H_2.

Thus, $FeCl_3$ easily available as acid wastes can be converted to an active, Cl-free Fe catalyst by using NH_3/NH_4Cl solution. However, there remain several problems. One is the use of more expensive NH_3 than $FeCl_3$. The preliminary experiments have suggested that cheap $Ca(OH)_2$ can be used as alternatives to NH_3/NH_4Cl solution. In this case Ca cations as well as Fe cations are incorporated into coal. The coexistence of Ca would enhance the activity of Fe catalyst (Ohtsuka et al., 1987a,b). A detailed study on the use of $Ca(OH)_2$ should be made. Another problem is that this method may be restricted to low-rank coals. Some pretreatment like mild oxidation to increase ion-exchangeable sites may be effective for the application to high-rank coals. Fe cations could be exchanged with graphite pretreated with nitric acid, and Fe promoted the gasification with H_2/H_2O (Hüttinger et al., 1986).

Catalytic State and Activity. The XRD measurements reveal that a Cl-free Fe catalyst exists in the form of Fe_3O_4 on devolatilization and during gasification (Figure 7), and the form does not change at all with the Fe loading, temperature, and char conversion. This form is exactly the same as predicted in pure steam from the phase diagram of Fe–O–H (von Bogdandy and Engell, 1971). The presence of Fe_3O_4 is also confirmed during Fe-catalyzed gasification of carbon with CO_2 by using an in situ high-temperature XRD technique (Ohtsuka et al., 1986). Fe_3O_4 enhances the gasification rate as observed in the present study. However, Fe_3O_4 identified by XRD is the bulk species, but not always the actual active species. The formation of iron carbides in the char after heat treatment in N_2 suggests that the reaction of Fe species with carbon may proceed readily under the present conditions, and H_2 evolved during gasification may reduce the surface of Fe_3O_4 particles. Therefore the surface species of Fe_3O_4 in the vicinity of the char reacting with steam may be converted into a higher reduced form such as FeO, metallic Fe, and iron carbides.

It has been considered that the catalyst dispersion on the surface of char is a key factor in determining the activity in the catalyzed gasification of Australian brown coals, because the surface area of char is almost independent of the extent of reaction and the presence of metal catalysts (Tomita et al., 1985; Ohtsuka, 1990). The average size of Fe_3O_4 crystallites derived from Cl-free catalysts was very small (<30 nm) on devolatilization irrespective of the coal type (Figure 8), in contrast with larger Fe_3O_4 crystallites (>100 nm) from impregnated $FeCl_3$. Fine dispersion with Cl-free Fe would arise from the presence of exchanged Fe which initially provides atomic dispersion. As the gasification proceeded, however, fine Fe_3O_4 particles agglomerated and the size increased (Figure 8). A smaller agglomeration rate of Fe_3O_4 particles was observed on SA char than on LY char, which may be attributable to the presence of a larger amount of exchanged Fe and the retardation of the agglomeration by inherent alkaline-earth metals present as mineral matter. Such a higher degree of Fe dispersion on SA char would lead to a larger rate enhancement. In both coals the lowered dispersion during gasification resulted in the decreased gasification rate at the latter stage of reaction (Figure 4). The coexistence of foreign additives like alkali and alkaline-earth metals increases the activity of Fe catalyst possibly by keeping it finely dispersed (Suzuki et al., 1985; Ohtsuka et al., 1987a,b; Haga and Nishiyama, 1989). The use of $Ca(OH)_2$ in place of NH_3/NH_4Cl would be desirable from this standpoint as well as a practical point of view, because not only Fe but also Ca cations can be incorporated into low-rank coals.

Conclusions

Steam gasification of low-rank coals using $FeCl_3$ is carried out, and the following conclusions are summarized:

1. A Cl-free Fe catalyst can be successfully prepared from $FeCl_3$ solution using NH_3/NH_4Cl solution.
2. Some Fe cations are exchanged with the protons in carboxyl groups and converted to the highly dispersed catalyst on devolatilization.
3. The Fe catalyst exhibits a high activity for gasification with steam at low temperatures of around 950 K.
4. The chemical form of Fe catalyst during gasification is Fe_3O_4, and the catalytic activity is correlated with the dispersion of Fe_3O_4 particles.

Acknowledgment

We gratefully acknowledge the assistance of Ms. Fumie Kinouchi and Ms. Naoko Yoshida in carrying out experiments. The advice of Prof. Osamu Ito in measuring FT-IR spectra is appreciated. Part of this work was carried out under the Japan–Australia Joint Research Program sponsored by the Ministry of Education, Science and Culture, Japan. We thank Mr. Ian Smith, CSIRO Division of Coal and Energy Technology, and Dr. David Allardice and Dr. Geoffrey Perry, Coal Corporation of Victoria, for their helpful discussions.

Registry No. $FeCl_3$, 7705-08-0; NH_3, 7664-41-7; NH_4Cl, 12125-02-9; Fe_3O_4, 1317-61-9; Fe, 7439-89-6.

Literature Cited

Adler, J.; Hüttinger, K. J. Mixtures of Potassium Sulphate and Iron Sulphate as Catalysts for Water Vapour Gasification of Carbon 1. Kinetic Studies. *Fuel* **1984**, *63*, 1393–1396.

Dack, S. W.; Hobday, M. D.; Smith, T. D.; Pilbrow, J. R. E.p.r. Study of Paramagnetic Metal Irons in Victorian Brown Coal. *Fuel* **1985**, *64*, 222–225.

Furimsky, E.; Sears, P.; Suzuki, T. Iron-Catalyzed Gasification of Char in CO_2. *Energy Fuels* **1988**, *2*, 634–639.

Haga, T.; Nishiyama, Y. Promotion of Iron-Group Catalysts by a Calcium Salt in Hydrogasification of Coal Chars. *Ind. Eng. Chem. Res.* **1989**, *28*, 724–728.

Hatswell, M. R.; Jackson, W. R.; Larkins, F. P.; Marshall, M.; Rash, D.; Rogers, D. E. Hydrogenation of Ion-Exchanged Victorian Brown Coals. *Fuel* **1980**, *59*, 442–444.

Hengel, T. D.; Walker, P. L., Jr. Catalysis of Lignite Char Gasification by Exchangeable Calcium and Magnesium. *Fuel* **1984**, *63*, 1214–1220.

Hippo, E. J.; Jenkins, R. G.; Walker, P. L., Jr. Enhancement of Lignite Char Reactivity to Steam by Cation Addition. *Fuel* **1979**, *58*, 338–344.

Hüttinger, K. J.; Schleicher, P. Kinetics of Hydrogasification of Coke Catalysed by Fe, Co, and Ni. *Fuel* **1981**, *60*, 1005–1012.

Hüttinger, K. J.; Adler, J.; Hermann, G. Iron-Catalyzed Water Vapour Gasification of Carbon, In *Carbon and Coal Gasification*; Figueiredo, J. Z., Moulijn, J. A., Eds.; NATO ASI Series; Martinus Nijhoff: Dordrecht, 1986; pp 213–229.

Kasaoka, S.; Sakata, Y.; Yamashita, H.; Nishino, T. Effects of Catalysis and Composition of Inlet Gas on Gasification of Carbon and Coal. *J. Fuel Soc. Jpn.* **1979**, *58*, 373–386. *Int. Chem. Eng.* **1981**, *21*, 419–434.

Ohtsuka, Y. Influence of Hydrogen Chloride Treatment on the Dispersion of Nickel Particles Supported on Carbon. *J. Mol. Catal.* **1989**, *54*, 225–235.

Ohtsuka, Y. Catalytic Pyrolysis and Gasification of Loy Yang Brown Coal. *Proc. Meet. Japan–Aust. Jt. Res. Program* **1990**, 25–29.

Ohtsuka, Y.; Tomita, A. Calcium Catalysed Steam Gasification of Yallourn Brown Coal. *Fuel* **1986**, *65*, 1653–1658.
Ohtsuka, Y.; Kuroda, Y.; Tamai, Y.; Tomita, A. Chemical Form of Iron Catalysts during the CO_2-Gasification of Carbon. *Fuel* **1986**, *65*, 1476–1478.
Ohtsuka, Y.; Tamai, Y.; Tomita, A. Iron-Catalyzed Gasification of Brown Coal at Low Temperatures. *Energy Fuels* **1987a**, *1*, 32–36.
Ohtsuka, Y.; Hosoda, K.; Nishiyama, Y. Rate Enhancement and in Situ Desulfurization by Iron-Calcium Catalyst in the Gasification of Coal Char. *J. Fuel Soc. Jpn.* **1987b**, *66*, 1031–1036.
Schafer, H. N. S. Factors Affecting the Equilibrium Moisture Contents of Low-Rank Coals. *Fuel* **1972**, *51*, 4–9.
Schafer, H. N. S. Organically Bound Iron in Brown Coals. *Fuel* **1977**, *56*, 45–46.
Suzuki, T.; Mishima, M.; Takahashi, T.; Watanabe, Y. Catalytic Steam Gasification of Yallourn Coal Using Sodium Hydridotetracarbonyl Ferrate. *Fuel* **1985**, *64*, 661–665.
Takarada, T.; Nabatame, T.; Ohtsuka, Y.; Tomita, A. New Utilization of NaCl as a Catalyst Precursor for Catalytic Gasification of Low-Rank Coal. *Energy Fuels* **1987**, *1*, 308–309.
Takarada, T.; Nabatame, T.; Ohtsuka, Y.; Tomita, A. Steam Gasification of Brown Coal Using Sodium Chloride and Potassium Chloride Catalysts. *Ind. Eng. Chem. Res.* **1989**, *28*, 505–510.
Tomita, A.; Ohtsuka, Y.; Tamai, Y. Low Temperature Gasification of Brown Coals Catalysed by Nickel. *Fuel* **1983**, *62*, 150–154.
Tomita, A.; Yuhki, Y.; Higashiyama, K.; Takarada, T.; Tamai, Y. Physical Properties of Yallourn Char during the Catalyzed Steam Gasification. *J. Fuel Soc. Jpn.* **1985**, *64*, 402–408.
von Bogdandy, L.; Engell, H.-J. *The Reduction of Iron Ores—Scientific Basis and Technology* (Engl. ed.); Springer-Verlag: New York, 1971; p 243.

Received for review September 24, 1990
Accepted May 2, 1991

Processing and Utilization of High-Sulfur Coals IV,
edited by P.R. Dugan, D.R. Quigley and Y.A. Attia

In situ sulfur capture during the calcium-catalyzed gasification of Illinois No. 6 coal

Yasuo Ohtsuka and Kenji Asami

Research Center for Carbonaceous Resources, Institute for Chemical Reaction Science (formerly Chemical Research Institute of Non-Aqueous Solutions), Tohoku University, Katahira, Sendai 980, Japan

Abstract

In situ desulfurization during the steam gasification of Illinois No. 6 coal with calcium catalyst has been studied with a fixed-bed reactor. $Ca(OH)_2$ used is added on the coal by kneading them in water. The Ca-loaded coal exhibits a large reactivity at 973-1073 K, and the rates with 4 wt% Ca are 10-15 times those without Ca. The addition of $Ca(OH)_2$ suppresses the sulfur evolution during gasification, showing that the in situ sulfur capture takes place in spite of differential reaction conditions using a high partial pressure of steam (70 kPa). The sulfur capture efficiency increases with increasing temperature and it reaches about 60 % at 1073 K. The XRD measurements reveal that pyritic sulfur in coal is readily transformed to FeO and Fe_3O_4, and $Ca(OH)_2$ is converted to CaO, which captures the sulfur evolved to form CaS. Most of the CaO unreacted with sulfur is too finely dispersed to be detected by XRD. Such the highly dispersed calcium promotes the gasification to a large extent. The desulfurization behavior by calcium can be explained on the basis of XRD results.

1. INTRODUCTION

Catalytic coal gasification has attracted increasing attention [1-3], because the utilization of a catalyst not only lowers the reaction temperature but also controls the composition of product gas. The lowering in gasification temperature would increase the thermal efficiency and enable the use of inexpensive plant material and waste heat. CH_4 and H_2, environmentally acceptable fuels because of reducing CO_2 emissions, can be directly and efficiently produced in the catalytic gasification with steam [4,5].

One of the indispensable requirements for realizing a catalytic gasification process is to use cheap and disposable catalyst materials like Fe and Ca compounds. Iron chloride, readily available as an acid waste from a steel pickling plant, can be converted to a chlorine-free, active iron catalyst [6]. The Ca ions incorporated into brown coals from $Ca(OH)_2$ achieve the complete gasification at around 1000 K in thermogravimetric experiments [7-9]. Further the pressurized fluidized bed gasification has

revealed that tarry materials evolved are also gasified completely with steam in the presence of Ca catalyst and thus 85 wt% of carbon in coal is converted to gas at 975 K [5].

Since calcium compounds like $CaCO_3$, CaO and $Ca(OH)_2$ are also sulfur sorbents, they can be used for in situ sulfur capture during coal gasification [10-13]. It has been reported that the sulfur capture efficiency during coal combustion is higher with the impregnated or ion-exchanged calcium than with the physically-mixed calcium [14,15], showing the importance of calcium dispersion within coal particles. We have also found that the finely-dispersed calcium prepared from $Ca(OH)_2$ not only promotes the steam gasification of high sulfur coals but also captures the sulfur evolved during gasification [8]. The advantage of in-bed sulfur removal is to simplify the catalytic gasification system, as suggested in simplified IGCC and mild gasification combined with simplified IGCC [16-18]. In the present paper, therefore, the rate enhancement and in situ desulfurization by $Ca(OH)_2$ during the steam gasification of Illinois No. 6 coal will be investigated in detail.

2. EXPERIMENTAL

2.1. Coal sample and calcium addition

Illinois No. 6 coal was employed in this study. The proximate analysis was: volatile matter, 38.9; fixed carbon, 50.2; ash, 10.9 wt%(dry). The ash analysis was: SiO_2, 48.2; Al_2O_3, 15.1; Fe_2O_3, 17.9; CaO, 6.3; MgO, 1.1; TiO_2, 0.9, Na_2O, 1.1; K_2O, 2.0 wt%. The ultimate analysis on a dry, ash-free coal basis was: C, 77.0; H, 5.2; N, 1.5; S, 3.6; O(diff.), 12.7 wt%. The particle size of the coal used for calcium addition was 0.1-0.5 mm.

$Ca(OH)_2$ was used as a precursor salt for both a gasification catalyst and an in situ desulfurizer. $Ca(OH)_2$ powder (J. T. Baker Chemical Co.) was usually loaded on coal by kneading them in water. The resulting slurry was then dried at 380 K in a N_2 stream. For the convenience of gasification experiments, dried fine powder (<0.02 mm) was pelletized into a disc, which was then cut down into coarse particles of 1-2 mm. For comparison $CaCO_3$-loaded coal was prepared in the same manner as above and $Ca(OH)_2$ powder was mechanically mixed with coal by grinding them in a dry atmosphere.

2.2. Gasification experiments

Coal was gasified with a thermobalance (Shinku-Riko, TGD-5000) or a quartz-made vertical fixed-bed reactor. Different Ca-loaded samples were used in thermogravimetric runs in order to examine the influence of the kind of precursor salt and the method of calcium addition on the reactivity of coal. The dried sample (about 20 mg) mounted onto a quartz cell in the thermobalance was heated at a rate of 300 K/min up to 1023 K under a H_2O (80 kPa)/N_2 flow, and it was soaked for 2 h at this temperature.

Schematic details of the fixed-bed reactor are illustrated in Figure 1. Only $Ca(OH)_2$-loaded coal prepared by kneading in water was used as a gasification sample for this reactor. About 600 mg of the dried coal was mount-

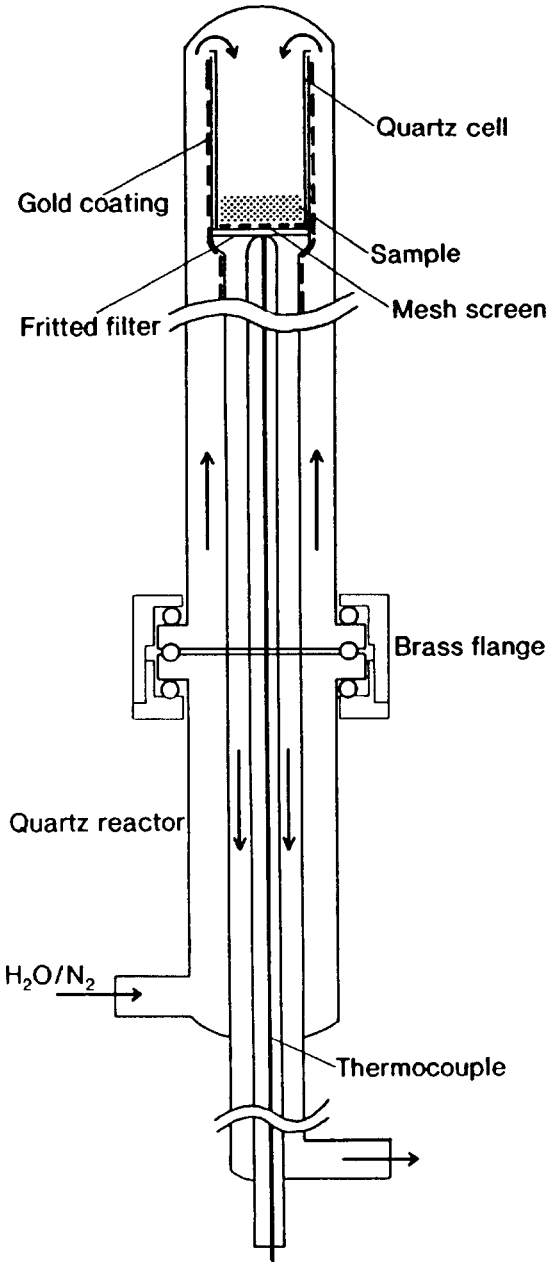

Figure 1. Schematic details of a quartz-made vertical fixed-bed reactor.

ed onto a quartz cell (15 mm inner diameter x 40 mm long) with a stainless steel mesh screen of 74 μm. The sample layer was very thin; around 5 mm in thickness. Thus the present condition may be regarded as a differential reaction condition. The outside part of the quartz cell was coated with gold film for attaining the isothermal heating by an infrared lamp. The coal in a H_2O (70 kPa)/N_2 stream was heated at 300 K/min up to a predetermined temperature, and gasified at a constant temperature. The devolatilization in pure N_2 was also conducted in the same manner as above.

Since raw coal was used in all gasification runs, the reaction consisted of the coal devolatilization and subsequent char gasification stages. The rate enhancement and in situ sulfur capture by calcium in the latter stage will be discussed throughout the present paper. Char conversion is expressed on a dry, volatile-, ash-, catalyst-free basis. Since the gasification rate is nearly proportional to the amount of residual char in the range of char conversion up to about 50 % [8,19], the average rate per unit weight of residual char, 1/h, is used as an index for the reactivity of char.

2.3. Analysis and characterization of calcium

The amounts of calcium ions in original and $Ca(OH)_2$-loaded coals were determined by leaching with HCl at 323 K, followed by analyzing the leachate using atomic adsorption spectroscopy. The content of the inherently-existing Ca was 0.3 wt%. The amount of the actually-loaded Ca, not including inherent Ca, was determined to be 4.0 or 7.9 wt%, which corresponds to the atomic ratio of Ca/S in the $Ca(OH)_2$-loaded coal of 1.1 or 2.3, respectively. The low loading of 4 wt% Ca was used for the fixed-bed gasification unless otherwise stated.

X-ray diffraction analysis (XRD) was carried out by using Cu-Kα (45 kv x 30 mA) to examine the chemical form and dispersion state of pyritic sulfur and calcium species on char. Char samples for the XRD measurements were prepared using the fixed-bed reactor; the char after devolatilization or steam gasification was quenched to room temperature in pure N_2. For the semi-quantitative discussion the ratio of diffraction intensity of CaS/SiO_2 or CaS/CaO was calculated from the height of main diffraction peaks of CaS, SiO_2 and CaO which appeared at 2θ (Cu-Kα) of 31.4, 26.7 and 37.4 degree.

2.4. Sulfur analysis

The S content in coal or char was determined with a sulfur analyzer (Horiba, EMIA-510); the sample was burned up in pure O_2 at 1723 K and the SO_2 evolved was detected by an on-line infrared spectrometer. The Standard Reference Material from the National Institute of Standards and Technology, U.S.A., was used for the calibration of the instrument. The S evolved during gasification was calculated by the amounts of S in both feed coal and residual char and it was expressed as wt%. The sulfur capture efficiency, %, was defined as [1-(S evolved with Ca)/(S evolved without Ca)] x 100. The atomic ratio of (S captured)/(Ca added) was also calculated by using both S and Ca contents in $Ca(OH)_2$-loaded coal and the capture efficiency.

3. RESULTS AND DISCUSSION

3.1. Catalyst effectiveness of $Ca(OH)_2$ in steam gasification

Figure 2 illustrates the profiles for the gasification of different Ca-loaded samples at 1023 K with a thermobalance. Actual Ca loadings were 4.0-4.5 wt%. When $Ca(OH)_2$ was ground with coal in a dry atmosphere or

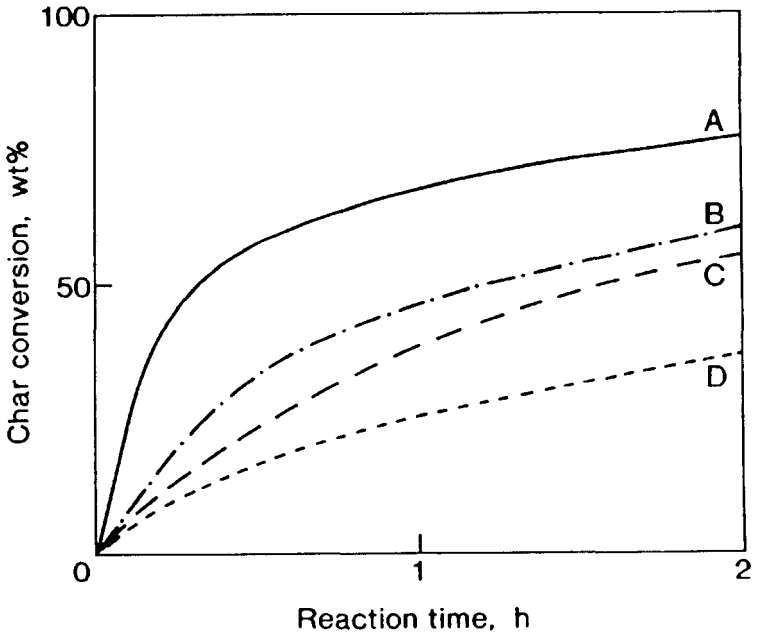

Figure 2. Profiles for the gasification of Illinois No. 6 coal at 1023 K with a thermobalance. A, $Ca(OH)_2$ kneaded in water; B, $CaCO_3$ kneaded in water; C, $Ca(OH)_2$ mixed in a dry atmosphere; D, no additives.

$CaCO_3$ was kneaded with coal in water, the calcium promoted the gasification, but the catalytic effect was not so large in both cases. $Ca(OH)_2$ kneaded in water was most effective among all the calcium examined, and the larger gasification rate was observed at the initial stage of reaction; about 60 wt% of char was gasified within 30 min. The difference in the effectiveness between these catalysts has also been observed in the gasification of brown coal [9], and may be ascribed to different dispersion states of calcium catalysts on devolatilization preceding char gasification. It has been shown that the most finely-dispersed calcium catalyst can be prepared from $Ca(OH)_2$ kneaded in water [9].

3.2. Rate enhancement by $Ca(OH)_2$ in fixed-bed gasification

Table 1 summarizes the gasification rate when $Ca(OH)_2$-kneaded coal is gasified using the fixed-bed reactor. The rate enhancement by calcium catalyst, defined as the ratio of the rates with and without $Ca(OH)_2$, was 15, 14 and 11 at 973, 1023 and 1073 K, respectively; thus it was slightly decreased with increasing temperature. The degree of the enhancement at 1023 K was quite similar between the fixed-bed and thermogravimetric runs. When the Ca loading was raised from 4.0 to 7.9 wt%, almost no further increase in rate enhancement was observed at 1023 K.

3.3. Sulfur capture during Ca-catalyzed gasification

Figure 3 illustrates the S evolved as H_2S and COS during the fixed-bed gasification at different temperatures. The S evolved without Ca addition

Table 1
Reaction rate for fixed-bed gasification

Ca loading, wt%	Gasification rate, 1/h		
	973 K	1023 K	1073 K
0	0.03	0.08	0.18
4.0	0.46	1.2	2.0
7.9	-	1.3	-

seemed independent of the temperature in the range of 973-1073 K, but it depended on char conversion. About 45 wt% of S in coal evolved at the conversion of zero, i.e., on devolatilization. The S evolved increased as the gasification proceeded, and it reached about 75 wt% at the conversion of 20 %. Thus the sulfur in coal was lost mostly in the initial step of gasification. The initial rapid sulfur evolution is caused partly by the transformation of FeS_2 (pyrite) to FeS (pyrrhotite), Fe_3O_4 (magnetite) and FeO (wüstite) as will be discussed later. The loss of less stable organic sulfur would also contribute partly to the initial sulfur emission [20].

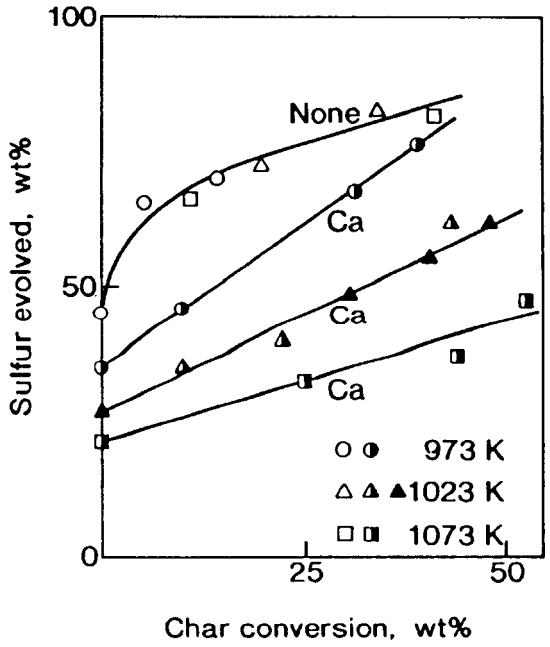

Figure 3. Sulfur evolution during the gasification of Illinois No. 6 coal without Ca (○, △, □) and with 4 wt% Ca (◑, ▲, ◨) and 8 wt% Ca (▲).

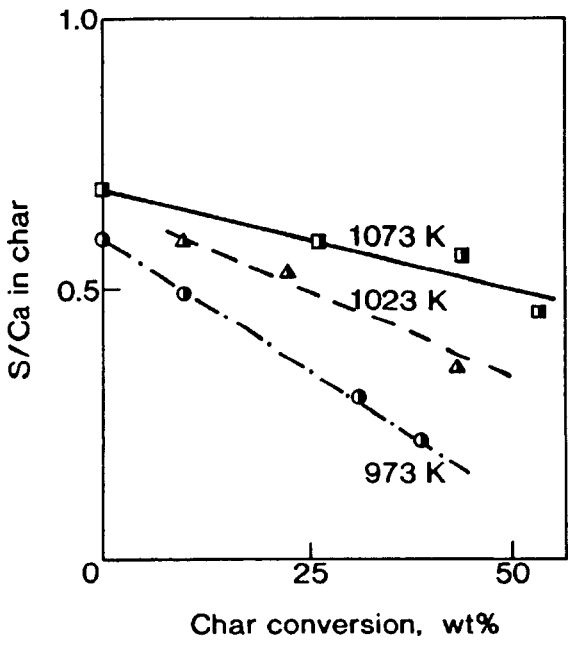

Figure 4. Change in the S/Ca ratio with char conversion during the Ca-catalyzed gasification.
Key as in Figure 3.

As is seen in Figure 3, the addition of calcium suppressed the sulfur evolution both on devolatilization and during gasification, which shows the in situ sulfur capture by calcium. The S evolved in the presence of calcium increased linearly with an increase in char conversion at every temperature. In contrast with the uncatalyzed gasification, the sulfur evolution in the Ca-catalyzed gasification depended strongly on the temperature, a lower S evolution being observed at a higher temperature. When the Ca loading was increased from 4.0 to 7.9 wt% at 1023 K, no further effect on the sulfur evolution was observed (Figure 3).

Figure 4 illustrates the atomic ratio of S/Ca in the Ca-bearing char as a function of char conversion. The sulfur remaining in char contains the sulfur both unreacted with steam and captured by calcium. The S/Ca ratio decreased linearly with increasing conversion at all the temperatures, but the slope of the straight line was smaller at higher temperatures. As the gasification proceeded, the amount of the sulfur unreacted at 973-1073 K decreased at almost the same rate irrespective of the temperature, as is seen without Ca in Figure 3. Therefore the smaller slope observed at higher temperatures suggests that the proportion of the sulfur captured increases as the temperature is raised.

Table 2 shows the sulfur capture efficiency defined as [1 - (S evolved with Ca)/(S evolved without Ca)]. The values of the S evolved without Ca at different char conversions and temperatures can be estimated from the curve in Figure 3. As can be expected from Figure 3, the efficiency at 973 K was the lowest in the range of 973-1073 K, and it decreased from about 20 % at the initial stage of gasification to 6 % at char conversion of 40 wt%. The XRD measurements of Ca-bearing chars after devolatilization and gasification revealed that $Ca(OH)_2$ incorporated into coal is transformed to CaO and CaS (Figure 5). CaS is formed by the following reactions of CaO with evolved H_2S and COS.

$$CaO + H_2S = CaS + H_2O \quad (1)$$

$$CaO + COS = CaS + CO_2 \quad (2)$$

Table 2
Sulfur capture efficiency and (S captured)/(Ca added) ratio during Ca-catalyzed gasification

Char conv., wt%	Sulfur capture efficiency, %			(S captured)/(Ca added)	
	973 K	1023 K	1073 K	973 K	1073 K
0	23	41	53	0.21	0.46
20	22	43	58	0.20	0.51
40	6	33	53	0.06	0.46

The decrease in the capture efficiency observed at 973 K shows that, as the gasification proceeds, some of CaS formed is converted to CaO mainly by the reverse reaction of eqn. (1) in the presence of excess amount of unreacted H_2O. As the temperature was raised, the capture efficiency increased considerably and reached 53-58 % at 1073 K. The efficiency at this temperature was almost independent of char conversion, suggesting that the CaS formed is more stable because of the reducing atmosphere around calcium species due to the higher gasification rate observed at 1073 K (Table 1). This point will be discussed in detail in the following section.

Thus, it is found that a significant amount of sulfur can be captured by calcium in spite of the differential reaction conditions with a large partial pressure of steam. If the chance of the contact between the sulfur evolved and the calcium introduced is further increased, the capture efficiency would be larger. In order to make clear this point, the thickness of the sample layer in the quartz cell was increased from the usual 5 to 30 mm by making the inner diameter of the cell shorter from 15 to 6 mm, and the $Ca(OH)_2$-loaded coal with 8 wt% Ca was gasified at 1023 K. The efficiency at char conversion of 50 wt% increased from 27 % under usual conditions to 40 %. This finding suggests that a much higher capture efficiency would be achieved under the integrated conditions like continuous fluidized-bed gasification.

3.4. XRD profiles during desulfurization

Figure 5 illustrates the XRD patterns for Ca-bearing chars after devolatilization in N_2 or gasification with steam at 973 K. Strong diffraction lines attributable to CaO (lime) and CaS (oldhamite) were observed on the devolatilized char, that is, at char conversion of zero. $Ca(OH)_2$ added was transformed to CaO and some CaO was converted to CaS according to eqns. (1) and (2). The Ca content at this stage was as large as about 7 wt%. Since the (S captured)/(Ca added) ratio was only 0.2 (Table 2), about 80 % of Ca added must exist in the form of CaO. Nevertheless the diffraction intensities of CaO were very low. This shows that a large part of CaO on the char is so finely dispersed that it can not be detected by XRD. When $Ca(OH)_2$ is incorporated into Yallourn brown coal with a low ash content of 1 wt% by the same method as in the present work, no diffraction lines from Ca species are observed on the char devolatilized at 973 K [7], showing the presence of ultra-fine particles of CaO. A highly dispersed calcium catalyst promotes the gasification considerably as is shown in Figure 2 and Table 1.

It has been reported in the gasification at high temperatures above 1300 K that calcium-based compounds added as sulfur-capturing sorbents react with the inherent silicates to form amorphous compounds, which are less effective for sulfur capture [13,21]. However, such the solid-solid reaction would proceed to a lesser extent under the present conditions of low temperatures and relatively low char conversions. A large rate enhancement by calcium catalyst observed in the present gasification runs (Table 1) would also show little significant formation of the compounds containing Ca and Si, because they are catalytically inactive for the gasification [22].

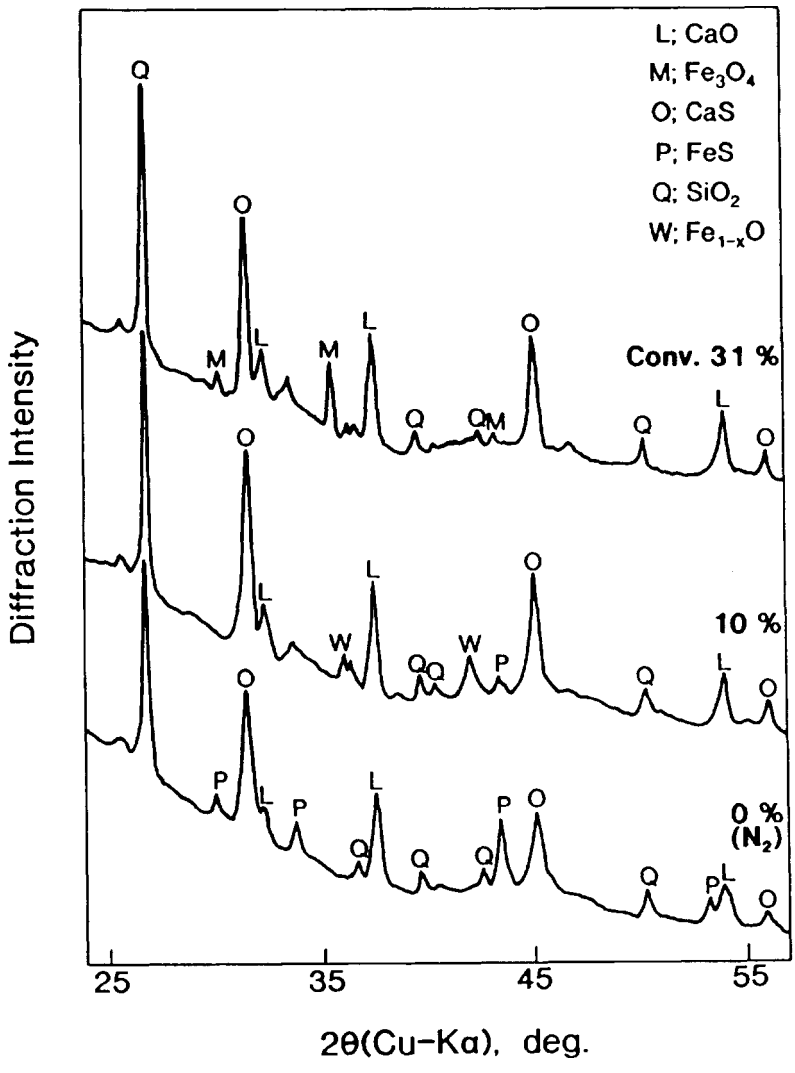

Figure 5. XRD patterns for different chars prepared from $Ca(OH)_2$-loaded Illinois No. 6 coal at 973 K.

With iron species derived from pyritic sulfur in coal, the XRD peaks due to FeS (FeS_{1+x} [23]; pyrrhotite) were detectable on the char devolatilized at 973 K, but any other distinct diffraction lines from iron species could not be detected (Figure 5). FeS_2 (pyrite) is reduced to FeS by the following reactions with H_2 and/or CO evolved during devolatilization, and some of H_2S and COS evolved is captured by CaO.

$$FeS_2 + H_2 = FeS + H_2S \quad (3)$$

$$FeS_2 + CO = FeS + COS \quad (4)$$

When the devolatilized char was gasified with steam, at char conversion of 10 wt%, the XRD intensities of FeS decreased and the diffraction lines

due to FeO (exactly $Fe_{1-x}O$; wüstite) newly appeared (Figure 5). FeO would be formed by eqn. (5) [24], followed by the capture of some of H_2S evolved by CaO (eqn. (1)).

$$FeS + H_2O = FeO + H_2S \quad (5)$$

As the gasification proceeded, at the conversion of 31 wt%, the XRD signals of FeS and FeO disappeared and instead the diffraction lines attributable to Fe_3O_4 (magnetite) appeared. FeO formed by the above reaction is further oxidized with excess steam according to eqn. (6). FeS may be directly converted to Fe_3O_4 by eqn. (7) [24].

$$3FeO + H_2O = Fe_3O_4 + H_2 \quad (6)$$

$$3FeS + 4H_2O = Fe_3O_4 + 3H_2S + H_2 \quad (7)$$

Thus two different iron species of FeO and Fe_3O_4 were observed during gasification. This is because the oxidation state of iron depends strongly on the gas atmosphere [25]. Since H_2 and CO are mainly produced during the Ca-catalyzed gasification [5], the gas in the vicinity of minerals is more reductive than feed steam. The char around pyritic sulfur may be selectively gasified at the beginning of reaction due to the catalysis of iron [26,27]. FeO is the stable species in the more reducing atmosphere [25].

As is shown for the chars after gasification in Figure 5, CaS existed stably in spite of the condition of a high partial pressure of steam (70 kPa). The ratio of diffraction intensity of CaS to SiO_2 (quartz) decreased with an increase in the conversion from 10 to 31 wt%, and correspondingly the (S captured)/(Ca added) ratio decreased from 0.29 to 0.13. These results show that part of CaS is converted to CaO. Since the char in the vicinity of calcium particles is consumed as the gasification proceeds, the atmosphere around the calcium would be rich in steam, and thus some CaS would be transformed to CaO by the reverse reaction of eqn. (1).

Figure 6 illustrates the XRD profiles for Ca-bearing chars at different temperatures. Char conversion was similar (39-44 wt%) among these samples, but the (S captured)/(Ca added) ratio was quite different among them; the values were 0.07, 0.28 and 0.45 at 973, 1023 and 1073 K, respectively. Correspondingly to the temperature change in this ratio, the ratio of diffraction intensity of CaS to SiO_2 increased with increasing temperature; the values were 0.5, 1.3 and 2.3 at 973, 1023 and 1073 K, respectively. As the temperature was raised, the diffraction intensity ratio of CaO/CaS decreased, and it was only 0.2 at 1073 K. However, the ratio of CaO/CaS actually present in char is estimated to be around unity from the (S captured)/(Ca added) ratio of 0.45. The discussion indicates that most of CaO in char is too fine to be detected by XRD. Such the finely dispersed calcium catalyst shows a high activity toward the gasification of char.

With iron species, the diffraction lines of Fe_3O_4 and FeO were observed at 973 and 1023 K, respectively, but no distinct XRD peaks due to iron compounds were detectable at 1073 K. Since the Ca-catalyzed gasification

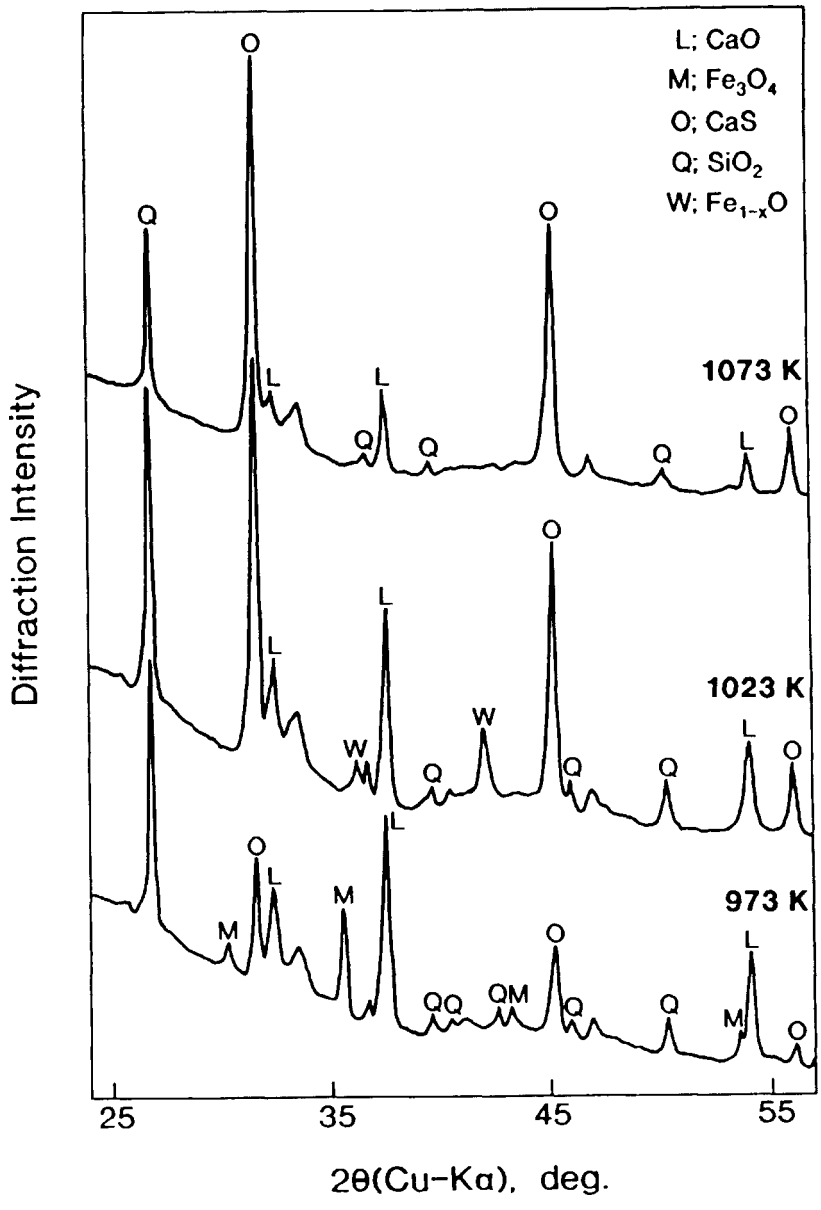

Figure 6. XRD patterns for Ca-bearing chars after gasification at different temperatures.

rate increases with increasing temperature (Table 1), the gas atmosphere around iron particles is more reductive at higher temperatures, which results in the more highly-reduced state of iron species. Therefore the iron at 1073 K is expected to exist in the form of metallic iron. Unfortunately, however, the main diffraction line of α-Fe appearing at 2θ (Cu-Kα) of 44.7 degree was masked by strong XRD peaks of CaS (Figure 6).

4. CONCLUSIONS

The conclusions are summarized as follows:

(1) $Ca(OH)_2$ kneaded with Illinois No. 6 coal in water promotes considerably the steam gasification at 973-1073 K, and a 10-15 fold rate enhancement by the addition of 4 wt% Ca is achieved with a fixed-bed reactor.

(2) Calcium catalyst captures in situ the sulfur evolved during gasification in spite of differential reaction conditions under a high partial pressure of steam. The sulfur capture efficiency depends strongly on the temperature and it reaches 50-60 % at 1073 K.

(3) Pyritic sulfur is easily transformed to Fe_3O_4, FeO and Fe via FeS during gasification. $Ca(OH)_2$ added is converted to CaO, which reacts with the sulfur evolved to form CaS. Most of the CaO unreacted is very finely dispersed on char and catalytically active for the steam gasification.

Acknowledgment

This work was supported in part by Tanikawa Fund Promotion of Thermal Technology. The authors would like to gratefully acknowledge the assistance of Ms. Naoko Yoshida, Ms. Fumie Kinouchi and Ms. Naomi Katahira in carrying out gasification experiments and elemental analysis.

References

1 J.L. Figueiredo and J.A. Moulijn (eds.), Carbon and Coal Gasification, NATO ASI Series, Martinus Nijhoff Publishers, Dordrecht, 1986.
2 J.A. Moulijn and F. Kapteijn (eds.), Special Issue of the International Symposium "Fundamentals of Catalytic Coal and Carbon Gasification", Fuel, 65 (1986) 1324.
3 M. Misono, A. Miyamoto and K. Wada, Appl. Catal., 65 (1990) N15.
4 T. Takarada, J. Sasaki, Y. Ohtsuka, Y. Tamai and A. Tomita, Ind. Eng. Chem. Res., 26 (1987) 627.
5 T. Takarada, Y. Ohtsuka and A. Tomita, J. Fuel Soc. Jpn., 67 (1988) 683.
6 Y. Ohtsuka and K. Asami, Ind. Eng. Chem. Res., in press.
7 Y. Ohtsuka and A. Tomita, Fuel, 65 (1986) 1653.
8 Y. Ohtsuka and K. Asami, Proc. 1989 International Conference on Coal Science, Tokyo, 1989, p. 353.
9 Y. Ohtsuka, Gypsum & Lime (Japan), No. 229 (1990) 35.
10 H.F. Feldmann and H.N. Conkle, Energy Progress, 3 (1983) 105.
11 J. Weldon, G.B. Haldipur, D.A. Lewandowski and K.J. Smith, Am. Chem. Soc., Div. Fuel Chem. Prepr., 31(3) (1986) 244.
12 Y. Ohtsuka, K. Hosoda and Y. Nishiyama, J. Fuel Soc. Jpn., 66 (1987) 1031.
13 S.D. Kline, D.M. Mason, R.H. Carty and S.P. Babu, in "Coal Science and Technology", Vol. 16 (R. Markuszewski and T.D. Wheelock, eds.), Elsevier, Amsterdam, 1990, p. 687.

14 J.J. Reuther, H.N. Conkle, P.R. Webb and H.F. Feldmann, in "Coal Science and Technology", Vol. 9 (Y.A. Attia, ed.), Elsevier, Amsterdam, 1985, p. 458.
15 K.K. Chang, R.C. Flagan, G.R. Gavalas and P.K. Sharma, Fuel, 65 (1986) 75.
16 J.E. Notestein, Proc. EPRI Coal Gasification Conference, Palo Alto, 1988, p. 1.
17 J. Haggin, Chem. Eng. News, (1990) May 21, 33.
18 M.D. Stephenson, A.D. Williams and C.W. Kruse, in "Coal Science and Technology", Vol. 16 (R. Markuszewski and T.D. Wheelock, eds.), Elsevier, Amsterdam, 1990, p. 665.
19 Y. Ohtsuka and A. Tomita, in "Calcium Magnesium Acetate: An Emerging Bulk Chemical for Environmental Applications", (D.L. Wise, Y.A. Levendis and M. Metghalchi, eds.), Elsevier, Amsterdam, 1990, p. 253.
20 G.J.W. Kor, ACS Symposium Series, 64 (1977) 221-247.
21 M.S. Najjar and D.Y. Jung, Am. Chem. Soc., Div. Fuel Chem. Prepr., 35(4) (1990) 1473.
22 T. Yamada, T. Asakura, A. Takahashi, T. Suzuki and T. Homma, J. Fuel Soc. Jpn., 67 (1988) 153.
23 J.M. Lambert, Jr., G. Simkovich and P.L. Walker, Jr., Fuel, 59 (1980) 687.
24 M.D. Stephenson, M. Rostam-Abadi, L.A. Johnson and C.W. Kruse, in "Coal Science and Technology", Vol. 9 (Y.A. Attia, ed.), Elsevier, Amsterdam, 1985, p. 353.
25 L. von Bogdandy and H.J. Engell, ed., "The Reduction of Iron Ores: Scientific Basis and Technology" (English Edition), Springer-Verlag, New York, 1971, p. 38.
26 Y. Ohtsuka, Y. Kuroda, Y. Tamai and A. Tomita, Fuel, 65 (1986) 1476.
27 Y. Ohtsuka, Y. Tamai and A. Tomita, Energy & Fuels, 1 (1987) 32.

Effect of Oxidants on the Oxidative Coupling of Methane over a Lead Oxide Catalyst

Kenji ASAMI,† Tsutomu SHIKADA,†† and Kaoru FUJIMOTO*
Department of Synthetic Chemistry, Faculty of Engineering, The University of Tokyo, Hongo 7-3-1, Bunkyo-ku, Tokyo 113
(Received July 3, 1990)

Oxidative coupling of methane was studied over a PbO/MgO catalyst using a variety of oxidants such as N_2O, NO, CO_2, and SO_2. While N_2O showed both high activity and selectivity for the title reaction, NO produced CO_2, exclusively. The coupling reaction was assumed to proceed via the redox cycle of Pb and PbO on each oxidant mentioned above. Carbon dioxide produced small amounts of C_2 hydrocarbons and CO, while SO_2, was inactive for the reaction. Oxygen, N_2O, CO_2 could oxidize the Pb/MgO which had been formed by the reaction of PbO/MgO with methane at 1023 K. Thus-prepared PbO/MgO produced C_2 hydrocarbons from methane. Even NO, which gave no C_2 hydrocarbons in the CH_4–NO cofeed reaction, converted the Pb/MgO to PbO/MgO and the PbO/MgO gave C_2 hydrocarbons exclusively upon reacting with CH_4. NO seems to oxidize the methyl radical, which is an intermediate of the coupling reaction to CO_2. The ineffectiveness of SO_2 as an oxidant was attributed to the formation of PbS, which is inactive in the methane activation.

Since the pioneering work by Keller and Bashin,[1] a great number of catalysts have been found to be effective for the title reaction. The reaction systems reported so far are classified into 4 groups:

(A) Metal oxides, which exhibit abilities to change the oxidation state easily under reaction conditions, such as PbO,[2,3] MnO,[5] Bi_2O_3,[6] NiO,[7] and Tl_2O_3.[8]

(B) Alkaline earth metal oxides, such as MgO and CaO, which are undoped[9,10] or doped with Li^+,[11–14] Na^+,[15] K^+,[16] alkaline earth metal halide[17,18] or rare earth oxides.[19]

(C) Rare earth oxides, which are undoped[20] or doped with alkali metal compounds.[21]

(D) Noncatalyzed gas-phase reaction.[22,23]

Active oxygen species for the catalysts which belong to group (A) have been claimed to be bulk oxygen in metal oxides,[7,24] while the surface oxide ion or adsorbed oxygen has been proposed for the catalysts of group (B) and group (C).[12,25,26]

Oxidants other than O_2, such as N_2O or CO_2, have been applied to the methane coupling reaction. Ito et al. compared the reactivity of dinitrogen monoxide to methane with O_2 over a lithium promoted magnesium oxide catalyst and concluded that dinitrogen monoxide is not a preferable oxidant.[12] Otsuka et al. studied the effect of N_2O oxidation over a series of rare earth oxides and confirmed that N_2O gave a lower conversion of methane but a higher selectivity for C_2 hydrocarbons than O_2.[27] Meng et al. examined methane activation by N_2O over lead oxide catalysts supported on γ-Al_2O_3 and NaY zeolite to find that C_2 hydrocarbons were formed with a selectivity of 40%.[28] Hutching et al. found that on a Li/MgO catalyst N_2O promoted CH_4 coupling but NO inhibited the reaction while giving CO_2, exclusively and claimed the presence of two oxidizing species on the catalyst.[29] We have reported that in the noncatalyzed gas-phase system N_2O gave a higher selectivity than O_2 for the formation of C_2 hydrocarbons from CH_4, whereas NO was inactive for the reaction.[22] We also reported that methane reacted with CO_2 to form C_2 hydrocarbons and CO over a PbO/MgO catalyst.[30] Aika and Nishiyama also reported a promotional effect of added CO_2 on the CH_4–O_2 cofeed reaction over PbO/MgO.[31]

In this study the effects of a series of oxidants such as O_2, N_2O, NO, SO_2 and CO_2 were examined systematically over a PbO/MgO catalyst in order to clarify how each oxidant activates methane and the active oxygen species for the coupling reaction.

Experimental

The catalyst used was 20 wt%-PbO/MgO, prepared by impregnating commercially available magnesium with lead(2) nitrate from aqueous solution and then calcining it at 800 °C.[10] Methane oxidation reactions were conducted with a fixed-bed flow-type reaction apparatus under atmospheric pressure; the catalyst charge was 1 g. The reactor was a quartz tube with an inner diameter of 10 mm, in which another quqartz tube (6 mm o. d.) was inserted as a thermocouple holder. Methane conversions were performed according to the following two procedures: One was a CH_4-oxidant cofeed reaction and another was a periodic oxidation-reduction reaction. The reaction conditions of the cofeed reaction were 650—800 °C, W/F=1 g h mol^{-1}, $P(CH_4)$=14 kPa, P(oxidant)=1—4 kPa, and helium balance. In the case of CO_2, the composition of the reactant was CH_4: CO_2=1:1 and W/F was 5 g h mol^{-1}.

A periodic reaction was conducted along the following flow module: Air oxidation⟶N_2 purge(5 min)⟶CH_4 reaction(20 min) N_2 purge(20 min)⟶Oxidation(10 min). The cycle of the CH_4 reaction and oxidation was repeated at least 2 times. The procedure of the periodic reaction has

Present address:
† Coal Chemistry Laboratory, Chemical Research Institute of Non-Aqueous Solutions, Tohoku University, Katahira 2-1-1, Aoba-ku, Sendai 980.
†† Technical Research Center, NKK Corporation, 1-1 Minamiwa, Kawasaki-ku, Kawasaki 210.

been described elsewhere.[24] However, the first activation of the catalyst was performed by oxygen (air); then the second and the third activations were performed by each oxidant. All of the reactions and products were analyzed by gas chromatography. The separation columns used were Porapak R for dinitrogen monoxide and sulfur dioxide and MS-13 X for nitrogen monoxide, respectively. The analysis methods for other reactants and produucts have been described elsewhere.[24] A Toshiba-Beckmann 951 NO/NO_x meter was also used for the analysis of nitrogen monoxide. X-Ray diffraction (XRD) measurements of the catalysts were recorded with a Rigaku Denki Ru-200 diffractometer with Ni-filtered Cu-K radiation.

Results and Discussion

Thermodynamic Consideration. The free-energy changes of ethane formation from methane with these oxidants are shown in Table 1. From a thermodynamic perspective, oxygen and nitrogen oxides are favorable oxidants for a coupling reaction ($G°_f<0$), whereas sulfur dioxide and carbon dioxide are unfavorable ($G°_f>0$). However, the equilibrium conversion of methane by CO_2 oxidation is about 10% under the conditions of 750 °C, $CH_4/CO_2=1$, and normal pressure.

CH_4-Oxidant Cofeed Reaction. In Fig. 1 are shown the space-time yields (STY) of the reaction products obtained by various cofeed reactions at 750 °C over a 20 wt%-PbO/MgO catalyst. The partial pressure of dinitrogen monoxide and nitrogen monoxide in the feed gas was set to be about twice that of oxygen in order to adjust the CH_4-O stoichiometry. In the case of the CH_4-CO_2 reaction, $P(CO_2)$ and the modified residence time (W/F) were 50 kPa and 5 g h mol^{-1}, respepctively, because of the low reaction rate.

(a) N_2O. Dinitrogen monoxide gave a similar STY of CH_4 oxidation (12.8 mmol g^{-1}h^{-1}) to that obtained by O_2 (11.6 mmol g^{-1} h^{-1}), the values of which correspond to CH_4 conversions of 8.5 and 8.1%, respepctively (Fig. 1). The product distribution was also similar to that of the CH_4-O_2 reaction, except for the lack of CO. The temperature dependence of the reaction using N_2O revealed that a higher temperature is favored for making C_2 hydrocarbons (Fig. 2), which is also similar to the case of O_2 oxidation.[10] We have reported that N_2O is effective to make C_2 hydrocarbons in a noncatalyzed system[22] while giving a higher selectivity (88%). However, the production rate was lower by about two orders of magnitude than that in the

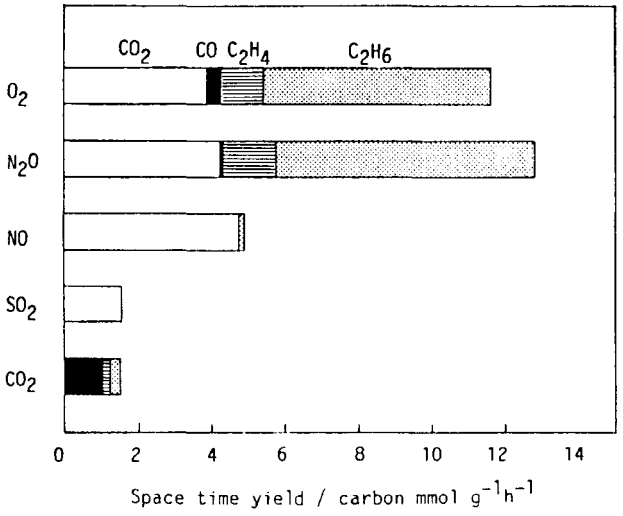

Fig. 1. Effect of oxidant on oxidative coupling of methane. Cat.; 20 wt%-PbO/MgO, 750 °C, W/F= 1.0 g h mol^{-1}, $P(CH_4)$=14 kPa, P(oxidant)=1.6 kPa (for O_2, N_2O, NO, SO_2), W/F=5.0 g h mol^{-1}, $P(CH_4)$= 5 kPa, $P(CO_2)$=5 kPa, (for CO_2).

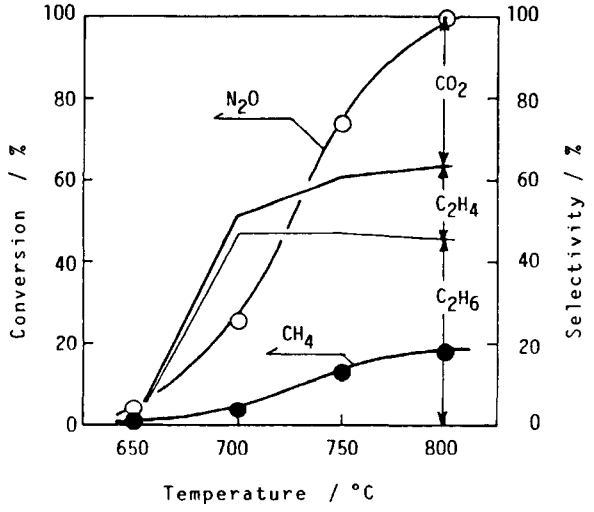

Fig. 2. Effect of temperature on the oxidative coupling of methane with N_2O as oxidant. Cat.; 20 wt%-PbO/MgO, 1.0 g h mol^{-1}, CH_4:N_2O:He= 10:4:86.

Table 1. Changes in Gibbs Free Energy in Oxidative Coupling of Methane with Various Oxidants

Reaction		$\Delta G_f°$/kcal mol^{-1}		
		700 °C	750 °C	800 °C
$2CH_4+1/2O_2 \rightarrow C_2H_6+H_2O$	(1)	−28.9	−28.1	−27.3
$2CH_4+N_2O \rightarrow C_2H_6+H_2O+N_2$	(2)	−66.2	−66.5	−66.7
$2CH_4+1/2NO \rightarrow C_2H_6+H_2O+1/2N_2$	(3)	−47.7	−46.8	−45.9
$2CH_4+1/2SO_2 \rightarrow C_2H_6+H_2O+S$	(4)	7.2	7.9	8.7
$2CH_4+1/3SO_2 \rightarrow C_2H_6+2/3H_2O+1/3H_2S$	(5)	6.2	6.6	7.0
$2CH_4+CO_2 \rightarrow C_2H_6+H_2O+CO$	(6)	17.8	17.4	16.9

present case, indicating that the reaction in the present system proceeds mainly on the catalyst surface.

The oxidative coupling of CH_4 over PbO/MgO has been clarified to be consist of a redox cycle between Pb and PbO; that is, a methane conversion into C_2 hydrocarbons by PbO (Eq. 7) and a reoxidation of metallic Pb with dioxygen (Eq. 8):

$$2\,CH_4 + PbO \longrightarrow C_2H_6 + H_2O + Pb, \quad (7)$$

and

$$Pb + 1/2O_2 \longrightarrow PbO. \quad (8)$$

The Gibbs free energy changes for the oxidation of Pb by N_2O oxidants shows as listed in Table 2 that the N_2O reaction with PbO (Eq. 9) is also thermodynamically favorable, as well as O_2. Therefore, the mechanism for the formation of C_2 hydrocarbons by N_2O is believed to be the same as that by O_2; namely, the reaction of CH_4 with PbO (Eq. 7) and the reoxidation reaction of reduced lead by N_2O (Eq. 9). We have confirmed that N_2O was completely decomposed to N_2 and O_2 on the PbO/MgO catalyst at 750 °C. Therefore, it is not clear whether N_2O reacts directly with Pb or after being converted to O_2.

(b) NO. Although a methane oxidation with NO is thermodynamically favorable (Table 1), the yield of C_2 hydrocarbons in the CH_4-NO reaction was much lower than those in the O_2-or N_2O- oxidation on the PbO/MgO catalyst, as indicated in Fig. 1. As shown in Table 3, CO_2 was formed exclusively (selectivity; >97%) under all reaction conditions. However, NO exhibited a strong oxidative ability of Pb; the oxidized Pb by NO gave C_2 hydrocarbons as well as N_2O or O_2 (Table 4). Therefore, the extremely low selectivity of C_2 hydrocarbons in a cofeed reaction might be interpreted in terms of the two prossible reasons given below.

[1] surface oxygen species derived from NO is active only for a complete oxidation of methane. The species would be an adsorbed one on PbO ($PbO-O_x$), since such a species derived from O_2 is considered to be active regarding the formation of carbon oxides.[24]

[2] NO inhibits a coupling reaction; thus molecular NO attacks the methyl radical, which is formed by the reaction of CH_4 with PbO, in the gas phase to form CH_3NO. It is then finally decomposed to CO_2. It is well-known that nitrogen monoxide is a radical inhibitor.[32] The fact that NO oxidized Pb to PbO and PbO oxidized CH_4 to C_2H_6 by periodic oxidation (Table 4 and Fig. 4) suggests that concept [2] is more plausible.

(c) SO_2. When sulfur dioxide was used as an oxidant, CO_2 was produced exclusively, as shown in Fig. 1. Though other by-products (not shown) were carbonyl sulfide and elemental sulfur, neither hydrogen sulfide nor methane thiol was formed. Further consideration is presented later.

(d) CO_2. It is noticeable that the oxidative coupling of methane proceeded to some extent by utilizing CO_2 as an oxidant (Fig. 1). The product distribution is explained by assuming the following reaction stoichiometry (Eq. 14—16):

$$CO_2 \longrightarrow CO + (O), \quad (14)$$

$$2\,CH_4 + (O) \longrightarrow C_2H_6 + H_2O, \quad (15)$$

Table 2. Changes in Gibbs Free Energy in Oxidation of Lead with Various Oxidants

Reaction		$\Delta G_f°$/kcal mol^{-1}		
		700 °C	750 °C	800 °C
$Pb+1/2O_2 \rightarrow PbO$	(8)	−29.6	−28.5	−27.4
$Pb+N_2O \rightarrow PbO+N_2$	(9)	−67.0	−66.9	−66.8
$Pb+NO \rightarrow PbO+1/2N_2$	(10)	−48.4	−47.2	−46.0
$Pb+1/2SO_2 \rightarrow PbO+1/2S$	(11)	6.4	7.5	8.6
$Pb+CO_2 \rightarrow PbO+CO$	(12)	17.0	16.9	16.8
$Pb+S \rightarrow PbS$	(13)	−22.5	−22.4	−22.4

Table 3. Methane Conversion by NO over 20 wt%-PbO/MgO Catalyst. W/F=1.0 g h mol^{-1}, He Balance

	Concentration/mol%				
CH_4	11.5	16.0	12.1	13.1	12.7
NO	1.5	3.7	7.5	3.7	3.7
Temperature/°C	750	750	750	800	700
Conversion/mol%					
CH_4	2.0	3.3	4.0	5.6	2.1
NO	6.3	7.2	19.4	24.5	3.5
Selectivity/C-mol%					
C_2H_6	1.7	1.0	0	2.5	0
CO_2	98.3	98.9	100	97.5	100

Table 4. Characterization of PbO Catalyst by XRD.[a] Same Experiments Shown in Figs. 3 to 6

	Oxidant	XRD peak		
		PbO	Pb	PbS
After oxidation	O_2	VS	—	—
	N_2O	VS	—	—
	NO	VS	—	—
	SO_2	W	—	S
	CO_2	VS	—	—
After CH_4 conversion	O_2	VW	VS	—
	N_2O	VW	VS	—
	NO	VW	VS	—
	SO_2	—	W	S
	CO_2	VW	VS	—

a) Peak intensity: VS; very strong, S; strong, W; weak, VW; very weak, —; not detected.

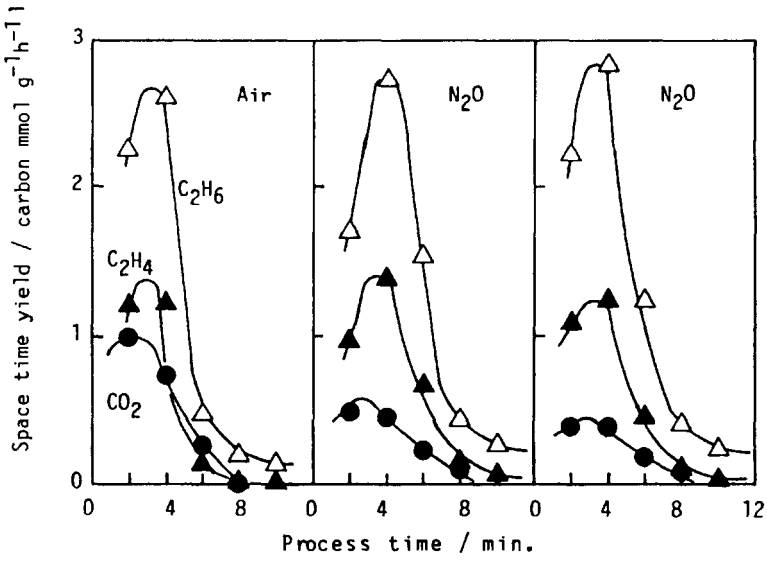

Fig. 3. Transient response of periodic CH_4 conversion: Effect of N_2O reoxidation. Cat.; 20 wt%-PbO/MgO, 750 °C, 4.3 g h mol^{-1}.

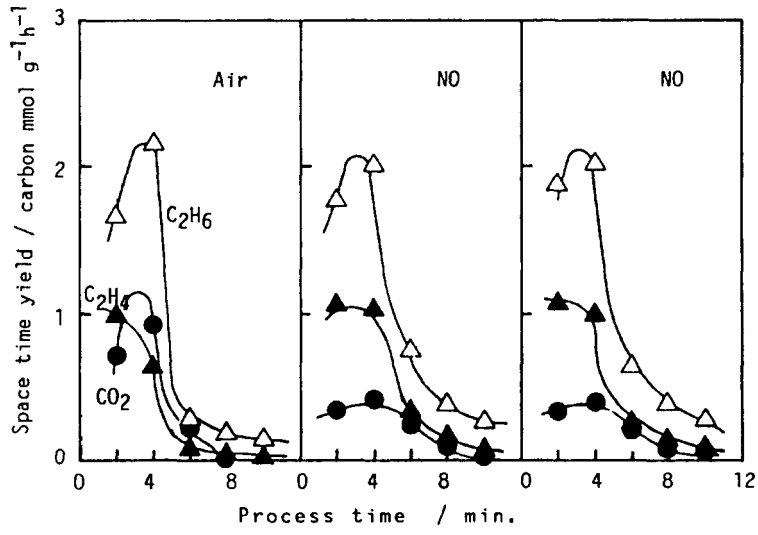

Fig. 4. Transient response of periodic CH_4 conversion: Effect of NO reoxidation. Cat.; 20 wt%-PbO/MgO, 750 °C, 4.3 g h mol^{-1}.

and

$$2\,CH_4 + 2\,(O) \longrightarrow C_2H_4 + 2H_2O. \quad (16)$$

Carbon dioxide is dissociated to carbon monoxide and a reactive surface oxygen species (O) (Eq. 14), which may react with methane to form ethane (Eq. 15) and ethylene (Eq. 16). In fact, CO_2 oxidized Pb to PbO and PbO oxidized CH_4 to C_2H_6 (Table 4 and Fig. 5). However, the amount of CO formed was larger than the amount calculated from reactions (14)—(16). Thus, reaction (17) should be accounted for. Reactions (14) and (17) are converted to the reaction stoichiometry shown in Eq. 18, which means that one fourth of the CO was formed from CH_4.

$$CH_4 + 3\,(O) \longrightarrow CO + 2\,H_2O \quad (17)$$

$$C^*H_4 + 3\,CO_2 \longrightarrow C^*O + 3\,CO + 2\,H_2O \quad (18)$$

The product distribution is shown as Fig. 1. Even at 800 °C the selectivity of C_2 hydrocarbons was not high. Thus low selectivity might be attributed to the formation of surface $MgCO_3$, which is not a favorable

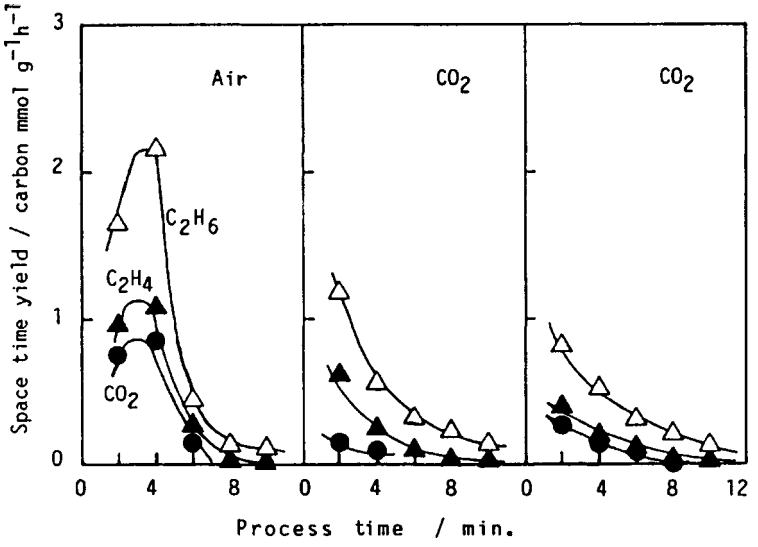

Fig. 5. Transient response of periodic CH_4 conversion: Effect of CO_2 reoxidation. Cat.; 20 wt%-PbO/MgO, 750 °C, 4.3 g h mol^{-1}.

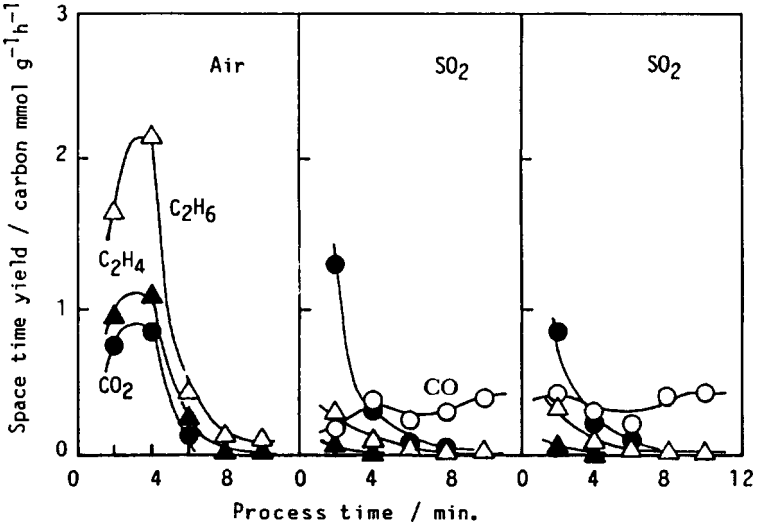

Fig. 6. Transient response of periodic CH_4 conversion: Effect of SO_2 reoxidation. Cat.; 20 wt%-PbO/MgO, 750 °C, 4.3 g h mol^{-1}.

support material. This subject will be discussed later.

Periodic Oxidation-Reduction Reaction. In the case of the CH_4–oxidant cofeed reaction, O_2 and N_2O exhibited excellent performance in the formation of C_2 hydrocarbons, similar to that of O_2, whereas other oxidants (NO, SO_2, and CO_2) did not produce the desired products selectively (as described above). However, a periodic oxidation-reduction reaction gave different results, as shown in Figs. 3 to 6. Also, the lead species identified after each reaction are shown in Table 4.

(a) N_2O, NO, and CO_2. Dinitrogen monoxide gave a similar result to that of the cofeed reaction containing O_2. Also, the periodic reaction gave C_2H_6 selectively over a catalyst which was oxidized by N_2O as demonstrated in Fig. 3. These facts correspond to that regarding O_2, which suggests that the oxidation state of lead oxidized by N_2O is similar to that oxidized by O_2 (Table 2).

Although little C_2 hydrocarbons were formed in a cofeed reaction containing NO (Fig. 1), they were formed with high selectivity in the CH_4–NO periodic reaction (Fig. 4). It was also clarified that NO has an ability to oxidize metallic Pb to PbO, and PbO gave C_2

hydrocarbons upon a reaction with CH_4, as demonstrated in Table 4. This means that although the redox cycle is possible in the CH_4–NO cofeed reaction system, NO inhibits the coupling reaction, probably because it reacts with the methyl radical to form CO_2. C_2 hydrocarbons were formed selectively at a comparable rate in a periodic CH_4–CO_2 operation (Fig. 5), while the rate of C_2 formation in a cofeed reaction was much lower than that in the O_2-containing cofeed reaction (Fig. 1). However, the amount of C_2 hydrocarbons formed in the second treatment was slightly smaller and the amount of CO formed was slightly larger than that obtained in the first treatment. This observation might be attributed to the formation of a surface carbonate species of carrier material of the catalyst (MgO) which is unfavorable for the coupling reaction.[24]

(b) SO_2. When sulfur dioxide was used as an oxidant, a small amount of C_2 hydrocarbons was formed in the periodic reaction (Fig. 6), although no C_2 hydrocarbons were formed at all in the cofeed reaction. The low CH_4 selectivity even in a periodic reaction, should be attribuuted to the formation of PbS according to Eqs. 11 and 13 during a reaction with SO_2 (Table 4), since PbS is never reduced by a reaction with CH_4. It is thus concluded that the redox cycle expressed as reactions (7) and (11) is inhibited by the formation of PbS.

Conclusion

Methane activation with a MgO-supported PbO catalyst was studied by using a variety of oxidants such as O_2, N_2O, NO, SO_2, and CO_2 resulting in the following conclusion:

1) In a CH_4–oxidant cofeed reaction, N_2O exhibited excellent activity and selectivity for the formation of C_2 hydrocarbons as well as O_2, whereas NO and CO_2 gave only small amounts of the desired product and SO_2 made no C_2 hydrocarbons.

2) Not only O_2 and N_2O, but also NO and CO_2, showed high selectivity for the formation of C_2 hydrocarbons in a periodic oxidation–reduction operation. This was because of the formation of PbO, which gave C_2 hydrocarbons upon a reaction with CH_4, with the reaction of a reduced catalyst and these oxidants as well as O_2 and N_2O. However, NO or CO_2 seems to have some inhibiting effect on the coupling reaction.

3) When SO_2 was used as an oxidant for methane conversion, lead sulfide was formed, which impeded the coupling reaction in either the cofeed reaction or the periodic reaction.

We thank Professor H. Tominaga for his discussion.

References

1) G. E. Keller and M. M. Bhasin, *J. Catal.*, **73**, 9 (1982).
2) W. Hinsen, W. Bytyn, and M. Baerns, *Proc. ICC, 8th*, **3**, 581 (1984).
3) K. Asami, S. Hashimoto, T. Shikada, K. Fujimoto, and H. Tomonaga, *Chem. Lett.*, **1986**, 1233.
4) G. Wendt, C. -D. Meinecke, and W. Schmitz, *Appl. Catal.*, **45**, 209 (1988).
5) J. A. Sofranko, J. J. Leonard, and C. A. Jones, *J. Catal.*, **103**, 311 (1987).
6) I. T. Ali Emesh and Y. Amenomiya, *J. Phys. Chem.*, **90**, 4785 (1986).
7) K. Otsuka, Q. Liu, M. Hatano, and A. Morikawa, *Chem. Lett.*, **1986**, 353.
8) K. Fujimoto and K. Asami, unpublished.
9) T. Mori, N. Takasaki, E. Iwamatsu, and K. Aika, *Chem. Lett.*, **1986**, 1165.
10) N. Yamagata, K. Tanaka, S. Sasaki, and S. Okazaki, *Chem. Lett.*, **1987**, 81.
11) T. Ito and L. Lunsford, *Nature*, **314**, 721 (1985).
12) T. Ito, J. -X. Wang, C. -H. Lin, and J. H. Lunsford, *J. Am. Chem. Soc.*, **107**, 5062 (1985).
13) S. J. Korf, J. A. Roos, N. A. deBruijn, J. G. Van Ommen, and J. R. H. Ross, *Catal. Today*, **2**, 535 (1988).
14) V. T. Amorebieta and A. J. Colussi, *J. Chem. Phys.*, **92**, 4576 (1988).
15) E. Iwamatsu, T. Moriyama, N. Takasaki, and K. Aika, *J. Catal.*, **113**, 25 (1988).
16) J. A. S. P. Carreiro and M. Baerns, *J. Catal.*, **117**, 396 (1989).
17) K. Fujimoto, S. Hashimoto, K. Asami, and H. Tominaga, *Chem. Lett.*, **1987**, 2157.
18) K. Fujimoto, S. Hashimoto, K. Asami, and H. Tominaga, *Appl. Catal.*, **50**, 223 (1989).
19) V. R. Choudhary, S. T. Chaudhari, A. M. Rajput, and V. H. Rane, *J. Chem. Soc., Chem. Commun.*, **1989**, 555.
20) K. Otsuka, Q. Liu, M. Hatano, and A. Morikawa, *Chem. Lett.*, **1986**, 467.
21) K. Otsuka, K. Jinno, and A. Morikawa, *Chem. Lett.*, **1985**, 499.
22) K. Asami, K. Omata, K. Fujimoto, and H. Tominaga, *Energy Fuels*, **2**, 574 (1988).
23) G. S. Lane and E. E. Wolf, *J. Catal.*, **113**, 144 (1988).
24) K. Asami, T. Shikada, K. Fujimoto, and H. Tominaga, *Ind. Eng. Chem. Res.*, **26**, 2348 (1987).
25) N. W. Cant, C. A. Lukey, P. F. Nelson, and R. J. Tyler, *J. Chem. Soc., Chem. Commun.*, **1988**, 766.
26) K. Otsuka, A. A. Said, K. Jinno, and T. Komatsu, *Chem. Lett.*, **1987**, 77.
27) K. Otsuka and T. Nakajima, *J. Chem. Soc., Faraday Trans. 1*, **83**, 1315 (1987).
28) H. Meng and R. D. Sanger, *Appl. Catal.*, **32**, 347 (1987).
29) G. J. Hutching, M. S. Scurrell, and J. R. Woodhouse, *J. Chem. Commun.*, **1989**, 765.
30) K. Asami, T. Shikada, K. Fujimoto, and H. Tominaga, Annual Meeting of the Chemical Society of Japan, Kyoto (1986).
31) K. Aika and T. Nishiyama, *J. Chem. Soc., Chem. Commun.*, **1988**, 70.
32) P. G. Ashmore, "Catalysis and Indibition of Chemical Reactions," Butterworths, London (1963).

Resources, Conservation and Recycling, 7 (1992) 69–82
Elsevier Science Publishers B.V.

In-bed sulfur removal during the fluidized bed combustion of coal impregnated with calcium magnesium acetate

Yasuo Ohtsuka and Kenji Asami
Research Center for Carbonaceous Resources, Institute for Chemical Reaction Science, Tohoku University, Katahira, Japan

(Accepted 2 April 1992)

ABSTRACT

Ohtsuka, Y. and Asami, K., 1992. In-bed sulfur removal during the fluidized bed combustion of coal impregnated with calcium magnesium acetate. *Resour., Conserv. Recycl.*, 7: 69–82.

Sulfur removal during the fluidized bed combustion of coal has been carried out at temperatures of 960–1140 K. Coal impregnated with calcium magnesium acetate (CMA) is used as a sulfur sorbent. The amount of CMA actually loaded is larger for brown coal with a higher ion-exchange capacity. CMA shows no significant effect on the burn-off irrespective of the coal type and temperature. However, calcium impregnation is effective for in-bed sulfur removal. The efficiency depends on the coal type, probably the type of sulfur in the coal; a high sulfur retention is attained for Illinois No. 6 coal with a large proportion of pyritic sulfur in spite of low Ca/S ratios of around 0.5. In the coprocessing of bituminous coal with impregnated low-sulfur brown coal, the highly dispersed calcium in the brown coal captures effectively the sulfur evolved during the combustion of the bituminous coal.

INTRODUCTION

Combustion of coal produces emissions of sulfur oxides which cause serious environmental problems. In order to reduce sulfur emissions, two different methods have been widely used; coal cleaning prior to combustion, and flue gas scrubbing after combustion. However, because of their high cost and complex operation, alternative methods of sulfur removal have been investigated. A more successful approach is to remove the sulfur during the fluidized combustion in a bed of a sulfur sorbent such as limestone or dolomite.

Since the desulfurization by calcium sorbents is a much slower solid–gas reaction than coal combustion, it would be desirable for improving sorbent utilization to enhance the reactivity. Impregnating coal with calcium using

Correspondence to: Y. Ohtsuka, Research Center for Carbonaceous Resources, Institute for Chemical Reaction Science, Tohoku University, Katahira, Sendai 980, Japan.

$Ca(CH_3COO)_2$ and $Ca(OH)_2$ produces a much higher reactivity due to very fine dispersion within the coal particles [1,2], compared with calcite and dolomite physically mixed with coal. It has been reported that the use of calcium-impregnated coal in pulverized firing is more effective for sulfur capture than the limestone injection method [3–5]. Since the operating temperature in fluidized combustion is lower than in pulverized firing, the $CaSO_4$ formed is thermodynamically more stable. Further, the complete mixing within the fluidized bed ensures good contact between sorbent and combustion gases. These advantages contribute to efficient sorbent utilization. In addition, the lower temperature of the bed may minimize the formation of thermal NO_x.

In the present paper, therefore, in-bed sulfur removal of calcium-impregnated coal is studied during fluidized combustion. Calcium magnesium acetate (CMA) is selected as a sulfur sorbent because its use for sulfur removal has been shown to be economically feasible by the simulation study [6]. Two different ranking high-sulfur coals, brown coal and bituminous coal, are used, and the effect of the coal type on sulfur removal efficiency and the influence of calcium impregnation on the burn-off are examined. A sufficient amount of calcium can not be loaded on high-sulfur bituminous coal because of the poor ion-exchange capacity. Thus, the coprocessing of bituminous coal with CMA-impregnated low-sulfur brown coal is carried out to capture the sulfur evolved from the bituminous coal.

EXPERIMENTAL

Coal sample

The proximate and elemental analysis of three coals examined are shown in Table 1. Loy Yang (LY) coal from Australia is a low-ash, low-sulfur brown coal; Leigh Creek (LC) coal from Australia is a high-sulfur brown coal with relatively large amounts of inherent Ca and Mg; Illinois No. 6 (IL) coal from

TABLE 1

Proximate and ultimate analysis of coals

Coal (country)	Code	Proximate analysis (wt%, dry)			Ultimate analysis (wt%, daf)					Inherent metal (wt%, dry)	
		VM[a]	FC[a]	Ash	C	H	N	S	O	Ca	Mg
Loy Yang (Australia)	LY	50.6	48.7	0.7	68.1	4.7	0.6	0.3	26.3	0.05	0.1
Leigh Creek (Australia)	LC	51.3	40.0	8.7	68.1	5.4	0.5	3.2	22.8	1.0	0.8
Illinois No.6 (USA)	IL	37.0	53.6	9.4	77.4	5.2	1.6	3.3	12.5	0.2	0.1

[a]VM, Volatile matter; FC, fixed carbon.

the USA is a high-sulfur bituminous coal. LC and IL coals are almost the same with regard to sulfur content. LY coal is used only for coprocessing with IL coal. The size of coal particles is 150–250 μm in every case.

Addition and determination of calcium magnesium acetate

Coal is simultaneously impregnated with an aqueous solution of $Ca(CH_3COO)_2$ and $Mg(CH_3COO)_2$ (CA and MA, respectively. Coal particles (30 g) dried in a stream of N_2 at 380 K are immersed in the solution (100 cm^3) in a glass flask, and the resulting mixture is then evacuated while rotating the flask at room temperature for 1 h and finally at 330 K for dryness. The nominal loading of CA or MA added to the dried coal in the impregnation step is usually 4 wt% as the metal. The dried lumps recovered from the flask are ground and sieved again to 150–250 μm. The sample prepared by this method will be denoted as impregnated coal throughout the present paper.

The amounts of Ca and Mg either actually loaded on coal or inherently present in coal are determined by atomic absorption spectroscopy (Japan Jarrell Ash Co., AA-855) after extraction with HCl at 320 K. The contents of inherent Ca and Mg are shown in Table 1.

Fluidized bed combustion

A quartz vertical reactor attached with a movable transparent electric furnace is used for the combustion experiments. The reactor consists of a fluidized zone (22 mm i.d.$\times$300 mm long) with fritted filter (pore size, 20–30 μm) and a freeboard zone (37 mm i.d.$\times$300 mm long). The amount of sample charged into the fluidized zone is 3.0–3.5 g, which corresponds to 15–20 mm bed height. No fluidized solids are used in the present work. The flow rate of air or Ar as a fluidized gas is 800 cm^3 (STP)/min. Temperatures of 1050–1100 K are primarily selected because the maximum sulfur removal efficiency in the fluidized combustion lies in this region [7].

Two different combustion runs are made — with and without pretreatment in Ar — depending on the type of sample. When impregnated IL or LC coal is used, the coal is preheated in Ar at 680 K for 30 min during fluidizing in order to decompose CMA, then cooled to room temperature, and again heated in air to a predetermined temperature. The pretreatment is effective in keeping the temperature of the fluidized bed constant during combustion. This point will be described later (Fig. 2). Original coals and the mixture of IL coal and impregnated LY coal are heated in air without any pretreatment.

The experimental procedure is as follows. The sample in the reactor is first kept in the fluidized state at room temperature, then heated rapidly (about 350 K/min) by raising the electric furnace and maintained at a predetermined temperature for 10 min. After 10 min the fluidized gas is switched from air to Ar and the reactor is quenched by lowering the furnace. The tem-

perature of the fluidized bed is measured by a chromel–alumel thermocouple inserted into the center of the bed and located at around 5 mm above the fritted filter. The temperature can be controlled within ± 15 K.

Sulfur determination

The S content in feed coal or combustion residue is determined with a sulfur analyser (Horiba, EMIA-510); the sample is burned up in a stream of O_2 at 1723 K and the SO_2 evolved is detected by an on-line IR spectrometer. The Standard Reference Materials from the National Institute of Standards and Technology, USA, are used for calibration of the instrument.

In the sulfur determination of the combustion residue a fixed amount of activated carbon is added to the residue prior to burning in order to promote the release of SO_2 from the incombustible sulfur such as CaS and $CaSO_4$. Fig. 1 illustrates the profiles for the evolution of SO_2 from pure $CaSO_4$. The re-

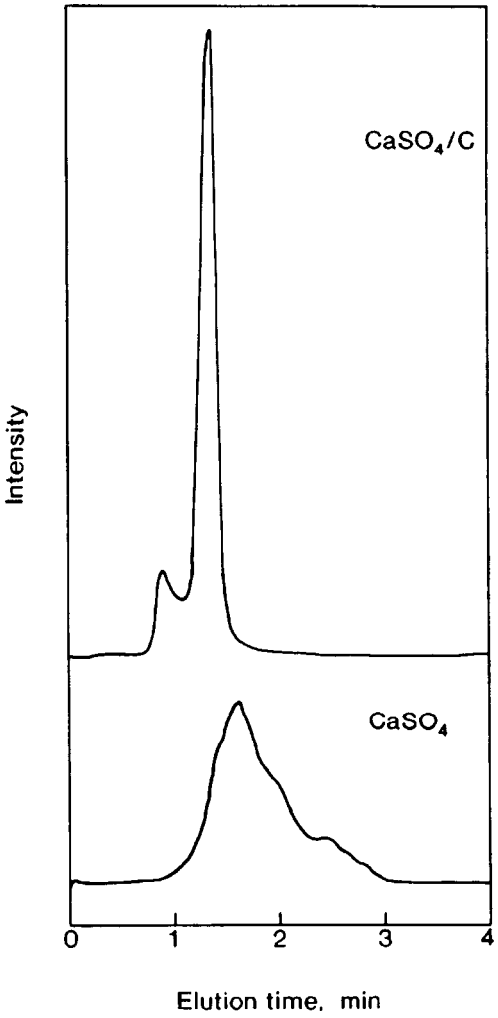

Fig. 1. Evolution of SO_2 from $CaSO_4$ with and without carbon.

lease of SO_2 without carbon is slow even at 1723 K. However, the evolution rate of SO_2 is increased by the addition of carbon, probably due to the heat of combustion, and thus the complete sulfur determination is attained within 2 min.

Characterization of the combustion residue

The amount of combustibles remaining in the residue is determined with a thermobalance (Sinku-Riko; TGD-7000); the residue (about 50 mg) mounted on a quartz cell in the thermobalance is heated at a rate of 20 K/min in a stream of air, and soaked at 1090 K until no further weight loss is observed.

X-Ray diffraction analysis of the combustion residue is made using Cu-K_α (45 kV×30 mA) to follow the change in the chemical form of CMA and pyritic sulfur during combustion.

Data processing

The sulfur retention, expressed as %, is calculated by the amounts of S in both feed coal and combustion residue. The burn-off is calculated from the amount of combustibles in these samples, and is expressed as wt% on a dry, ash-free, CMA-free basis.

RESULTS AND DISCUSSION

Actual metal loading

The relationship between the nominal and actual loading is given in Table 2, where the metal loading is defined as wt% of Ca or Mg metal to CMA-free coal, and the inherent metal is excluded from the actual loading. The amount of metal actually loaded is found to depend strongly on the coal type. The actual loading of each metal is nearly equal to the nominal one with LY coal. About 90% of the nominal loading is actually loaded onto LC coal irrespec-

TABLE 2

Nominal and actual loadings of Ca and Mg

Coal	Mg loading (wt%)		Ca loading (wt%)	
	Nominal[a]	Actual[b]	Nominal[a]	Actual[b]
LY	4.0	4.0	4.0	3.9
LC	4.0	3.5	4.0	3.7
IL	2.0	1.2	2.0	1.3
IL	4.0	1.9	4.0	1.9

[a]Calculated from the amount of metal added to coal in the impregnation step.
[b]Determined by atomic absorption spectroscopy of impregnated coal.

tive of the kind of metal. With IL coal, however, the proportion of actual to nominal loading decreases considerably; 60–65% and < 50% at nominal loadings of 2 and 4 wt%, respectively.

Since some ion-exchange between Ca and Mg cations and the protons in COOH groups proceeds even under the present impregnation conditions [2,8], the difference among these coals is probably related to different amounts of free COOH groups not associated with metal ions. Quite a low ash content and very small amounts of inherent Ca and Mg in LY coal, as seen in Table 1, show that most of the total COOH content (1.6 meq/g coal) exists as free COOH. Although similar oxygen contents in LY and LC coal suggest similar total COOH contents, the amount of free COOH would be lower in LC coal owing to a higher ash content and larger amounts of inherent Ca and Mg (Table 1). The demineralization of LC coal with HCl–HF aqueous solution prior to CMA impregnation would increase actual metal loadings, but the residual halogen in the demineralized coal would impair the calcium dispersion [1,9] and may cause corrosive problems on various parts of materials. Total COOH content in IL coal is less than one-fifth of that in LY coal [10], which results in a very small ion-exchange capacity of IL coal. Although the pretreatment of coal such as mild oxidation with air [4,6] or dilute nitric acid [11] improves the exchange capacity, the loss in the calorific value of coal during oxidation is inevitable.

XRD measurements after the pyrolysis of calcium-impregnated coals reveal that no diffraction lines due to calcium species are detectable on the chars derived from brown coals [1,2], whereas strong XRD peaks of $CaCO_3$ and CaO are observed on the chars from bituminous coals like IL coal [2,12]. These observations show that calcium is very finely dispersed on the surface of brown coal, and the dispersion is less on bituminous coal. The fine dispersion of calcium would be due to some ion-exchange, which initially provides essentially atomic dispersion.

Temperature profile of fluidized bed

Typical profiles of the bed temperature are illustrated in Fig. 2, where the nominal content of CMA is given. When impregnated IL coal is heated in air without any pretreatment, the bed temperature rises steeply at around 900 K during heating and reaches 1300 K. This probably arises from explosive combustion of inflammable organic gases evolved by decomposition of CMA. A similar phenomenon is observed for impregnated LC coal. However, when the sample preheated in Ar at 680 K is heated again in air, the temperature is uniform within ± 15 K, as seen from the solid line in Fig. 2. Since the decomposition of CMA into $CaCO_3$ and MgO is completed during pretreatment, no inflammable organic gases evolve on reheating in air.

Fig. 2 also shows that when the mixture of IL coal and impregnated LY coal is heated in air without being preheated, the uniform bed temperature is also

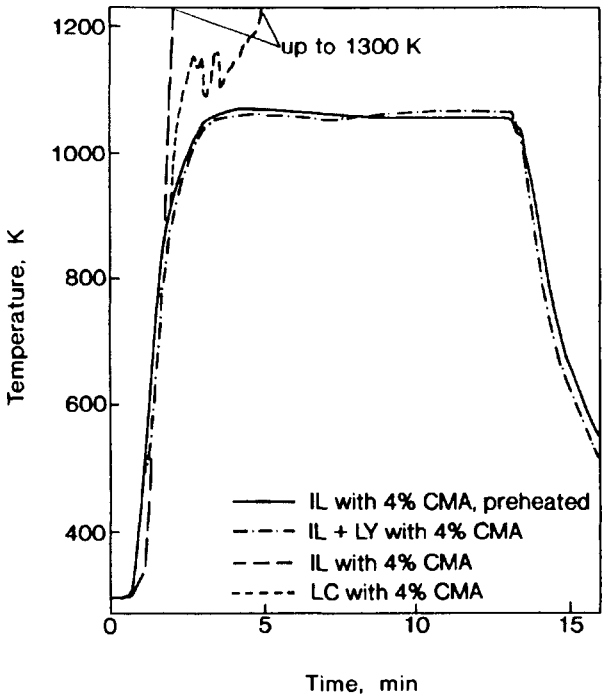

Fig. 2. Temperature profiles of fluidized bed for different samples.

attained. The amounts of Ca and Mg actually loaded are almost the same between the above mixture and impregnated IL coal, as is shown in Table 4. Nevertheless, the bed temperature without pretreatment in Ar is uniform only for the former. This difference may be caused by different chemical states of CMA loaded between impregnated LY and IL coal. As discussed above, some ion-exchange proceeds between CMA and LY coal with a large amount of free COOH groups. However, little ion-exchange takes place with IL coal because of the poor exchange capacity, and thus a large part of the metals loaded exist in the form of acetates which evolve inflammable organic gases on combustion. A lower proportion of acetates with impregnated LY coal would lead to a uniform bed temperature.

Combustion of Leigh Creek coal

Table 3 summarizes the burn-off and sulfur retention for the combustion of Leigh Creek coal. The addition of CMA (Ca content, 4.7 wt%) has almost no effect on the burn-off, irrespective of temperature. It has been reported that a small amount of CMA of 1 wt% markedly promotes the steam gasification of coal [2], and that impregnated calcium enhances the combustion rate of low reactive chars [13,14]. Since these reactions are chemical reaction limited, the calcium shows a catalytic effect on reactivity enhancement. On the other hand, the rate of the present combustion is quite high, and also only a small increase in the burn-off with increasing temperature is observed (Ta-

TABLE 3

Burn-off and sulfur retention for the combustion of Leigh Creek coal

Temperature (K)	Ca content[a] (wt%)	Ca/S[b]	Burn-off (%, daf)	S retention (%)
970	1.0	0.29	85	36
960	4.7	1.4	83	41
1100	1.0	0.29	94	33
1080	4.7	1.4	96	40

[a]Content of inherent and Ca actually loaded in coal.
[b]Atomic ratio of (inherent and actually loaded Ca)/S.

ble 3). These observations suggest the gas-film diffusion controlled reaction, as is well established in coal combustion. Calcium impregnation is ineffective for the diffusion-controlled combustion. Table 3 shows that the sulfur retention is enhanced by the addition of CMA at the atomic Ca/S ratio of 1.4, but the increase is small, and is not improved at a higher temperature of around 1100 K.

The XRD patterns for combustion residues at around 1100 K are illustrated in Fig. 3. Strong diffraction lines attributable to CaS (oldhamite) and $CaSO_4$ (anhydrite) are observed even without CMA, indicating the sulfur capture by inherent Ca. The following reactions for this are

$$CaO + H_2S \text{ (or COS)} = CaS + H_2O \text{ (or } CO_2) \quad (1)$$

$$CaS + 2O_2 = CaSO_4 \quad (2)$$

$$CaO + SO_2 + 1/2O_2 = CaSO_4 \quad (3)$$

Judging from the absence of distinct XRD peaks of other Ca species and the Ca/S ratio of about 1 in the residue, most of the inherent Ca is found to be transformed to CaS and $CaSO_4$. No Fe species can be detected by XRD, which means that only a slight amount of pyritic sulfur is contained in LC coal, in contrast with the observation for IL coal (Fig. 5).

MgO (periclase) is the only Mg species for the XRD profiles with CMA. The diffraction lines of CaS and $CaSO_4$ are detectable similarly as without CMA, but $CaCO_3$ is the major Ca species. Thus, the reaction of $CaCO_3$ with the sulfur evolved may be given instead of Eqns. 1 and 3.

$$CaCO_3 + H_2S = CaS + H_2O + CO_2 \quad (4)$$

$$CaCO_3 + SO_2 + 1/2O_2 = CaSO_4 + CO_2 \quad (5)$$

However, the presence of $CaCO_3$ as the major species shows that most of the CMA remains unreacted, as is reflected by a small enhancement of sulfur retention (Table 3). The reason for such a poor calcium utilization is not clear

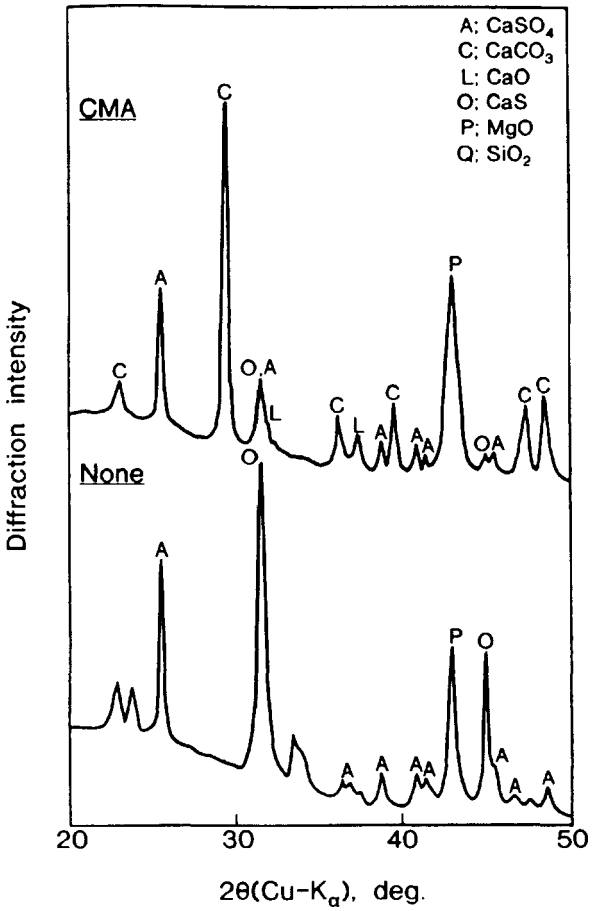

Fig. 3. XRD patterns for the residues after combustion of Leigh Creek coal with and without calcium magnesium acetate.

at present, but some speculations may be possible. The main reason may be the type of coal, in particular, the type of sulfur. As is shown in Fig. 4, a higher sulfur retention is attained in the combustion of impregnated IL coal in spite of lower Ca/S ratios. A comparison of XRD patterns between original LC and IL coals (Figs. 3 and 5) reveals that pyritic sulfur is rich in IL coal, whereas organic sulfur is rich in LC coal, because it is well accepted that pyritic and organic sulfur together account for the majority of sulfur in coal [15]. Pyritic sulfur is selectively oxidized with air and thus more easily removed than organic sulfur [16,17]. Most of the organic sulfur in LC coal might be incombustible and flown away as it is under the present conditions. Another reason may be a relatively low O_2 concentration. The formation of $CaSO_4$ may be thermodynamically favored under O_2-rich conditions. The combustion run of impregnated LC coal is tested at the partial pressure of O_2 of 0.4 atm, but unfortunately the uniform temperature of the fluidized bed is not obtained due to the rapid combustion.

Combustion of Illinois and Loy Yang coal

Table 4 summarizes the burn-off for both IL coal and the mixture of IL and LY coal. The burn-off for original and impregnated IL coal is 73–81 wt% at 1050–1060 K. The presence of CMA (Ca content, 1.4 and 2.0 wt%) shows no significant effect on the burn-off. A quite similar phenomenon is observed for the mixture of IL and LY coal; the burn-off is not changed significantly by the addition of CMA at 1040–1070 K.

In Fig. 4 the sulfur retention for these samples is plotted as a function of

TABLE 4

Burn-off for the combustion of Illinois No. 6 and Loy Yang coal

Temperature (K)	Feed coal[a] (g)		Ca content[b] (wt%)	Burn-off (%, daf)
	IL	LY		
1050	3.0	0	0.2	81
1050[c]	3.0	0	0.2	78
1050[c]	3.2	0	1.4	75
1060[c]	3.5	0	2.0	73
1040	1.5	1.5	0.1	81
1060	1.5	1.5	2.0	84
1070[c]	1.5	1.5	2.0	84
1040	1.0	2.0	2.6	86
1140	1.5	1.5	2.0	90

[a]CMA-free basis with impregnated coal.
[b]Content of inherent and Ca actually loaded in coal.
[c]Preheated in Ar at 680K prior to combustion.

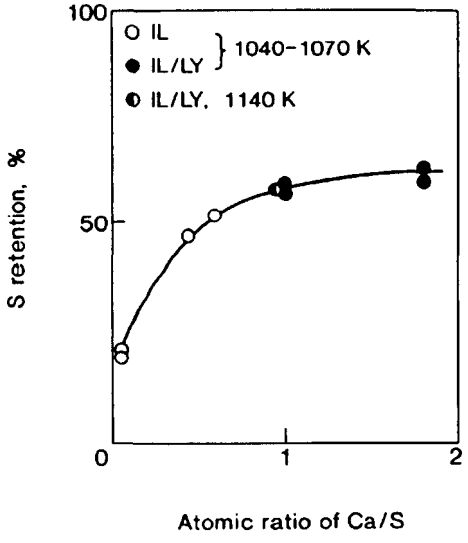

Fig. 4. Effect of Ca/S ratio on sulfur retention during the combustion of Illinois No. 6 coal and coprocessing of Illinois No. 6 and impregnated Loy Yang coal.

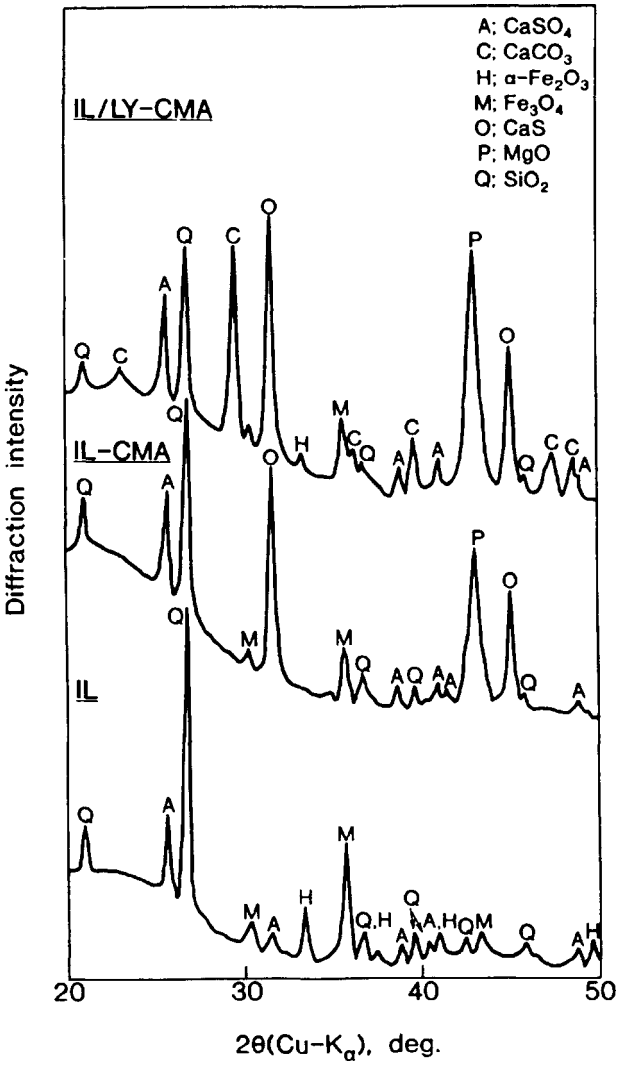

Fig. 5. XRD patterns for the residues after combustion of Illinois No. 6 coal and coprocessing of Illinois No. 6 and impregnated Loy Yang coal.

the atomic ratio of Ca/S. The sulfur retention for IL coal increases considerably with increasing ratio—from 20% without CMA to about 50% with CMA. When the mixture of IL coal and impregnated LY coal is used (IL/LY in Fig. 4) the sulfur retention reaches around 60% at the Ca/S ratio of about 1, but a further increase in the ratio has no significant effect on the retention. Thus, in contrast with LC coal (Table 3), impregnation with CMA can easily capture the sulfur from IL coal in spite of relatively low Ca/S ratios. Further, low-sulfur brown coal impregnated with CMA is found be effective for sulfur removal during the combustion of high-sulfur bituminous coal. The finely dispersed calcium on LY brown coal would be able to readily capture the sulfur evolved. This finding would be noteworthy from a practical point of view

because when bituminous coal alone is used in the fluidized combustion a mild oxidation process is essential for obtaining a sufficient Ca/S ratio, whereas the pretreatment is unnecessary in the coprocessing of bituminous coal with impregnated brown coal.

The XRD patterns for combustion residues at 1050–1070 K are illustrated in Fig. 5, where IL, IL-CMA and IL/LY-CMA denote original, impregnated IL coal and the mixture of IL coal and impregnated LY coal as starting samples, respectively. Weak diffraction lines of $CaSO_4$ are observed for IL. Some of the sulfate comes from sulfates naturally present, because bassanite ($CaSO_4 \cdot 1/2H_2O$) exists in the low-temperature ash prepared using a plasma asher [18]. The XRD profiles also reveal the presence of Fe_2O_3 (hematite) and Fe_3O_4 (magnetite), most of which are formed by oxidation of pyritic sulfur according to the following equations [19,20].

$$FeS_2 + 11/4O_2 = 1/2Fe_2O_3 + 2SO_2 \quad (6)$$

$$FeS_2 + 8/3O_2 = 1/3Fe_3O_4 + 2SO_2 \quad (7)$$

The products from pyrite oxidation depend on temperature and partial pressure of O_3. Pyritic sulfur may also react with the reducing gas produced by the partial oxidation of coal to form pyrrhotites (FeS_{1+x}) [12,19], which are then oxidized to Fe_3O_4 and Fe_2O_3.

$$FeS_2 + H_2 = FeS + H_2S \quad (8)$$

$$FeS_2 + CO = FeS + COS \quad (9)$$

The presence of these iron oxides means that IL coal is rich in pyritic sulfur, in contrast with LC coal (Fig. 3).

MgO is the only Mg species detectable by XRD with impregnated samples (IL-CMA and IL/LY-CMA). For impregnated IL coal with the Ca/S ratio of 0.6, CaS and $CaSO_4$ alone are detectable as the Ca species, and the Ca/S ratio in the residue is determined as 1.2. These results show that a large part of the loaded calcium acts as a sulfur-capturing agent. When the Ca/S ratio in the starting sample (IL/LY-CMA) is further increased to 1, however, some of the calcium remains unreacted and exists as $CaCO_3$. The XRD signals of Fe_3O_4 and α-Fe_2O_3 can be detected. Since pyritic sulfur reacts more readily with O_2 than organic sulfur [16,17], it is likely that most of the CaS and $CaSO_4$ are formed by the reaction of Ca species with the sulfur compounds evolved from pyritic sulfur. Calcium impregnation is also effective for removing pyritic sulfur during coal gasification [12].

If unreacted $CaCO_3$ could be converted to CaS and $CaSO_4$, a higher sulfur retention would be attained. An increase in the height of the fluidized bed increases the residence time of both gases and solids and thus would be expected to improve the sulfur removal efficiency [7]. Therefore the combustion run is tested under the conditions where the bed height is increased two-

fold and the molar ratio of O_2/coal is kept unchanged, but the sulfur retention is not improved significantly.

The coexistence of CaS and $CaSO_4$ in combustion residues (Figs. 3 and 5) suggests that the atmosphere in the present fluidized bed is relatively reductive. Under such conditions, part of the $CaSO_4$ formed may be reconverted to CaO (Eqns. 10 and 11) [7], which results in a lowering of the sulfur retention.

$$CaSO_4 + CO = CaO + SO_2 + CO_2 \quad (10)$$

$$CaSO_4 + H_2 = CaO + SO_2 + H_2O \quad (11)$$

Thus, the fluidizing gas is changed from air to 40% O_2–Ar, but the bed temperature is not uniform and the formation of slag due to local overheating is observed. Fuel-lean conditions may be desirable for higher sulfur removal efficiency.

CONCLUSIONS

(1) In CMA impregnated coal, the actual loading is larger for brown coal with higher ion-exchange capacity.
(2) Burn-off of coal in the fluidized bed combustion is not changed significantly by CMA impregnation.
(3) Impregnation with calcium is effective for in-bed sulfur removal, but the efficiency is probably dependent on the type of sulfur in the coal; a high sulfur retention is obtained for Illinois No. 6 coal rich in pyritic sulfur.
(4) Finely dispersed calcium on brown coal can readily capture the sulfur evolved from bituminous coal in the coprocessing.

ACKNOWLEDGEMENTS

The authors gratefully acknowledge the assistance of Ms. Naomi Katahira and Ms. Naoko Yoshida in carrying out sulfur analysis, sample preparation and preparing the manuscript. This work was supported in part by the Japan Association of Chemistry, and Iketani Science and Technology Foundation.

REFERENCES

1 Ohtsuka, Y. and Tomita, A., 1986. Fuel 65: 1653.
2 Ohtsuka, Y. and Tomita, A., 1990. In: D.L. Wise, Y.A. Levendis and M. Metghalchi (Editors), Calcium Magnesium Acetate: An Emerging Bulk Chemical for Environmental Applications. Elsevier, Amsterdam, p. 253.
3 Freund, H. and Lyon, R.K., 1982. Combust. Flame, 45: 191.
4 Chang, K.K., Flagan, R.C., Gavalas, G.R. and Sharma, P.K., 1986. Fuel, 65: 75.

5 Reuther, J.J., Conkle, H.N., Webb, P.R. and Feldmann, H.F., 1985. In: Y.A. Attia (Editor), Coal Science and Technology, Vol. 9. Elsevier, Amsterdam, p. 458.
6 Manivannan, S. and Wise, D.L., 1990. In: D.L. Wise, Y.A. Levendis and M. Metghalchi (Editors), Calcium Magnesium Acetate: An Emerging Bulk Chemical for Environmental Applications. Elsevier, Amsterdam, p. 297.
7 IEA Coal Research, 1989. In: The Problems of Sulphur (Reviews in Coal Science), Butterworths, London, p. 82.
8 Schafer, H.N.S., 1970; Fuel, 49: 197.
9 Hengel, T.D. and Walker, P.L., Jr., 1984. Fuel, 63: 1214.
10 Takarada, T., Nabatame, T., Ohtsuka, Y. and Tomita, A., 1987. In: J.A. Moulijn, K.A. Nater and H.A.G. Chermin (Editors), Coal Science and Technology, Vol. 11. Elsevier, Amsterdam, p. 547.
11 Ohtsuka, Y., Itagaki, K., Higashiyama, K., Tomita, A. and Tamai, Y., 1981. J. Fuel Soc. Jpn., 60: 437.
12 Ohtsuka, Y. and Asami, K., 1991. In: P.R. Dugan, D.R. Quigley and Y.A. Affria (Editors), Coal Science and Technology Vol. 18. Elsevier, Amsterdam, p. 139.
13 Levendis, Y.A., Nam, S.W., Loewenberg, M., Flagen, R.C. and Gavalas, G.R., 1989. Energy and Fuels, 3: 256.
14 Levendis, Y.A., 1990. In: D.L. Wise, Y.A. Levendis and M. Metghalchi (Editors), Calcium Magnesium Acetate: An Emerging Bulk Chemical for Environmental Applications. Elsevier, Amsterdam, p. 221.
15 IEA Coal Research, 1989. In: The Problems of Sulphur (Reviews in Coal Science). Butterworths, London, p. 5.
16 Sinha, R.K. and Walker, P.L., Jr., 1972. Fuel, 51: 125.
17 Block, S.S., Sharp, J.B. and Darlage, L.J., 1975. Fuel, 54: 113.
18 Ohtsuka, Y., Wang, Z-Y and Tomita, A., 1987 J. Fuel Soc. Jpn., 66: 189.
19 Stephenson, M.D., Rostam-Abadi, M. Johnson, L.A. and Kruse, C.W., 1985. In: Y.A. Attia (Editor), Coal Science and Technology, Vol. 9. Elsevier, Amsterdam, p. 353.
20 Tsai, S.C., 1986. Ind. Eng. Chem. Process. Des. Dev. 25: 126.

Reprinted from ENERGY & FUELS, 1992, 6.

Large Rate Enhancement by Iron Catalysts in the Low-Temperature Hydrogasification of Brown Coal under Pressure

Yasuo Ohtsuka,*,† Kenji Asami,† Tetsuo Yamada,‡ and Tsuneyuki Homma‡

Research Center for Carbonaceous Resources, Institute for Chemical Reaction Science, Tohoku University, Katahira, Aoba-ku, Sendai 980, Japan, and Kitami Institute of Technology, Koen-cho, Kitami 090, Japan

Received April 23, 1992. Revised Manuscript Received June 19, 1992

The direct conversion of coal into CH_4 with a catalyst is one of the most attractive of processes which utilize coal in an environmentally acceptable manner. Among the many gasification catalysts, nickel is more suitable for producing a high concentration of CH_4 in one pass from low-rank coal and pressurized steam at around 850 K.[1] However, the use of expensive nickel would not be practical. Iron is promising as an alternative to nickel, and the iron chlorides and sulfates readily available as acid wastes from steel pickling and TiO_2 production plants are the most desirable iron catalyst sources.[2] We have recently found that $FeCl_3$ can be successfully converted to a Cl-free iron catalyst active for the steam gasification of low-rank coals.[3] However, the effectiveness is small at the low temperatures, 800–850 K, favorable for CH_4 formation from coal and steam. The present study focuses on applying this iron to the hydrogasification reaction where CH_4 is produced by the reaction of coal with H_2, because an iron catalyst is more effective at low temperatures in H_2 than in steam.[4] In this communication, the Cl-free iron from $FeCl_3$ is found to show an exceptionally high catalytic activity in the low-temperature, pressurized hydrogasification of brown coal.

Loy Yang brown coal supplied from the Coal Corporation of Victoria, Australia, was crushed to 150–250 μm. The proximate analysis was ash, 0.5, volatile matter, 52.4, and fixed carbon, 47.1 wt % (dry), and the ultimate analysis was as follows: C, 66.7; H, 4.6; N, 0.5; S, 0.3; O, 27.9 wt % (daf). Iron cations alone were incorporated into the coal from an aqueous solution of $FeCl_3$ by using NH_3; after a sufficient amount of NH_3/NH_4Cl solution was added into the mixture of coal particles and $FeCl_3$ solution, the iron-bearing coal was separated from the solution by filtration, washed with deionized water, and then dried at 380 K in N_2. The details of the procedure have been described elsewhere.[3] Actual iron loadings were 5 and 9 wt %. Since a higher equilibrium concentration of CH_4 is obtained at a lower temperature and higher pressure,[5] the gasification run with a thermobalance (Shimadzu RT-1HP) was carried out at temperature of <1000 K and at pressures of H_2 of 3.5 and 7.0 MPa. In this thermobalance, the weight change can be monitored with a microbalance enclosed in the pressure chamber, and the influence of the change in buoyancy on the weight can be corrected electrically.[6] About 0.2 g of the dried coal was mounted onto quartz wool in a quartz cell, at the bottom of which several small holes were open for attaining a good contact between the coal and H_2. The sample was heated in an H_2 flow at 10 K/min, the flow rate being 0.5 L(STP)/min unless otherwise stated.

Table I. Mössbauer Parameters[a]

iron species	IS, mm/s	QS, mm/s	*H*, kOe
present iron (5 wt %)	0.39	0.97	0
present iron (9 wt %)	0.39	0.97	0
α-FeOOH[b]	0.57	0.40	360
fine FeOOH[c]	0.41	0.89–0.92	0

[a] IS, isomer shift relative to α-Fe at room temperature; QS, quadrupole splitting; *H*, hyperfine field. [b] Commercial bulk compound (99.999% pure). [c] Reference 7; FeOOH particles finely dispersed on brown coal.

The Cl determination by a standard Eschka method showed that the Cl contents in iron-bearing samples, 0.04–0.06 wt %, are nearly equal to that (0.08 wt %) in original coal. Accordingly, every iron-loaded coal is free from Cl contamination from $FeCl_3$, because all of the Cl ions from $FeCl_3$ are removed as ammonium chloride. Mössbauer spectra revealed that every iron catalyst shows a doublet, which differed from those of bulk compounds of $Fe(OH)_3$ and FeOOH. The Mössbauer parameters are summarized in Table I. The comparison of the parameters observed and those reported suggested that the present iron may exist in the form of fine particles of FeOOH. The FT-IR spectra also showed that part of Fe ions incorporated are exchanged with the protons in COOH groups in coal.[3] From these observations the iron catalyst was found to be very highly dispersed on the coal surface. The X-ray diffraction (XRD) analysis showed that the catalyst is reduced to fine particles of metallic iron (α-Fe) up to 700 K.

* Author to whom correspondence should be addressed.
† Tohoku University.
‡ Kitami Institute of Technology.

(1) Takarada, T.; Sasaki, J.; Ohtsuka, Y.; Tamai, Y.; Tomita, A. *Ind. Eng. Chem. Res.* 1987, *26*, 627–629.
(2) Hüttinger, K. J.; Adler, J.; Hermann, G. In *Carbon and Coal Gasification*; Figueiredo, J. L., Moulijn, J. A., Eds.; NATO ASI Series; Martinus Nijhoff: Dordrecht, The Netherlands, 1986; pp 213–229.
(3) Ohtsuka, Y.; Asami, K. *Ind. Eng. Chem. Res.* 1991, *30*, 1921–1926.
(4) Ohtsuka, Y.; Tamai, Y.; Tomita, A. *Energy Fuels* 1987, *1*, 32–36.
(5) Walker, P. L., Jr.; Rusinko, F., Jr.; Austin, L. G. In *Advances in Catalysis*; Eley, D. D., Selwood, P. W., Weisz, P. B., Eds.; Academic Press: New York, 1959; Vol. XI, pp 133–221.
(6) Sasaki, M.; Homma, T.; Yamada, T.; Makino, K. *Bunseki Kagaku* 1969, *18*, 1179–1183.
(7) Cook, P. S.; Cashion, J. D. *Fuel* 1987, *66*, 661–668.

0887-0624/92/2506-0678$03.00/0

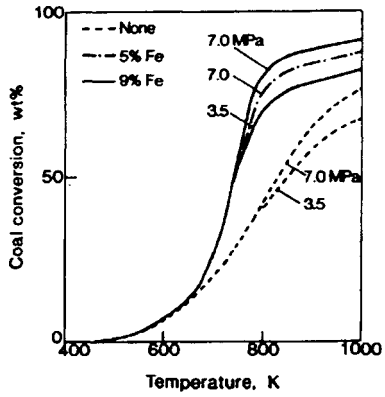

Figure 1. Profiles for the temperature-programmed hydrogasification of Loy Yang coal at 3.5 and 7.0 MPa.

Profiles for the temperature-programed hydrogasification are illustrated in Figure 1, where coal conversion is expressed as wt % on a dry, ash- and catalyst-free basis. When the flow rate of H_2 was increased from the normal level of 0.5 to 2 L(STP)/min, no significant effects on the gasification profiles were observed, which means that the reaction under the present conditions is free from the gas film diffusion control. Coal devolatilization in the absence of catalyst was almost complete at temperatures up to 800 K, followed by char gasification. The reaction rate was larger at a higher pressure of 7.0 MPa.

The iron-catalyzed gasification proceeded in two stages: in other words, rapidly between 700 and 800 K and slowly beyond 800 K. The iron catalyst enhanced the reaction rate even in the conversion range up to about 50%, namely, the devolatilization step. In this region the deposition of carbon (or carbon precursor) from tarry materials evolved and the subsequent hydrogenation may proceed on the catalyst surface, as observed with the nickel-catalyzed gasification.[8,9] As is well known, volatile hydrocarbons are decomposed to form highly reactive carbon and coke over Fe and Ni metals.[10] Another possibility is that the iron may promote the reaction of devolatilizing coal with H_2, the so-called rapid hydrogenation.[11,12] Thus, the iron catalyst seems to greatly promote CH_4 formation at the expense of tarry materials. Char gasification followed the hydrogenation of deposited carbon, and the gasification rate was larger at a higher iron loading and pressure of H_2. The conversion up to 800 K after the completion of the first rapid stage reached 80% at 9 wt % Fe and 7.0 MPa, whereas it was only 40% without iron. The reaction rate in the second slow stage beyond 800 K was rather lower in the presence of catalyst, but the conversion up to 1000 K at 9 wt % Fe, 90%, was much larger than that (75%) without catalyst. The XRD measurements of iron-bearing char after gasification showed that the crystallite size of α-Fe is too large to be determined by XRD. Therefore, the decreased rate in the second stage may be attributable to the catalyst deactivation due to agglomeration of iron particles. These observations suggest that the optimum temperature region for producing CH_4 efficiently with an iron catalyst may be below 800 K. The residual iron-rich char after CH_4 production may be burned in a blast furnace and converted to pig iron.

In conclusion, a Cl-free, finely dispersed iron catalyst prepared from $FeCl_3$ shows a large rate enhancement in the pressurized hydrogasification of brown coal at low temperatures of 700–800 K.

Registry No. Fe, 7439-89-6.

(8) Tomita, A.; Watanabe, Y.; Takarada, T.; Ohtsuka, Y.; Tamai, Y. *Fuel* **1985**, *64*, 795–800.
(9) Takarada, T.; Ohtsuka, Y.; Tomita, A. *J. Fuel Soc. Jpn.* **1988**, *67*, 683–692.
(10) Albright, L. F., Baker, R. T. K., Eds. *Coke Formation on Metal Surfaces*; ACS Symposium Series 202; American Chemical Society: Washington, DC, 1982.
(11) Johnson, J. L. In *Coal Gasification*; Massey, L. G., Ed.; Advances in Chemistry Series 131; American Chemical Society: Washington, DC, 1974; pp 145–178.
(12) Anthony, D. B.; Howard, J. B. *AIChE J.* **1976**, *22*, 625–656.

T. Inui et al. (Editors), *New Aspects of Spillover Effect in Catalysis*

Catalytic behavior of iron in the gasification of coal with hydrogen

Kenji Asami and Yasuo Ohtsuka

Research Center for Carbonaceous Resources, Institute for Chemical Reaction Science
Tohoku University, Sendai 980, Japan

Abstract

Three kinds of iron catalysts are precipitated onto an Australian brown coal from an aqueous solution of $FeCl_3$ by using urea, $Ca(OH)_2$, or NH_3 as an additive. All the iron species on coal are found to be finely dispersed FeOOH by the XRD and ESCA measurements, and they are reduced to metallic iron during pyrolysis. The use of urea gives the highest metal dispersion. All the catalysts show gasification activities in atmospheric H_2 at 873 K and the iron catalyst prepared with urea is most effective. These observations suggest that the metal dispersion is a key factor for controlling the catalytic activity and that the present hydrogasification may proceed through a hydrogen spillover mechanism.

1. INTRODUCTION

Hydrogasification of coal is an important process for producing CH_4 (SNG). Since the reaction rate is extremely low at lower temperatures which are thermodynamically favorable for CH_4 formation, the use of a catalyst is essentially needed in this process. Inexpensive Fe is one of the most promising catalysts, and Fe chloride and sulfate as acid wastes from steel pickling plants are the most desirable catalyst sources. We have recently found that a Cl-free Fe catalyst can be successfully prepared from $FeCl_3$ solution [1,2], and it exhibits high activity for the hydrogasification of low rank coals under pressure [3] and at relatively high temperatures of 1050–1200 K [4]. The present paper focuses on the catalytic behavior of this iron in the hydrogasification at a low temperature of 873 K.

2. EXPERIMENTAL

2.1. Coal sample and catalyst preparation

The coal sample used was Australian Loy Yang brown coal with a low ash content of 0.5 wt% and a large surface area of about 250 m^2/g. The elemental analysis was C, 66.7; H, 4.6; N, 0.5; S, 0.3; O, 27.9 wt% on a dry, ash-free basis.

Three kinds of Fe catalysts, abbreviated as Fe(U), Fe(C), and Fe(A), were precipitated onto coal from an aqueous solution of $FeCl_3$ by using urea, $Ca(OH)_2$, or NH_3 as additives. The use of urea is known to be effective for precipitating fine FeOOH particles [5], and $Ca(OH)_2$ or NH_3 was used instead of urea. After the aqueous mixture of coal, $FeCl_3$, and each additive was stirred either at 370 K for urea or at room temperature for other additives, the Fe-loaded coal was separated from the solution and finally

washed with water to remove Cl ions. The details of the procedure have been described elsewhere [2].

2.2. Hydrogasification

The gasification experiments were carried out with a thermobalance. All the samples were heated at 300 K/min up to 873 K under atmospheric H_2 of 250 cm^3(STP)/min, and soaked for 60 min. The pyrolysis of coal first occurred during heating, and almost completed within a few minutes. Then the residual solid char was gasified with H_2. The reactivity of char is expressed by char conversion on a dry, ash-free and catalyst- free basis.

2.3. Characterization

The XRD measurements of Fe-bearing samples were made with Mn-filtered Fe-Kα radiation. The average crystallite size of metallic Fe was determined according to the Debye-Shörrer method. The ESCA spectra were also measured using Mg-Kα radiation.

3. RESULTS AND DISCUSSION

3.1. Catalyst State

The chemical analysis of Fe-bearing coals showed that actual Fe loadings were 3.4, 4.7, and 4.6 wt% for Fe(U), Fe(C), and Fe(A), respectively, and also revealed that any catalysts were not contaminated by the Cl ions from $FeCl_3$, but a small amount of Ca was retained with Fe(C).

No XRD lines attributable to Fe species were detectable for all the catalysts, which suggests a high degree of catalyst dispersion in every case. Table 1 summarizes ESCA spectra. The binding energy of Fe $2p_{3/2}$ for each catalyst was in agreement with that of FeOOH reported previously. The presence of this species was supported by the elemental analysis of Fe-bearing coals. These observations show that every catalyst exists in the form of FeOOH finely dispersed on coal.

Table 1
Binding energies of Fe $2p_{3/2}$ ESCA spectra of Fe-bearing samples

Sample	Fe(U)	Fe(C)	Fe(A)	FeOOH[1)]
Fe $2p_{3/2}$ (eV)	711.6	712.4	712.1	710.7-712.1

[1)]References [6,7]

Figure 1 shows the XRD patterns for Fe catalysts after pyrolysis at 873 K, in other words, immediately before gasification. α-Fe was the major species irrespective of the catalyst type, indicating the reduction of FeOOH to metallic Fe during pyrolysis. The average crystallite size of α-Fe was 10, 28, and 45 nm for Fe(U), Fe(C), and Fe(A), respectively. Therefore the degree of metal dispersion evaluated from the size became higher in the order of Fe(A) < Fe(C) < Fe(U).

3.2. Catalyst effectiveness

Figure 2 shows the gasification profiles at 873 K. Char conversion without catalyst would be attributable mostly to a slow release of the volatile matter remaining in the char formed after pyrolysis. The presence of the Fe catalyst increased char conversion

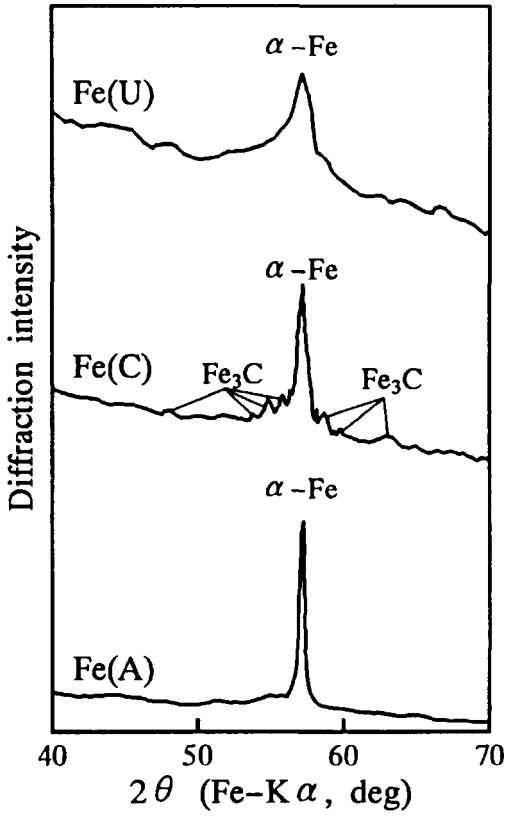

Figure 1. XRD patterns of iron catalysts on the chars pyrolyzed in H_2.

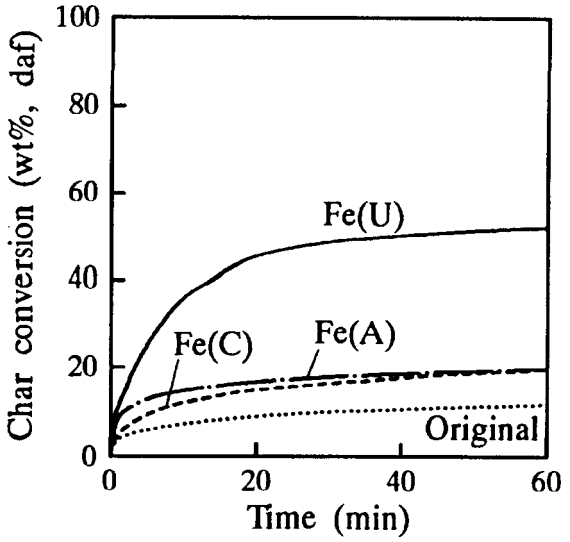

Figure 2. Hydrogasification of Loy Yang coal with iron catalysts.

in every case, showing the promotion of char gasification by this catalyst. Fe(U) was the most active catalyst, and the conversion after 60 min reached about 50%, where the

gasification appeared to be stopped. The rate enhancement by Fe(C) and Fe(A) was not so large.

Although the mechanism for the metal-catalyzed hydrogasification at low temperatures is not fully elucidated, the present gasification may proceed through the spillover mechanism [8,9] where the dissociated hydrogen atoms spill over from iron metal to react with the char. The metal dispersion is a key factor in controlling the catalytic activity in this mechanism. The comparison of Figures 1 and 2 points out that Fe(U) with the highest degree of metal dispersion is most effective for the low temperature hydrogasification of brown coal. Ni and Co metals also promoted the gasification in this temperature region, and they were more effective than Fe(U) [10]. When the average size of Ni crystallites exceeded about 30 nm, the catalytic activity was drastically decreased [11]. Therefore a smaller activity of Fe(C) or Fe(A) may be ascribed to a larger crystallite size of Fe metal.

Figure 2 also shows that the conversion with Fe(U) leveled off at the latter stage of reaction. There are two reasons for this rate retardation; one is the lowering of catalyst dispersion due to the agglomeration of Fe particles, and another is the consumption and concurrent crystallization of reactive char (carbon). If the former is main as suggested in the Ni-catalyzed gasification [10], the hydrogen adsorption or spillover might be a rate-limiting step in the present Fe-catalyzed gasification.

4. CONCLUSIONS

Hydrogasification of brown coal with fine FeOOH particles precipitated from $FeCl_3$ solution by adding urea, $Ca(OH)_2$, and NH_3 is carried out at a low temperature of 873 K under atmospheric pressure. FeOOH is reduced to metallic Fe in the step of coal pyrolysis preceding char gasification. The Fe catalyst prepared by using urea gives the highest metal dispersion and shows the largest activity for the gasification. The finely dispersed metallic Fe seems to play a key role for hydrogen spillover.

5. ACKNOWLEDGMENTS

Ms. Naoko Yoshida and Ms. Naomi Katahira are gratefully acknowledged for their assistance in carrying out experiments. This work was partly supported by a Grant-in-Aid for Scientific Research from the Ministry of Education, Science and Culture, Japan.

6. REFERENCES

1 Y. Ohtsuka and K. Asami, Ind. Eng. Chem. Res., 30 (1991) 1921.
2 K. Asami and Y. Ohtsuka, submitted to Ind. Eng. Chem. Res.
3 Y. Ohtsuka, K. Asami, T. Yamada and T. Homma, Energy & Fuels, 5 (1992) 678.
4 K. Asami and Y. Ohtsuka, Prep. 204th ACS National Meeting., Div. Fuel Chem., 4 (1992) 1951 .
5 K. Kaneko, S. Ozeki, and K. Inouye, J. Chem. Soc. Jpn., (1985) 1351.
6 N.S. McIntyre and D.G. Zetaruk, Anal. Chem., 49 (1977) 1521.
7 D.T. Harvey and R.W. Linton, Anal. Chem., 53 (1981) 1684.
8 A. Tomita and Y. Tamai, J. Catal., 27 (1972) 293.
9 T. Inui, K. Ueno, M. Funabiki, M. Suehiro, T. Sezume, and Y. Takegami, J. Chem. Soc., Faraday Trans. I, 75 (1979) 1495.
10 Y. Ohtsuka, Y. Tamai, and A. Tomita, Energy & Fuels, 1 (1987) 32.
11 Y. Ohtsuka, J. Mol. Catal., 54 (1989) 225.

Reprinted from I&EC RESEARCH, 1993, 32.

Highly Active Iron Catalysts from Ferric Chloride for the Steam Gasification of Brown Coal

Kenji Asami* and Yasuo Ohtsuka

Research Center for Carbonaceous Resources, Institute for Chemical Reaction Science, Tohoku University, Aoba-ku, Sendai 980, Japan

A new method for preparing active iron catalysts for coal gasification at low temperatures has been studied by using $FeCl_3$ as a raw material. Iron catalysts are precipitated onto brown coal probably in the form of FeOOH from an aqueous solution of $FeCl_3$ by using three additives (urea, $Ca(OH)_2$, and ammonia) and by hydrolysis. The use of $Ca(OH)_2$ gives the highly dispersed, most active iron catalyst, which achieves complete gasification in steam within 60 min at 973 K and at 5 wt % Fe. The specific gasification rate with the most active catalyst is about 20 times that without catalyst, and it increases as the reaction proceeds. The X-ray diffraction measurements show that Fe_3O_4 is the stable species throughout the gasification regardless of the catalyst preparation method. The sequence of catalyst effectiveness and the difference in the rate profiles among these catalysts can be elucidated on the basis of the degree of Fe_3O_4 dispersion.

Introduction

Catalytic gasification of coal has a great potential (Figueiredo and Moulijn, 1986; Moulijn and Kapteijn, 1986), because this process can produce environmentally acceptable fuels and chemical feedstocks at low temperatures (Misono et al., 1990). Fe catalyst is known to show gasification activity in every gas of steam, CO_2, and H_2, and thus it would be one of the most promising catalysts (Hüttinger et al., 1986; Ohtsuka and Asami, 1991a). Since abundance and inexpensiveness are indispensable requirements for catalyst sources from a practical point of view, we have focused on new utilization of acid wastes from metal pickling and titanium oxide production plants as Fe catalyst sources. When iron chloride and sulfate of the major components were added to coal by the conventional impregnation method, they unfortunately showed only a very small catalyst effectiveness for the gasification at low temperatures of around 950 K because of rapid agglomeration of catalyst particles (Ohtsuka et al., 1987). However, we have recently found that a Cl-free Fe catalyst finely dispersed on coal can be successfully prepared from an aqueous solution of $FeCl_3$ using NH_3/NH_4Cl solution, and this catalyst exhibits high activity for the low-temperature gasification of low-rank coals with steam (Ohtsuka and Asami, 1991a). Some Fe ions in the Cl-free catalyst may precipitate on the coal.

In the present work several alternatives to NH_3/NH_4Cl solution are studied. Urea is first selected since it is effective for homogeneous precipitation of fine Fe particles from aqueous solutions of iron chloride and sulfate (Kaneko et al., 1985; Kaneko, 1987). Further, inexpensive $Ca(OH)_2$ is used in place of urea, and hydrolysis of $FeCl_3$ without any base is also examined. All the Fe catalysts incorporated on brown coal are much more active for the steam gasification than the previous catalyst. Thus, some factors controlling these activities are clarified.

Experimental Section

Coal Sample. Loy Yang brown coal from Australia was crushed and sieved to 0.15–0.25 mm. The proximate analysis was ash, 0.5; volatile matter, 52.4; fixed carbon, 47.1 wt % (dry); and the ultimate analysis was C, 66.7; H, 4.6; N, 0.5; S, 0.3; O, 27.9 wt % (daf).

Catalyst Preparation. Fe catalysts were precipitated onto brown coal from an aqueous solution of $FeCl_3$ by four different methods, that is, by use of urea ($(NH_2)_2CO$), $Ca(OH)_2$, and NH_3/NH_4Cl and by hydrolysis at an elevated temperature; these catalysts were abbreviated as Fe(U), Fe(C), Fe(A), and Fe(N), respectively. In every precipitation 12 g of coal and 200 mL of 0.2 N $FeCl_3$ solution were used unless otherwise stated. The details of each procedure are as follows.

To prepare the Fe(U) catalyst, 3.6 g of urea was added the mixture of coal and $FeCl_3$ solution. Then, the resulting aqueous mixture was stirred, heated gradually up to 370 K, and soaked for 4 h. It took 90 min to heat it. With the Fe(C) catalyst, $Ca(OH)_2$ powder with a molar ratio of $Ca(OH)_2/FeCl_3$ of 1.5 was first added instead of urea. Then the aqueous mixture was stirred for 2 h at room temperature. The change in the pH during stirring was monitored; it increased from the initial value of 1.5 to about 5 on the addition of $Ca(OH)_2$ and finally became constant at 4. Fe loading was varied by changing the initial concentration of $FeCl_3$. Subscript "L" or "H" in $Fe(C)_L$ or $Fe(C)_H$ catalyst means low or high loading, respectively. The preparation method of Fe(A) catalyst using NH_3/NH_4Cl buffer solution has been described elsewhere (Ohtsuka and Asami, 1991a). When the Fe(N) catalyst was prepared, the mixture of coal and $FeCl_3$ solution was heated in laboratory air at 370 K for 8 h so that FeOOH could be precipitated (Matijević and Scheiner, 1978; Musić et al., 1982).

After every precipitation, the solution was filtered off, and the Fe-bearing coal was washed with deionized water repeatedly to remove the Cl^- or Ca^{2+} ions. The Ca-exchanged catalyst, abbreviated as Ca(E), was also prepared by exchanging H^+ in COOH groups in coal with Ca^{2+} in a saturated aqueous solution of $Ca(OH)_2$ (Ohtsuka and Tomita, 1986) to examine the influence of residual Ca on the activity of Fe(C) catalyst.

Steam Gasification. About 20 mg of the original or catalyst-loaded coal mounted on quartz wool in a quartz cell was dried in a N_2 stream at 380 K prior to the gasification run. Then the sample was heated quickly in an atmospheric steam up to a predetermined temperature of 873–1073 K, and the weight loss during the isothermal gasification was monitored with a thermobalance. The

* To whom correspondence should be addressed.

0888-5885/93/2632-1631$04.00/0

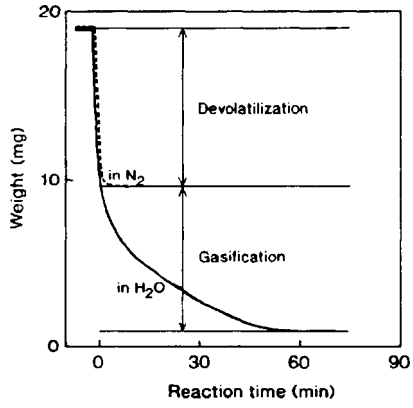

Figure 1. Thermogravimetric curves for the gasification in steam and the devolatilization in N_2 of Fe-loaded coal at 973 K.

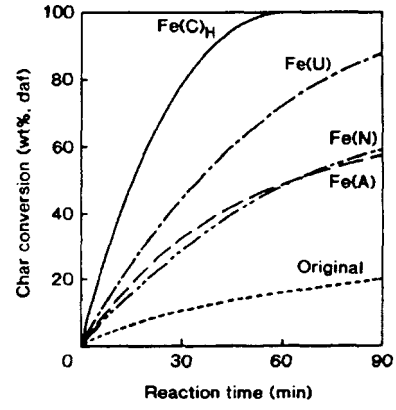

Figure 2. Steam gasification of Loy Yang coal with several Fe catalysts at 973 K.

details of the procedure have been described elsewhere (Ohtsuka and Asami, 1991a).

Figure 1 shows an example of the thermogravimetric curve for the gasification of Fe-loaded coal in steam. When the sample was heated at a rate of about 300 K/min, as is seen in the solid line in Figure 1, the coal devolatilization first took place, and after completion within a few minutes the char gasification started. The activity of Fe catalyst in the latter stage will be discussed throughout the paper. The reactivity of char after devolatilization is expressed by using two indexes: char conversion on a dry ash free and catalyst free basis, and the specific rate of char, that is, the gasification rate per unit weight of remaining char. Since the amount of volatile matter is needed for evaluating the reactivity of char, every sample was devolatilized in pure N_2 under the same heating conditions as above, to compare with reaction in steam, and the weight loss was regarded as the volatile matter for the gasification run. This example is also illustrated as the dotted line in Figure 1. The devolatilization experiment in pure N_2 was necessary especially for the catalyst-bearing coal showing large gasification reactivity, because it was difficult to distinguish the dividing point between the coal devolatilization and the following char gasification step in steam.

Data Processing. Raw data in the char gasification step shown in Figure 1 were processed by a personal computer system with a digitizer, and they were directly converted to both the char conversion vs reaction time figure and the specific rate vs char conversion figure with a plotter. In this processing, the ash content, the catalyst amount, the volatile matter, and more than 50 data points for each thermogravimetric curve were input into the computer system.

The same gasification run was repeated at least twice, the reproducibility being within ±5% or ±10% for char conversion or the specific rate, respectively. The apparent activation energy and frequency factor were calculated from the temperature dependence of specific rate by the least-squares method. The error for the activation energy was within ±6 or ±9 kJ/mol for noncatalyzed or Fe-catalyzed gasification, respectively.

Characterization. The amounts of Fe and Ca in the original and catalyst-loaded coal were determined by atomic absorption spectroscopy after extraction of metals from the coal with hot HCl for 2 h. The residual content of Cl in the coal was determined by a standard Eschka method (ISO 587-1981 (E)). X-ray diffraction (XRD) measurements of Fe-bearing coal and char were made with Mn-filtered Fe Kα radiation to clarify the chemical form and dispersion state of Fe catalyst. The char for XRD was prepared in a thermobalance in the same manner as the gasification run. The average crystallite size of Fe_3O_4 was determined by the Debye–Shörrer method.

Table I. Contents of Fe, Ca, and Cl in Coal

sample	additive	Fe (wt %)	Ca (wt %)	Cl (wt %)
Fe(U)	$(NH_2)_2CO$	3.4		0.04
Fe(C)$_H$	$Ca(OH)_2$	4.7	0.51	0.04
Fe(C)$_L$	$Ca(OH)_2$	1.0	0.16	
Fe(A)	NH_3/NH_4Cl	4.6		0.06
Fe(N)	none	0.95		0.66
Ca(E)			0.41	
original		0.02	0.07	0.08

Results

Fe, Ca, and Cl Contents. Table I shows the Fe, Ca, and Cl contents in the coal specimen used in this study. Most of Fe ions in $FeCl_3$ solution were actually loaded onto coal with Fe(C)$_H$, Fe(U), and Fe(A) catalysts. On the other hand, the actual loading for the Fe(N) catalyst was at the highest 1 wt %. The Ca retention was observed for both Fe(C) catalysts, which shows that some Ca ions from $Ca(OH)_2$ are exchangeable with COOH groups in brown coal (Ohtsuka and Tomita, 1986), and exchanged Ca cannot easily be removed by a simple water washing.

As is seen in Table I, the Cl contents in Fe(U), Fe(C), and Fe(A) samples were nearly equal to the level of Cl inherently present in the original coal. Thus, Cl ions from $FeCl_3$ were completely removed by water washing. On the other hand, some Cl, though small, was retained in the Fe(N) sample.

Gasification Reactivity. Figures 2 and 3 show the profiles for the steam gasification with different Fe catalysts at 973 and 1023 K, respectively. Every Fe catalyst showed activity in the gasification of char. The effectiveness was dependent on the catalyst type, in the sequence of Fe(A), Fe(N) < Fe(U) < Fe(C)$_H$. Char was completely gasified within 60 min at 973 K for the most active Fe(C)$_H$ catalyst. When the temperature was raised to 1023 K, the time required for the complete gasification was shortened to 25 min. With the Fe(U) catalyst char conversion at 973 K reached about 90% after 90 min, and the gasification at 1023 K was completed within 80 min. The activity of Fe(N) catalyst was comparable to that of Fe(A) catalyst in spite of a lower Fe loading. The conversion after 90 min at 973 K increased from 20% for original coal to about 60% in the presence of Fe.

Figure 4 illustrates the gasification profiles at 973 and 1023 K for the Fe(C)$_L$ catalyst. The reactivity of char was

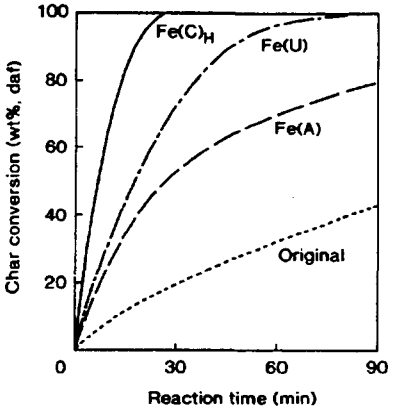

Figure 3. Steam gasification of Loy Yang coal with several Fe catalysts at 1023 K.

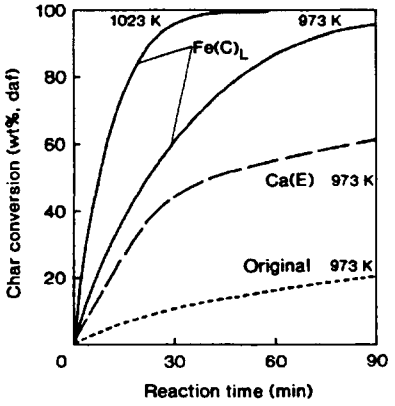

Figure 4. Steam gasification of Loy Yang coal with Fe and Ca catalysts at 973 and 1023 K.

largely enhanced in spite of small loading of 1 wt %: the conversion at 973 K reached more than 90% after 90 min and the gasification at 1023 K was complete within 60 min. The gasification rate with $Fe(C)_L$ catalyst was found to be higher than with Fe(U) catalyst with 3.4 wt % Fe (Figures 2 and 4). The reactivity of char with Ca(E) catalyst at 973 K is also shown in Figure 4, where the Ca loading, 0.4 wt %, is close to the Ca retention (0.5 wt %) in the $Fe(C)_H$ sample. The Ca(E) catalyst was active especially at the beginning of reaction, but the degree of rate enhancement seemed to level off in the higher conversion range.

Figure 5 shows the specific gasification rate as a function of char conversion for $Fe(C)_H$, Fe(U), Fe(A), and Fe(N) catalysts at 973 and 1023 K. The rates for Fe(A) and Fe(N) catalysts decreased gradually with increasing conversion. On the contrary, the rates for Fe(C) and Fe(U) catalysts increased gradually as the gasification proceeded, and especially the rates at these temperatures for the $Fe(C)_H$ catalyst increased exponentially at the latter stage of gasification. The initial rate in the conversion range of 10–20% with the $Fe(C)_H$ catalyst was about 20 times as large as that without catalyst irrespective of temperature. A 6–9-fold rate enhancement was observed in the initial step of the gasification with the Fe(U) catalyst.

Figure 6 illustrates the relationship between the specific rate and the conversion for $Fe(C)_L$ and Ca(E) catalysts. Initial gasification rates at 973 and 1023 K with the $Fe(C)_L$ catalyst were about 15 times those for original coal, and the degree of rate enhancement by this catalyst

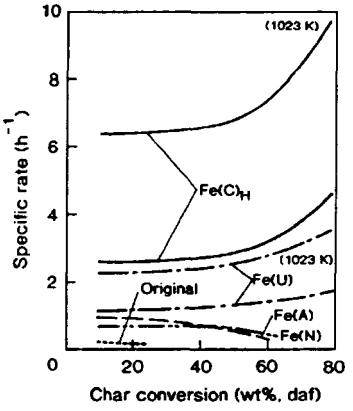

Figure 5. Profiles for specific gasification rates with several Fe catalysts at 973 and 1023 K.

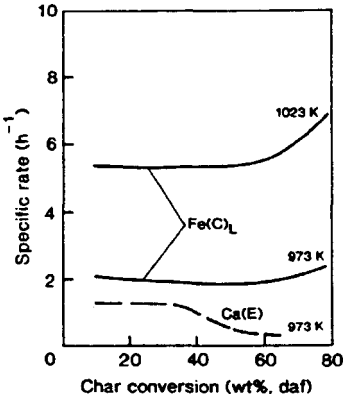

Figure 6. Profiles for specific gasification rates with Fe and Ca catalysts at 973 and 1023 K.

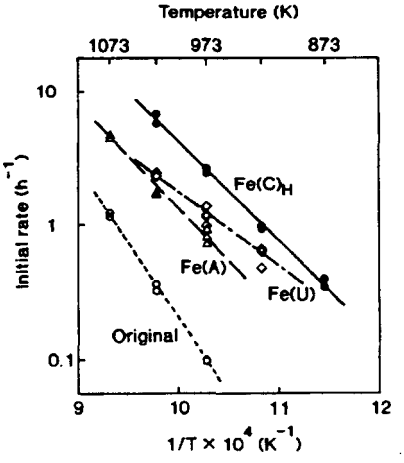

Figure 7. Arrhenius plots for noncatalyzed and Fe-catalyzed gasification.

increased with increasing conversion especially at the higher level, similarly as for the $Fe(C)_H$ catalyst. By contrast, the rate at 973 K with the Ca(E) catalyst decreased rapidly in the conversion range beyond 40%.

The Arrhenius plots for noncatalyzed and Fe-catalyzed gasification are shown in Figure 7, where the initial rate denotes the average specific rate in the conversion range of 10–20%. The apparent activation energies for $Fe(C)_H$, Fe(U), and Fe(A) catalysts and original coal were 140, 110, 160, and 190 kJ/mol, and the frequency factors were

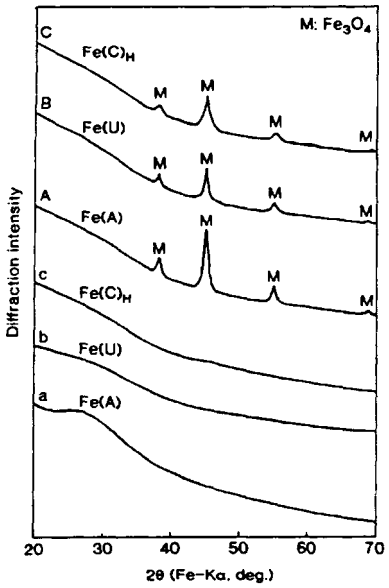

Figure 8. XRD patterns of Fe-bearing samples without heat treatment (a, b, c) and after devolatilization in steam at 973 K (A, B, C).

1.2×10^8, 6.6×10^5, 1.6×10^8, and 3.2×10^9 h^{-1}, respectively. The values of the activation energies show that the gasification rate is controlled by the chemical reaction step in every case. Not only the activation energy but also the frequency factor was lower in the presence of every Fe catalyst. These observations suggest that the Fe catalyst may not increase the number of reaction sites but may increase the rate of the limiting step in the reaction sequence.

The degree of lowering in the gasification temperature by Fe addition can also be evaluated from Figure 7. The difference in the temperature required for obtaining the reaction rate of 1 h^{-1} with and without catalyst was 140, 110, and 80 K for $Fe(C)_H$, Fe(U), and Fe(A) catalysts, respectively. Since the temperature difference can be regarded as an index that represents the catalyst effectiveness quantitatively, the sequence of the effectiveness based on this criterion was Fe(A) < Fe(U) < $Fe(C)_H$. This sequence agreed with that observed in the gasification profile (Figure 2). Accordingly the $Fe(C)_H$ catalyst was the most effective, and the presence of this catalyst lowered the temperature by 140 K.

Chemical Form and Dispersion. Figure 8 shows the XRD profiles for Fe-bearing samples without any heat treatment and immediately after completion of the devolatilization step in steam at 973 K. Any XRD lines attributable to Fe crystallites could not be detected for any of the untreated Fe-loaded coals (Figure 8a–c) including the Fe(N) sample (not shown in Figure 8). When the coals were devolatilized, only the XRD signals due to Fe_3O_4 appeared (Figure 8A–C). This observation was identical as predicted from phase diagrams for Fe–O–H and Fe–O–C systems (von Bogdandy and Engell, 1971). The XRD intensity of Fe_3O_4 on devolatilization was small in every case in spite of a relatively high Fe content (7–9 wt % Fe), showing the low crystallinity of Fe_3O_4, in other words, the high dispersion of Fe catalyst. The chemical form of Fe_3O_4 was retained throughout the subsequent char gasification in every Fe catalyst. No diffraction peaks of Ca species were detectable for the chars derived from the $Fe(C)_H$ sample with residual Ca because of a small quantity and the high degree of dispersion.

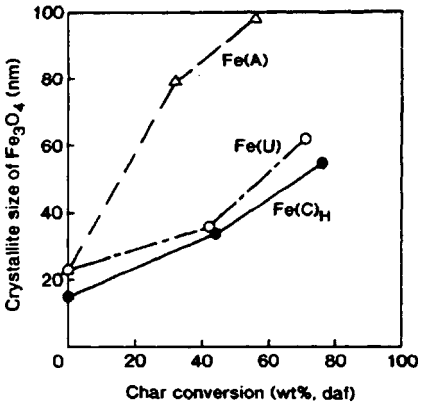

Figure 9. Relationship at 973 K between char conversion and average crystallite size of Fe_3O_4.

Figure 9 shows the change in average crystalline size of Fe_3O_4 as a function of char conversion at 973 K with $Fe(C)_H$, Fe(U) and Fe(A) catalysts. The size of Fe_3O_4 at the conversion of zero, namely, on devolatilization, was very small, 15–23 nm, for every catalyst. The size increased with conversion in each case because Fe_3O_4 particles agglomerated due to the consumption of char. However, the agglomeration behavior depended strongly on the catalyst type. The growth of Fe_3O_4 crystallites proceeded most slowly with the $Fe(C)_H$ catalyst showing the highest activity in steam gasification; the average size of Fe_3O_4 was as small as 55 nm even at the conversion of 75 wt %. The growth rate with the Fe(U) catalyst was a little larger despite a lower Fe loading, compared with the $Fe(C)_H$ catalyst. In the case of Fe(A) catalyst, on the other hand, Fe_3O_4 particles aggregated rapidly in the beginning step of gasification.

Discussion

Precipitated Iron. Urea is well-known to be effective for precipitation of pure metal salts from a homogeneous solution (Willard and Tang, 1937), and this method is applicable to the preparation of metal hydroxides as catalyst precursors (Kayama, 1974). When urea was used with $FeCl_3$ solution, fine particles of FeOOH precipitated on carbon (Kaneko et al., 1985). FeOOH particles were also formed by hydrolysis of $FeCl_3$ solution at elevated temperatures (Matijević and Scheiner, 1978; Musić et al., 1982). Therefore the Fe(U) and Fe(N) catalysts in the present study would also exist in the form of FeOOH. The chemical form of Fe(C) catalyst prepared by using $Ca(OH)_2$ was probably FeOOH because of precipitation in the same acidic region as in the preparation method using urea (Kayama, 1974). This form was also supported by the elemental analysis of Fe(C) sample. No XRD lines of Fe species were detectable with all these Fe catalysts, which suggests that FeOOH particles formed on brown coal are too fine to be detected by XRD. This corresponded to the observations by Mössbauer spectroscopy (Cook and Cashion, 1987; Ohtsuka et al., 1992) and extended X-ray absorption fine structure spectroscopy (Yamashita et al., 1991). Unfortunately, the preparation method using $Ca(OH)_2$ could not be successfully applied to some coals with lower oxygen contents or higher mineral contents than the present brown coal. These observations suggest that Fe^{3+} ions in the precipitation process interact strongly

with free oxygen-functional groups in no association with metal cations. Since Loy Yang coal with a very low content of minerals has a large number of exchangeable sites (Schafer, 1991), some Fe^{3+} ions in these precipitated catalysts may exchange with H^+ in COOH groups, as observed with the Fe(A) catalyst (Ohtsuka and Asami, 1991a).

Table I reveals that Fe(U), Fe(C), and Fe(A) catalysts are free from Cl contamination, but the Fe(N) catalyst contains some Cl ions. This difference may be related to the conversion extent of $FeCl_3$ to FeOOH. Most of the Fe^{3+} ions in $FeCl_3$ solution were incorporated into coal with these Cl-free catalysts, whereas only a small amount of Fe was loaded with the Fe(N) catalyst (Table I). The precipitation of FeOOH by hydrolysis of $FeCl_3$ in the absence of base would proceed mainly through the replacement of Cl ions by OH^- groups (Musić et al., 1982). The adsorption of Fe^{3+} ions on surface functional groups like COOH in coal would not be so easy in the strong, acidic region without any base, and the replacement would be incomplete. Consequently, the preparation of Fe(N) catalyst would be followed by a small Fe loading with some Cl retention.

Catalyst Effectiveness. When iron chloride or sulfate was loaded onto coal by the impregnation method where coal was soaked in the aqueous solution and then water was evaporated, the catalyst effectiveness for the steam gasification was quite small at low temperatures of around 950 K (Ohtsuka et al., 1987; Ohtsuka and Asami, 1991a), whereas the effectiveness was improved at higher temperatures and in the coexistence of H_2 (Kasaoka et al., 1979; Hüttinger and Schleicher, 1981). However, the evolution of Cl- or S-containing gas during gasification was inevitable, and it caused some serious problems like corrosion. Thus, our target is to prepare active Fe catalysts without such pollutants. The preparation method using NH_3/NH_4Cl solution has enabled the incorporation of a large amount of Cl-free Fe ions into low-rank coals from $FeCl_3$ solution (Ohtsuka and Asami, 1991a). However, the use of NH_3, which is more expensive than $FeCl_3$, would not be practically feasible.

In the present study, when inexpensive $Ca(OH)_2$ was used instead of NH_3/NH_4Cl, a much more effective Fe(C) catalyst was prepared, and consequently the complete gasification was achieved. The higher the Fe loading and the temperature were, the shorter the time required for the complete gasification was (Figures 2–4). Such an extremely large activity of Fe(C) catalyst is ascribed probably to a high degree of catalyst dispersion not only on devolatilization but also at the latter stage of gasification (Figure 9). The retention of a small amount of Ca from $Ca(OH)_2$ in the Fe(C) catalyst may suggest the synergetic effect of Fe and Ca on the gasification. However, the contribution of residual Ca to the rate enhancement by Fe(C) catalyst would be minor at least in the latter part of gasification, because the intrinsic activity of finely dispersed FeOOH was high as in the Fe(U) catalyst (Figure 2) and the change in rate with conversion was different between the Fe(C) and Ca(E) catalysts (Figures 5 and 6). The Ca retention is rather favorable to in situ sulfur removal during gasification. The Ca incorporated into coal can efficiently capture the sulfur-containing gas evolved during steam gasification despite differential reaction conditions like the fixed bed gasification (Ohtsuka and Asami, 1991b).

It may be noteworthy from a practical point of view that the Fe(N) catalyst promoted the gasification at a low loading of 1 wt %, since the Fe(N) catalyst can be prepared simply, and most of the Cl in $FeCl_3$ may be recovered as HCl during preparation. The relatively high activity of Fe(N) catalyst might be attributable to the monodispersed state of FeOOH particles formed by hydrolysis (Matijević, 1981).

Catalyst State, Activity, and Behavior. Although many studies on the Fe-catalyzed gasification have been carried out so far, it seems very elusive to determine the actual catalytically-active species during the gasification in the oxidizing gas like steam, because the chemical form of Fe catalyst is very sensitive to the temperature and atmosphere in the vicinity of catalyst particles. Our previous study using an in situ high-temperature XRD technique has shown that the gasification rate is enhanced even under the conditions where Fe_3O_4 alone is stable (Ohtsuka et al., 1986). In the present study, every precipitated Fe, probably FeOOH, on brown coal was reduced to Fe_3O_4, which was the only stable species detected by XRD and catalytically active in every case. However, these observations do not necessarily mean that Fe_3O_4 is the actual active species because of the bulk chemical form identified by XRD. Since H_2 evolved during gasification and Fe particles readily reacted with carbon (Ohtsuka and Asami, 1991a), the surface of Fe_3O_4 may be in a higher reduced state. Thus, the gasification may proceed through the oxygen-transfer mechanism involving the redox cycle of iron oxides (McKee, 1981; Hüttinger et al., 1986). A recent EXAFS study suggests that the highly dispersed FeOOH may play an important role as the intermediate for this mechanism (Yamashita et al., 1991). If the present gasification is the case, the chemical form of precipitated catalyst, FeOOH, may be maintained up to the gasification step.

As is shown in Figure 9, the sequence of the agglomeration rate of Fe_3O_4 crystallites was F(C) < Fe(U) ≪ Fe(A), which means that the degree of catalyst dispersion during gasification is high in the order of Fe(A) ≪ Fe(U) < Fe(C). This order corresponded to the sequence of catalyst effectiveness, Fe(A) < Fe(U) < Fe(C). These findings show that the dispersion of Fe_3O_4 particles is a suitable index to elucidate the catalytic behavior of precipitated iron.

It has been reported by many investigators that the specific rate of the Fe-catalyzed gasification drops as the reaction proceeds (Hippo et al., 1979; Adler and Hüttinger, 1984; Furimsky et al., 1988). Contrarily, the rates for Fe(U) and Fe(C) catalysts increased exponentially in the latter part of gasification (Figures 5 and 6). The change in specific rate with char conversion would be determined by the balance between catalyst agglomeration and enrichment due to the consumption of char, since the surface area of the char from catalyst-loaded brown coal was not changed significantly with the extent of reaction (Tomita et al., 1985). The rapid agglomeration of catalyst particles observed for the Fe(A) catalyst resulted in the decreased gasification rate with conversion. When the agglomeration rate was rather small as with Fe(U) and Fe(C) catalysts (Figure 9), however, the catalyst enrichment, in other words, the increase of catalytically active sites per unit of remaining char, would be predominant and consequently the gasification rate increased as the reaction proceeded. The present exponential rate increase is, to the authors' knowledge, the first example observed in Fe-catalyzed gasification, though similar phenomena have been shown frequently in K-catalyzed gasification where no catalyst agglomeration occurs because of the liquidlike state (Verra and Bell, 1979; Takarada et al.,

1983; van Heek and Mühlen, 1991). Further study on the behavior of Fe(U) and Fe(C) catalysts should be made.

Conclusions

Iron catalysts are precipitated onto brown coal from $FeCl_3$ solution by several methods, and their activities in steam gasification are examined. The conclusions can be summarized as follows:

1. All the catalysts promote the gasification at low temperatures of around 950 K, but the effectiveness depends strongly on the preparation method.

2. The use of $Ca(OH)_2$ gives the most effective iron catalyst, which is Cl-free and contains a small amount of Ca.

3. The gasification rate with the most active catalyst at 5 wt % Fe is about 20 times that without iron, and increases as the reaction proceeds. This catalyst realizes complete gasification within a short time.

4. FeOOH as a probable precipitated form is reduced to finely dispersed Fe_3O_4 particles on coal devolatilization, and this form is held during gasification. The sequence of catalyst effectiveness among these catalysts can be correlated with the degree of Fe_3O_4 dispersion.

Acknowledgment

Ms. Naoko Yoshida and Ms. Naomi Katahira are gratefully acknowledged for their assistance in carrying out experiments. This work was partly supported by a Grant-in-Aid for Scientific Research from the Ministry of Education, Science and Culture, Japan (Nos. 0245082 and 03203204). We also thank Prof. Y. Nishiyama of our Institute and Prof. H. Sasaki and Dr. A. Muramatsu of the Institute for Advanced Materials Processing for their helpful discussions. The Coal Corporation of Victoria, Australia, is appreciated for kindly supplying Loy Yang brown coal.

Nomenclature

$Ca(E)$ = calcium catalyst prepared by ion exchange
$Fe(A)$ = iron catalyst prepared with ammonia
$Fe(C)_H$ = iron catalyst prepared with $Ca(OH)_2$, high loading
$Fe(C)_L$ = iron catalyst prepared with $Ca(OH)_2$, low loading
$Fe(N)$ = iron catalyst prepared by hydrolysis
$Fe(U)$ = iron catalyst prepared with urea

Literature Cited

Adler, J.; Hüttinger, K. J. Mixtures of Potassium Sulphate and Iron Sulphate as Catalysts for Water Vapour Gasification of Carbon 1. Kinetic Studies. *Fuel* **1984**, *63*, 1393–1396.

Cook, P. S.; Cashion, J. D. Mössbauer Study of Iron Exchanged into Victorian Brown Coal. *Fuel* **1987**, *66*, 661–668.

Figueiredo, J. L., Moulijn, J. A., Eds. *Carbon and Coal Gasification*; NATO ASI Series; Martinus Nijihoff Publishers: Dordrecht, 1986.

Furimsky, E.; Sears, P.; Suzuki, T. Iron-Catalyzed Gasification of Char in CO_2. *Energy Fuels* **1988**, *2*, 634–639.

Hippo, E. J.; Jenkins, R. G.; Walker, P. L., Jr. Enhancement of Lignite Char Reactivity to Steam by Cation Addition. *Fuel* **1979**, *58*, 338–344.

Hüttinger, K. J.; Schleicher, P. Kinetics of Hydrogasification of Coke Catalysed by Fe, Co, and Ni. *Fuel* **1981**, *60*, 1005–1012.

Hüttinger, K. J.; Adler, J.; Hermann, G. Iron-Catalyzed Water Vapour Gasification of Carbon, In *Carbon and Coal Gasification*; Figueiredo, J. L., Moulijn, J. A., Eds.; NATO ASI Series; Martinus Nijihoff Publishers: Dordrecht, 1986; pp 213–229.

Kaneko, K. Anomalous Micropore Filling of NO on α-FeOOH-Dispersed Activated Carbon Fibers. *Langmuir* **1987**, *3*, 357–363.

Kaneko, K.; Ozeki, S.; Inouye, K. The Adsorption of Nitrogen Monoxide on Iron-Treated Activated Carbon Fibers. *J. Chem. Soc. Jpn.* **1985**, 1351–1359.

Kasaoka, S.; Sakata, Y.; Yamashita, H.; Nishino, T. Effects of Catalysis and Composition of Inlet Gas on Gasification of Carbon and Coal. *J. Fuel Soc. Jpn.* **1979**, *58*, 373–386; *Int. Chem. Eng.* **1981**, *21*, 419–434.

Kayama, I. Catalyst Preparation by a Homogeneous Precipitation Method. *Catalyst (J. Catal. Soc. Jpn.)* **1974**, *16*, 18–24.

Matijević, E. Monodispersed Metal (Hydrous) Oxides-A Fascinating Field of Colloid Science. *Acc. Chem. Res.* **1981**, *14*, 22–29.

Matijević, E.; Scheiner, P. Ferric Hydrous Oxide Sols. III. Preparation of Uniform Particles by Hydrolysis of Fe(III)-Chloride, -Nitrate, and -Perchlorate Solutions. *J. Colloid Interface Sci.* **1978**, *78*, 509–524.

McKee, D. W. The Catalyzed Gasification Reaction of Carbon. *Chem. Phys. Carbon* **1981**, *16*, 1–118.

Misono, M.; Miyamoto, A.; Wada, K. Catalytic Coal Gasification to Produce Super-Clean Fuels. *Appl. Catal.* **1990**, *65*, N14–N15.

Moulijn, J. A., Kapteijn, F., Eds. Special Issue of the International Symposium "Fundamentals of Catalytic Coal and Carbon Gasification". *Fuel* **1986**, *65*, 1324–1478.

Musić, S.; Vértes, A.; Simmons, G. W.; Czakó-Nagy, I.; Leidheiser, H., Jr. Mössbauer Spectroscopic Study of the Formation of Fe(III) Oxyhydroxides and Oxides by Hydrolysis of Aqueous Fe(III) Salt Solutions. *J. Colloid Interface Sci.* **1982**, *85*, 256–266.

Ohtsuka, Y.; Tomita, A. Calcium Catalysed Steam Gasification of Yallourn Brown Coal. *Fuel* **1986**, *65*, 1653–1658.

Ohtsuka, Y.; Asami, K. Steam Gasification of Low-Rank Coals with a Chlorine-Free Iron Catalyst from Ferric Chloride. *Ind. Eng. Chem. Res.* **1991a**, *30*, 1921–1926.

Ohtsuka, Y.; Asami, K. In Situ Sulfur Capture during the Calcium-Catalyzed Gasification of Illinois No. 6 Coal. In *Coal Science and Technology*; Dugan, P. R., Quigley, D. R., Attia, Y. A., Eds.; Elsevier: Amsterdam, 1991b; Vol. 18, pp 139–151.

Ohtsuka, Y.; Kuroda, Y.; Tamai, Y.; Tomita, A. Chemical Form of Iron Catalysts during the CO_2-Gasification of Carbon. *Fuel* **1986**, *65*, 1476–1478.

Ohtsuka, Y.; Tamai, Y.; Tomita, A. Iron-Catalyzed Gasification of Brown Coal at Low Temperatures. *Energy Fuels* **1987**, *1*, 32–36.

Ohtsuka, Y.; Asami, K.; Yamada, T.; Homma, T. Large Rate Enhancement by Iron Catalyst in the Low Temperature Hydrogasification of Brown Coal under Pressure. *Energy Fuels* **1992**, *6*, 678–679.

Schaefer, H. N. S. Functional Groups and Ion Exchange Properties. In *the Science of Victorian Brown Coal: Structure, Properties and Consequence for Utilization*; Durie, R. A., Ed.; Butterworth-Heinemann: Oxford, 1991; pp 323–357.

Takarada, T.; Ohtsuka, Y.; Tomita, A.; Tamai, Y. Activity Sequence of Catalysts on Catalytic Coal Gasification. Effect of Coal Type and Gasifying Agent. *J. Fuel Soc. Jpn.* **1983**, *62*, 414–420.

Tomita, A.; Yuhki, Y.; Higashiyama, K.; Takarada, T.; Tamai, Y. Physical Properties of Yallourn Char during the Catalyzed Steam Gasification. *J. Fuel Soc. Jpn.* **1985**, *64*, 402–408.

van Heek, K. H.; Mühlen, H.-J. Chemical Kinetics of Carbon and Char Gasification. In *Fundamental Issues in Control of Carbon Gasification Reactivity*; Lahaye, J., Ehrburger, P., Eds.; NATO ASI Series; Kluwer Academic Publishers: Dordrecht, 1991; pp 1–34.

Verra, M. J.; Bell, A. T. Effect of Alkali Metal Catalysts on Gasification of Coal Char. *Fuel* **1979**, *57*, 194–200.

von Bogdandy, L.; Engell, H.-J. *The Reduction of Iron Ores—Scientific Basis and Technology* (Engl. Ed.); Springer-Verlag; New York, 1971; p 243.

Willard, H. H.; Tang, N. K. A Study of the Precipitation of Aluminum Basic Sulfate by Urea. *J. Am. Chem. Soc.* **1937**, *59*, 1190–1196.

Yamashita, H.; Yoshida, S.; Tomita, A. Local Structures of Metals Dispersed on Coal. 2. Ultrafine FeOOH as Active Iron Species for Steam Gasification of Brown Coal. *Energy Fuels* **1991**, *5*, 52–57.

Received for review April 20, 1992
Revised manuscript received October 29, 1992
Accepted April 19, 1993

Reprinted from ENERGY & FUELS, 1993, 7.

Selective Conversion of Coal Nitrogen to N_2 with Iron

Yasuo Ohtsuka,* Hiroshi Mori, Katsutoshi Nonaka, Takashi Watanabe, and Kenji Asami

Research Center for Carbonaceous Resources, Institute for Chemical Reaction Science, Tohoku University, Katahira, Aoba-ku, Sendai 980, Japan

Received June 3, 1993. Revised Manuscript Received August 3, 1993•

Brown coal with iron catalyst precipitated from $FeCl_3$ solution has been pyrolyzed in He or H_2 at 600–900 °C with a fluidized bed reactor. The presence of the iron at loadings of 3–7 wt % changes dramatically the fate of coal nitrogen during pyrolysis at 900 °C; 50–60% of coal nitrogen is readily converted to N_2, resulting in a low residual nitrogen in the char. Changing the fluidizing gas from He to H_2 shows no significant effect on the conversion to N_2. It is probable that ultrafine iron particles of around 50 nm in the reduced state are responsible for the present nitrogen removal.

Nitrogen oxides (NO_x) emitted from coal combustion to generate electricity have been implicated in acid rain and photchemical smog. Considerable effort has therefore been devoted to reduce the NO_x emissions by combustion modification and flue gas treatment.[1-3] However, since 75–95% of the NO_x emissions originates from coal nitrogen in pulverized coal-fired boilers,[2,3] the removal of nitrogen prior to coal combustion would be one of the most essential approaches to meet more stringent regulations on NO_x emissions. As is well-known, coal nitrogen is present predominantly as the thermally stable aromatic ring structures like pyridines and pyrroles.[4,5] The physical removal seems almost impossible accordingly, but the conversion of coal nitrogen into inert substances may be feasible. The present article shows a novel nitrogen removal method of converting coal nitrogen mainly into N_2 gas during the pyrolysis with iron in an inert atmosphere.

Loy Yang brown coal of size fraction 150–250 μm was used; the ultimate analysis was C 65.9; H 4.7; N 0.60; S 0.27; and O 28.5 wt % (daf). The iron catalyst was precipitated onto coal from an aqueous solution of $FeCl_3$ by using $Ca(OH)_2$; $Ca(OH)_2$ powder was added into the mixture of coal particles and $FeCl_3$ solution during stirring at room temperature, and then the Fe-bearing coal was separated from the solution by filtration. The procedure has been described in more detail elsewhere.[6]

Pyrolysis experiments were carried out with a fluidized bed reactor; coal particles (5 g) were first fluidized in atmospheric He or H_2 of 0.2 L(STP)/min, and then heated at 600–700 °C/min up to 600–900 °C by elevating the preheated, transparent electric furnace, the solid residence time being 10 min. The reactor effluent was collected as gas in a plastic bag after being passed two traps. For some materials recovered from the first trap heated at 120 °C, the fraction soluble in tetrahydrofuran is denoted as tar throughout the paper, the remainder being as coke which includes a small amount of char entrained from the reactor. The material condensed in the second trap cooled at −70 °C is denoted as oil, which includes water. The char remained in the reactor was also recovered. The material balance for every run revealed that 92–97 wt % of coal fed could be recovered as gas, oil, tar, coke, and char. The product distribution at 900 °C and 3–7 wt % Fe was gas, 27–31; oil, 9–14; tar, 5–6; coke, 1–2; and char, 46–47 wt %. Coal nitrogen evolution was monitored in terms of N_2 and the nitrogen contents of tar and char, but HCN and NH_3 were not determined because the quantitative analysis was difficult due to being soluble in water evolved from coal and iron catalyst. The reproducibility of the results was within ±5%.

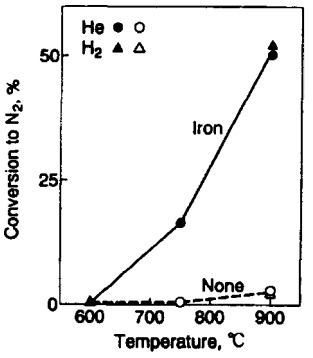

Figure 1. Conversion of coal nitrogen to N_2 during pyrolysis at different temperatures under atmospheric pressure.

Figure 1 illustrates the effects of pyrolysis temperature, catalyst addition, and fluidizing gas on the conversion of coal nitrogen to N_2. The conversion without catalyst slightly increased with increasing temperature, and it was very small, less than 3% even at 900 °C. Major nitrogen-containing gas would be HCN in this temperature region.[7,8] In contrast with the uncatalyzed pyrolysis, the conversion to N_2 with catalyst, at 7 wt % Fe, increased considerably

* Author to whom correspondence should be addressed.

• Abstract published in *Advance ACS Abstracts*, October 1, 1993.

(1) Hjalmarsson, A-K. In *NOx Control Technologies for Coal Combustion*; IEA Coal Research: London, 1990; IEACR/24, pp 1–62.

(2) Unsworth, J. F.; Barratt, D. J.; Roberts, P. T. In *Coal Quality and Combustion Performance*; Coal Science and Technology Vol. 19; Elsevier: Amsterdam, 1991; pp 579–590.

(3) Boardman, R.; Smoot, L. D. In *Fundamentals of Coal Combustion for Clean and Efficient Use*; Smoot, L. D., Ed.; Coal Science Technology Vol. 20; Elsevier: Amsterdam, 1993; pp 433–509.

(4) Solomon, P. R.; Colket, M. B. *Fuel* 1978, *57*, 749–755.

(5) Whitehurst, D. D. In *Organic Chemistry of Coal*; Larsen, J. W., Ed.; ACS Symposium Series 71; American Chemical Society: Washington DC, 1978; pp 1–35.

(6) Asami, K.; Ohtsuka, Y. *Ind. Eng. Chem. Res.* 1993, *32*, 1631–1636.

(7) Nelson, P. F.; Kelly, M. D.; Wornat, M. J. *Fuel* 1991, *70*, 403–407.

(8) Chen, J. C.; Castagnoli, C.; Niksa, S. *Energy Fuels* 1992, *6* 264–271.

0887-0624/93/2507-1095$04.00/0

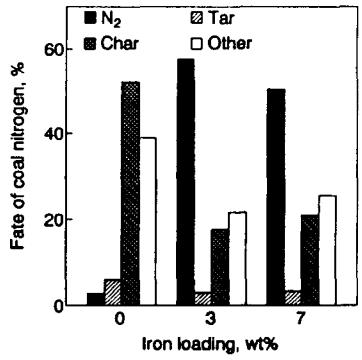

Figure 2. Fate of coal nitrogen during pyrolysis in He at 900 °C.

with increasing temperature, and it reached 50% at 900 °C. Thus, the amount of N_2 formed at 900 °C was drastically enhanced by iron addition, and it was about 20 times that without iron. When the fluidizing gas in the iron-catalyzed pyrolysis at 900 °C was changed from He to H_2, as is seen in Figure 1, no further improvement on the conversion to N_2 was observed. This finding is noteworthy from a practical point of view, because expensive H_2 is unnecessary for this conversion.

The fate of coal nitrogen during the pyrolysis in He at 900 °C is illustrated in Figure 2, where the difference in the nitrogen balance is labeled as "other", which includes HCN, NH_3, and oil nitrogen. Nearly 60% of coal nitrogen was converted into N_2 even at a low loading of 3 wt % Fe. Further increase in the loading from 3 to 7 wt % showed almost no improvement on the conversion, but rather a slight decrease, which may suggest the presence of the optimum loading. Not only the tar yield but also the nitrogen content in the tar was lower in the presence of the iron catalyst, and consequently the conversion to tar nitrogen at 3 wt % Fe was less than half of that without iron (Figure 2). The char yield increased slightly from 44 wt % without iron to 46 and 47 wt % at 3 and 7 wt % Fe, respectively. On the contrary, the nitrogen contents in Fe-bearing chars were lower, and they were almost one-third of that without iron. Figure 2 shows as a result that the Fe-bearing chars retain only 18–21% of coal nitrogen, whereas the original char does 50%. The change of the fluidizing gas from He to H_2 had no significant effect on the conversion to char nitrogen, as observed in the formation of N_2 (Figure 1). As is seen in Figure 2, the conversion of coal nitrogen to other nitrogen-containing compounds was also reduced by catalyst addition.

It has been shown that the iron precipitated onto brown coal by the present method exists in the form of fine particles of FeOOH.[6] The X-ray diffraction measurements revealed that FeOOH remained partly oxidized after the pyrolysis in He or H_2 at 750 °C, but it was completely reduced to α-Fe and Fe_3C at 900 °C irrespective of the fluidizing gas. Thus, the kind of the gas did not affect any crystalline form of iron catalyst, indicating the evolution of sufficient reducing gases such as H_2, CO, and hydrocarbons for catalyst reduction. This is the probable reason why the use of H_2 instead of He had no effect on the fate of coal nitrogen. The transmission electron microscope showed that the particle size of the iron catalyst was as small as 30–50 nm at 900 °C. The finely dispersed catalyst in the reduced state would be responsible for the present nitrogen removal.

Some mechanisms can be speculated for the dramatically increased conversion to N_2 and consequent decreased residual nitrogen in the char with the iron catalyst. When coal is pyrolyzed, coal nitrogen can initially be either retained in the char or released as volatile nitrogen, which can then be decomposed into HCN, NH_3, and tar nitrogen.[4] Part of the volatile nitrogen may also be reincorporated into carbon and soot may be formed during the secondary decomposition,[7,8] which results in the increased nitrogen retention in the char. Since metal particles finely dispersed on coal can catalyze secondary decomposition reactions of the volatiles released during pyrolysis,[9-11] the present iron may change the fate of volatile nitrogen. In other words, the nitrogen may be converted selectively to N_2 and nitrogen-free (or nitrogen-poor) carbon on the catalyst surface. Another speculated mechanism is that the iron catalyst may promote the reactions to extract N_2 from char. The first mechanism may be more predominant, since the occurrence of the latter solid-catalyzed solid-phase reactions is not so easy because of small chance of contact between char nitrogen and iron particles.

In conclusion, when brown coal with fine iron particles is pyrolyzed in an inert gas at 900 °C, 50–60% of coal nitrogen can easily be converted to N_2 with the corresponding low nitrogen retention in the char.

Acknowledgment. We thank the Iketani Science and Technology Foundation for partial financial support and Miss N. Katahira for help with elemental analyses.

(9) Tyler, R. J.; Schafer, H. N. S. *Fuel* **1980**, *59*, 487–494.
(10) Franklin, H. D.; Cosway, R. G.; Peters, W. A.; Howard, J. B. *Ind. Eng. Chem. Process Design Dev.* **1983**, *22*, 39–42.
(11) Tomita, A.; Watanabe, Y.; Takarada, T.; Ohtsuka, Y.; Tamai, Y. *Fuel* **1985**, *64*, 795–800.

Wise et al. (Eds.), Calcium Magnesium Acetate

Chapter 10

CATALYTIC GASIFICATION OF LOW-RANK COALS WITH CALCIUM ACETATE

Yasuo OHTSUKA[1] and Akira TOMITA[2]
[1]Coal Chemistry Laboratory
[1,2]Chemical Research Institute of Non-Aqueous Solutions, Tohoku University, Katahira, Sendai 980 (Japan)

10.1 INTRODUCTION

Catalytic coal gasification has attracted increasing attention, because a lowering of the gasification temperature has several advantages, such as the direct production of methane, less severe material problem and the use of waste heat. Therefore a number of studies on the catalytic gasification have been carried out, as is reflected by the increasing research effort (refs. 1,2). Among many catalysts reported so far (refs. 3,4), it has been generally accepted that alkali metal compounds like K_2CO_3 are the most effective catalysts for the steam gasification of coal.

In previous works (refs. 5-7), we have found that nickel catalyst markedly promotes the steam gasification of brown coal at low temperatures, around 800 K. K_2CO_3 is inactive in this temperature region. The continuous fluidized bed gasification of brown coal with nickel has shown that more than 80 wt% of the coal is converted to very clean gas containing neither tarry materials nor H_2S (ref. 8) and methane-rich gas is directly produced under pressure (ref. 9). We believe that the realization of such a low temperature gasification with less expensive catalysts than nickel should be a final target for the catalytic coal gasification. Therefore we have recently started the study on the development of cheap and disposable catalysts in place of nickel. It has been found that iron catalyst in hydrogen exhibits a high activity comparable to that of nickel catalyst (refs. 10,11), and active, chlorine-free alkali catalysts can easily be prepared from aqueous solutions of NaCl and KCl (refs. 12,13).

Cheap calcium compounds are also one of the promising disposable raw materials as gasification catalysts. With low rank coals, some calcium are inherently present with carboxyl functional groups and these exchangeable calcium cations promote the steam gasification (refs. 14-16). When the catalyst effectiveness of externally-added calcium is examined, these raw coals are usually demineralized with HCl-HF aqueous solution before the incorporation of calcium cations into the acid sites. However, the residual halogen in the demineralized coals may deactivate the calcium catalyst (ref. 17). In most studies, calcium-loaded coals are devolatilized at >1000 K prior to the gasification, but the pretreatment at high temperatures accelerates the

agglomeration of catalyst particles (refs. 18,19). Consequently the activity of calcium catalyst may be deteriorated.

We have reported that, without both demineralization and heat treatment, the calcium impregnated on coal is very effective for the steam gasification even at low temperatures of around 950 K (refs. 20-22). In the present work, we will investigate the steam gasification of low rank coals with $Ca(CH_3COO)_2$ in detail in order to clarify some factors controlling the catalyst effectiveness of this compound, for example, the conditions of catalyst preparation, the co-existence of $Mg(CH_3COO)_2$, the coal type, the amount of inherent calcium, and the reaction temperature.

10.2 EXPERIMENTAL

10.2.1 Coal sample

Nine low rank coals from four countries were used, the starting size of coal particles being 1-2 mm in diameter in every case. Among them an Australian Yallourn brown coal was investigated in detail. It was received in a briquette form and then crushed into particles of 1-2 mm in diameter. The ultimate and proximate analyses of all coals used are given in Table 10.1. The amount of exchangeable calcium ions inherently present in coal was determined by leaching with 1 N ammonium acetate solution (ref. 16). The details of the procedure have been described elsewhere (ref. 23).

TABLE 10.1

Ultimate and proximate analyses of coals.

Coal	Code	Country	Ultimate analysis (wt%, daf)					Proximate analysis (wt%, dry)		
			C	H	N	S	O	VM[a]	Ash	FC[a]
Rhein Braun	RB	F.R.G.	65.8	5.5	0.8	0.3	27.6	54.8	2.9	42.3
Yallourn	YL	Australia	67.1	4.8	0.8	0.3	27.0	55.2	0.9	43.9
Morwell	MW	Australia	67.9	5.0	0.5	0.3	26.3	51.6	1.5	46.9
Velva	VL	U.S.A.	69.1	4.9	1.4	0.6	24.0	47.7	8.8	43.5
South Beulah	SB	U.S.A.	71.6	4.8	1.4	2.9	19.3	38.6	13.7	47.7
Colowyo	CW	U.S.A.	74.0	5.0	1.9	0.4	18.7	36.3	6.3	57.4
Wandoan	WD	Australia	75.8	6.8	1.0	0.3	16.1	53.9	16.9	29.2
Taiheiyo	TH	Japan	77.0	6.3	1.5	0.3	14.9	49.4	11.5	39.1
Illinois No.6	IL	U.S.A.	77.0	5.2	1.5	3.6	12.7	38.9	10.9	50.2

[a]VM, volatile matter; FC, fixed carbon.

10.2.2 Catalyst material and addition

$Ca(CH_3COO)_2$ was usually used as a catalyst precursor among different calcium compounds examined. Water-soluble salts like $Ca(CH_3COO)_2$, $Ca(NO_3)_2$ and $CaCl_2$ were impregnated on raw coal by grinding coal particles in their aqueous solutions. For water-insoluble salts like $Ca(OH)_2$, $CaCO_3$, CaS and $CaSO_4$ they were kneaded with coal in water. The resultant mixture was then dried at 380 K in a N_2 stream. In order to make clear the gasification activity of calcium magnesium acetate (CMA), $Ca(CH_3COO)_2$ and $Mg(CH_3COO)_2$ were simultaneously impregnated on coal in the same way as above. Furthermore, for comparison of the effectiveness of calcium catalyst, K, Mg, Ba, Fe and Ni as well as Ca were impregnated on coal from aqueous solutions of nitrates. In every case a nominal catalyst content is expressed as wt% of metal in the dried sample.

10.2.3 Steam gasification

The gasification experiments were carried out with an atmospheric thermobalance (Shinku-Riko, TGD-3000). The coals (about 20 mg) mounted onto a quartz cell were rapidly heated at a rate of about 300 K/min in a H_2O (66 kPa)/N_2 stream, and soaked for 2 h at a constant temperature, usually 923 K. Since raw coal was used in all runs instead of devolatilized char as a starting material, the reaction consisted of the coal devolatilization and subsequent char gasification stages. The reactivity of char in the latter stage will be discussed throughout the present paper. Data is processed as follows. Char conversion is expressed as wt% on a dry, volatile-free, ash-free, catalyst-free basis. The specific rate of char, the gasification rate per the unit weight of residual char, was almost independent of the conversion up to 50-60 %. Thus the average rate in this range was used as an index for the reactivity of char.

10.2.4 Characterization of catalyst

X-ray diffraction analysis (XRD) was carried out by using Cu-Kα radiation (45 kV x 30 mA) to characterize calcium catalyst in the coal devolatilization step prior to char gasification. The samples for XRD were prepared in a thermobalance by heating calcium-loaded coals in pure N_2 and then quenching the resulting chars to room temperature. Unless otherwise stated, the heating conditions were as follows: heating rate, 300 K/min; devolatilization temperature, 923 K; soaking time, 5 min. Temperature changes in chemical form of $Ca(CH_3COO)_2$ physically-mixed with YL coal were followed *in situ* by using a high temperature X-ray diffraction (HTXRD; Shimadzu XD3A/HX3) technique (refs. 21,24). The HTXRD measurements were carried out during heating the samples up to 923 K at a rate of 10 K/min in a N_2 stream. The average crystallite size of calcium species was determined by the Debye-Scherrer method.

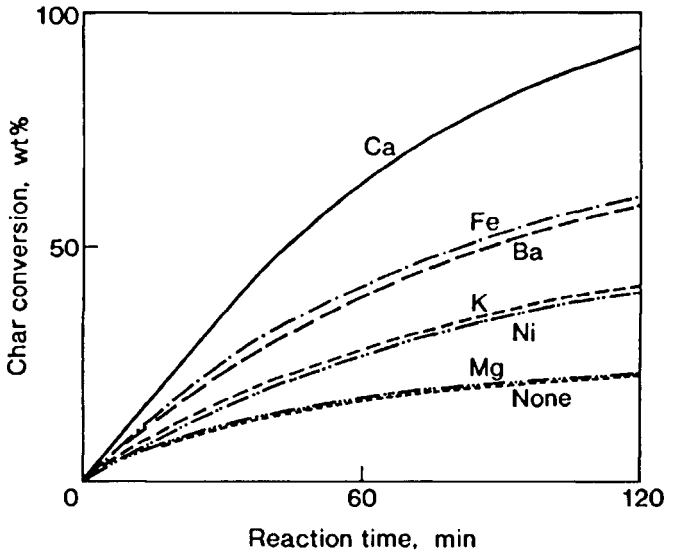

Fig. 10.1 Gasification profile of Yallourn brown coal with various metal nitrates at 923 K.

10.3 RESULTS

10.3.1 Calcium and other metals

Figure 10.1 illustrates the gasification profile of YL coal with several metals at a loading of 1 %. Magnesium was inactive, but all the other metals exhibited the catalytic effect. Among active catalysts the calcium was most effective; char conversion at 923 K reached more than 90 % in 120 min. Interestingly, iron was more active than nickel, and barium was less active than calcium. The rate enhancement by nickel or potassium was small at a low loading of 1 %.

10.3.2 Calcium compounds

Figure 10.2 illustrates the influence of the kind of calcium salts on the gasification reactivity of YL coal. The calcium loading was 5 %. The catalysts from $Ca(CH_3COO)_2$, $Ca(NO_3)_2$, $Ca(OH)_2$ and $CaCO_3$ enhanced the gasification rate to a quite similar extent. Coal was completely gasified within 60-70 min in every case. It is noteworthy from a practical point of view that cheap $Ca(OH)_2$ and $CaCO_3$ are effective. The details of the coal gasification with $Ca(OH)_2$ have been described elsewhere (refs. 20,22). $CaCl_2$ and CaS also promoted the gasification, and the degree of rate enhancement by these compounds was slightly lower than that of above four salts. Since some Cl- or S-containing compounds evolved during the gasification with $CaCl_2$ or CaS would cause some problems like corrosion, the practical use of these compounds seems not so easy. The catalyst from $CaSO_4$ showed only a slight activity.

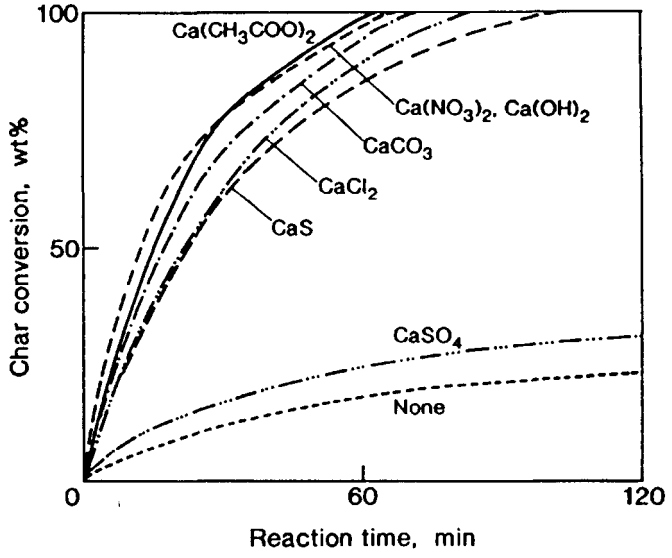

Fig. 10.2 Gasification reactivity of Yallourn coal with different calcium compounds at 923 K.

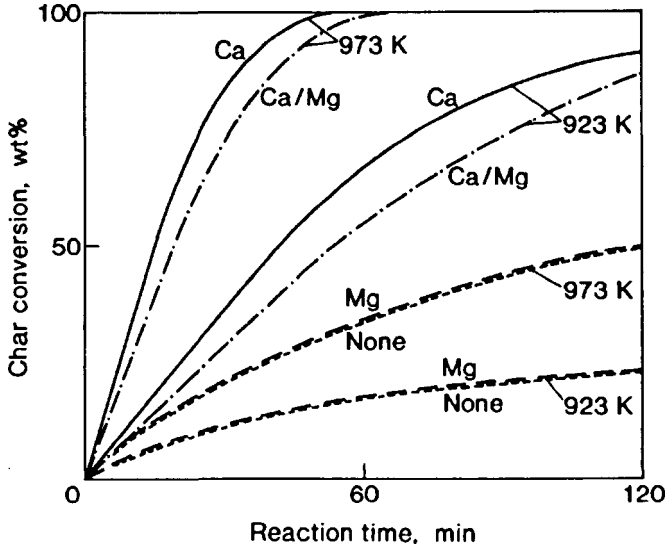

Fig. 10.3 Reactivity of Yallourn coal in the co-existence of $Ca(CH_3COO)_2$ and $Mg(CH_3COO)_2$ at 923 and 973 K.

10.3.3 Coexistence of calcium acetate and magnesium acetate

In order to clarify the catalyst effectiveness of CMA, YL coal was gasified in the co-existence of $Ca(CH_3COO)_2$ and $Mg(CH_3COO)_2$ at a loading of 1 % Ca and 1 % Mg. Figure 10.3 illustrates the gasification profiles at 923 and 973 K. $Mg(CH_3COO)_2$ alone showed no catalytic effect in this temperature range, similarly as in the case of $Mg(NO_3)_2$ (Fig. 10.1). However, the co-impregnated $Ca(CH_3COO)_2$ and $Mg(CH_3COO)_2$ markedly promoted the gasification. At 923 K char

conversion reached 85 % in 120 min, and at 973 K the coal was completely gasified within 70 min. The effectiveness of this mixture was a little smaller than that of $Ca(CH_3COO)_2$ alone. Figure 10.3 reveals that CMA can be used instead of pure $Ca(CH_3COO)_2$ as a catalyst raw material for coal gasification.

10.3.4 Coal particle size

The catalytic effectiveness in coal gasification is often dependent on the size of coal particles, in other words, the degree of contact between coal and catalyst. The method of catalyst addition used in the present study reduced the starting particle size to <0.02 mm. Thus the contact between coal and catalyst was very intimate. In order to examine the effect of particle size on the gasification reactivity, coarse particles of YL coal with the size of 0.25-0.50 mm in diameter were immersed in an aqueous solution of $Ca(CH_3COO)_2$ and the resulting particles were dried at 380 K in a N_2 stream. The reactivity of this sample was almost equal to that for fine powders of <0.02 mm; the average gasification rate at 5 % Ca and at 923 K was 3.0 and 3.4 h^{-1} for coarse particles and fine powders, respectively. The size effect was not so appreciable under these conditions. This can be attributed to the great adsorptive ability of low rank coals.

10.3.5 Coal type

The catalytic effectiveness of $Ca(CH_3COO)_2$ in the gasification of nine coals with different carbon and sulfur contents was examined at a loading of 1 %. The

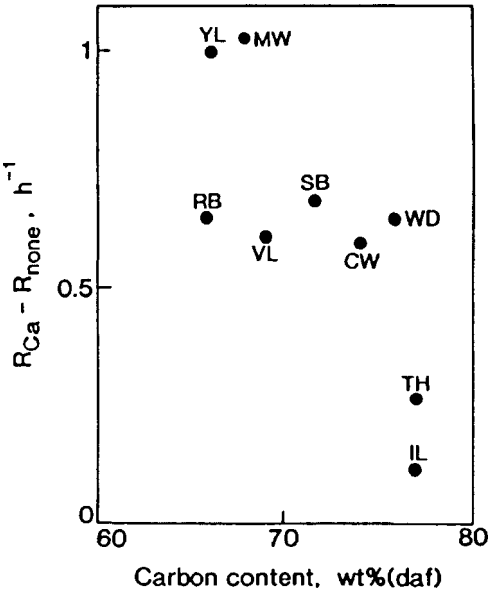

Fig. 10.4 Effectiveness of calcium catalyst for the gasification of several coals at 923 K.

difference in gasification rates with and without calcium, (R_{Ca}-R_{none}), is used as an index of the effectiveness. A plot of (R_{Ca}-R_{none}) versus carbon content in coal is illustrated in Figure 10.4, where the symbols designate the names of the examined coals (see Table 10.1). The effectiveness of calcium depended on the coal type; the larger effectiveness was observed for the coals with lower carbon contents. Since the effectiveness for VL and SB coals with high sulfur contents was almost similar as that for RB and CW coals with low sulfur contents, there may be little dependence on the sulfur content.

10.3.6 Calcium loading

Figure 10.5 illustrates the influence of the amount of added calcium on the gasification rates for YL, MW, SB and CW coals. The rates for YL and CW coals increased almost linearly with the calcium loading, whereas the rates for MW and SB coals tended to level off at around 5 %. Walker and co-workers (refs. 15,17) also observed that the effect of calcium loading on the gasification rates of American lignites depended on the coal type. At 5 % Ca all these coals were completely gasified within at least 100 min; the rates for YL, CW, MW and SB coals with calcium were 28, 27, 6 and 3 times those without catalyst, respectively. The degree of rate enhancement by calcium addition was much larger for YL and CW coals which showed lower reactivities without catalyst.

10.3.7 Temperature dependence

The gasification rates of $Ca(CH_3COO)_2$-impregnated YL and SB coals were determined at different temperatures. In both coals the calcium showed no catalytic activity at a low temperature of 773 K, in contrast with an extremely

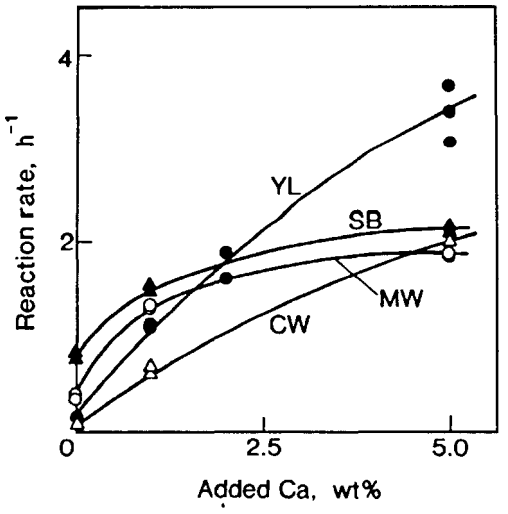

Fig. 10.5 Effect of calcium loading on the gasification rates of several coals at 923 K.

high activity of nickel catalyst in this temperature region (refs. 5-7). The rate enhancement by calcium was appreciable at > 850 K. The gasification rate increased with temperature and the complete conversion of YL or SB coal with 5 % Ca was achieved within 25 or 40 min at 973 K.

Figure 10.6 illustrates the Arrhenius plots. The apparent activation energies and frequency factors for YL coal were 170, 170 and 140 kJ/mol, and 4.7×10^8, 7.7×10^9 and 3.2×10^8 h^{-1} at 0, 1 and 5 % Ca, respectively. These values for SB coal, though the data at 1 % Ca were not shown in the figure, were 160, 160 and 130 kJ/mol, and 1.4×10^9, 1.5×10^9 and 2.4×10^7 h^{-1} at 0, 1 and 5 % Ca, respectively. For both coals, the activation energy remained unchanged and only the frequency factor was increased by the addition of 1 % Ca, and a slight decrease in the activation energy was observed in the presence of 5 % Ca. Otto et al. (ref. 25) also observed that the apparent activation energy for the steam gasification of bituminous coal char slightly decreased at a higher calcium loading. The catalysis of calcium at low loadings may be due to an increase in the reaction-site density (ref. 25).

Figure 10.6 also shows that, in order to attain a practically sufficient reaction rate, say 1 h^{-1}, with YL coal, a temperature of 1020 K is required

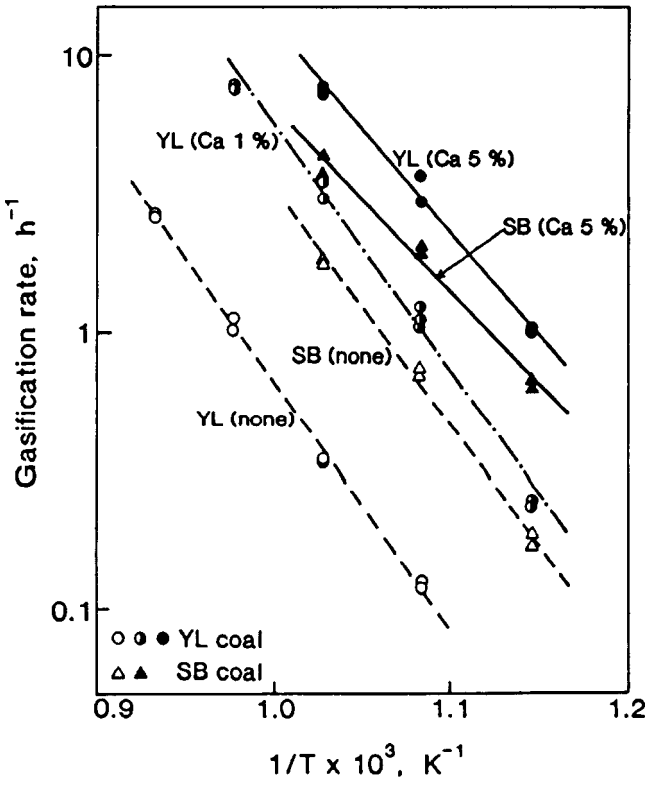

Fig. 10.6 Arrhenius plots for the gasification of Yallourn and South Beulah coals.

without catalyst, whereas 920 and 870 K are enough with 1 and 5 % Ca, respectively. In other words, the presence of 1 and 5 % Ca could lower the gasification temperature by 100 and 150 K, respectively. With SB coal the addition of 5 % Ca lowered the temperature by 50 K only.

10.3.8 XRD profiles of calcium-bearing chars

Figure 10.7 illustrates XRD patterns for different chars prepared from $Ca(CH_3COO)_2$-loaded coals. In every case the calcium loading was 5 % on the coal before char preparation. For YL coal impregnated with $Ca(CH_3COO)_2$, no XRD lines from calcium species were detectable for the char devolatilized at 923 K (Fig. 10.7A). This observation shows that the calcium catalyst is very finely dispersed on the surface of char. When the devolatilization temperature was raised to 1023 K, the small and broad peaks attributable to CaO appeared (Fig. 10.7B), the average crystallite size being determined to 21 nm. Thus the heat treatment at higher temperatures accelerated the crystallization of calcium species.

When the $Ca(CH_3COO)_2$ physically-mixed with YL coal was used instead of the impregnated-$Ca(CH_3COO)_2$, the diffraction peaks from this compound were detectable even at room temperature. Thus the change in chemical form with temperature could be followed by HTXRD. The dehydration of $Ca(CH_3COO)_2$ completed at <570 K. At around 700 K the XRD lines of anhydrous $Ca(CH_3COO)_2$ disappeared, and instead the peaks of $CaCO_3$ appeared. The diffraction intensity of $CaCO_3$ peaks increased with increasing the temperature. At a constant temperature of 923 K, the decomposition of $CaCO_3$ to CaO proceeded gradually with the soaking time and completed in 40 min. Figure 10.7C shows the XRD profile for the char prepared from the physical mixture of YL coal and $Ca(CH_3COO)_2$. The strong and sharp lines of $CaCO_3$, together with the small peaks of CaO, were observed. The crystallite size of $CaCO_3$ was as large as 40 nm. The comparison with XRD patterns for the chars from $Ca(CH_3COO)_2$-impregnated coals reveals that the physical mixing of $Ca(CH_3COO)_2$ with coal gives the poorly dispersed calcium.

Figures 10.7D and 7E illustrate XRD profiles for calcium-bearing chars from $Ca(CH_3COO)_2$-impregnated SB and TH coals, respectively. No XRD lines of calcium species were observed with SB char, similarly as the case of YL char (Fig. 10.7A), whereas the signals from $CaCO_3$ crystallites were detectable with TH char. These observations show the decreased dispersion of calcium catalyst on the surface of TH char.

The chemical form and dispersion of the catalysts from other calcium salts than $Ca(CH_3COO)_2$ were examined with YL coal in the same manner as in Fig. 10.7A. Strong and sharp peaks due to $CaSO_4$ were observed in the case of $CaSO_4$

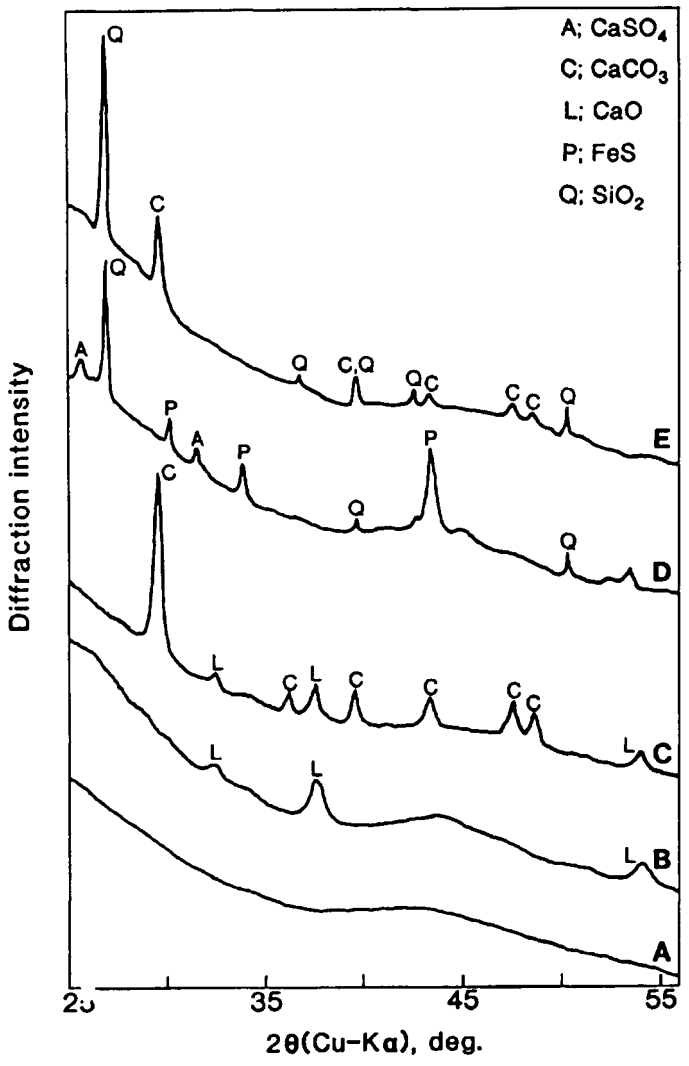

Fig. 10.7 XRD profiles of different calcium-bearing chars.
The conditions of char preparation are as follows; A, D, E, from $Ca(CH_3COO)_2$-impregnated YL, SB, and TH coals at 923 K, respectively; B, from $Ca(CH_3COO)_2$-impregnated YL coal at 1023 K; C, from the physical mixture of YL coal and $Ca(CH_3COO)_2$ at 923 K.

(ref. 21). With the CaS-loaded coal, the small peaks of $CaCO_3$ and CaO as well as CaS were detected, indicating that some CaS are converted to $CaCO_3$ and CaO. On the other hand, for $Ca(NO_3)_2$-, $Ca(OH)_2$- and $CaCl_2$-loaded coals, no XRD lines from calcium species were detectable on these chars prepared at 923 K (ref. 21), similarly as the case of $Ca(CH_3COO)_2$ (Fig. 10.7A). Calcium species derived from these compounds were found to be highly dispersed. Although the absence of XRD signals gave no information on their chemical forms, the XRD results for $Ca(CH_3COO)_2$ physically-mixed with YL coal or impregnated on TH coal suggest that $CaCO_3$ is the predominant species at 923 K (Figs. 10.7C and 7E). When the

devolatilization temperature was raised to 1023 K, the broad peaks attributable to CaO appeared with these three chars. The decomposition of $CaCO_3$ to CaO proceeded easily in an inert atmosphere at 1023 K.

10.3.9 Catalyst preparation

Table 10.2 summarizes how both the method of catalyst addition and the heat treatment prior to steam gasification, that is, the devolatilization of calcium-loaded coal, affect the catalyst dispersion and subsequent char reactivity. When YL coal impregnated with $Ca(CH_3COO)_2$ was heated rapidly (300 K/min) up to 923 K and soaked for 5 min, the specific rate of the resulting char, 3.3 h^{-1}, was almost the same as that (3.4 h^{-1}) without heat treatment. The calcium on the surface of this char was very finely dispersed because no XRD lines attributable to calcium species were detected. The dispersion of calcium catalyst lowered with increasing severity of conditions of heat treatment, in other words, with decreasing the heating rate, increasing the temperature, and increasing the soaking time. The severer conditions resulted in lower gasification reactivities of chars; the reaction rate decreased from 3.3 h^{-1} for the char of 300 K/min - 923 K - 5 min to 1.8 h^{-1} for the char of 10 K/min - 1023 K - 30 min. The devolatilization of the physical mixture of YL coal and $Ca(CH_3COO)_2$ at 923 K gave the formation of larger $CaCO_3$ particles (40 nm), which resulted in the considerable decrease in the rate. Thus a good

TABLE 10.2

Influence of conditions of catalyst preparation on the dispersion of calcium catalyst and the gasification rate of char.

Method of catalyst addition[a]	Conditions of heat treatment			Calcium catalyst		Specific rate at 923 K (h^{-1})
	Heat. rate (K/min)	Temp. (K)	Soaking time (min)	Chemical form	Crystal. size (nm)	
Impregnation	No treatment			-	-	3.4
Impregnation	300	923	5	n.d.[b]	-	3.3
Impregnation	10	923	30	n.d.	-	2.6
Impregnation	300	1023	30	CaO[c]	21	2.1
Impregnation	10	1023	30	CaO	24	1.8
Physical mix	300	923	5	$CaCO_3$[d]	40	0.5

[a]YL coal; $Ca(CH_3COO)_2$ (Ca, 5 %).

[b]Not detectable by XRD (Fig. 10.7A).

[c]Shown in Figure 10.7B

[d]With the small peaks of CaO (Fig. 10.7C).

correlation was observed between the catalyst dispersion and the char reactivity.

10.4 DISCUSSION

10.4.1 Reaction scheme

In a previous study using the HTXRD technique (ref. 21), it has been suggested that the calcium-catalyzed gasification at low temperatures of around 950 K may proceed through the following carbonate-oxide cycle.

$$CaCO_3 + C = CaO + 2CO \quad (10.1)$$

$$H_2O + CO = H_2 + CO_2 \quad (10.2)$$

$$CaO + CO_2 = CaCO_3 \quad (10.3)$$

McKee (ref. 26) investigated the catalysis of alkaline earth salts in the steam gasification of graphite at high temperatures of 1100-1300 K, and suggested that the catalytic mechanism may involve a carbonate-oxide oxidation-reduction cycle. The mechanism proposed by McKee has been modified as the above reaction scheme for explaining the catalysis of calcium in the low temperature region.

The occurrence of eqn. 10.1, that is, the promotion of the decomposition of $CaCO_3$ by carbon, was confirmed also in the present study; the TPXRD experiment of the physical mixture of YL coal and $Ca(CH_3COO)_2$ revealed that the decomposition of $CaCO_3$ to CaO at 923 K completed in 40 min on the surface of char, whereas it took much more than 90 min for the completion of $CaCO_3$ decomposition on inert Al_2O_3 (ref. 21). Since the calcium catalyst was more finely dispersed with the impregnated $Ca(CH_3COO)_2$ than with the physically-mixed one (Figs. 10.7A and 7C), the reaction rate of eqn. 10.1 would be larger in the former case. With eqn. 10.2, a high partial pressure of steam (66 kPa) in the present study would favor the shift conversion of CO formed, and further calcium catalyst considerably promotes this reaction during steam gasification (ref. 27). The regeneration of $CaCO_3$ from CaO (eqn. 10.3) proceeded readily in the presence of CO_2 and at temperatures of <1000 K (ref. 21), though the regeneration was not so easy at higher temperatures even in the presence of CO_2. Thus the catalytic gasification of low rank coals with $Ca(CH_3COO)_2$ at around 950 K may proceed via a carbonate-oxide cycle mechanism.

10.4.2 Importance of catalyst dispersion

Walker and co-workers (refs. 18,19) reported that the heat treatment of calcium-exchanged lignite decreased the dispersion of calcium and consequently

lowered the catalytic activity toward the subsequent reaction of char with air. As is shown in Table 10.2, the degree of catalyst dispersion was well correlated with the gasification rate of calcium-bearing char. This finding points out that the catalyst dispersion is an important factor which controls the rate enhancement by calcium also in the gasification of coal with steam. When $Ca(CH_3COO)_2$ was impregnated on YL coal and then devolatilized at 923 K, calcium species were not detectable by XRD (Fig. 10.7A) and thus very finely dispersed on the surface of char. Since some exchange of calcium ions with oxygen functional groups in YL coal takes place in the impregnation step, such a high degree of dispersion would be brought about by the presence of ion-exchanged calcium. The increase in severity of conditions of devolatilization of calcium-loaded coal accelerated the agglomeration of calcium particles, and the decreased dispersion of calcium catalyst resulted in the small rate enhancement (Table 10.2). Although the ion exchange or impregnation method provides essentially atomic dispersion in the step of catalyst addition, the heat treatment prior to the gasification decreases the catalyst dispersion and thus lowers the inherent catalytic activity. Therefore the gasification catalyst should be used without such the pretreatment so that the inherent activity can be maximally exhibited in the gasification step.

For TH coal with a smaller content of surface oxygen groups than YL coal, the formation of $CaCO_3$ crystallites was observed on the devolatilized char (Fig. 10.7E). The sintering of $CaCO_3$ particles would arise from a lower exchange extent of calcium ions with these acid cites. The smaller catalyst effectiveness of calcium observed for TH coal, as shown in Figure 10.4, is ascribed partly to the decreased dispersion.

Table 10.2 shows that the catalyst dispersion is affected also by the method of catalyst addition. In contrast with the highly dispersed calcium observed for the impregnated $Ca(CH_3COO)_2$, the physically-mixed $Ca(CH_3COO)_2$ gave large $CaCO_3$ particles in the devolatilization step (Fig. 10.7C). Since no ion exchanges occur in the catalyst addition like physical mixing, the absence of exchanged calcium would be the reason for the poor dispersion. The catalytic effect of poorly dispersed calcium was quite small (Table 10.2).

10.4.3 Effectiveness of calcium catalyst

The effectiveness of various catalysts in the steam gasification of coal has been studied by many investigators, and found to depend on several factors, such as the catalyst loading, the kind of precursor salt, the coal type and the reaction temperature. In this section the catalyst effectiveness of calcium will be discussed from these point of view.

(i) Comparison with other metals. As shown in Figure 10.1, at a low loading of 1 %, the calcium was the most active catalyst among different metals examined in the present study. Although alkali-metal compounds have been generally accepted to be most effective, the potassium at 1 % was less active than calcium. When the catalyst loading was increased up to 10 %, however, the effectiveness of potassium was very large for the gasification of many coals from lignite to anthracite (refs. 28,29). The activity of nickel was not so high in this work, but the nickel at a high loading of 10 % exhibited an extremely high activity toward the gasification of brown coals with low sulfur contents even at low temperatures of < 800 K (refs. 5-7). Other catalysts than nickel, potassium, calcium and iron, were inactive in this temperature region.

With the activity sequence of alkali earth metals, it has been reported that barium is more active than calcium at temperatures of >1000 K (refs. 25,26,30). In the present work, however, the reverse sequence was observed (Fig. 10.1). Calcium catalyst was still more active than barium catalyst even when the activity at 923-973 K was compared at the same atomic per cent, say 0.7 at.% (1.5 wt% Ca and 5.0 wt% Ba) (ref. 21). The difference in activity sequence between the earlier studies and the present work can be explained on the basis of the above-mentioned reaction mechanism. The mechanism suggests that, if alkaline earth metal can readily cycle between carbonate and oxide, the metal is more active. The interconversion between $CaCO_3$ and CaO is easy at around 950 K, but it is difficult at high temperatures of >1000 K because CaO is very stable. On the other hand, the barium shows the reverse behavior. Consequently the difference would be observed. The detailed discussion has been described

TABLE 10.3

Lowering in gasification temperature, ΔT, by catalyst addition in the steam gasification of Yallourn brown coal.

Catalyst			ΔT
Metal	Precursor Salt	Amount (%)	(K)
Fe[a]	$Fe(NO_3)_3$	10	50
Na[b]	NaCl	5	120
Ca	$Ca(CH_3COO)_2$	5	150
K[b]	KCl	10	170
Ni[c]	$Ni(NH_3)_6CO_3$	10	300

[a]Ref. 10.
[b]Ref. 12; metal ions alone are incorporated into coal by the ion exchange method using a pH adjusting agent.
[c]Ref. 5.

elsewhere (ref. 21).

Figure 10.6 shows that the gasification temperature for YL coal can be lowered by 100 and 150 K with the aid of 1 and 5 % Ca, respectively. The degree of the lowering in gasification temperature by catalyst addition is a convenient index that represents the catalyst effectiveness quantitatively. This index (ΔT) in the steam gasification of YL coal with different catalysts is summarized in Table 10.3, where the values for nickel, iron, sodium and potassium catalysts have already been shown elsewhere (refs. 5,10,13). On this criterion, the calcium prepared from $Ca(CH_3COO)_2$ was more effective than sodium and iron, but less effective than nickel and potassium. With the most effective nickel catalyst, however, the expensive nickel of a large amount of 10 % is essential for such the large effectiveness, and 15 wt% of coal remains ungasified because of the rapid deactivation of nickel catalyst (refs. 5,7). With potassium catalyst, KCl as a catalyst precursor is inexpensive, but the use of a pH adjusting agent like NH_3 or $Ca(OH)_2$ is unavoidably necessary for preparing the active, chlorine-free catalyst (ref. 13). The application of this catalyst to the coals with high ash contents seems not so easy because of the catalyst deterioration by the reaction with alumino-silicate compounds in minerals (ref. 31). On the other hand, with calcium catalyst, the complete conversion of coal can easily be achieved (Fig. 10.2), and this catalyst is applicable to the coals with high ash and high sulfur contents (ref. 22). Furthermore, there is the advantage that cheap raw materials like $Ca(OH)_2$, $CaCO_3$ and CMA can be used (Figs. 10.2 and 10.3). Therefore it can be concluded that the calcium is the most promising catalyst for coal gasification.

(ii) Influence of catalyst precursor. Figure 10.2 shows that $Ca(NO_3)_2$, $Ca(OH)_2$, $CaCO_3$ and $CaCl_2$ exhibit similar catalyst effectiveness as $Ca(CH_3COO)_2$. Large effectiveness of calcium catalysts from these precursors would be ascribed to the high degree of catalyst dispersion. Interestingly even CaS promoted the gasification to a large extent (Fig. 10.2). The XRD measurement for the CaS-loaded coal revealed the presence of $CaCO_3$ and CaO as well as CaS on the devolatilized char. This observation means that some CaS are converted to $CaCO_3$ and CaO by the reaction with H_2O and CO_2 evolved during devolatilization according to the following equations.

$$CaS + CO_2 + H_2O = CaCO_3 + H_2S \qquad (10.4)$$

$$CaS + H_2O = CaO + H_2S \qquad (10.5)$$

Since the concentrations of H_2O and CO_2 around CaS particles become higher during steam gasification, the reaction rates of eqns. 10.4 and 10.5 would be

larger. $CaCO_3$ and CaO formed would promote the gasification through the carbonate-oxide cycle. With the $CaSO_4$-loaded coal, no XRD lines from $CaCO_3$ and CaO were detectable on the char, indicating that no change in the form of $CaSO_4$ takes place. Therefore little effectiveness was observed with $CaSO_4$.

(iii) Influence of coal type. As is seen in Figure 10.4, the effectiveness of calcium catalyst for high sulfur coals (VL, SB) was almost the same as that for low sulfur coals (RB, CW). This suggests that calcium catalyst is hardly deactivated by the sulfur compounds like H_2S evolved during the devolatilization and subsequent gasification. However, Otto et al. (ref. 25) observed that calcium catalyst was severely poisoned by externally-added H_2S in the steam gasification of coal chars. This difference can be explained from the different reaction conditions. The conditions of Otto et al., an extremely low partial pressure of steam (2.7 kPa) and a relatively high temperature of 1023 K, favor thermodynamically the reactions of $CaCO_3$ and CaO with H_2S, that is, the reverse reactions of eqns. 10.4 and 10.5. However, the present conditions of both a high partial pressure of steam (66 kPa) and a low temperature of 923 K are unfavorable to the poisoning of calcium catalyst by H_2S. This would be supported by the fact that the catalyst derived from CaS exhibits a high activity (Fig. 10.2).

It is well known that alkali and alkali earth metal cations exchanged with carboxyl groups naturally exist in low rank coals. Takarada et al. (ref. 23) have shown that the amount of such metal ions, especially Ca and Na, controls the reactivity of low rank coals in steam. The presence of inherent, exchangeable calcium ions may also affect the degree of rate enhancement by

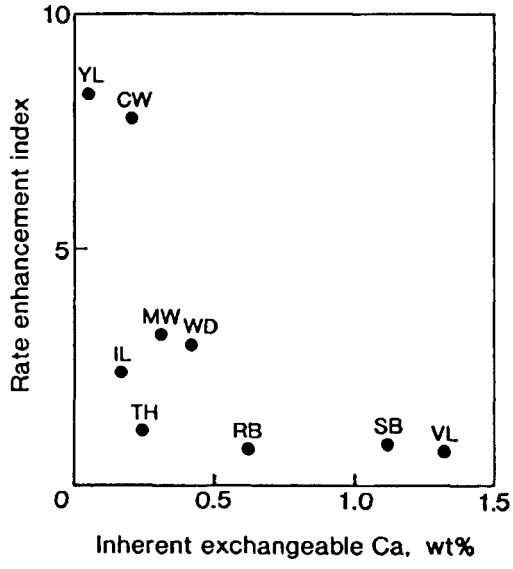

Fig. 10.8 Influence of the amount of inherent exchangeable calcium on the rate enhancement indexes for various low rank coals.

externally-added calcium in the gasification of these coals. A rate enhancement index, $(R_{Ca}-R_{none})/R_{none}$, may be convenient for expressing quantitatively the difference of rate enhancement among several low rank coals. In Figure 10.8, this index at a loading of 1 % Ca is plotted as a function of the amount of inherent, exchangeable calcium. A relatively good correlation between the two, except for TH and IL coals, was observed; the enhancement index decreased with an increase in the amount of inherent calcium. The indexes for TH and IL coals deviated from the expected correlation curve. This deviation would be ascribed to the poor dispersion of calcium catalyst on these chars, as indicated by the fact that the catalyst dispersion was poorer on TH char than on YL and SB chars (Fig. 10.7).

10.5 CONCLUSION

Calcium catalyst prepared from $Ca(CH_3COO)_2$ promoted the steam gasification of low rank coals at low temperatures of around 950 K. The catalytic effectiveness of $Ca(CH_3COO)_2$ depended on the coal type; the larger rate enhancement by calcium was observed for the coals with smaller amounts of inherent exchangeable calcium, such as Yallourn, Colowyo and Morwell coal. The gasification rate increased with the calcium loading, the degree of rate increase being also dependent on the coal type. With Yallourn coal, calcium catalyst was effective even at a low loading of 1 %, and most active among the examined metals like K, Mg, Ba, Fe and Ni. The presence of 5 % Ca lowered the gasification temperature of Yallourn coal by 150 K. Cheap and effective calcium is found to be the most promising catalyst for coal gasification. The co-impregnated $Ca(CH_3COO)_2$ and $Mg(CH_3COO)_2$ also enhanced the reactivity of Yallourn coal to a similar degree as the case of $Ca(CH_3COO)_2$ alone. This finding shows that CMA can also be used as a catalyst raw material. The dispersion of calcium catalyst was affected by the conditions of catalyst preparation. The devolatilization of calcium-loaded coal, that is, the heat treatment prior to the gasification, brought about the decreased catalyst dispersion, which resulted in the lowering of gasification activity. Therefore the gasification catalyst should be used without the pretreatment to gain the maximal activity.

ACKNOWLEDGMENT

The authors gratefully acknowledge the assistance of Miss Fumie Hamaoka, Miss Meiko Nishiyama (presently Mrs. Meiko Kuramoto) and Miss Naoko Yoshida in carrying out experiments.

REFERENCES

1 J.L. Figueiredo and J.A. Moulijn (Editors), Carbon and Coal Gasification, NATO ASI Series, Martinus Nijhoff Publishers, Dordrecht, 1986.
2 J.A. Moulijn and F. Kapteijn (Editors), Special Issue of the International Symposium on Fundamentals of Catalytic Coal and Carbon Gasification, Fuel, 65 (1986) 1324-1478.
3 J.L. Johnson, The Use of Catalysts in Coal Gasification, Catal. Rev. Sci. Eng., 14 (1976) 131-152.
4 D.W. McKee, The Catalyzed Gasification Reactions of Carbon, Chem. Phys. Carbon, 16 (1981) 1-118.
5 A. Tomita, Y. Ohtsuka and Y. Tamai, Low Temperature Gasification of Brown Coals Catalysed by Nickel, Fuel, 62 (1983) 150-154.
6 K. Higashiyama, A. Tomita and Y. Tamai, Action of Nickel Catalyst during Steam Gasification of Bituminous and Brown Coals, Fuel, 64 (1985) 1157-1162.
7 Y. Ohtsuka, A. Tomita and Y. Tamai, Catalysis of Nickel in Low Temperature Gasification of Brown Coal, Appl. Catal., 28 (1986) 105-117.
8 A. Tomita, Y. Watanabe, T. Takarada, Y. Ohtsuka and Y. Tamai, Nickel-Catalysed Gasification of Brown Coal in a Fluidized Bed Reactor at Atmospheric Pressure, Fuel, 64 (1985) 795-800.
9 T. Takarada, J. Sasaki, Y. Ohtsuka, Y. Tamai and A. Tomita, Direct Production of Methane-Rich Gas from the Low-Temperature Steam Gasification of Brown Coal, Ind. Eng. Chem. Res., 26 (1987) 627-629.
10 Y. Ohtsuka, Y. Tamai and A. Tomita, Iron-Catalyzed Gasification of Brown Coal at Low Temperatures, Energy & Fuels, 1 (1987) 32-36.
11 K. Asami and Y. Ohtsuka, Gasification of Low Rank Coals with Chlorine-free Iron Catalyst from Ferric Chloride, Proc. 1989 Int. Conference on Coal Science, Tokyo, October 23-27, 1989, pp. 357-360.
12 T. Takarada, T. Nabatame, Y. Ohtsuka and A. Tomita, New Utilization of NaCl as a Catalyst Precursor for Catalytic Gasification of Low-Rank Coal, Energy & Fuels, 1 (1987) 308-309.
13 T. Takarada, T. Nabatame, Y. Ohtsuka and A. Tomita, Steam Gasification of Brown Coal Using Sodium Chloride and Potassium Chloride Catalysts, Ind. Eng. Chem. Res., 28 (1989) 505-510.
14 J.L. Johnson, Relationship between the Gasification Reactivities of Coal Char and the Physical and Chemical Properties of Coal and Char, Am. Chem. Soc. Div. Fuel Chem., 20 (1975) 85-101.
15 E.J. Hippo, R.J. Jenkins and P.L. Walker, Jr., Enhancement of Lignite Char Reactivity to Steam by Cation Addition, Fuel, 58 (1979) 338-344.
16 R.J. Lang and R.C. Neavel, Behaviour of Calcium as a Steam Gasification Catalyst, Fuel, 61 (1982) 620-626.
17 T.D. Hengel and P.L. Walker, Jr., Catalysis of Lignite Char Gasification by Exchangeable Calcium and Magnesium, Fuel, 63 (1984) 1214-1220.
18 L.R. Radovic, P.L. Walker, Jr. and R.G. Jenkins, Importance of Catalyst Dispersion in the Gasification of Lignite Chars, J. Catal., 82 (1983) 382-394.
19 L.R. Radovic, P.L. Walker, Jr. and R.G. Jenkins, Effect of Lignite Pyrolysis Conditions on Calcium Oxide Dispersion and Subsequent Char Reactivity, Fuel, 62 (1983) 209-212.
20 T. Nabatame, Y. Ohtsuka, T. Takarada and A. Tomita, Steam Gasification of Brown Coal Impregnated with Calcium Hydroxide, J. Fuel Soc. Japan, 65 (1986) 53-58.
21 Y. Ohtsuka and A. Tomita, Calcium Catalysed Steam Gasification of Yallourn Brown Coal, Fuel, 65 (1986) 1653-1657.
22 Y. Ohtsuka and K. Asami, Steam Gasification of High Sulfur Coals with Calcium Hydroxide, Proc. 1989 Int. Conference on Coal Science, Tokyo, October 23-27, 1989, pp. 353-356.
23 T. Takarada, Y. Tamai and A. Tomita, Reactivities of 34 Coals under Steam Gasification, Fuel, 64 (1985) 1438-1442.

24 Y. Ohtsuka, Y. Kuroda, Y. Tamai and A. Tomita, Chemical Form of Iron Catalysts during the CO_2-Gasification of Carbon, Fuel, 65 (1986) 1476-1478.
25 K. Otto, L. Bartosiewicz and M. Shelef, Effects of Calcium, Strontium, and Barium as Catalysts and Sulphur Scavengers in the Steam Gasification of Coal Chars, Fuel, 58 (1978) 565-572.
26 D.W. McKee, Catalysis of the Graphite-Water Vapor Reaction by Alkali Earth Salts, Carbon, 17 (1979) 419-425.
27 T. Takarada, Y. Ohtsuka and A. Tomita, Pressurized Fluidized-Bed Gasification of Catalyst-Loaded Yallourn Brown Coal, J. Fuel Soc. Japan, 67 (1988) 683-692.
28 T. Takarada, Y. Ohtsuka, A. Tomita and Y. Tamai, Activity Sequence of Catalysts on Catalytic Coal Gasification, J. Fuel Soc. Japan, 62 (1983) 414-420.
29 T. Takarada, Y. Tamai and A. Tomita, Effectiveness of K_2CO_3 and Ni as Catalysts in Steam Gasification, Fuel, 65 (1986) 679-683.
30 T. Yamada and T. Homma, Catalytic Effect of Alkaline Earth Salt on the Reaction of Char from Phenol-Aldehyde Resin with Carbon Dioxide, J. Fuel Soc. Japan, 58 (1979) 11-17.
31 D.W. McKee, C.L. Spiro, P.G. Kosky and E.J. Lamby, The Catalysis of Coal Gasification, Chemtech, (1983) 624-629.

天然ガスから化学製品を
ーメタンの酸化カップリング反応ー

Kenji ASAMI
朝見賢二

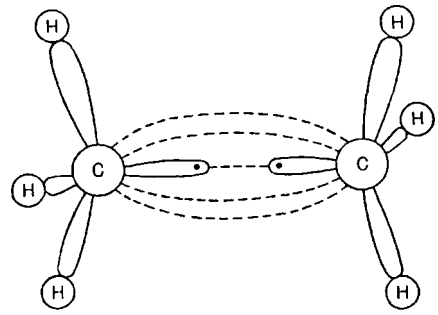

カット：メチルラジカルのカップリング。

天然ガスは，資源量が多く安価で，燃焼に伴う二酸化炭素発生量が少ないため，クリーンなエネルギー源として注目され，その使用量は年々増加している。しかしこれをただ燃やしてしまうだけではもったいないのではなかろうか？　石油や石炭のような複雑な混合物でない天然ガスは，化学製品を大量に生みだす可能性を秘めている。本稿では，化学品の原料であるエチレンを天然ガスから合成する方法について紹介したい。

はじめに

天然ガス資源とその利用

天然ガスとは，一般に天然に産する可燃性のガスをいい，その主成分はメタンである。世界の天然ガスの確認埋蔵量は約 120 兆 m^3 (1991 年) である。これは東京ドームと同じ大きさをもつ巨大なガスタンクに 100 気圧ずつ充填しても約 100 万基に及ぶ膨大なものであり，エネルギー換算では原油の資源量に匹敵する。この内の大部分は発電用や都市ガスなどの燃料として用いられ，化学製品の原料に使用される量は極めて少ない。これは，メタンが非常に安定で反応性に乏しいからである。

現在，工業化されている技術としては，メタンを水蒸気改質反応（1）により合成ガス（CO, H_2）に変換し，この CO や H_2 を原料としてメタノールやアンモニアを合成するという方法がある。また，塩素化によるクロロメタン類の合成や熱分解によるアセチレンの製造も行なわれている。

$$CH_4+H_2O\longrightarrow CO+3\,H_2 \qquad (1)$$

メタンから C_2 炭化水素へ

天然ガス（メタン）から炭素数が 2 以上の炭化水素を得る方法としては，上述の合成ガスを利用したフィッシャー・トロプシュ反応や，メタノールからガソリンを合成する MTG 法などの間接的方法があり，直接的方法には以下の脱水素カップリングと酸化カップリングの二つがある。

メタンは 1,000 ℃ 以上に加熱すると脱水素しながらカップリングする（(2)〜(4)）。高温ほど平衡転化率は上昇し，主生成物は C_2H_2 になるが，化学品原料としては C_2H_4 の方が重要である。また大きな吸熱を伴うので熱力学的には不利である。

$$2\,CH_4\longrightarrow C_2H_6+H_2 \qquad (2)$$

$$2\,CH_4\longrightarrow C_2H_4+2\,H_2 \qquad (3)$$

$$2\,CH_4\longrightarrow C_2H_2+3\,H_2 \qquad (4)$$

酸素共存下で水を生成させると，反応は発熱に変わり，熱力学的に有利となる。これがメタンの酸化カップリング反応である（(5)，(6)）。

$$4\,CH_4+O_2\longrightarrow 2\,C_2H_6+2\,H_2O \qquad (5)$$

$$2\,CH_4+O_2\longrightarrow C_2H_4+2\,H_2O \qquad (6)$$

このような反応が進行する可能性が初めて示されたのは，1982 年のことであり[1]，その 2 年後触媒反応で C_2 炭化水素を合成する報告がなされた[2]。しかし同時に進行する完全酸化反応（(7)，(8)）

$$2CH_4+3O_2 \longrightarrow 2CO+4H_2O \quad (7)$$

$$CH_4+2O_2 \longrightarrow CO_2+2H_2O \quad (8)$$

のため，C_2H_6，C_2H_4 の収率，選択率は低かった。

筆者らは 1984 年に本反応に注目した。メタンからエチレンが定量的に得られれば，石油によらない「天然ガスからの化学品製造」が可能になるものと期待し，研究に着手した。本稿では筆者らが行なった研究の中から酸化鉛を触媒とする系と加圧無触媒系について概説する。

担持酸化鉛触媒の C_2 炭化水素生成活性と選択性

担体の効果

酸化カップリング反応によりメタンから C_2 化合物を製造するためのキーポイントは，優れた触媒の開発にあった。予備的な実験の結果から，酸化鉛（PbO）を主触媒に用いることにした。Hinsen らの報告[2]と同様，PbO 触媒では SiO_2 担持と Al_2O_3 担持で C_2 の収率や選択率が大きく異なっていた。そこで，担体の酸塩基性が酸化鉛触媒の活性，選択性に及ぼす影響を検討した[3]。図 1 に各種担体に担持した触媒上での C_2 の選択率と収率の関係を示す。酸性担体では燃焼反応が優先し，C_2 収率，選択率とも低かった。中性担体では C_2 選択性は増すものの，反応性が極端に低下した。これらに対し，塩基性担体，特に MgO や β''-Al_2O_3（Al_2O_3，K_2O の層状化合物）が優れた結果を与えた。反応条件を選ぶと，PbO/MgO 触媒は 750 ℃ において C_2 生成速度 11.1 mmol/g·h，選択率 85.3% という非常に高い活性，選択性を示した。ほぼ同時期に本反応に有効な触媒が報告され[4~7]，これらはいずれも塩基性物質を含んでおり，その重要性が認識された。

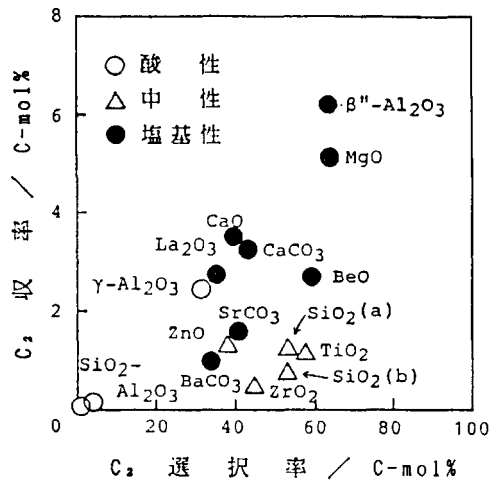

図 1 PbO 触媒の担体効果。反応条件：750 ℃，$CH_4:O_2:N_2=14:1.6:84.4$，$W/F=1\,g\cdot h\cdot mol^{-1}$。

反応機構

反応の経路は次のように考えられる。まず活性な酸素種により，CH_4 から水素が引き抜かれてメチルラジカル（$CH_3\cdot$）が生成する。これが二量化して C_2H_6 を与え，C_2H_4 はその酸化脱水素で生成する。では，活性な酸素種とは何であろうか？

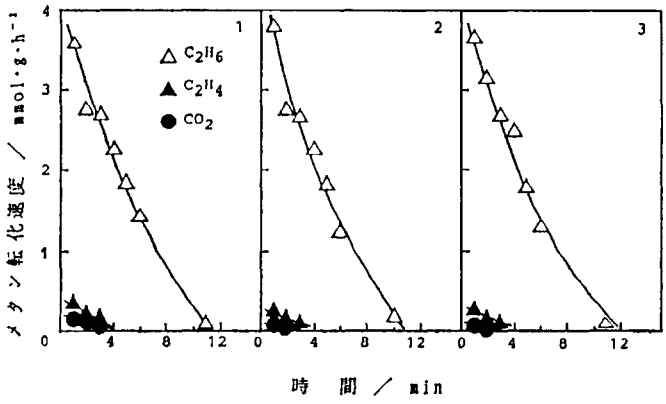

図 2 PbO/MgO 触媒とメタンの反応。反応条件：750 ℃，$W/F=4.3\,g\cdot h\cdot mol^{-1}$。

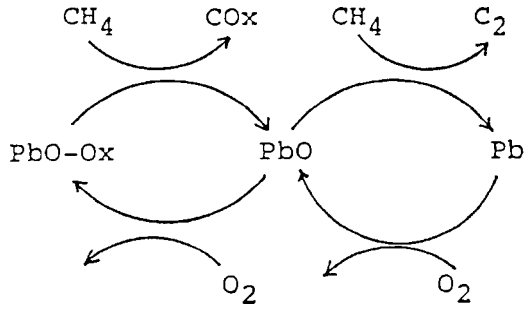

図 3 PbO/MgO の触媒サイクル。

これを解明するために，触媒上に Air→N_2→CH_4→N_2 の順でガスを流し，触媒中の酸素とメタンを反応させる周期反応を行なった[8]。図2に各生成物への CH_4 転化速度を示す。気相に酸素が存在しないと，選択的に C_2H_6 が生成することがわかる。X線回折の結果から，反応前と空気による再酸化後の鉛の状態は PbO であり，CH_4 と反応すると Pb になった。つまり C_2 生成の活性酸素種は PbO の格子酸素であり，0価と2価の酸化還元で反応が進行することが明らかとなった。一方，完全酸化の活性種は，触媒表面の吸着酸素と推定され，PbO/MgO 触媒上では図3に示す機構で反応が進行すると結論された。

酸素以外の酸化剤の効果

メタンの酸化カップリング反応は通常酸素を酸化剤として行なう。しかしながら，工業的な意味は別として，ほかの酸化剤の使用も可能である。そこで筆者らは，N_2O, NO, SO_2, CO_2 を酸化剤に用いて反応を行なった[9]。CH_4 との混合ガスによる反応では，N_2O が O_2 と同等の C_2 収率，選択率を示した。CO_2 も少量の C_2 を与え，CH_4-CO_2 同時変換による C_2 製造への可能性を示した。ところで，PbO/MgO 触媒の C_2 生成の活性酸素種は PbO の格子酸素である。そこで，O_2 の代わりにこれらの酸化剤を用いて周期反応を行なってみた。すると N_2O のみならず NO や CO_2 も有効な酸化剤として機能し，O_2 と同様選択的に C_2 を生成することが判明した。このことより，これらの物質がうまく濃縮できれば，NO_x の除去や CO_2 の還元再資源化の方法となり得る。

触媒は本当に必要か？ —気相加圧系

高圧反応器の試作とブランクテスト

筆者には CO 水素化などの高圧反応に対する経験があったので，本触媒系での加圧下での挙動に興味があった。CH_4-O_2 の混合ガスを 700 °C 以上にして加圧するなどという無謀な（？）研究者がいなかったせいか，加圧下での研究例は全くなかったので，反応器の設計，試作から行なった。反応器の外側は耐熱性合金（インコロイH），内側には金属表面での反応を避けるための石英管という構造にした（図 4-a）。高温での耐圧性や爆発しないことを確かめるためのテストのときである。触媒なしのブランクテストだったので，まさか反応はするまいと思ったが，念のために出口ガスを分析してみたところ，C_2H_6, C_2H_4 が生成していた。しかもその生成量は圧力を上げると増加した。つまり，無触媒で酸化カップリングが進んでいたのである。そこで，反応器を図 4-b のように改良

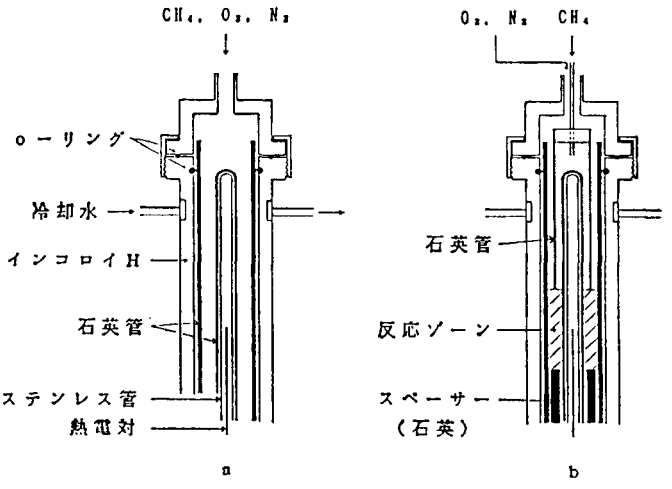

図 4 高圧反応器。

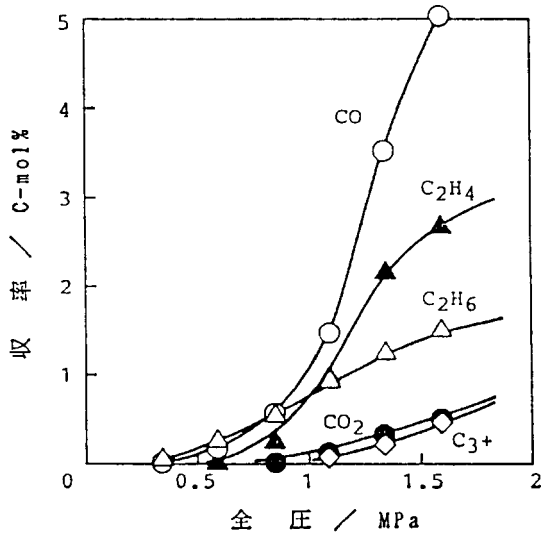

図 5 気相反応の圧力依存性。反応条件：750 ℃, $CH_4 : O_2 : N_2 = 14 : 1.6 : 84.4$, 350 $ml \cdot min^{-1}$。

して（aの構造ではどこで反応が起こるのか不明なので），加圧下での気相無触媒反応の詳細を検討した[10]。

気相反応の特徴

図5に示すように，常圧（0.1 MPa）では反応は全く起こらないが，圧力を増すに従って反応が起こるようになった。これに伴い C_2 収率も増加し，高圧になるほどエチレンの比率が大きくなった。C_2 選択率は反応圧 0.6 MPa の場合の約 60% から徐々に減少する傾向をみせた。触媒反応における燃焼反応の生成物は，大部分 CO_2 であるが，この系では CO が主生成物であり，実用的には好ましい。

加圧下において無触媒で反応が進行することは，二つの機構によって説明される。一つは，この系での活性酸素は気相の酸素分子であるが，酸素分子による水素引き抜き（9）が遅いために，常圧では反応が起こらない。加圧によって衝突頻度が

$$CH_4 + O_2 \longrightarrow CH_3\cdot + HO_2\cdot \qquad (9)$$

増し，この反応が進行するようになったためである。もう一つは，二つの $CH_3\cdot$ が結合して生成する C_2H_6 分子は，過剰なエネルギーをもつ励起分子であり（10），第三体（M）との衝突による安定化（11）が起こらなければ再び解離してしまう。圧力を増すとこの第三体の分圧が増加し，安定化

$$CH_3\cdot + CH_3\cdot \rightleftarrows C_2H_6^* \qquad (10)$$

$$C_2H_6^* + M \longrightarrow C_2H_6 + M \qquad (11)$$

が効率よく行なわれるようになるためであると考えられる。

なお，圧力が増加すると反応器内での線流速は遅くなるので，反応物の滞留時間は長くなる。このことによって高圧になるほど転化率が上昇することが考えられるが，その影響はそれほど大きくないことが別の実験で確認されており，本質的な圧力効果は上記のものであるといえる。

おわりに

以上，メタンの酸化カップリング反応に関して著者らの研究の一端を紹介した。この反応に関する研究は，ここ 10 年で膨大な数におよび，世界各国で行なわれている。このことから，天然ガスを化学原料にすることに対していかに関心が高いかがうかがえる。まだまだ問題点は多いと思うが，実用化に向けた研究も行なわれつつあり，基礎研究に携わった者としては，一日も早く工業化されてプラントが稼働し始めるのを望んで止まない。

本研究は東京大学工学部合成化学科冨永博夫教授（現名誉教授），藤元 薫助教授のご指導のもとに行なわれたものであり，両先生ならびに共同研究者諸氏に深く感謝の意を表する。

引用文献

1) G. E. Keller and M. M. Bhasin, *J. Catal.*, **73**, 9(1982).
2) W. Hinsen, W. Bytyn, and M. Baerns, *Proc. 8th Int. Cong. Catal.*, 3, 581 (1984).
3) K. Asami, S. Hashimoto, T. Shikada, K. Fujimoto, and H. Tominaga, *Chem. Lett.*, 1986, 1233.
4) K. Otsuka, K. Jinno, and A. Morikawa, 1985, 499.
5) T. Ito, J.-X. Wang, C.-H. Lin, and J. H. Lunsford, *J. Am. Chem. Soc.*, 107, 5062 (1985).
6) H. Imai and T. Tagawa, *J. Chem. Soc. Chem. Commun.*, 1986, 52.
7) T. Moriyama, N. Takasaki, E. Iwamatsu, and K. Aika, *Chem. Lett.*, 1986, 1165.

石炭ガス化の新触媒

東北大 反応研

酸洗廃液や石灰石から作る

低温、高効率でガス化

鋼板の表面処理工程で大量に発生する鉄を含む廃液（鉄鋼酸洗廃液）や石灰石（炭酸カルシウム）が、石炭ガス化（「ハイテクき～わ～ど」参照）触媒に有望なことを東北大学の研究グループが突き止めた。触媒を使う石炭のガス化は、次世代のガス化法として注目されているが、決め手となる触媒がまだ登場していない。試作した触媒は高効率、低温で石炭をガス化できることが分かった。触媒の製作も極めて簡単だ。触媒を使った石炭ガス化の実用化に道を開く成果として注目されそうだ。

この研究を行ったのは、東北大学反応化学研究所炭素資源反応研究センターの大塚康夫助教授、朝見賢二助手らのグループ。

新手法は、石炭粒子の周りに数十ナノ（一ナノは十億分の一）㍍単位の微細な石灰石か鉄微粒子を担持し、これを低温でガス化するという方式。つくり方は極めて簡単。石灰石の場合は石炭と石灰石を水中で混合、これをろ過、乾燥するだけでよい。

鉄微粒子の場合もほぼ同様で、塩酸か硫酸で洗った鉄鋼酸洗廃液に石炭と水酸化カルシウムを入れ、ろ過、乾燥する。水酸化カルシウムは、石炭燃焼時に発生する塩素や硫黄を無害な塩化カルシウムや硫化カルシウムに変える役割を演ずる。

実験に使った石炭は、発熱量が低いためほとんど利用されていないロイヤン褐炭。豪州炭の一種で、埋蔵量は二〇〇〇億㌧にも達すると推定されている。

実験は石灰石、鉄微粒子をそれぞれ三%担持したロイヤン褐炭の粒子を七〇〇―七五〇度Cの温度で水蒸気を吹き込みながら常圧でガス化した。

この結果、石灰石を担持した石炭は七〇〇度C、二十分間で九〇―九五%がガス化した。これは石灰石を担持しない場合に比べて、七十―百倍もガス化速度が早いという。生成したガスはおよそ六〇%が水素、残りが一酸化炭素（CO）と炭酸ガス（CO_2）。

一方、鉄微粒子を担持した石炭は、七〇〇度Cでは六十分間、七五〇度Cでは二十分間で完全にガス化。ガスの組成は水素が約七〇%、残りがCOとCO_2という。また、五〇気圧の条件で水蒸気の代わりに水素を吹き込み、ガス化すると八〇%の収率でメタンガスが生成できた。

ハイテクき～わ～ど

石炭ガス化

一五〇〇度C程度の高温で、水蒸気や酸素を吹き込みながら石炭を熱分解すると、水素や合成ガス（水素と一酸化炭素の混合ガス）などのガスが発生する。これらのガスは複合発電、燃料電池、都市ガスや、C1化学の原料として使える。現在日本でも水素製造を目的とした商業用の石炭ガス化炉が稼働している。

ただ、高温なため装置に耐熱材料を使ったり高価な酸素を使ったりする必要があり、コスト高になる問題がある。これに対して、触媒を使った石炭のガス化は六〇〇―七〇〇度Cという低温で処理でき、しかもガス化効率がよいため、次世代のガス化法として脚光を浴びている。

future research would focus on devising processes for the recapture and recirculation of the catalyst within the gasification process, as well as working on in-bed simultaneous removal of sulfur and nitrogen compounds during catalytic gasification.

Current coal gasification processes do not use catalysts, but next-generation gasifiers are expected to rely on catalysts, especially if these catalysts can be made of inexpensive raw materials, and if the additional cost of adding and recovering the catalyst can be minimized. Use of a catalyst in coal gasification would not only lower the temperature of the gasification process, but also could control the composition of the product gas.

The Japanese researchers say they have identified catalysts that allow for direct conversion of coal into methane or hydrogen at temperatures of 600 C to 700 C and that allow for high gasification efficiencies. The catalysts are obtained from limestone and acid wastes that are generated in large volumes when iron and steel plate surfaces are washed with acid.

In experiments conducted gasifying Australian Loy Yang subbituminous coal, which has a 68.1 percent carbon weight, the Tohoku University researchers evaluated the use of limestone (CaCO3) and iron and steel acid washing wastes (FeCl3, FeSO2) as catalyst raw materials. The coal comes from a vast 43-billion-mt reserve in Victoria.

In the experiments, limestone powder was mixed with 0.07 to 0.15-mm coal particles in water while iron hydroxide was precipitated onto the coal by adding Ca(OH)2 powder into an aqueous solution of iron or steel acid-washing wastes dispersed with brown coal.

Coal, containing either 3 percent calcium or 3 percent iron was heated with steam to temperatures of 700 C to 750 C and gasified at ambient pressure. The coal containing calcium was gasified by 90 percent to 95 percent in 20 minutes at a temperature of 700 C. The gasification rate was as large as 70 to 100 times that of coal gasified with no catalyst. Some 60 percent of the generated gas in the fluidized bed gasification consisted of hydrogen with the remainder consisting of carbon monoxide and carbon dioxide.

The coal containing the iron catalyst was gasified completely in an hour at 700 C and in 20 minutes at 750 C. The gas formed under excess steam consisted of about 70 percent hydrogen, with the remainder consisting of carbon monoxide and carbon dioxide.

When hydrogen was used instead of steam and the coal was gasified at a pressure of 7 MPa, methane was generated at a yield of 80 percent at about 550 C.

INTERNATIONAL

Research in Japan shows potential for catalyst use in gasification

LONDON — Researchers at Japan's Institute for Chemical Reaction Science at Tohoku University have determined that steel acid washing wastes and limestone could eventually prove to be an inexpensive catalyst in the gasification of low-grade coal.

The researchers are currently looking for funding to continue the research on a larger scale, and plan to report on their findings in a technical journal later this summer. In a recent interview with *McGraw-Hill's Coal Tech International*, Prof. Yasuo Ohtsuka of the Institute for Chemical Reaction Science noted that

ENTERPRISE

GE announces new ammonia-based flue gas desulfurization process

LEBANON PA — General Electric Environmental Systems has reported that it has developed a new ammonia-based flue gas desulfurizaion process which

(Continued on page 4)

科学・技術

燃焼前に石炭無公害化

含有窒素 鉄担持で窒素ガス化

大塚東北大助教授グループ

東北大学反応化学研究所・炭素資源反応研究センターの大塚康夫助教授らの研究グループは、豪州産石炭に水酸化鉄を担持しヘリウム雰囲気の流動層で常圧熱分解を行うと、発生する石炭中の窒素の五〇％以上が窒素ガスに転換されることを確認した。通常の燃焼ではタールやチャー（未燃焼窒素）に移行する窒素が、水酸化鉄の還元で生成する鉄の超微粒子によって脱窒素反応が促進された結果、と同グループでは考えている。今後、石炭の種類を変えるなどの実験を行い、無害化除去法としての確立を目指す。

高温燃焼で発生する窒素酸化物は大気汚染物質として排出が規制されている。石炭は地球温暖化物質とされる二酸化炭素、酸性雨の原因物質と見込まれる硫黄化合物、窒素化合物を燃焼時に大量発生することから、燃料として使用する発電所などでは大規模な装置で排ガス処理が行われている。

大塚助教授らの研究グループは、これらの問題に対処する狙いから石炭中の窒素を燃焼する前に無害化除去する事前脱窒素する方法の研究開発を進めてきた。研究は石炭中の窒素分を無害な窒素ガスにすることを目指し、豪州炭を試料に常圧下の流動層で検討を行った。

実験は塩化第二鉄水溶液中に試料の石炭を入れた後、水酸化カルシウムを添加し、試料に水溶液鉄を沈でん担持させる。これを流動層に入れ、常圧のヘリウム雰囲気中で熱分解し、石炭中の窒素の窒素ガスへの転換率を測定した。

図は鉄担持石炭および通常の石炭の窒素ガスへの転換率の結果。未処理の石炭は九百度Cで窒素ガスへの転換率は二・五％と低いが、鉄担持石炭は温度とともに転換率が上昇し、七百五十度Cで一五％、九百度Cでは五五％まで増加した。

またチャーへの窒素移行率は未処理では八百―九百度Cで頭打ちとなり、五五％がチャーに残留する。一方、鉄担持では窒素発生量の増加にともない移行率は急速に減少し、九百度Cでは二〇％以下に低下した。

さらに鉄担持は未処理に比較し、タールの生成量や窒素含有量が著しく低下し、これまでの実験から鉄の担持量が一―三wt％、水素不要の条件下で最も速く反応が進むことが確認されている。担持した水酸化鉄は熱分解時には三十―五十ナノメートルの超微粒子として存在することが確かめられている。

これらから熱分解初期に発生する揮発分窒素が窒素と窒素フリー炭素に分解する反応、およびチャー中の残留窒素からの個相脱窒素反応の二反応が鉄微粒子により促進された結果、脱窒素反応が進むと考えられている。

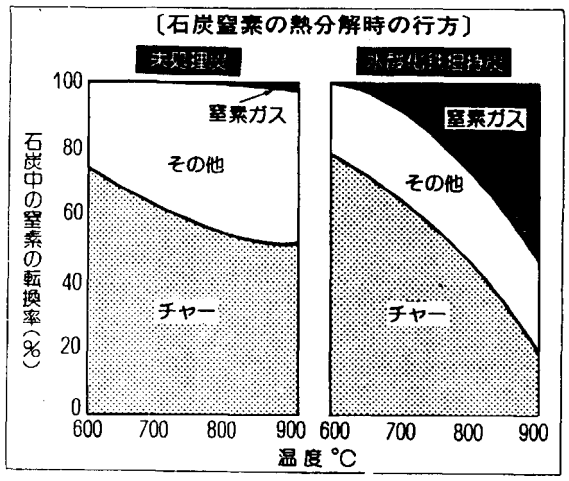

科学技術

亜瀝青炭からBTX留分

11・7%の高収率達成

東北大・富田教授グループ

東北大学反応化学研究所の富田彰教授らの研究グループは、亜瀝青炭から石炭重量比で一一・七%という高効率でベンゼン・トルエン・キシレン（BTX）留分を製造することに成功した。加圧水素下の石炭熱分解で発生する揮発分をニッケル／タングステン／硫黄／アルミーゼオライト（NiWSAl－ゼオライト）触媒上で改質した結果で過去最高の収率となっている。一連の研究から熱分解温度は八百度C前後、改質段階の温度は六百度C前後で収率が最高になることを確認している。今後、触媒の研究を進めてさらに収率を高め、製鉄所における実用を目指すことにしている。

〔亜瀝青炭からのBTX留分製造装置フロー〕

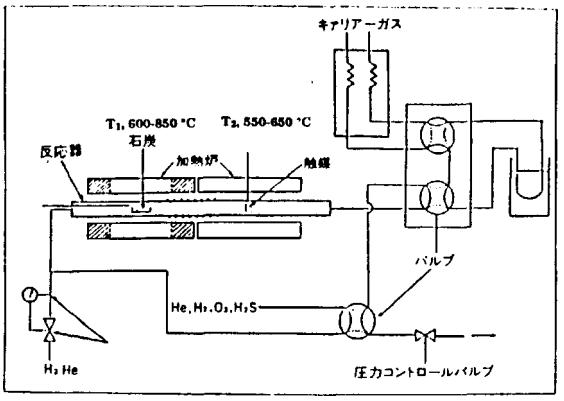

触媒にNiWS Al－ゼオライト

最適温度で2段階反応

富田教授らの研究グループはかねてから石炭の熱分解反応における反応条件を変化させることにより生成するBTX留分を最大にする研究を進めてきた。具体的には石炭のハイドロパイロリシスで生成する揮発分をさらに水素加圧下（五気圧）、触媒の存在下で温度を制御する二段階反応でBTX留分の収率を上げる実験を行ってきたもの。

これまでの研究から石炭は亜瀝青炭がほかの石炭に比べBTX収率が高くなることなどが確認されており、豪州産のミルメラン炭（亜瀝青炭、炭素分七六・九%）を中心に図のような構造の実験装置で第一次、第二次の反応温度、触媒などの条件を変化させて最高のBTX収率を目指してきた。

最近の実験で第一次反応温度八百度C－第二次反応温度六百二十度Cで、市販のニッケル／モリブデン／アルミナ触媒の存在下でBTX収率が使用石炭の重量比で初めて二ケタの一〇・四%を達成したもの。

さらに触媒をニッケル／タングステン／硫黄／アルミーゼオライト触媒に変え、第一次および第二次反応温度を変化させた実験から第一次反応温度八百度C－第二次反応温度六百度Cの条件下でこれまで報告されているなかでは最高の一一・七%の収率を達成した。

これまでの結果から第一次反応温度は高すぎると過度の熱分解が進み、また低すぎると揮発分の生成が少なくなることから八百度C前後が最適であること、また第二次反応温度にも約六百度C付近に最適条件が存在することを確認した。

富田教授らのグループはこれまでの知見をもとに、今後は触媒を変えることでBTX留分の収率をさらに高めることを目指している。

JOURNAL OF CATALYSIS 140, 168–172 (1993)

Regeneration of Nickel Catalyst on Carbon

TETSUYA HAGA AND YOSHIYUKI NISHIYAMA[1]

Institute for Chemical Reaction Science, Tohoku University, Katahira, Sendai-980, Japan

Received January 3, 1991; revised October 6, 1992

Catalytic activity of nickel for carbon gasification is initially high at 500–700°C, but it disappears when the reaction is repeated or the specimen is preheated in an inert atmosphere above 700°C. The deactivated catalyst was found to be regenerated by a treatment with steam at 700–800°C and subsequent reduction at 350°C. The surface state of nickel on carbon was inferred by temperature-programmed desorption of hydrogen, and a correlation was found between the TPD patterns and the catalytic activity for gasification. Catalytic activity of the nickel for CO_2 conversion in $1\%CO_2+99\%H_2$ mixture deactivated, and the catalyst was regenerated in a similar way as that observed for gasification. Redispersion of nickel and, possibly, removal of contaminants are thought to be responsible for the observed catalyst regeneration.

INTRODUCTION

It is well known that some transition metals such as nickel and cobalt catalyze carbon gasification in two temperature regions: the lower one between 400 and 700°C and the higher one above 750°C (*1*, *2*). The lower temperature reaction (LTR) takes place nearly in the same temperature region irrespective of the nature and pressure of gasifying agent (*3*), and the reaction rate is reported to decrease from 600 to 700°C (*4*, *5*). This is different from the higher temperature reaction (HTR), which proceeds without serious deactivation as long as carbon substrate remains (*6*, *7*). A similar deactivation to that observed for the LTR was seen in hydrogenation of CO or CO_2 catalyzed by nickel on carbon during gasification in a somewhat wider temperature region of 500–700°C (*8*). The sintering of nickel particles and carbon deposition onto or into nickel are possible causes of deactivation.

The carbon conversion in LTR can be enhanced by modifying the reaction system (*9–13*). Here, we tried to regenerate the catalytic activity of nickel in the LTR region during hydrogasification, and found that it can be restored by a steam treatment and subsequent reduction in hydrogen.

EXPERIMENTAL

A calcined pitch coke, supplied by Nittetsu Chemical Industry Co., was crushed to 0.25–0.5 mm and heated to 750°C to remove residual volatile matter (0.3 wt%). As the surface state of this carbon was not suitable for catalyst loading, the carbon was treated at 850°C for 1 h with $50\%H_2O$–He, which caused a weight decrease of about 1% and an enlargement in surface area measured by nitrogen adsorption from 0.5 to 3 m^2/g (*9*). The treated specimen is hereafter referred to as SPC. The SPC was impregnated with nickel nitrate to load 5 wt% of nickel, and dried at 50°C in vacuum. The nitrate was reduced to nickel at 350°C by hydrogen before use.

In the present study, three temperature-programmed methods were employed. In hydrogasification, referred to as H_2-TPG, approximately 1 g of the Ni-loaded sample was packed in a quartz tube of 15 mm I.D., and was heated up to 1000°C at a rate of 5°C/min in a flow of pure hydrogen, 100 cm^3/min (20°C, 1 atm). In another temperature-programmed reaction, designated as $1\%CO_2/H_2$-TPR, about 0.1 g of the speci-

[1] To whom correspondence should be addressed.

0021-9517/93 $5.00

men was heated in a flow of 1%CO_2+99%H_2 under the same temperature and flow rates as H_2-TPG. The state of nickel was inferred by temperature-programmed desorption of hydrogen (H_2-TPD). In H_2-TPD, the specimen was exposed to hydrogen for 5 min at 300°C and 1 atm and cooled in hydrogen to 25°C. Then, after the hydrogen in the gas phase was purged, the specimen was heated to 300°C at 30°C/min in a flow of pure argon, 30 cm^3/min (20°C, 1 atm), and the amount of hydrogen evolved was quantified using a thermal conductivity detector (TCD).

After a reaction, either H_2-TPG or 1%CO_2/H_2-TPR, the specimen was treated with 50%H_2O–He at 1 atm for various times at temperatures between 300 and 800°C to alter the state of nickel. After the treatment, nickel (nickel oxide) was reduced by hydrogen at 350°C and 1 atm for 1 h. The 50%H_2O treatment and the succeeding reduction are hereafter referred to simply as "steam treatment" and denoted by a code such as T(700,3), which express the temperature (°C) and the duration (h) of exposure to 50%H_2O–He. During all the reactions and treatments, C-containing components (CO, CO_2, and CH_4) in the effluent gases were monitored by a gas chromatograph, from which reaction rates (R) were calculated. These are expressed on a basis of mol converted per unit weight of catalyst on the carbon specimen.

RESULTS

Hydrogasification Runs Repeated with Intermediate Steam Treatment

The H_2-TPG of the 5%Ni-SPC specimen was repeated with intermediate steam treatment, varying the treating temperature and duration. The profiles of methane formation in H_2-TPG are depicted in Fig. 1. The fresh specimen is gasified in the temperature ranges 400–700°C(LTR) and above 700°C(HTR) as described above. Noncatalytic hydrogasification occurred only above 750°C at a small rate. The carbon conversion in the initial run was about 3%. The methane formation profile in the second or later runs, when the H_2-TPG was repeated without intermediate steam treatment, is shown by a dotted line in Fig. 1a as "Deactivated." The LTR is totally lacking, indicating a change in the reaction system. As the deactivation is also caused by heating in helium or CO_2, the notation is used regardless of the heating atmosphere.

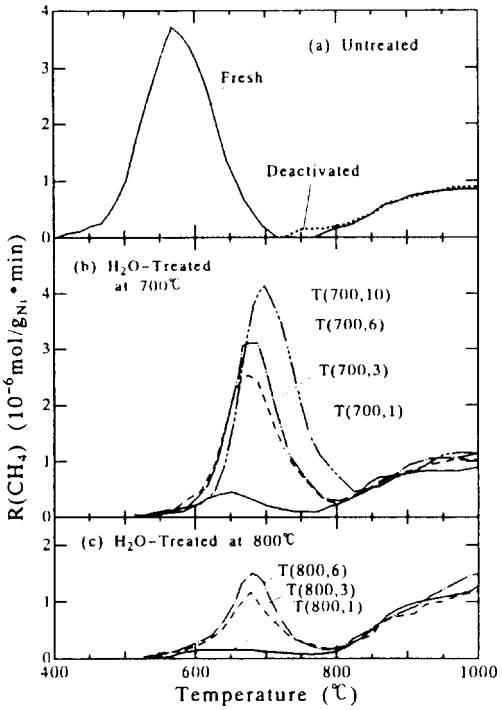

FIG. 1. Methane formation profiles in H_2-TPG of 5%Ni-SPC for a series of gasification–steam treatment experiments. (a) Untreated, (b) treated at 700°C, and (c) treated at 800°C. The H_2-TPGs were conducted in the order (a), (b), (c), and from shorter duration to longer ones.

Methane formation profiles after the steam treatment below 500°C were the same as that of the deactivated. By raising the treatment temperature to 700°C or higher, LTR was observed again as seen in Fig. 1, though methane was formed in a temperature range a little higher than that of the fresh sample. Thus, the nickel catalyst deactivated in LTR can be regenerated by treating the specimen with steam at a

temperature between 700 and 800°C and reducing at 350°C. The methane formation profiles after regeneration depend somewhat on the history of the specimen, but the main features are the same irrespective of the deactivation–regeneration sequence. Also, the steam treatment at 700°C appears to be more effective than that at 800°C. Carbon conversion in H_2-TPG after regeneration was less than 2%.

It is important that a similar treatment of the deactivated specimen with 100% CO_2 at 1 atm for 1 to 10 h at temperatures from 300 to 800°C did not cause any regeneration. The weight losses in the steam treatment were less than 1%, while a larger weight loss was observed during CO_2-treatment at 700°C.

The H_2-TPD Study

As a probe of the changes in the state of nickel on carbon, the H_2-TPD experiments were conducted on fresh, deactivated, and steam-treated specimens. Figure 2 displays the H_2-TPD profiles for the specimens after hydrogasification up to a temperature between 400 and 700°C. The pattern for a freshly prepared specimen is almost the same as that of the specimen heated to

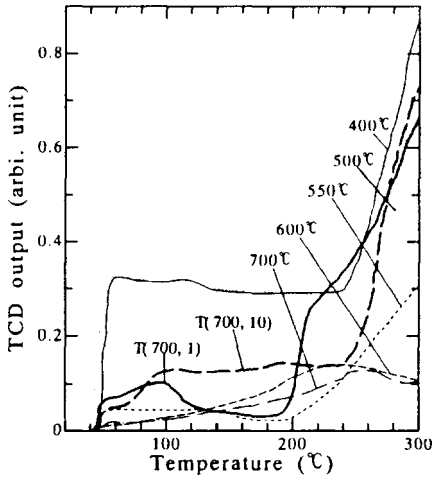

FIG. 2. H_2-TPD profiles of 5%Ni-SPC heated in hydrogen up to the temperature shown in the figure. The steam treatments were conducted for specimens gasified up to 700°C.

400°C. The profiles indicate the existence of at least two kinds of hydrogen-adsorbing sites. Also drawn in Fig. 2 are H_2-TPD profiles of two steam-treated specimens. They have a small peak at 100°C and a sharp rise near 300°C, and resemble somewhat those of the specimens gasified up to 500 or 550°C, suggesting that the state of nickel after the steam treatment is similar to those on partially gasified specimens.

The 1%CO_2/H_2-TPR Study

The deactivation and the regeneration of nickel on carbon were also examined for CO_2 hydrogenation catalyzed by the nickel using 1%CO_2/H_2-TPR method. In 1%CO_2+99%H_2, CO_2 was converted into CO and CH_4 by the reverse shift and methanation reactions, respectively. We estimated the rate of individual reactions, by using the observed rates of disappearance of CO_2, formation of CO and CH_4, and hydrogasification measured separately. In doing so, assumptions were made about the additivity of the rates and the inhibition of the Boudouard reaction in a large excess of hydrogen (*8*). In Fig. 3, parts of the results are presented. $R(-CO_2)$ is the rate of disappearance of CO_2 and $R(CH_4^*)$ is the difference in the rates of methane formation between 1%CO_2+99%H_2 run and 100%H_2(H_2-TPG); the former is believed to correspond to the activity for reverse shift reaction and the latter to methanation of CO and CO_2.

The nickel on SPC as prepared is very active for converting CO_2 in the range of 350 to 600°C, but loses its activity after heated above 700°C, similar to the deactivation in gasification. The catalytic activities for CO_2 conversion and methane formation are also regenerated by the steam treatment. It is again noted that the active region shifted to a higher temperature side after the steam treatment. It was observed that the rate of conversion after regeneration is somewhat affected by the maximum temperature of preceding reaction; heating to a higher temperature resulted in a lower rate

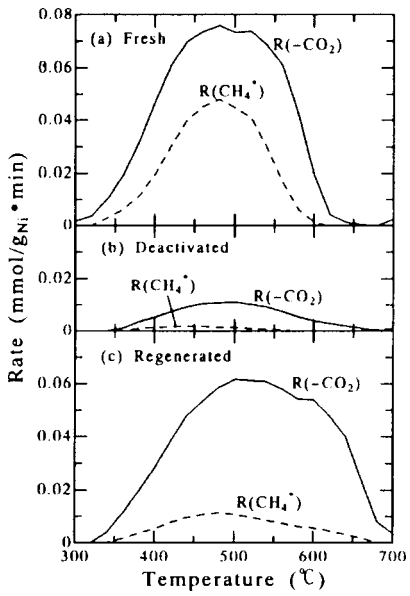

FIG. 3. The rates of disappearance of CO_2 [$R(-CO_2)$] and methane formation other than hydrogasification [$R(CH_4^*)$] on the 5%Ni-SPC in $1\%CO_2+99\%H_2$. (a) Fresh, (b) after H_2-TPG up to 700°C, and (c) regenerated by a steam treatment [T(700,1)].

even after the regeneration, as illustrated in Fig. 4.

DISCUSSION

The present work showed that a nickel catalyst deactivated by hydrogasification or in a $1\%CO_2+99\%H_2$ mixture at temperature up to 700°C can be regenerated by the steam treatment. In this system, three possible reasons for the deactivation are agglomeration of nickel or loss of contact to carbon, encapsulation or embedding into the substrate, and/or a change in the chemical form such as carbide formation.

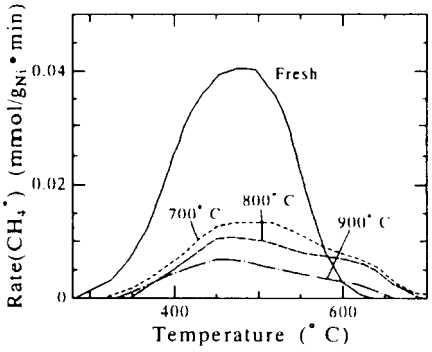

FIG. 4. Dependence of methane formation rate [$R(CH_4^*)$] on the prior history of heating. Specimens were heated in $1\%CO_2+99\%H_2$ flow up to the temperature indicated in the figure and then steam treated at 700°C for 1 h, except for the fresh specimen.

Though a definite conclusion cannot be drawn from the present study alone, we think it most feasible to suppose that the deactivation is caused by the sintering of nickel which was initially well dispersed, and the steam treatment results in a redispersion of nickel. At the same time, some contribution may occur from removal of carbon contamination, either covering over or dissolving into nickel (*14*). The results of H_2-TPD are in accord with the above view. We suppose that the agglomerated nickel in a metallic state was oxidized by steam, spread over the carbon substrate, and was reduced there, resulting in a redispersion. In another study of nickel on silica, we also noted the redispersion of nickel by oxidation–reduction treatment (*15*). It was found that the redispersion was accomplished at some limited temperature program; treatment at higher temperature reduced the effect similarly to the present results. These results might be explained by supposing that the spreading in the oxide form is balanced with their own coalescence, and is sensitive to the treatment temperature. It is possible that oxygen was incorporated with the carbon surface by the steam treatment, so that some alteration of the carbon surface may contribute to the restoring of the activity. Baker *et al.* (*16*) reported the change in the state of nickel on graphite by steaming. In another study, nickel wetted the graphite surface more in steam when hydrogen was absent (*17*).

Removal of carbon contaminants may contribute to some degree to the regeneration, but the nature of contamination is not clear. At least this cannot be the deposition from the gas phase, as the deactivation took place under conditions where nickel is catalyzing carbon gasification. The carbon re-

moval did not appear to be the main reason for the regeneration, as the CO_2 treatment which gasifies carbon does not cause regeneration. In CO_2, the surface state of carbon as well as the chemical form of nickel would be different from that in steam.

So far, in considering the behavior of nickel, we did not discriminate between gasification, CO_2 conversion, and methanation, but they are not the same, and there are some differences in the temperature range and the degree of deactivation as well as the degree of regeneration for the same treatment. Naturally, the activity or turnover frequency of a catalyst is determined by a number of parameters, depending on the nature of reaction, e.g., activity for gasification may be more sensitive to the number of contacts between carbon and nickel, while methane formation from carbon oxides may be sensitive to the surface structure of nickel. The similarity in the change of activities can be taken to indicate that there is one dominate parameter.

Although the catalytic activity for lower temperature reactions is restored by the steam treatment, the nickel-loaded carbon after regeneration is not totally the same as the fresh one, and the reaction occurred at some higher temperature ranges. The H_2-TPD after the regeneration resembles somewhat that on the specimen heated up to 550°C in hydrogen. It may be that the steam-treated sample no longer contains very small nickel particles, and incomplete redispersion of nickel by the treatment resulted in the shift in the active temperature region.

It is interesting to add that the activity for HTR is always the same regardless of the state of nickel (Fig. 1). This can be understood by the carbon-dissolution-into-nickel mechanism in which the surface state of nickel is not the controlling factor.

ACKNOWLEDGMENTS

This study was supported by the Ministry of Education, Science, and Culture (Grant-in-Aid for Energy Research). We appreciate the assistance of Mr. Kenji Murakami in experimental work.

REFERENCES

1. Tomita, A., and Tamai, Y., *J. Catal.* **27,** 293 (1972).
2. Tomita, A., Sato, N., and Tamai, Y., *Carbon* **12,** 143 (1974).
3. Tamai, Y., Watanabe, H., and Tomita, A., *Carbon* **15,** 103 (1977).
4. Figueiredo, J. L., Rivera-Utrilla, J., and Ferro-Garcia, M. A., *Carbon* **25,** 703 (1987).
5. Lund, C. R. F., *Carbon* **25,** 337 (1987).
6. Baker, R. T. K., and Sherwood, R. D., *J. Catal.* **70,** 198 (1981).
7. Tamai, Y., Nishiyama, Y., and Hagiwara, H., *Nippon Kagaku Kaishi,* 1670 (1978).
8. Haga, T., and Nishiyama, Y., *in* "Proceedings, 1989 International Conference on Coal Science," p. 401. New Energy and Industrial Technology Development Organization (NEDO).
9. Haga, T., and Nishiyama, Y., *Carbon* **21,** 219 (1983).
10. Nishiyama, Y., Haga, T., Tamura, O., and Sonehara, N., *Carbon* **28,** 185 (1990).
11. Haga, T., and Nishiyama, Y., *J. Catal.* **81,** 239 (1983).
12. Haga, T., and Nishiyama, Y., *Ind. Eng. Chem. Res.* **26,** 1202 (1987).
13. Haga, T., and Nishiyama, Y., *Ind. Eng. Chem. Res.* **28,** 724 (1989).
14. Colle, K. S., Kim, K., and Wold, A., *Fuel* **62,** 155 (1983).
15. Nakayama, T., Arai, M., and Nishiyama, Y., *J. Catal.* **87,** 108 (1984); **79,** 497 (1983).
16. Baker, R. T. K., Sherwood, R. D., Simoens, A. J., and Derouane, E. G., *in* "Metal–Support and Metal Additive Effects in Catalysis" (B. Imelik *et al.*, Eds.), p. 149. Elsevier, Amsterdam, 1982.
17. Baker, R. T. K., Chludzinski, Jr., J. J., and Sherwood, R. D., *Carbon* **23,** 245 (1985).

Reprinted from The Journal of Physical Chemistry, 1993, 97.

Effect of Ferrocene on the Carbonization of Poly(vinylidene chloride)

Jun-ichi Ozaki,* Tatsuya Watanabe, and Yoshiyuki Nishiyama

Institute for Chemical Reaction Science, Tohoku University, 1-1, Katahira 2 chome, Aoba-ku, Sendai 980, Japan

Received: September 29, 1992; In Final Form: November 23, 1992

Iron-containing carbons (0.4–8.9 wt % Fe) were prepared by pyrolysis at 400 °C of poly(vinylidene chloride) physically mixed with ferrocene. The electrical conductivity of the carbons with a small amount of iron is higher by 10 orders of magnitude at maximum than the carbon without iron. Comparison of the degree of carbonization of the iron-containing carbons with that of the carbon without iron using π-electronic excitations for infrared ray revealed that the effect of iron addition is to promote carbonization. X-ray diffraction observation also indicated the development of graphitic structure with the increase in the iron content. From X-ray photoelectron spectroscopy and electron paramagnetic resonance measurements, the effective iron species for the promotion of carbonization reaction seems to be small iron clusters with lower valence state. Addition of iron species can be one way to modify the electrical properties of carbons prepared at lower temperatures.

Introduction

Carbonization can be recognized as formation of condensed aromatic systems with the elimination of foreign atoms other than carbon atom and unstable carbon containing fragments from the original organic substances. As the condensed aromatic polycyclic sheets have mobile π-electrons, the electrical conductivity of carbons increases during carbonization lower than 1000 °C, due to development of the size of the graphitic sheets. The present authors have been interested in the drastic change in the electrical conductivity during carbonization, because of the possibility of producing materials with electronic functions by controlling the carbonization process. We have paid attention to the π-electronic excitation by infrared radiation and have shown that a parameter obtained by an analysis of the absorption edge gives an estimation of the volume fraction of π-electron containing constituents in carbonized materials.[1,2] We also have shown an application of π-electron excitation by infrared radiation to a photoconductive device.[3]

We think there are two ways to control the electrical properties. One is to control the carbonization conditions, such as temperature, reaction period, and starting materials. Another is modification by adding other elements or compounds such as halogens, alkali metals, etc. The latter is widely investigated on conductive polymers. Tanaka et al. studied the doping effect on polyacenic materials[4-7] and coals.[8] We also studied the effect of bromine doping to the carbons derived from poly(vinylidene chloride) (PVDC) and presented a model to explain the increase in electrical conductivity with the bromine addition.[9]

The catalytic effect of foreign elements on graphitization has been widely investigated. Marsh and Warburton reviewed catalysis of graphitization.[10] Promotive effects on graphitization were found for many elements, such as iron,[11-13] ferrosilicon,[13] titanium oxide,[14] etc. The admixing methods for these studies were physical mixing of powders of metals or metallic compounds and carbon. Kammereck, Nakamizo, and Walker[15] and Nakamizo[16] tried carbonization of copolymers consisting of furfuryl alcohol and vinyl ferrocene or ferrocene dicarboxylic acid to obtain homogeneously dispersed iron-containing glassy carbons. Yasuda et al. prepared metal-containing carbons by pyrolysis of metal–polymer complexes.[17] Although there are many studies on the effect of metallic element on graphitization, there are only a few studies for carbonization at lower than 1000 °C.

Carmona and Delhaes considered carbons derived from anthracene as inhomogeneous materials; that is to say, carbons consist of graphitic phase and disordered phase, and hence the properties of them are determined by the composition of the constituents.[18] We extended this concept to a three-phase model, which includes a conductor phase, a semiconductor phase, and an insulator phase.[2] We believe that the inhomogeneous structures of carbons are essential for developing semiconductive properties of carbon as a whole, because the changes in electrical conductivity by adsorption of gases or absorption of radiations are remarkable for semiconductive materials. Construction of conjugated π-electron systems is one of the most interesting problems in physical chemistry with hopes for developing optical or electronic functions. We consider carbonization as one way to obtain conjugated π-electron systems and are very interested in the way to control the sizes of the graphitic sheets while maintaining the inhomogeneous nature of carbons. As the structures of carbons heat-treated at higher temperatures approach that of graphite, the carbonization temperature must be as low as possible to obtain the inhomogeneous structures.

In our laboratory, carbon deposition off metals and carbon gasification by metal catalysts have been studied, and we have information on the interactions between carbons and metals: the interaction between iron or nickel and carbons is moderate for chemical reactions.[19,20] Although there are differences in the manner of the two carbon formation reactions, carbon deposition and carbonization of polymers, there could be the same elemental reaction step in the carbonization of polymers with metals as in the carbon deposition on metal surfaces. In planning this work, we chose iron as the modifying element because of the moderate interaction between iron and carbon.

The purpose of this study is to know the effect of iron on carbonization by observing the electrical conductivity of carbons.

Experimental Section

Sample Preparation. We prepared two kinds of samples: one is iron-containing carbon and another is a control. The procedure of preparation of the iron-containing carbons is as follows. The mixture of predetermined amounts of poly(vinylidene chloride) (PVDC) (Asahi Chemical Industry Co. Ltd.) and ferrocene (Aldrich) was dissolved in warm tetrahydrofuran (THF) in an alumina mortar. The solvent was evaporated by stirring in air followed by drying under vacuum at room temperature for 1 h. Precarbonization was done by heating samples in a helium flow at 350 °C for 1 h. The precarbonized samples were pulverized into the range of 45–125 μm. The ground samples were subjected to carbonization in a helium flow at 400 or 800 °C for 1 h. The iron content of resultant carbons was determined by combustion

0022-3654/93/2097-1400$04.00/0

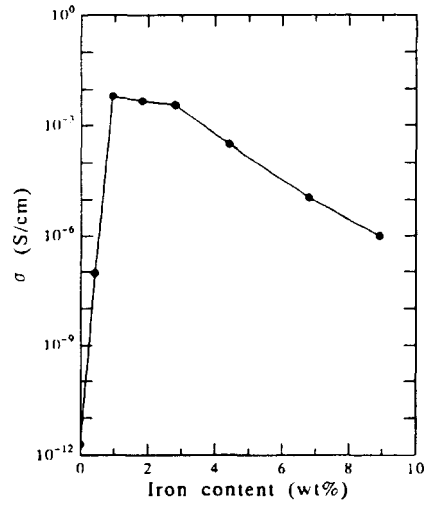

Figure 1. Changes in the electrical conductivity with iron content for F400-*X*'s.

TABLE I: Elemental Analyses

sample	C (wt %)	H (wt %)	Cl (wt %)	Fe (wt %)
F400-0.4	78.4	2.0	18.6	0.4
F400-0.9	88.5	1.9	7.9	0.9
F400-1.8	90.9	1.8	4.3	1.8
F400-2.8	87.0	1.9	5.1	2.8
F400-4.4	81.0	2.1	6.1	4.4
F400-6.8	78.1	2.6	8.3	6.8
F400-8.9	71.9	2.9	12.3	8.9
S400	72.0	2.1	23.3	
S500	80.9	1.7	10.8	
S550	88.8	1.5	3.7	
S600	91.0	1.6	0	
S700	90.8	1.0	0	
S800	93.0	0.9	0	

in air at 800 °C. These samples are referred to by their carbonization temperatures and iron content following a prefix F. For example, F400-1.8 stands for the sample carbonized at 400 °C with the iron content of 1.8 wt %.

Samples of the second series were obtained by pyrolysis of PVDC without ferrocene additive and with varying carbonization temperature, but the preparation procedure was the same as for F-series samples; these samples are referred to as S-series.

The elemental composition of the samples used here are presented in Table I.

Electrical Conductivity. The electrical conductivity of powder sample was measured by using an apparatus consisting of two piston-type electrodes. Details are described elsewhere.[2]

Infrared Absorption. IR spectra were obtained by the diffuse reflectance method for carbons diluted by potassium bromide powder with an FTIR spectrometer, JIR-100 (JEOL). The spectra showed a broad π-electron excitation absorption continued from the near-IR region to the far-IR region with an absorption edge. The absorption near the edge was simulated by an equation of optical absorption for amorphous semiconductors as reported before:[1]

$$(\hbar\omega\alpha)^{1/2} = A(\hbar\omega - E_0) \qquad (1)$$

where $\hbar\omega$ is the energy of the photon, α is the Kubelka–Munk function, E_0 is the optical gap, and A is the infrared absorption parameter. We have assumed that this parameter is proportional to the volume fraction of the π-electron-containing part in carbons. The unit of this quantity is $eV^{-0.5}$.

X-ray Photoelectron Spectroscopy. Photoelectron spectra of Fe $2p_{3/2}$ were measured after argon ion etching for 3 min in the spectrometer, by using an ESCA750 spectrometer (Shimadzu) with a Mg X-ray source.

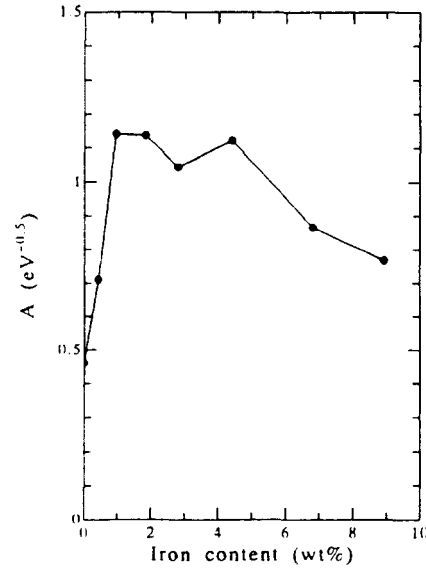

Figure 2. Changes in the infrared parameter (eq 1) with iron content for F400-*X*'s.

Electron Paramagnetic Resonance. The samples for this measurement were diluted by potassium bromide powder. This mixture was charged in a quartz tube and was evacuated by a rotary pump for 20 min to eliminate effects of adsorbed oxygen. The spectra were measured at room temperature by using an E-4 ESR spectrometer (Varian) with X-band microwave. Calibrations for the magnetic field and the spin concentration were done by using diphenylpicrylhydrazyl (DPPH) as reference.

Other Instrumental Analysis. An X-ray diffractogram was obtained by an XD-D1 diffractometer (Shimadzu) with Cu Kα radiation. Transmission electron microscopic (TEM) observation was done for several representative samples using an H-300 Model (Hitachi).

Results

Electrical Conductivity. Figure 1 shows the electrical conductivity of the F400-*X* (*X* stands for iron content in weight percent) series with the content of iron. An increase in the iron content to 1–3 wt % gives rise to the maximum increase in the electrical conductivity by about 10 orders of magnitude relative to that of the $X = 0$ sample. Introduction of more than 3 wt % iron brings about a decrease in the electrical conductivity. Possible explanations for the changes in the electrical conductivity are (1) introduction of iron induces some structural changes in carbon matrix and (2) the electrical conduction process varied with the addition of iron. The following experiments were performed to investigate which explanation is more plausible.

States of Carbon Matrix. The IR parameter A is plotted against the iron content in Figure 2. The parameter A increases in the range of 0–1 wt % iron content. At an iron content higher than 5 wt %, this quantity decreases. This behavior is similar to that of electrical conductivity (Figure 1) to some extent.

Figure 3 shows diffractograms of several F400-*X* samples. Carbons show a diffraction peak at about 42–43° by a Cu Kα ray which corresponds to the (10) reflection of the graphitic net plane. With the increase in iron content up to 3 wt %, the development of the (10) peak is observed. This indicates enlargement of the hexagonal net plane in the carbon matrix.

The EPR spectra comprise two absorptions: one is very broad, and the other is narrow, as shown in Figure 4. As the broad one cannot be seen for the S400 sample, we considered that the broad

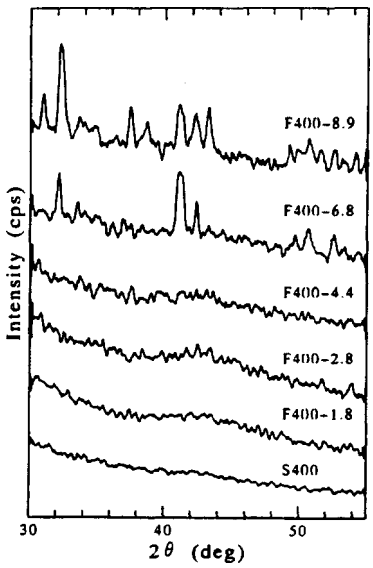

Figure 3. Cu Kα X-ray diffractograms of F400-X's.

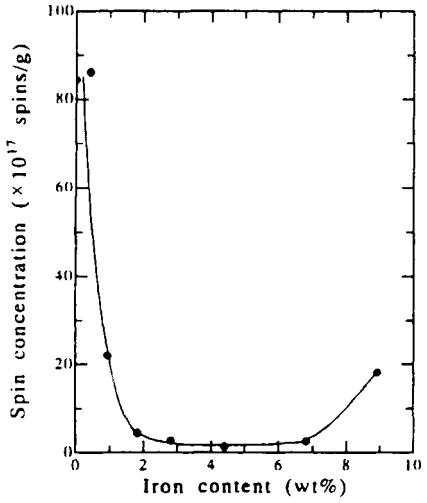

Figure 5. Variation of the spin concentration of organic radicals with iron content.

peak originates from iron species and the narrow one from organic radicals. Figure 5 shows the variation of the spin concentration calculated from peak area of narrow absorption. Introduction of iron up to 2 wt % decreases the spin concentration to several tenths of the S400 sample.

States of Iron in Carbons. The states of iron in carbon matrix were investigated by XRD, EPR, XPS, and TEM. There are no diffraction peaks that can be assigned to iron compounds for iron content lower than 5 wt %, as shown in Figure 3. For samples higher than 5 wt % in iron content, some sharp peaks are detected. These peaks can be assigned to $FeCl_2$ and $FeCl_3$. When the F400-8.9 sample was immersed in ethanol to prepare the TEM sample, the supernatant liquid turned to green. This observation agrees with the existence of $FeCl_2$ by XRD for higher iron content samples.

The variation of the intensity of broad EPR absorption in Figure 4a is plotted as a function of iron content in Figure 6. The intensity shows a maximum at an iron content of 4 wt %.

Figure 7 shows the Fe $2p_{3/2}$ XPS spectra. There is a difference at a lower binding energy end, about 709 eV, between samples higher and lower than 5 wt % in iron content. This implies that there are different states of iron contained in the carbon matrix. Peak separation analysis was performed using three Gaussian functions, which locate at the binding energies of 709 and 711 eV, and the remaining shake-up satellite. Figure 8 shows the variation of the amounts of the 711- and 709-eV components. While the amount of the 711-eV component almost monotonously increases with the iron content, the amount of the 709-eV component shows a maximum at 4 wt % of iron content. The feature of 709 eV is similar to that of the intensity of the broad EPR peak shown in Figure 6.

A few TEM images are presented in Figure 9. The lower iron content samples, S400 (Figure 9a) and F400-1.8 (Figure 9b), appear similar to one another, and the highest iron content sample, F400-8.9 (Figure 9c), shows fibril structures beside solid blocks similar to the lower iron content samples. Iron particles are hardly seen in Figure 9a,b, but spots which can be considered to be iron particles are seen in Figure 9c.

Leaching by Acid Wash. Elimination of iron particles from several samples was performed to investigate the role of iron additive to the electrical conduction process. The samples were

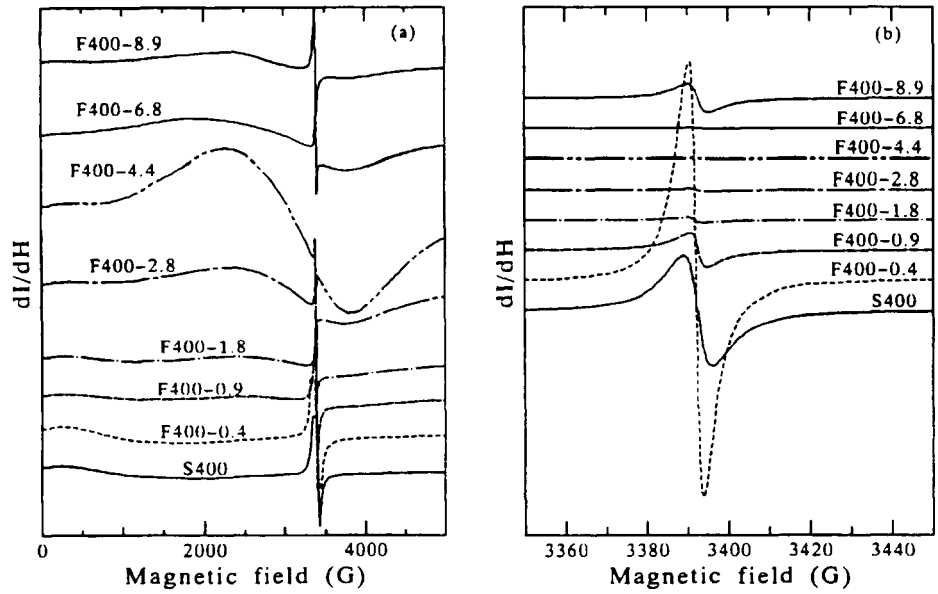

Figure 4. EPR spectra of S400 and F400-X samples: (a) for wide range scanning and (b) for narrow range scanning focused on organic radicals.

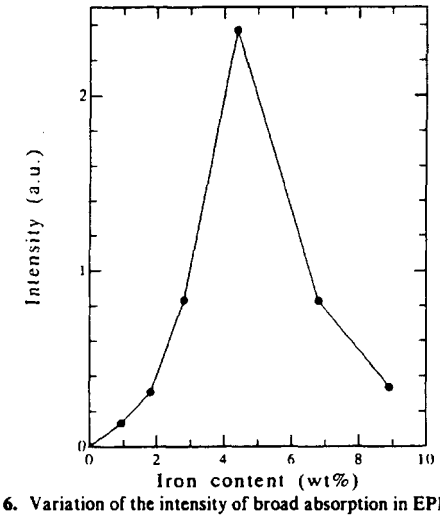

Figure 6. Variation of the intensity of broad absorption in EPR spectra with iron content.

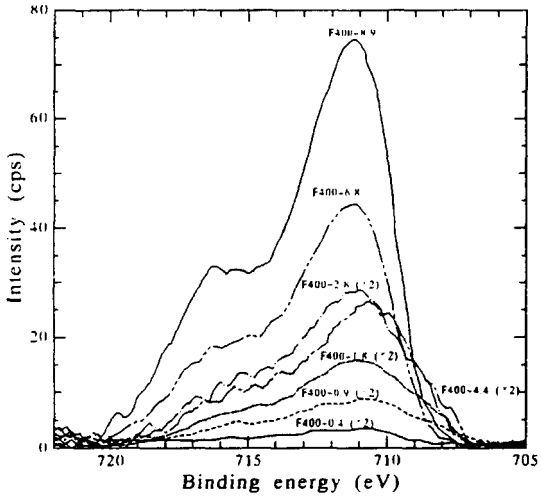

Figure 7. Fe $2p_{3/2}$ X-ray photoelectron spectra of F400-X's.

immersed in 2 M HCl solutions and shaken for 5 h. Then, the samples were washed with ion-exchanged water and dried in vacuum. The electrical conductivity and the iron content of acid-washed samples are presented in Table II. The iron contents did not decrease by acid washing for lower iron content samples. For higher iron content samples, F400-8.9, the iron content decreased to one-third of the as-prepared sample by acid washing; however the electrical conductivity did not show any significant change upon acid washing.

Discussion

Promotive Effect of Iron on Carbonization. The infrared parameter (see eq 1) is a useful one for describing the degree of the carbonization reaction. In this section, some comparisons of F-series with S-series are made by using the IR parameter A.

The IR parameter varied with the iron content shown in Figure 2. As this parameter can be taken to be proportional to the volume fraction of π-electron-containing constituents in the carbons, the authors infer the introduction of small amounts of iron promotes the carbonization reaction. This is evidenced by X-ray diffraction studies shown in Figure 3.

Figure 10 shows a plot of electrical conductivity of the S-series, F400-X, and F800-X samples as a function of A. The behaviors of the F-series show tendencies similar to those of the S-series

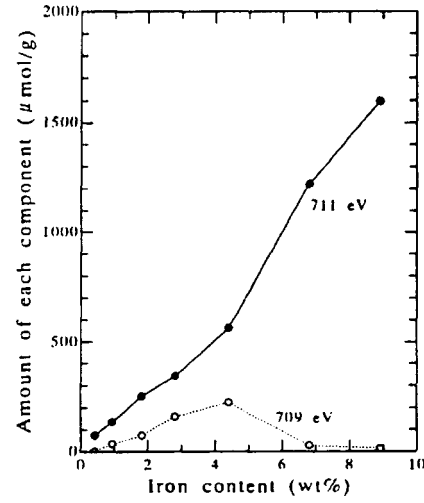

Figure 8. Changes in the amounts of 711- and 709-eV components in Fe $2p_{3/2}$ XPS spectra with iron content.

against A, but the carbonization temperatures differ significantly between them. The electrical conductivity of about 10^{-2} S/cm was attained by carbonization at about 600 °C for the S-series, while it was attained at 400 °C by introduction of 1–3 wt % of iron. This observation also indicates a promotive effect of iron on the carbonization reaction.

To know how the iron promotes the carbonization reaction at a low temperature, the chemical compositions of carbonized polymers were plotted as a function of A in Figure 11. As can be seen in Figure 11a, the decrease in the Cl/C ratio shows the same behavior as that in the S-series. The decreasing manner of H/C for the F400-X series is somewhat different from that for the S-series viewed in the light of a higher H/C ratio.

The possibility of modification of the electrical conduction process by iron seems very low from the results of acid washing. Thus we conclude that the role of iron additive is to modify the structure of the carbon matrix.

Effective Iron Species. The amount of the higher binding energy component in the separated Fe $2p_{3/2}$ peak increases with the iron content, as shown in Figure 8. This component can be assigned to $FeCl_2$ (710.8 eV) or $FeCl_3$ (711.5 eV) according to Carver et al.[21] This assignment agrees with the XRD studies. Although the origin of the 709-eV peak is not clear, the similarity between the variation of this peak and that of the intensity of the broad EPR absorption with iron content shown in Figure 6 suggests the same origin. As the clusters of paramagnetic elements show broad EPR peaks,[22,23] we inferred that these signals originate from small clusters of the lower valence state of iron.

Carbonization is considered to consist mainly of two reactions: one is elimination of heteroatoms and another is formation of condensed aromatic systems. The addition of iron results in a decrease in the chlorine content, and the effect is maximum at 2–4 wt % of iron content (Table I). The electrical conductivity (Figure 1) and the IR parameter A (Figure 2) take maximum values at 0.4–4 wt % of iron content, so that the introduced iron promotes the formation of condensed aromatic rings in this iron content range. The tendency of the above two effects with the iron content, promotion of chlorine elimination and condensed aromatic ring formation, has some parallelism to that of the amount of the small clusters of the lower valence state of iron. Thus the authors conclude that the effective iron species for promotion of carbonization is small iron clusters with lower valence state, and these clusters catalyze the chlorine elimination and the aromatic ring formation. This catalytic mechanism is now under investigation.

Variation in Conductivity with Iron Content. The electrical

(3) Ozaki, J.; Nishiyama, Y. *J. Appl. Phys.* **1991**, *69*, 324.
(4) Tanaka, K.; Yamanaka, S.; Koike, T.; Yamabe, T.; Yoshino, K.; Ishii, G.; Yata, S. *Phys. Rev.* **1985**, *B32*, 6675.
(5) Tanaka, K.; Ohzeki, K.; Yamabe, T. *Synth. Met.* **1984**, *9*, 41.
(6) Tanaka, K.; Koike, T.; Nishino, H.; Yamabe, T. *Synth. Met.* **1987**, *18*, 521.
(7) Tanaka, K.; Koike, T.; Yamabe, T.; Yamauchi, J.; Deguchi, Y.; Yata, S. *Phys. Rev.* **1987**, *B35*, 8368.
(8) Tanaka, K.; Koike, T.; Sasaki, T.; Kobashi, M.; Yamabe, T. *Solid State Commun.* **1988**, *66*, 237.
(9) Ozaki, J.; Sumami, I.; Nishiyama, Y. *J. Phys. Chem.* **1990**, *94*, 3839.
(10) Marsh, H.; Warburton, A. P. *J. Appl. Chem.* **1970**, *20*, 133.
(11) Oberlin, A.; Rouchy, J. P. *Carbon* **1971**, *9*, 39.
(12) Courtney, R. L.; Duliere, S. F. *Carbon* **1972**, *10*, 65.
(13) Varaniecki, C.; Pinchbeck, P. H.; Pickering, F. B. *Carbon* **1969**, *7*, 213.
(14) Millet, J.; Rogue, J.; Vivares, A.; Descomps, A.; Millet, J. *J. Chim. Phys. Phys.-Chim. Biol.* **1965**, *62*, 46.
(15) Kammereck, R.; Nakamizo, M.; Walker, P. L., Jr. *Carbon* **1974**, *12*, 281.
(16) Nakamizo, M. *Carbon* **1991**, *29*, 757.
(17) Yasuda, H.; Miyanaga, S. *Hyoumen* **1989**, *27*, 490.
(18) Carmona, F.; Delhaes, P. *Chemistry and Physics of Carbon*; Walker, P. L., Jr., Thrower, P. A., Eds.; Dekker: New York, 1981; Vol. 17, p 89.
(19) Nishiyama, Y. J. *Jpn. Pet. Inst.* **1974**, *17*, 454.
(20) For example, his recent review appeared in: Nishiyama, Y. *Fuel Proc. Technol.* **1991**, *29*, 31.
(21) Carver, J. C.; Schweitzer, G. K. *J. Chem. Phys.* **1972**, *57*, 973.
(22) Ito, O.; Tsuchibe, K.; Ohtsuka, Y.; Iino, M. *Carbon* **1989**, *27*, 325.
(23) Dack, S. W.; Hobday, M. D.; Smith, T. D.; Pilbrow, J. R. *Fuel* **1985**, *64*, 222.

Fuel Processing Technology, 29 (1991) 31-42
Elsevier Science Publishers B.V., Amsterdam

Review

Catalytic gasification of coals – Features and possibilities

Yoshiyuki Nishiyama

Institute for Chemical Reaction Science, Tohoku University, Katahira, Aobaku, Sendai 980 (Japan)

(Received July 10th, 1991; accepted July 18th, 1991)

Abstract

Catalysis in coal gasification is reviewed in relation to the author's own research. The features of three catalyst groups, alkali, alkaline earth and iron-group metals, are compared and the rate change during gasification is discussed. Effect of substrate properties, especially surface area and state of char, on the activity of catalyst is stated. Steam gasification with catalyst is shown to yield more carbon dioxide when gasification activity is high, except for nickel. Possible applications are briefly mentioned.

INTRODUCTION

Among coal utilization processes, gasification is gaining more significance as a route of better efficiency in energy consumption. Needless to say, coal gasification aims at producing fuel gases or gaseous materials which can be converted into useful chemicals. Gasification can be conducted without catalyst at higher temperatures and practical processes seem well mature [1,2].

Studies on catalysis of coal gasification have two purposes: (1) to understand the kinetics of gasification of coals which contain catalytically active minerals; and (2) to design and evaluate possible gasification processes using catalysts. The use of catalysts lowers the gasification temperature thereby attaining an advantage in product composition determined by chemical equilibrium, in addition to some merits in thermal efficiency and/or reactor materials. However, a catalytic process rarely competes with non-catalytic ones under normal circumstances, except when a cheap catalyst that is highly active at low temperature is employed.

Research on catalysis of gasification cover a wide range of subjects: basic chemistry, application problems and engineering. The state of research up to 1984 was compiled by Pullen [3] and there are several excellent review articles on the subject [4–7]. In the last decade, a number of basic researches have been published and the chemistry of catalysis has made good progress, though

0378-3820/91/$4.20

not yet complete. In these researches, graphite or activated carbon was frequently used as the model substrate. Coals have widely diverse properties which influence catalysis. It is important to clarify the influence of the nature of substrate on catalysis. The author has been working to elucidate the parameters influencing catalytic gasification and activating catalytic systems. This article reviews briefly recent progress in the area of his own interest.

BASIC CHEMISTRY OF CATALYSIS IN GASIFICATION

Comparison of gasification catalysts

Catalysis in carbon gasification has long been recognized and the following conditions are well agreed.
(1) Salts of alkali and alkaline earth metals as well as transition metals in the eighth group are active catalysts for gasification.
(2) Activity depends on the gasifying conditions, and especially on the gasifying agent. However, behaviors in oxidative gasifications bear some resemblance to one another.
(3) The main mechanism of catalysis using alkali and alkaline earth metal salts in steam or carbon dioxide gasifications involves the supply of oxygen from the catalyst to carbon, perhaps through the formation and decomposition of a C–O complex [5,7].

The mechanism of hydrogasification catalyzed by iron or nickel is still vague. The catalyst is active in the metallic state and two catalytic steps, hydrogen dissociation and carbon activation, seem to work. For the latter, a route of carbon dissolution into and diffusion through catalyst particles [8–11] seems well supported [12,13]. It should be noted that gasification proceeds in two stages, each of differing temperature range and thermal behaviors [14,15], so that a single mechanism cannot explain the whole reaction and hydrogen activation can still be a role of the catalyst.

Calcium as the catalyst has been studied by several research groups [16–21]. This catalyst has very high activity in the initial period when it is well dispersed, but loses its activity with burn-off. The chemical state and dispersion were studied by CO_2 chemisorption, X-ray diffraction and others, and the existence of two or more states of calcium compound [18] as well as the formation of a surface oxygen complex was elucidated [21].

The comparison of three catalyst groups, alkali, alkaline earth and iron group metals, would be interesting and is given in Table 1 and Fig. 1, from the author's limited experience. Figure 1 depicts typical kinetic patterns of gasification [22]. Interestingly, the rate increases with burn-off for sodium, rapidly decreases for calcium and is invariable for nickel. Note that the comparison given in Fig. 1 looks similar to that given by Moulijn and Kapteijn [7], but is

TABLE 1

Comparison of catalyst group

Item	Alkali (K, Na)	Alkaline earth (Ca)	Iron group (Fe, Ni)
Influence of surface area	Small	Large	Large
Influence of surface state of carbon	Insensitive	Insensitive	Sensitive
Effect of minerals	Easily poisoned	(Not clear)	Relatively insensitive
Main C1 product in steam gasification	CO_2	CO_2	The same as uncatalyzed
Effect of the amount[a]	Roughly proportional	Easy to level-off	Proportional

[a]In case of a substrate of large surface area.

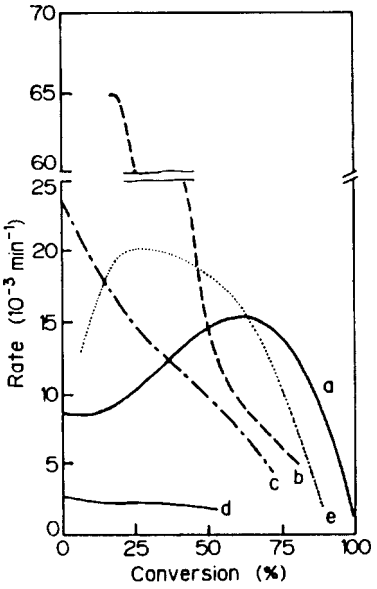

Fig. 1. Typical reaction patterns of steam gasification of an activated carbon with three catalysts, 0.375 mol% to carbon for each. Reaction at 800°C in 50% H_2O-He with (a) Na, (b) Ca and (c) Ni as catalyst or (d) without catalyst and at 850°C in 50% H_2O-H_2 with (e) Ni as catalyst. The rate is expressed in units of 10^{-3} g carbon gasified/min g carbon initially charged.

different in that the ordinate is not the apparent rate coefficient but the rate itself.

Changes in the activity of catalyst during gasification

Catalysis in gasification is unique as compared with usual heterogeneous catalysis in that the catalyst is very short-lived and is effective only while it is in contact with a particular substrate which eventually changes. The kinetics

of catalytic gasification is complicated, even when using a model carbon, due to unstable changes in the reaction rate, and it is difficult to give an unequivocal definition of the activity.

The rate increase with burn-off in the case of an alkali metal catalyst has been explained by the change in catalyst dispersion with burn-off and the increase in the ratio of catalyst/carbon in the later stage of gasification on the grain reaction model [23]. We also noted such rate increases when a demineralized char was the substrate [24,25], as shown in Fig. 2. In this figure, the product composition is shown to alter with burn-off, but most of the carbon monoxide is ascribed to the non-catalytic reaction. Other possible explanations for the rate increase would be the change in surface area or diffusibility by pore opening, the change in the chemical state of the catalyst and the change in the dispersion of catalyst. The CO formation profile in Fig. 2 suggests that surface area or diffusibility does not limit the reaction rate. So, for the rate change, the explanation by the change in chemical state of catalyst or catalyst-carbon system seems most feasible. Matsukata et al. [26] indicated the existence of three types of potassium compounds on the carbon surface. Some of the characteristic behaviors of alkali metal compounds is related to the mobility of the catalytic species over the substrate surface.

In the case of nickel-catalyzed hydrogasification, another rate increase was observed (Fig. 1, curve e), but its behavior is not the same as above. It was found to be sensitive to the surface state of the substrate and disappeared by preheating carbon in hydrogen prior to catalyst loading [27]. The rate change is ascribed to the diminishing poisonous effect of heteroatoms on the carbon surface to nickel or iron.

There are other changes which mostly bring about deactivation of the catalyst, for example, agglomeration of catalyst particles, carbon deposition (coking) or carbon dissolution, and reaction with sulfur or other elements.

Immobile catalysts such as calcium or iron usually agglomerate during gas-

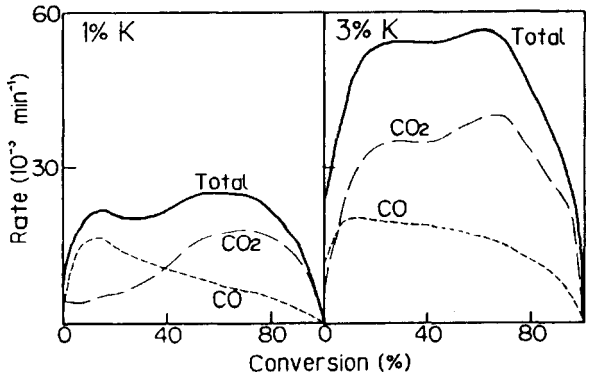

Fig. 2. Reaction of potassium-catalyzed steam gasification of Blair Athol char (demineralized) at 850 °C in 50% H_2O-He.

ification and deactivate with burn-off, but the agglomeration can be prevented or lessened by some suitable methods. Part, at least, of the synergistic effect of calcium and sodium seen in steam gasification [22] could be due to the prevention of agglomeration of calcium by a sodium compound [28]. Another example is the effect of adding calcium to an iron group catalyst, which has been shown to result in pronounced activation and one of the reasons is the better dispersion or slow agglomeration of the catalyst [14,29,30]. Suzuki et al. [31] used cyclic feed of carbon dioxide and inert gas to suppress the deactivation of iron catalyst. Thus, elucidation of the causes of changes in activity of catalyst, especially deactivation, and its utilization are important problems for catalysis.

PROBLEMS ASSOCIATED WITH APPLICATION TO COAL

Effect of nature of substrate

The activity of a catalyst depends profoundly on the nature of substrate and gasifying conditions. Thus, it is necessary to elucidate the factors influencing the activity and to design an effective catalyst for individual coals. The main properties of the substrate related to the activity are: (1) reactivity of carbonaceous constituents; (2) catalytic effect of minerals; and (3) effect of minerals on the activity of added catalyst.

As stated above, it is difficult, if not impossible, to assign a fixed rate constant to a catalytic reaction system, so that the term "activity" can be of qualitative significance, but comparison of the rate at a fixed time or burn-off can indicate the role played by the catalyst. Although, in most experimental studies, factors related to the activity of catalyst given above are not well separated, the following can be said to be general trends.

(1) The reactivity of the organic part of coals in relation to coal rank is of some ambiguity. Takarada et al. [32] showed that nickel catalysts are more effective for lower rank coals, while efficacy of potassium is nearly independent of coal rank, if the differences in the reactivity with and without catalyst are compared. The nickel catalyst was found to be well dispersed on lower rank coals. However, if the ratio of catalytic rate to non-catalytic rate is considered, the influence of nickel is generally larger for higher rank coals. In any case, the coal rank as given by the carbon content to designate the degree of coalification is not an appropriate parameter to predict the catalyst activity.

(2) One of the factors related to the activity is the surface area of coal or char. In a simple picture of catalysis, the activity of a catalytic system is determined primarily by the number of active sites which is under the influence of the catalyst. The surface area can be related to the number of active sites in cases when the amount of catalyst is large enough to cover the available surface area at the time of loading. So, if the catalyst is immobile, catalytic conversion

in a fixed time is almost proportional to the initial surface area, when several chars are compared, as given in Fig. 3 [25]. Here, carbon conversions of chars with 2 wt% of nickel or calcium are shown to change in a similar manner to the surface area (5–180 m^2/g) measured by CO_2 adsorption. Supposing that a limited fraction of surface determined by CO_2 adsorption is available to the catalyst (or its precursor) solution at the time of impregnation, the density of catalyst (2.5–90 $Å^2$ of surface per metal atom) would be enough to occupy active sites so that the activity is related to the apparent surface area. In the case of a potassium catalyst which is said to be mobile at the working state, the activity is not directly related to the surface area of the char.

(3) There are additional properties of carbon to surface area which influence catalysis. The behavior of iron or nickel catalyst is found to be sensitive to the surface state of carbon as stated above. By a pretreatment of an activated carbon, more than 80% of carbon could be gasified within 15 min at 650°C by either steam or carbon dioxide using 2–3% of nickel as catalyst [27]. Though the pretreatment cannot be directly applied to coal as a practical process, the result suggests that a suitable selection of coal species or processing can enhance the activity of catalysts. Also, we have empirically found that a parameter derived from X-ray diffraction can be related to the catalytic activity [33]. The true nature of the effect is not elucidated yet.

(4) The effect of mineral material on catalysis is double-faced; some minerals containing active elements such as alkali and alkaline earth metals catalyze the reaction and others, such as silica and alumina, interact with the added catalyst to deactivate it. Both forms of the influence is well documented in the literature. In our own study, demineralization resulted in an enhance-

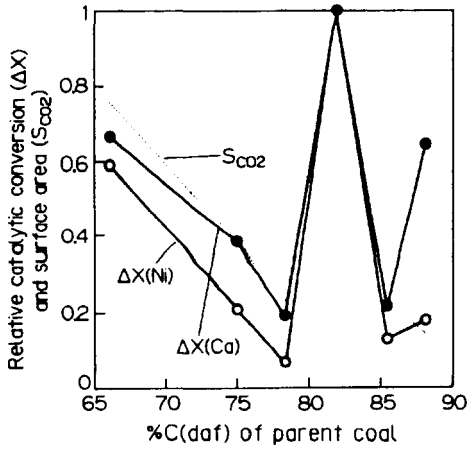

Fig. 3. Relation of catalytic reactivity to the surface area of chars. ΔX is the difference in carbon conversions with and without added catalyst (2 wt% of Ni or Ca). Reaction at 750°C for 30 min (Ni) or 60 min (Ca). S_{CO_2} is the surface area measured by CO_2 adsorption at 0°C. Data are expressed as the relative values to the most reactive coal (Blair Athol char at C = 82%).

ment of activity noticeably for potassium and only slightly for calcium and nickel [24].

Method of catalyst loading

It is well known that the manner of the loading is essential for the activity. The catalyst should have a definite contact with both the solid substrate and the gaseous reactant. For that purpose, loading to form minute particles on the surface is essential if the catalyst component is not mobile under gasifying conditions. Incipient wetness impregnation method is convenient in the laboratory, but would be inadequate for large scale operation and simple methods such as soaking should be tried. In connection with catalyst loading, the following would be worth mentioning:
(1) When a catalyst is loaded from an aqueous solution, a carbon surface of hydrophobic nature was found to result in a finer dispersion of the catalyst than a hydrophilic surface [34], in contrast to empirical feeling. The effect is tentatively correlated with surface hydroxyl groups which governs the deposition from aqueous solution [35].
(2) In spite of large structural changes during devolatilization, catalyst added before and after devolatilization behaved almost identically; in other words, devolatilization had slight influence on the activity of the catalyst [36].
(3) As a method of addition, vapor phase impregnation was tried and pentacarbonyl iron was successfully deposited as fine iron particles on the carbon surface [36].

Product composition in steam gasification

Steam is the main gasifying agent for a practical gasification process to produce a fuel gas or synthesis gas. Reaction of steam with carbon yields hydrogen, carbon monoxide and carbon dioxide with a small amount of methane. When the ratio of hydrogen to carbon monoxide is important, a shift reactor is necessary. It would be advantageous if the ratio can be controlled by the catalyst as a side effect. Here, the factors determining the H_2 to CO ratio is investigated and the result is expressed not by H_2/CO but CO–CO_2 composition, for experimental convenience. The CO fraction in the product was compared for several coals and was seen to be rich in CO for higher rank coals without added catalyst in accord with a previous report [37], when partial pressure of steam is high enough to expect a CO_2-rich gas in equilibrium. In cases of catalytic gasification, the fraction varies depending on the catalyst species. Then, the relation between gasification activity and CO–CO_2 composition in the product was examined using an activated carbon as a substrate with which CO was the main product in the absence of a catalyst. Interestingly, nickel did not alter the composition while other metals produced more CO_2 when the gasification activity

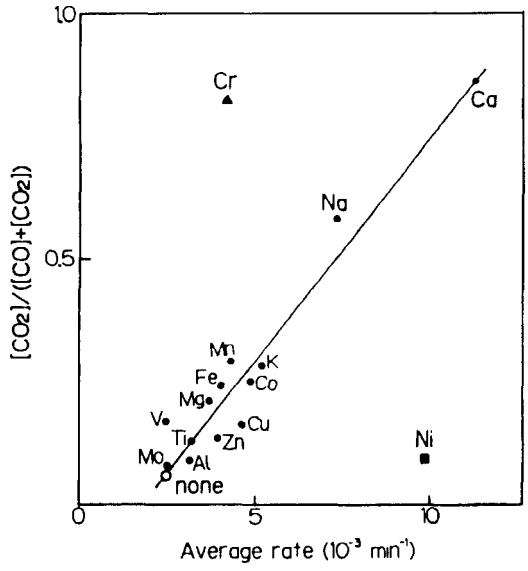

Fig. 4. Relation between gasification activity and $CO-CO_2$ composition in steam gasification at 800°C of an activated carbon with 0.25 mol% of metal element to carbon. The abscissa, average rate in gasification for the first 60 min, is used to denote catalyst activity.

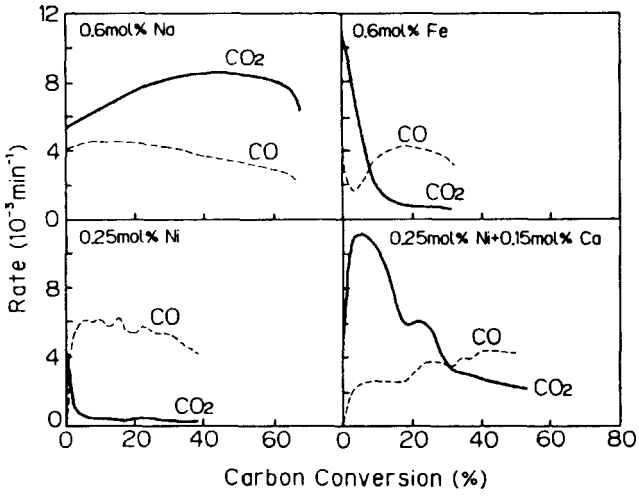

Fig. 5. Changes in the product composition during catalytic steam gasification of an activated carbon at 800°C in 50% H_2O-He at 1 atm.

is higher and a linear correlation was found between the activity and CO_2 fraction as illustrated in Fig. 4 [38]. In the presence of calcium or chromium, an equilibrium in the shift reaction was attained. The latter element is interesting in that it strongly accelerates the shift reaction in spite of rather low activity for gasification.

The correlation of gasification activity and product composition was unchanged when the above elements were mixed. Thus, a combination of nickel and alkali metal salt is attractive as they form a synergistically active catalyst.

By an appropriate application of these results, better use of the catalyst could be designed.

Examination of the change in product composition with burn-off is illustrated in Fig. 5 [38]. The general trend is in accord with the above; more CO is formed when the catalyst activity becomes low. Thus, product composition is a good clue for a diagnosis of the state of the catalyst. If the number of active site changes during gasification, product composition is expected to remain unchanged, as a first approximation.

Effect of product gases on catalyst activity

Among several parameters which causes deterioration of catalyst, gases evolved from coal could contain components harmful to the catalyst. So, the effect of the presence of product gas was examined by using, not a differential, but an integral type reactor. The average conversions with or without catalyst naturally decreased due to the decrease in steam partial pressure at downstream side, when the height of the fixed bed was increased from 1 to 30 cm, keeping the feed-rate of steam constant [36]. The conversion vs bed height was much the same for nickel and sodium catalyzed cases with non-catalytic ones. This was taken to indicate that the state and activity of the catalyst in steam gasification with sodium or nickel catalyst was not so much changed even when the catalyst was exposed to the product gases containing heavy tars and sulfur compounds.

POSSIBLE CATALYTIC PROCESSES

Catalytic process of coal gasification in large scale operations can be economical only when some special limitation in the process is imposed. There can be several possible applications but their evaluation depends on the circumstances especially on the whole energy strategy. A few possibilities are briefly mentioned here.

(1) Production of methane-rich gas at lower temperature, utilizing the advantage in equilibrium [39,40] is the main aim of the process developed by Exxon.

(2) Utilization of heat from gas-cooled reactor to supply the endothermic reaction of steam gasification indicated by a German group [4].

(3) Hydrogasification, which is quite slow without catalyst, is one component of clean fuel from coal plan proposed by Steinberg [41]. This reaction can be easily conducted by the presence of a catalyst.

(4) Another possibility would be that gasification is conducted in a small scale unit where ease of operation is given first priority. For example, a fuel cell to supply electricity to some limited unit would need low temperature gasification.

(5) A gasification process can be coupled with ore refinery to yield fuel gas and metals [42,43].

(6) Calcium catalyst can be endowed additional roles such as product selectivity or purification. Calcium is seen to trap sulfur-containing components in the product, and contribute to environmental problems [16,44].

Catalysts are required in a variety of coal utilization process such as liquefaction, purification or upgrading. Catalyst usefulness in gasification is quite different from these in that the reactant does not by itself come to contact with the catalyst. In case when the catalyst has to maintain contact with the substrate, then the study on gasification can be applicable. One such case is the pyrolysis of coal to yield liquid and gaseous materials [45–49]. In pyrolysis, a catalyst may alter the product composition, but the actual reaction step is not clear. There are some reports showing that the product of pyrolysis can be altered by adding a catalyst. The catalyst may work on solid material in gasification, on liquid material in liquefaction or in upgrading [49]. At present, there seems to be no clear evidence of the influence of a catalyst on solid substrate in pyrolysis, but a decrease in char yield is indicated [48]. Then, catalytic pyrolysis can be coupled with gasification to convert whole carbonaceous materials into fluid form. Also, it is suggested that conversion of biomass into gaseous fuel can be assisted by catalyst, similarly to coal [50]. Utilization of biomass has to be developed and catalysts may find new application here. Such a possibility has not been fully explored and the present author hopes a new type of catalyst and sophisticated methods of utilization may come onto the stage in the near future.

ACKNOWLEDGMENT

The author appreciates the cooperation of Dr T. Haga throughout his study on coal gasification.

REFERENCES

1 Wilson, J.S., Halow, J. and Ghate, M.R., 1988. Gasification: Key to chemicals from coal. CHEMTECH, 18: 123-128.
2 Keller, J., 1990. Diversification of feedstocks and products: Recent trends in the development of solid fuel gasification using the TEXACO and the HTW process. Fuel Processing Technol., 24: 247-268.
3 Pullen, J.R., 1984. Catalytic coal gasification. IEC Coal Research, London, 57 pp.
4 Jüntgen, H., 1983. Application of catalysts to coal gasification processes. Incentives and perspectives. Fuel, 62: 234-238.
5 Wood, B.J. and Sancier, K.M., 1984. The mechanism of the catalytic gasification of coal char: A critical review. Catal. Rev.-Sci. Eng., 26: 233-279.
6 Hüttinger, K.J., 1988. The potential of catalysed coal gasification. Erdöl u. Kohle, 41: 376-378.
7 Moulijn, J.A. and Kapteijn, F., 1987. The mechanism of the alkali metal catalyzed gasification of carbon. Erdöl u. Kohle, 40: 15-21.

8 Hahn, R. and Hüttinger, K.J., 1978. Kinetik der eisenkatalysierten Wasserstoff-Druck Vergasung von Koks. Chem.-Ing.-Tech., 50: 954.
9 Figueiredo, J.L. and Trimm, D.L., 1975. Gasification of carbon deposits on nickel catalysts. J. Catal., 40: 154-159.
10 Baker, R.T.K. and Sherwood, R.D., 1981. Catalytic gasification of graphite by nickel in various gaseous environments. J. Catal., 70: 198-214.
11 Keep, C.W., Terry, S. and Wells, M., 1980. Studies of the nickel-catalyzed hydrogasification of graphite. J. Catal., 66: 451-462.
12 Goethel, P.J., Tsamopoulos, J.T. and Yang, R.T., 1989. AIChE J., 35: 686-689.
13 Haga, T. and Nishiyama, Y., 1987. Promotion of iron-group catalysts by a calcium salt in hydrogasification of carbons at elevated pressures. Ind. Eng. Chem. Res., 26: 1202-1206.
14 Haga, T. and Nishiyama, Y., 1983. Promotion of nickel-catalyzed hydrogasification of carbon by alkaline earth compounds. J. Catal., 81: 239-246.
15 Haga, T. and Nishiyama,Y., 1983. Enhancements in nickel-catalysed hydrogasification of carbon by surface treatments. Carbon, 21: 219-223.
16 Ohtsuka, Y. and Asami, K., 1989. Steam gasification of high sulfur coals with calcium hydroxide. Proc. 1989 Int. Conf. Coal Sci., 1: 353-356.
17 Salinas-Martínez de Lecea, C., Almela-Alarcón, M. and Linares-Solano, A., 1990. Calcium-catalysed carbon gasification in CO_2 and steam. Fuel, 69: 21-27.
18 Joly, J.P., Cazorla-Amoros, D., Charcosset, H., Linares-Solano, A., Marcilio, N.R., Martinez-Alonso, A. and Salinas-Martínez de Lecea, C., 1990. The state of calcium as a char gasification catalyst — A temperature-programmed reaction study. Fuel, 69: 878-884.
19 Mühlen, H.-J., 1990. Finely dispersed calcium in hard and brown coals: Its influence on pressure and burn-off dependencies of steam and carbon dioxide gasification. Fuel Processing Technol., 24: 291-297.
20 Levendis, Y..A., Nam, S.W., Lowenberg, M., Flagen, R.C. and Gravalas, G.R., 1989. Catalysis of the combustion of synthetic char particles by various forms of calcium additives. Energy Fuels, 3: 28-37.
21 Zhang, Z.-G., Kyotani, T. and Tomita, A., 1989. Dynamic behavior of surface oxygen complexes during O_2 chemisorption and subsequent temperature-programmed desorption of calcium-loaded coal chars. Energy Fuels, 3: 566-571.
22 Haga, T., Nogi, K., Amaya, M. and Nishiyama, Y.,1991. Composite catalysts for carbon gasification. Appl. Catal., 67: 189-202.
23 Mühlen, H.-J., 1989. Impact of potassium dispersion and mass transfer on the kinetics of catalysed H_2O and CO_2-gasification. Proc. 1989 Int. Conf. Coal Sci., 1: 449-452.
24 Ozaki, J., Haga, T. and Nishiyama, Y., 1986. A comparison of the features of catalysis in coal gasification. Nenryo Kyokaishi, 65: 187-193 (in Japanese).
25 Haga, T., Sato, M., Nishiyama, Y., Agarwal, P.K. and Agnew, J.B., 1991. Influence of structural parameters of coal char on K- and Ca-catalyzed steam gasifications. Energy Fuels, 5: 317-322.
26 Matsukata, M., Fujikawa, T., Kikuchi, E. and Morita, Y., 1989. Quantitative behavior of potassium species on an amorphous carbon under steam gasification conditions. Energy Fuels, 3: 336-341.
27 Nishiyama, Y., Haga, T., Tamura, O. and Sonehara, N., 1990. A kinetic feature of catalytic gasification of carbons — Activation of nickel and iron catalysts during gasification. Carbon, 28: 185-191.
28 Pereira, P., Csencsits, R., Somorjai, G.A. and Heineman, H., 1990. Steam gasification of graphite and chars ate temperatures < 1000 K over potassium-calcium-oxide catalysts. J. Catal., 123: 463-476.
29 Haga, T. and Nishiyama, Y., 1989. Promotion of iron-group catalysts by a calcium salt in hydrogasification of coal chars. Ind. Eng. Chem. Res., 28: 724-728.

30 Nishiyama, Y., 1986. Catalytic behavior of iron and nickel in coal gasification. Fuel, 65: 1404-1409.
31 Suzuki, T., Chouchi, H., Naito, K. and Watanabe, Y., 1989. Cyclic feed CO_2 gasification of iron-loaded coal char. Approach to activate iron catalyst in coal gasification. Energy Fuels, 3: 535-536.
32 Takarada, T., Tamai, Y. and Tomita, A., 1986. Effectiveness of K_2CO_3 and Ni as catalysts in steam gasification. Fuel, 65: 679-683.
33 Haga, T. and Nishiyama, Y., 1988. Influence of structural parameters on coal char gasification. 2. Ni-catalyzed steam gasification. Fuel, 67: 748-752.
34 Nishiyama, Y. and Sonehara, N., 1989. Effect of pretreatment of carbon support on the activity of nickel catalyst. Tanso, no. 140: 314-315 (in Japanese).
35 Guo, S.-L., Arai, M. and Nishiyama, Y., 1990. Activation of a silica-supported nickel catalyst through surface modification of the support. Appl. Catal., 65: 31-44.
36 Haga, T. and Nishiyama, Y., unpublished. Preliminary results are given in the reports of Researches Grant-in-aid of Scientific Research of the Ministry of Education, Science and Culture, Japan: SPEY 16, 1987, pp. 99-104 and Energy, DEc. 1990, pp. 5-10.
37 Hashimoto, K., Miura, K. and Ueda, T., 1986. Correlation of gasification rates of various coals measured by a rapid heating method in a steam atmosphere at relatively low temperatures. Fuel, 65: 1516-1523.
38 Nishiyama, Y., Haga, T., Terada, K., Amaya, M. and Nogi, K., 1989. Product selectivity in catalytic gasification of carbons with steam. Proc. 1989 Int. Conf. Coal Sci., 1: 365-368.
39 Nahas, N.C., 1983. Exxon catalytic coal gasification process. Fuel, 62: 239—241.
40 Takarada, T., Sasaki, J., Ohtsuka, Y., Tamai, Y. and Tomita, A., 1987. Direct production of methane-rich gas from the low-temperature steam gasification of brown coal. Ind. Eng. Chem. Res., 26: 627-629.
41 Steinberg, M., 1988. A clean carbon fuel from coal. Fuel Processing Technol., 18: 313-315.
42 Tamai, Y. and Tomita, A., 1984. Production of synthesis gas and nickel metal. Nickel-catalyzed gasification of brown coal. Erdöl u. Kohle, 37: 474.
43 Weeda, M., Tromp, P.J.J., Van der Linden, B. and Moulijn, J.A., 1990. High temperature gasification of coal under severely product inhibited conditions: The potential of catalysis. Fuel, 69: 846-850.
44 Ohtsuka, Y., Hosoda, K. and Nishiyama, Y., 1987. Rate enhancement and *in situ* desulfurization by iron-calcium catalyst in the gasification of coal char. Nenryo Kyokaishi, 66: 1031-1036 (in Japanese).
45 Snape, C.E., Lafferty, C.J., Stephens, H.P., Dosch, R.G. and Klavetter, E., 1991. Effect of catalyst precursors on coal reactivity in catalytic hydropyrolysis. Fuel, 70: 393-395.
46 Matsui, H., Yamauchi, S. and Xu, W.-C., 1991. Coal flash pyrolysis — Catalytic effect of various metals loaded by ion-exchange method. Nenryo Kyokaishi, 70: 81-87 (in Japanese).
47 Maa, P.S., Veluswamy, L.R. and Gorbaty, M.L., 1989. Catalytic coal hydropyrolysis. Proc. 1989 Int. Conf. Coal Sci., 1: 643-646.
48 Kai, T., 1990. Asahikasei flash hydropyrolysis process. Nenryo Kyokaishi, 69: 701-704 (in Japanese).
49 Khan, M.R. and Seshadri, K., 1991. Compositional changes in the mild gasification liquids produced in the presence of calcium compounds. Fuel Processing Technol. 27: 83-94.
50 Kannan, M.P. and Richards, G.N., 1990. Gasification of biomass chars in carbon dioxide: dependence of gasification rate on the indigenous metal content. Fuel, 69: 747-753.

論文リスト

1．炭素資源反応研究センター

［論文］

T. Takanohashi, M. Iino
Insolubilization of Coal Soluble Constituents by Refluxing with Pyridine
Energy Fuels, **5**, 708 (1991)

M. Iino, T. Takanohashi, T. Ohkawa, T. Yanagida
On the Solvent Soluble Constituents Originally Existing in Zao Zhuang Coal
Fuel, **70**, 1236 (1991)

O. Ito, T. Ishizuka, M. Iino, M. Matsuda, T. Endo, T. Yokozawa
Kinetics of Ring-Opening Radical Polymerization of Vinyloxiranes
Int. J. Chem. Kinet., **23**, 853 (1991)

O. Ito, T. Kakuta, M. Iino
Modification of Mesophase Formation during the Carbonization of Acenaphthylene by the Addition of Acenaphthene
Carbon, **29**, 541 (1991)

J-L. Shen, T. Takanohashi, M. Iino
Thermal Behavior of Coals at Temperatures as Low as 100－350℃: Heat Treatment of THF-Insoluble Extract from CS2－NMP Mixed Solvent Extraction of Zao Zhuang Coal
Energy Fuels, **6**, 854 (1992)

M. Fujiwara, H. Ohsuga, T. Takanohashi, M. Iino
Swelling of the Extracts and Residues from Carbon Disulfide－N-Methyl-2-pyrrolidinone Mixed Solvent Extraction
Energy Fuels, **6**, 859 (1992)

T. Takanohashi, T. Ohkawa, T. Yanagida, M. Iino
Effect of Maceral Composition on the Extraction of Bituminous Coals with Carbon Disulfide－N-Methyl-2-pyrrolidinone Mixed Solvent at Room Temperature
Fuel, **72**, 51 (1993)

T. Ishizuka, T. Takanohashi, O. Ito, M. Iino
Effects of the Additives and Oxygen on Extraction Yield with Carbon Disulfide-N-Methyl-2-pyrrolidinone Mixed Solvent for Argonne Premium Coal Samples
Fuel, **72**, 579 (1993)

鷹觜利公, 劉　宏涛, 沈　建立, 飯野　雅
液化残査の構造と水素供与能
日エネ誌, **72**, 958 (1993)

H-T. Liu, T. Ishizuka, T. Takanohashi, M. Iino
Effect of TCNE Addition on the Extraction of Coals and Solubility of Coal Extracts
Energy Fuels, **7**, 1108 (1993)

Y. Ohtsuka, K. Asami
Steam Gasification of Low-Rank Coals with a Chlorine-Free Iron Catalyst from Ferric Chloride
Ind. Eng. Chem. Res., **30**, 1921 (1991)

Y. Ohtsuka, K. Asami
In Situ Sulfur Capture during the Calcium-Catalyzed Gasification of Illinois No. 6 Coal
Coal Sci. Technol., **18**, 139 (1991)

K. Asami, T. Shikada, K. Fujimoto
Effect of Oxidant on the Oxidative Coupling of Methane over a Lead Oxide Catalyst
Bull. Chem. Soc. Japan, **64**, 266 (1991)

Y. Ohtsuka, K. Asami
In-Bed Sulfur Removal during the Fluidized Bed Combustion of Coal Impregnated with Calcium Magnesium Acetate
Resour. Conserv. Recycl., **7**, 69 (1992)

Y. Ohtsuka, K. Asami, T. Yamada, T. Homma
Large Rate Enhancement by Iron Catalysts in the Low-Temperature Hydrogasification of Brown Coal under Pressure
Energy Fuels, **6**, 679 (1992)

K. Asami, Y. Ohtsuka
Catalytic Behavior of Iron in the Gasification of Coal with Hydrogen
Stud. Surf. Sci. Catal., **77**, 413 (1993)

K. Asami, Y. Ohtsuka
Highly Active Iron Catalysts from Ferric Chloride for the Steam Gasification of Brown Coal
Ind. Eng. Chem. Res., **32**, 1631 (1993)

Y. Ohtsuka, H. Mori, K. Nonaka, T. Watanabe, K. Asami
Selective Conversion of Coal Nitrogen to N_2 with Iron
Energy Fuels, **7**, 1095 (1993)

[総説・著書]

鷹觜利公, 飯野　雅
石炭構造－溶媒抽出からのアプローチ
燃協誌, **70**, 802 (1991)

飯野　雅
石炭の溶媒抽出と膨潤
石油学会誌, **35**, 26 (1992)

鷹觜利公
“地下深く眠る石炭”その不思議な構造 －石炭の非共有結合構造－
化学と工業, **46**, 234 (1993)

鷹觜利公, 飯野　雅
石炭架橋への溶媒の浸透
日エネ誌, **72**, 362 (1993)

Y. Ohtsuka, A. Tomita
Calcium Magnesium Acetate －An Emerging Bulk Chemical for Environmental Applications (Eds. D. L. Wise, Y. A. Levendis, M. Metghalchi), Chap. 10, Elsevier, Amsterdam, pp. 253-271 (1991).

朝見賢二
天然ガスからの化学製品 －メタンの酸化カップリング反応－
化学と工業, **45**, 305 (1992).

大塚康夫, 富田　彰
コークス製造のための乾留制御, 第3章
日本鉄鋼協会, pp. 69-94 (1993).

2．協力研究分野

［論文］

N. Sonobe, T. Kyotani, A. Tomita
Formation of Graphite Thin Film from Polyfurfuryl Alcohol and Polyvinyl Acetate Carbons Prepared between the Lamellae of Montmorillonite
Carbon, **29**, 61 (1991)

H. Yamashita, S. Yoshida, A. Tomita
Local Structures of Metals Dispersed on Coal. 2. Ultrafine FeOOH as Active Iron Species for Steam Gasification of Brown Coal
Energy Fuels, **5**, 52 (1991)

R. R. Martin, J. A. MacPhee, T. Kyotani, S. Hayashi, A. Tomita
SIMS Study on $^{18}O_2$-Gasification of Ca-Loaded Graphite
Carbon, **29**, 475 (1991)

A. Tomita
Reactivity of Char -- Effect of Coal Rank -- 14 Years Later
Carbon, **29**, 753 (1991)

沙　興中, 京谷　隆, 富田　彰
煤焦着火点与其気化活性的関係
燃料化学学報, **19**, 185 (1991)

H. Yamashita, S. Yoshida, A. Tomita
Local Structures of Metals Dispersed on Coal. 3. Na K-Edge XANES Studies on the Structure of Sodium Gasification Catalyst
Ind. Eng. Chem. Res., **30**, 1651 (1991)

T. Kyotani, S. Hayashi, A. Tomita
Study of Ca Catalysis on Carbon Gasification with $^{18}O_2$
Energy Fuels, **5**, 683 (1991)

H. Yamashita, H. Yamada, A. Tomita
Reaction of Nitric Oxide with Metal-Loaded Carbon in the Presence of Oxygen
Appl. Catal., **78**, L1 (1991)

Y.-H. Huang, H. Yamashita, A. Tomita
Gasification Reactivities of Coal Macerals
Fuel Process. Technol., **29**, 75 (1991)

H. Yamashita, Y. Machida, A. Tomita
Oxidative Coupling of Methane with Peroxide Ions over Barium-, Lanthanum-Oxygen Mixed Oxide
Appl. Catal., **79**, 203 (1991)

山下弘巳，許　維春，陳岡俊哉，V. Shrotori，羽島雅之，富田　彰
キュリーポイントパイロライザを用いた石炭の接触水素化熱分解の研究
日エネ誌，**71**，189 (1992)

T. Kyotani, S. Hayashi, A. Tomita, J. A. MacPhee, R. R. Martin
Three-Dimensional SIMS Imaging of $^{18}O_2$ Oxidized Calcium-Loaded Graphite
Fuel, **71**, 655 (1992)

H. Yamashita, M. Nomura, A. Tomita
Local Structures of Metals Dispersed on Coal. 4. Local Structure of Calcium Species on Coal after Heat Treatment and CO_2 Gasification
Energy Fuels, **6**, 656 (1992)

D. Cazorla-Amoros, A. Linares-Solano, C. Salinas-Martinez de Lecea, T. Kyotani, H. Yamashita, A. Tomita
Carbon Gasification Catalyzed by Calcium: A High Vacuum Temperature Programmed Desorption Study
Carbon, **30**, 995 (1992)

T. Kyotani, N. Sonobe, A. Tomita
Carbonization of Polyfurfuryl Alcohol Prepared between the Lamellae of Saponite
Tanso, **155**, 301 (1992)

T. Kyotani, H. Yamada, H. Yamashita, A. Tomita, L. R. Radovic
On the Use of Transient Kinetics and Temperature-Programmed Desorption to Predict Carbon/Char Reactivity: The Case of Cu-Catalyzed Gasification of Coal Char in Oxygen
Energy Fuels, **6**, 865 (1992)

H. Yamashita, A. Tomita, H. Yamada, T. Kyotani, L. R. Radovic
Influence of Char Surface Chemistry on the Reduction of Nitric Oxide with Chars
Energy Fuels, **7**, 85 (1993)

D. Cazorla-Amoros, A. Linares-Solano, C. Salinas-Martinez de Lecea, H. Yamashita, T. Kyotani, A. Tomita, M. Nomura
XAFS and Thermogravimetry Study of the Sintering of Calcium Supported on Carbon
Energy Fuels, **7**, 139 (1993)

T. Kyotani, K. Suzuki, N. Sonobe, A. Tomita, Y. Chida, R. Hara
Potassium-Graphite Intercalation Compounds from Thin Carbon Films Prepared between Montmorillonite Lamellae
Carbon, **31**, 149 (1993)

H. Yamashita, A. Tomita
Local Structures of Metals Dispersed on Coal. 5. Effect of Coal, Catalyst Precursor and Catalyst Preparation Method on the Structure of Iron Species during Heat Treatment and Steam Gasification
Ind. Eng. Chem. Res., **32**, 409 (1993)

D. Cazorla-Amoros, A. Linares-Solano, C. Salinas-Martinez de Lecea, M. Nomura, H. Yamashita, A. Tomita
Local Structures of Calcium Species Dispersed on Carbon: Influence of the Metal Loading Procedure and Its Evolution during Pyrolysis
Energy Fuels, **7**, 625 (1993)

山下弘巳, 庄　前林, 京谷　隆, 富田　彰
NEDOL残渣中のFe触媒の形態
日エネ誌, **72**, 993 (1993)

T. Kyotani, K. Kubota, J.-Q. Cao, H. Yamashita, A. Tomita
Combustion and CO_2 Gasification of Coals in a Wide Temperature Range
Fuel Process. Technol., **36**, 209 (1993)

T. Kyotani, K. Suzuki, H. Yamashita, A. Tomita
Formation of Carbon-Metal Composites from Metal Ion Exchanged Graphite Oxide
Tanso, **160**, 255 (1993)

T. Haga, K. Nogi, M. Amaya, Y. Nishiyama
Composite Catalysts for Carbon Gasification
Appl. Catal., **67**, 189 (1991)

T. Haga, Y. Nishiyama, P. K. Agarwal, J. B. Agnew
Surface Structural Changes of Coal upon Heat Treatment at 200-900℃
Energy Fuels, **5**, 312 (1991)

T. Haga, M. Sato, Y. Nishiyama, P. K. Agarwal, J. B. Agnew
Influence of Structural Parameters of Coal Char on K- and Ca-Catalyzed Steam Gasification
Energy Fuels, **5**, 317 (1991)

J. Ozaki, Y. Nishiyama
Infrared Photoresponse of Carbon Films Prepared by Plasma Decomposition of Propylene
J. Appl. Phys., **69**, 324 (1991)

T. Haga, J. Ozaki, K. Suzuki, Y. Nishiyama
Role of MgO and CaO Promoters in Ni-Catalyzed Hydrogenation Reactions of CO and Carbon
J. Catal., **134**, 107 (1992)

T. Haga, Y. Nishiyama
Regeneration of Nickel Catalyst on Carbon
J. Catal., **140**, 168 (1993)

J. Ozaki, T. Watanabe, Y. Nishiyama
Effect of Ferrocene on the Carbonization of Poly(vinylidene chloride)
J. Phys. Chem., **97**, 1400 (1993)

［総説］

京谷　隆，富田　彰
粘土層間を利用した２次元状炭素の合成
セラミックス，**26**，322（1991）

富田　彰
ホストゲスト反応を利用した新しい炭素の合成
セラミックス，**27**，427（1992）

山下弘巳，富田　彰
Ｘ線を利用した構造解析 —XRD，XAFS—
日エネ誌，**71**，1199（1992）

京谷　隆，富田　彰
石炭ガス化反応機構—表面含酸素化合物の役割—
日エネ誌，**72**，378（1993）

京谷　隆，富田　彰
分子サイズの鋳型を利用した高分子の新しい炭素化法
表面，**31**，578（1993）

京谷　隆，富田　彰
ゼオライトを鋳型として用いた高分子の新しい炭素化法
ペトロテック，**16**，841（1993）

富田　彰，京谷　隆
粘土を利用した新しい炭素材料の創製
スメクタイト，**3**，2（1993）

Y. Nishiyama
Catalytic Gasification of Coals - Features and Possibilities
Fuel Process. Technol., **29**, 31 (1991)